# Volcanology of the Raventhorpe and Pokeno West Volcanic Complexes, South Auckland Volcanic Field.

A thesis submitted in partial fulfilment
of the requirements for the degree
of
**Master of Science**
**in Earth and Ocean Sciences**
at
**The University of Waikato**
by

**Simon Nicholas Taylor**

---

The University of Waikato
2012


THE UNIVERSITY OF
WAIKATO
*Te Whare Wānanga o Waikato*

# Abstract

The South Auckland volcanic field hosts at least 82 volcanic centres throughout the Pukekohe, Bombay, Tuakau, Pukekawa and Onewhero regions. The monogenetic basaltic volcanic field was active between 1.59 to 0.51 Ma, producing tuff rings, maar craters, scoria cones, and basaltic lava flows covering an area of 300 $km^2$.

Two volcanic complexes have been studied in this thesis: the Raventhorpe volcanic complex, and the Pokeno West volcanic complex. The Raventhorpe complex hosts six interconnected and overlapping tuff rings (the Raventhorpe and five Ingram Road tuff rings) and the Rutherford Road scoria cone with several lava flows. The Pokeno West volcanic complex hosts a single tuff ring and surrounding lava flows. Each complex has been mapped and stratigraphic logs of exposed sections have been constructed. Measurements have been made of componentry (juveniles, lithics, crystals) and vesicularity of juvenile clasts. Petrography of the tuff rings, mineralogy (including selected electron microprobe analyses) and geochemistry by XRF has been undertaken to characterise the deposits. These data have been compiled and used for facies analysis, and to determine styles of eruption and their controlling factors.

The tuff ring facies of Raventhorpe include finely fragmented laminated to thinly bedded surge beds, coarse planar fall beds, and a massive magmatic block and bomb bed. The data show evidence for eruption drying out in the early stages moving to a Strombolian phase before reverting back to a phreatomagmatic style. Petrographic data indicates the Kaawa Formation aquifers were very important in the eruption dynamics, with the localisation of vents controlled by the St. Stevens Fault.

The facies of the Pokeno West tuff ring include finely fragmented laminated or thinly bedded surge beds, cross bedded surge beds, planar bedded fall beds, and massive magmatic coarse lapilli beds. The data suggest variable eruption styles occurred alternating between phreatomagmatic and Strombolian. Petrographic analysis of lithic clasts indicates the Kaawa Formation aquifers were important in the eruption dynamics and the localisation of the tuff ring could be related to the Waikato or Pukekawa faults. The presence of the Kidnappers Ignimbrite allows for a new age constraint based on stratigraphy (>1.0 Ma).

GIS analysis of the South Auckland volcanic field indicates fault location is the main control on the distribution of volcanic centres. The type of volcanism occurring is related to the hydrogeological parameters of underlying strata, which throughout the Manukau Lowlands is the Kaawa Formation. However, there are several dry magmatic volcanic centres in the Manukau Lowlands which could indicate another control by rate of magma flux which if rapid enough could prevent water-magma interaction. The distribution of age constrained centres has been statistically verified to be random.

# Acknowledgements

I would like to acknowledge and thank the many people who have assisted me throughout the duration of this thesis.

My primary thanks goes to Associate Professor Roger Briggs, and Dr. Adrian Pittari of the University of Waikato which, with their guidance and knowledge, has made this study possible.

I am grateful to all the landowners who welcomed me on their property and allowed me to collect samples. A special thanks to Quentin and Katie Ross and Margret Hopkins. I thank Dougal McFarlane for granting access onto Winstone Aggregates land.

I would like to acknowledge all those who have given technical assistance and time to this study including, Renat Radosinsky and Annette Rodgers for lab assistance, Helen Turner for support with the SEM, and Ritchie Sims of Auckland University for help and assistance with the electron microprobe.

I thank the Waikato Regional Council for supplying digital data when requested.

I am grateful to the funding I received from the University of Waikato Masters Research Scholarship, the AUSIMM Education Endowment Trust Scholarship, and the Broad Memorial Fund.

To all my friends and colleagues, Josh, Karl, Megan, Anna, Kirsty, Mike, and Sean thanks for all the discussions (and laughs).

I thank my family for supporting me throughout my time at university.

I am grateful to you all.

# Table of Contents

# List of Figures

# List of Tables

# Chapter One

# Introduction

## 1.1 Introduction

The South Auckland volcanic field (SAVF) is one example of several monogenetic volcanic fields throughout New Zealand, still preserved in the geological record. Activity ceased 0.5 Ma ago after the field's 1 Ma lifespan and represents a complete history of a monogenetic field. Many of the ~82 centres presently known are exposed and accessible, but many others are buried by younger lava flows. Study of these preserved volcanic fields and centres can help improve our understanding of controls, dynamics, and eruptive histories of monogenetic fields, tuff rings, maars, and effusive centres, both in the SAVF and other comparable fields.

## 1.2 Objectives

The first objective of this thesis is to reconstruct the eruption and emplacement processes of two volcanic complexes consisting of tuff rings and scoria cones, using stratigraphic data, facies analysis, geochemical data, and petrographic data. The second objective is to determine spatial and temporal controls on the localisation and occurrence of volcanic centres, and the evolution of the SAVF.

## 1.3 Study Area Locations

The SAVF covers an area of 300 $km^2$ (Schofield, 1958a; Rafferty & Heming, 1979, Weaver & Smith, 1989) across the Bombay-Tuakau-Pukekawa-Onewhero regions (Briggs *et al.*, 1994). The two study areas chosen are the Raventhorpe volcanic complex, and the Pokeno West volcanic complex. The Raventhorpe volcanic complex is situated in the centre of the field, 10 km east of Pukekohe,

and consists of 6 interconnected tuff rings, five Ingram Road tuff rings and the breached Raventhorpe tuff ring. The Pokeno West volcanic complex occurs 1 km southeast of Pokeno Township, in the southeast region of the field. The complex consists of the Pokeno West tuff ring, which State Highway One crosses, and the Bluff Road cone to the southwest.

## 1.4 Field Study

Field work was undertaken over a four week period during December 2010 and January 2011 in the two study areas. GPS co-ordinates were used to determine location. Photographs were taken of the outcrops and samples.

Two stratigraphic logs were constructed of exposed tuff deposits at the Raventhorpe volcanic complex. The sections were sampled, as were numerous boulder fields and lava flows in the area. Three stratigraphic columns were constructed of exposed tuff at Pokeno West, with samples taken at all three locations at various intervals of interest. A large ignimbrite exposure in the area was sampled along with basalt boulders from the Bluff Road cone.

## 1.5 Laboratory Methods

181 thin sections from the two field areas were made from samples representative of stratigraphic change, facies change, and layers of interest, and were analysed petrographically using an Olympus BH2 petrographic microscope. 56 thin sections were made from deposits of the Raventhorpe volcanic complex, including tuff (46), juvenile clasts (8), and lithics (2). 86 thin sections were made from the deposits of the Pokeno West volcanic complex, including tuff (57), and juvenile clasts (29). 39 sections were cut from boulder field and lava flow samples in the two study areas. Modal analysis of 141 slides was undertaken using a Swift Model F point counter.

Representative samples of ash, and juvenile basalt were viewed with a Hitachi S-4100 Field Emission Scanning Electron Microscope (SEM) with X-ray analyser from the University of Waikato.

Three polished thin sections of tuff, two from Raventhorpe and one from Pokeno West, were made to determine mineral geochemistry. A JEOL JXA-840A electron probe micro-analyser was used at the School of Environment, The University of Auckland, with the assistance of Ritchie Sims.

Major and trace elements were determined using an X-ray Fluorescence (XRF) spectrometer at the University of Waikato. 13 samples were analysed. Samples were powdered using a tungsten carbide ring mill. Major element geochemistry was analysed using fused glass disks. Trace element compositions were analysed using pressed powder pellets using the XRF. Loss on ignition (LOI) was determined by heating 2 g of powder in silica crucibles in a Bradway Fusion Furnace at 1100°C for one hour, measuring the difference in weight before and after heating.

Vesicularity and density were measured using vesicular basalt, lavas, and boulders from the two study area locations by the method and calculations of Houghton and Wilson (1989) for smaller samples. Specific gravity (SG) and vesicularity (V) were determined using the formulas:

$$SG = \frac{W_{clast}^{air}}{W_{clast}^{air} + W_{sheet}^{water} - (W_{clast+sheet}^{water} - W_{sinker}^{water})} \qquad \textbf{Equation 1}$$

$$V = \frac{100(DRE\ density - clast\ density)}{DRE\ density} \qquad \textbf{Equation 2}$$

where w is weight, and DRE is dense rock equivalent.

For larger samples vesicularities were measured using the Quantichrome Instruments Ultrapycnometer running nitrogen gas, with 1” or 1.5” cores, at the University of Waikato using the method and calculations of Formenti and Druitt (2003). Total vesicularity ($X_t$) and connected vesicularity ($X_c$) were determined using the formulas:

$$X_t = 1 - \frac{m_{sam}}{\rho_s V_{sam}} \qquad \textbf{Equation 3}$$

$$X_c = 1 - \frac{V_{meas}}{V_{sam}} \qquad \textbf{Equation 4}$$

where $m_{sam}$ is the mass of each cube, $\rho_s$ is the density, $V_{sam}$ is the total volume, and $V_{meas}$ is the volume of the solid calculated by the pycnometer.

Spatial and temporal analyses were undertaken at the University of Waikato using a Dell Precision T5500 with ArcGIS, ArcINFO desktop 10.0 software. ArcMap, ArcScene, ArcCatalogue, and ArcReader were used, alongside the Spatial analyst, 3D analyst, and Geostatistical analyst extensions. The data used were created by Landcare Research 2002 (digital elevation model), and QMAP GNS Science 2009. Other data produced were based on previous research (Greig, 1989; Viljevac *et al.*, 2002), or from stereoscopic observation, or location data based on academic works.

## 1.6 Chapter Outlines

Chapter 2 outlines the geological setting of the study area. The New Zealand tectonic development, current tectonic setting and intraplate volcanism in the North Island are discussed, with emphasis on fields within the Auckland Province. Previous studies of the SAVF are discussed as well as the centres at the two main study areas.

Chapter 3 focuses on the stratigraphy and geomorphology of the Raventhorpe and Pokeno West volcanic complexes, presenting stratigraphy and facies from field work, and componentry and vesicularity data.

Chapter 4 concerns the petrographic analysis of the lavas and tuff within the two study areas. Samples are classified as group A or B basalts, and descriptions and quantitative results are presented.

Chapter 5 concerns the bulk geochemical analysis of lava and juvenile basalts, and the geochemistry of crystals within the tuff. The major and trace elements are described with the mineral geochemistry occurring within the tuffs.

Chapter 6 focuses on spatial and temporal analysis on the SAVF and the two study locations. Slope analysis is presented in each study area, the relationship between age and location is described, as are the main controls of volcanism.

Chapter 7 interprets the data presented in the preceding chapters and summarises the eruption styles, and histories of the two volcanic complexes. Comparisons to other centres studied are presented and the conclusions are given.

# Chapter Two

# Geological Setting

## 2.1 Introduction

This chapter concerns the previous studies relating to the geological evolution of New Zealand with regard to the SAVF. The tectonic setting of New Zealand is briefly described along with other North Island intraplate fields. The geology and volcanic centres in the SAVF, and previous studies at the Raventhorpe and Pokeno West tuff rings are summarised.

## 2.2 New Zealand's Tectonic Setting

The current convergent boundary of the Australian and Pacific plates passes to the east of the North Island at the Hikurangi Trench, whereby the Pacific Plate is subducted underneath the Australian Plate (Fig. 2.1). The plate boundary then moves onto land at Kaikoura, and down the west of the South Island where compressional strike slip tectonics have, and still are, actively producing the Southern Alps. To the south of the Alps the Australian Plate is subducted underneath the Pacific Plate at the Puysegur Trench, forming New Zealand's complex tectonic setting. This boundary development has had a large influence on the volcanism of the North Island through the Neogene and Quaternary.

The New Zealand landmass was located on the eastern side of Gondwana during the Mesozoic, and consisted of several basement terranes (King, 2000). These terranes were uplifted, faulted, and folded due to the extensional deformation regime New Zealand was experiencing during the rifting from Gondwana, prior to the development of the plate boundary structure before 25 Ma (Furlong & Kamp, 2009). The movement of the Pacific Plate pole southward set the precursors for subduction to begin at the Hikurangi and Puysegur Trenches. This began the

movement of the New Zealand tectonic system away from an extensional regime and toward one of transpression (Furlong & Kamp, 2009).

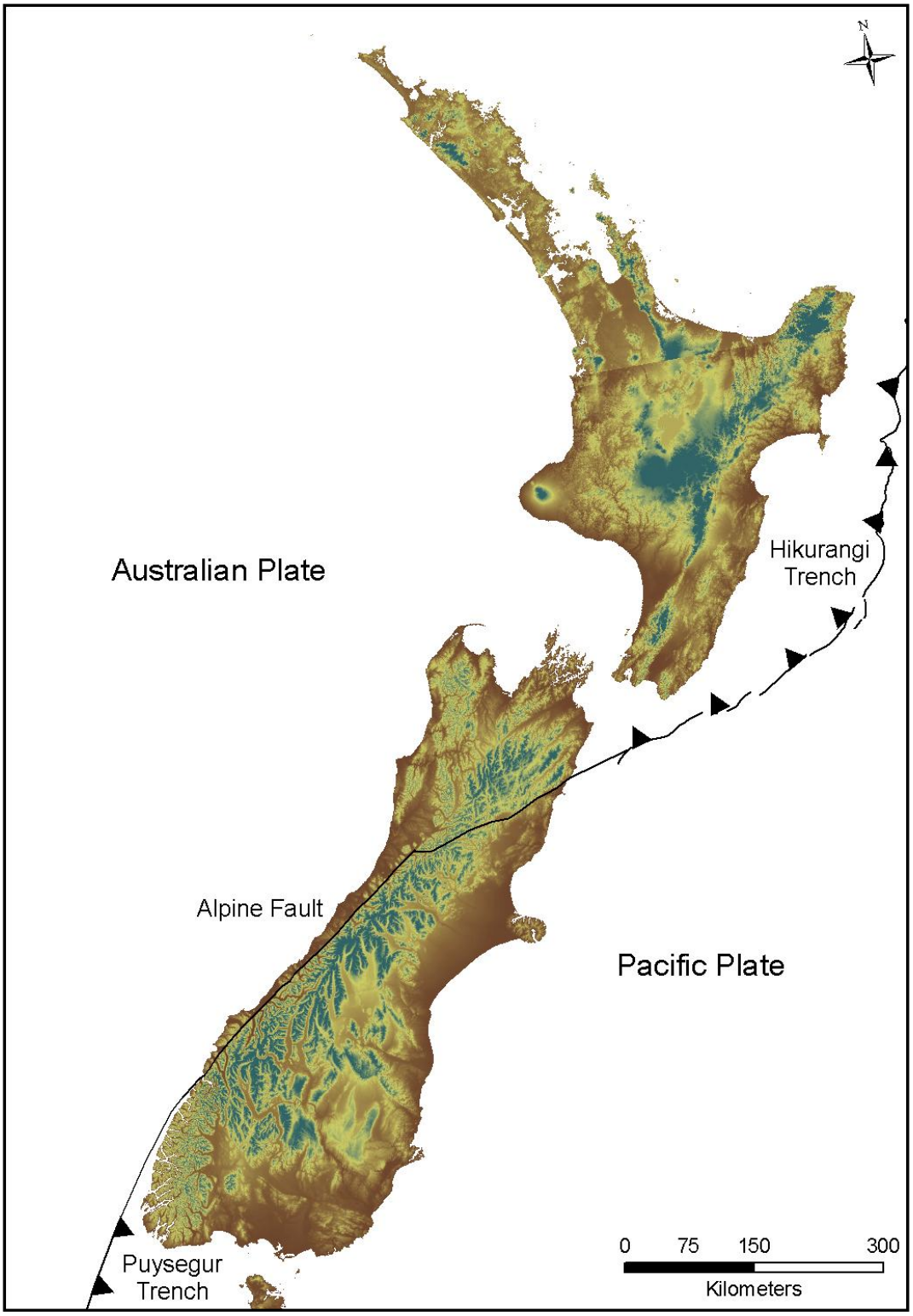


**Figure 2.1:** Tectonic setting of New Zealand. DEM basemap sourced from Landcare Research (2002).

Post 25 Ma the New Zealand landmass deformed under transpression, as the initial stages of subduction had started, and the slab had begun to migrate south (Furlong & Kamp, 2009). The Rakaia Terrane, forming the main South Island body, moved south off the East Coast of the North Island to the middle of what is now the current South Island (Furlong & Kamp, 2009). The plate boundary began propagating through the New Zealand landmass, producing the onset of arc volcanism in Northland and the Coromandel in the Late Miocene (Cole, 1986). The propagation of the plate boundary through New Zealand produced both uplift, and basin subsidence along with the reactivation of faults trending northward in the Auckland region (Edbrooke, 2001).

Between 15-10 Ma the east coast block began rotating clockwise (King, 2000), as the South Island body moved alongside the Buller Terrane of the western South Island. The West Coast block continued rotating clockwise until residing in its final position adjacent to the North Island (King, 2000; Kamp & Furlong 2009). During the last 5 Ma, the movement of the plate boundary shifted arc volcanism away from the Coromandel Volcanic Zone (CVZ), with rhyolitic volcanism becoming inactive by about 1.9 Ma (Briggs *et al.*, 2005). The northwest orientation of the Northland-Coromandel volcanic arc shifted orientation to the presently active, northeast trending Kermadec-Taupo Volcanic Zone (TVZ), where andesitic volcanism has been active since c. 2 Ma (Wilson *et al.*, 1995).

## 2.3 North Island Intraplate Volcanism

Volcanism through the Cenozoic is a dominant feature in the geological development of the North Island of New Zealand (Cook *et al.*, 2005). In the Late Miocene intraplate basaltic fields in Northland began to develop, and are still present in New Zealand's geological record (Cook *et al.*, 2005). Basaltic intraplate volcanism in New Zealand occurs in two provinces in the North Island on the Australian Plate, and several areas in the South Island located on, or near the plate boundary (Weaver & Smith, 1989). This review concerns only the North Island volcanic fields with particular emphasis on the SAVF.

The North Island volcanic fields are present through Kaikohe and Whangarei, southward to Auckland, South Auckland, Ngatutura, and Okete. The northern fields of Kaikohe and Whangarei reside in the Northland Volcanic Province, 150-250 km to the north of the currently active Auckland Volcanic Province, which includes the fields of Auckland, South Auckland, Ngatutura, and Okete (Cook *et al.*, 2005) (Fig. 2.2).

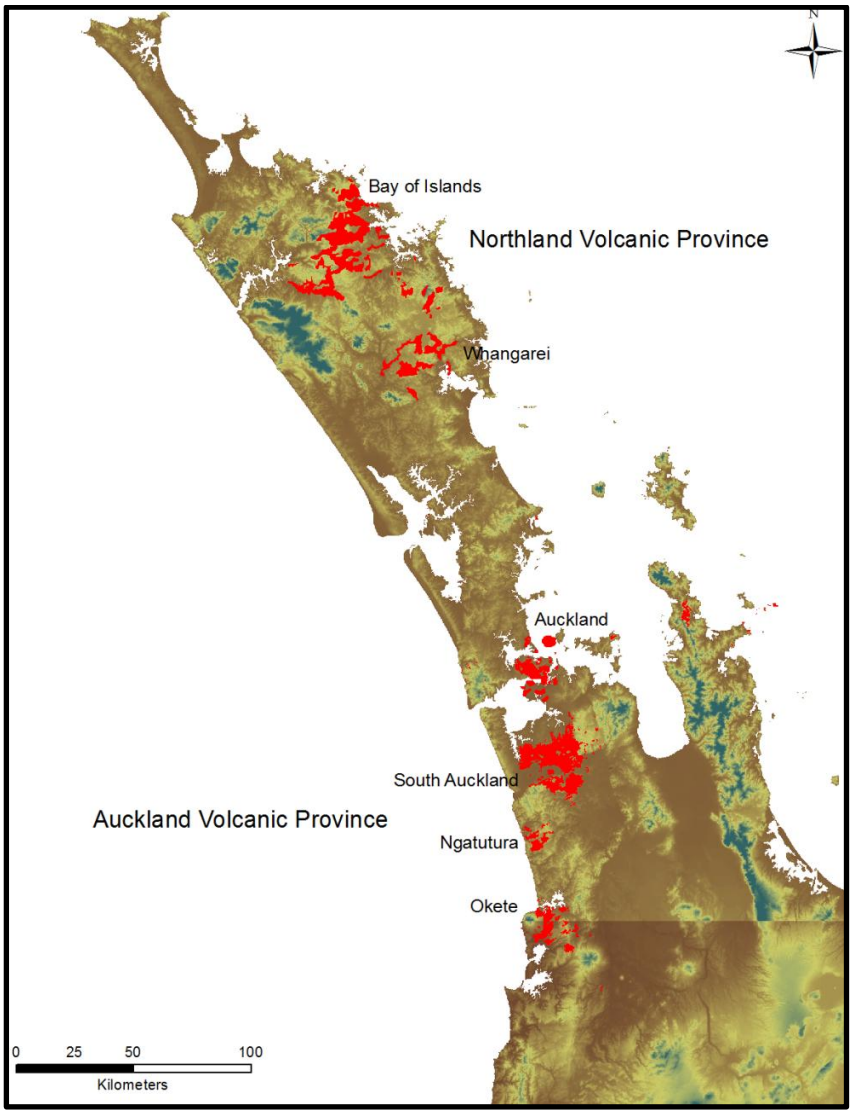


**Figure 2.2:** Intraplate volcanic fields of North Island, New Zealand. DEM basemap sourced from Landcare Research (2002), geological units from QMAP, GNS Science (2009).

These intraplate fields of the North Island contain numerous small volume centres, and are most commonly monogenetic (Cook *et al.*, 2005), with one nearby exception, Rangitoto volcano in the Auckland Volcanic Field (AVF) (Needham *et al.*, 2011). Such polygenetic volcanism has implications for hazard assessment. Needham *et al.* (2011) concluded that the earliest Rangitoto magma resulted from

~1% partial melting of a garnet peridotite, while the second magma resulted from 6% partial melting, erupting c. 500 years BP with about 60 years between eruptions. Activity throughout the Northland Province began c. 10 Ma and continued into recent times (Smith *et al.*, 1993).

The Auckland Volcanic Province lies between the Northland Peninsula and the actively mobile eastern segment of the North Island (Briggs *et al.*, 1994). Within the Auckland Volcanic Province, the fields of Okete (2.69-1.8 Ma), Ngatutura (1.83-1.54 Ma), SAVF (1.59-0.51 Ma), and AVF (0.26 Ma- 500 yr.) young in age progressively to the north (Briggs *et al.*, 1994). Several theories have been proposed regarding the distribution of volcanic fields within the Auckland Volcanic Province (Hodder, 1984; Briggs *et al.*, 1994; Spörli & Eastwood, 1997). The progressive younging of fields to the north indicates migration of the mantle source to the north, however if the spatial trend of these fields were related to plate movement over a stationary source, the youngest fields would be to the south (Briggs *et al.*, 1994). Briggs *et al.* (1994) proposed that the northern migration of magma sources within the Auckland Volcanic Province could be due to the onset of subduction at the southern end of the convergent plate boundary to the southeast of the province. Hodder (1984) and Spörli and Eastwood (1997) proposed that the development of the Hauraki Rift and lithospheric fracturing could account for the observed migration.

## 2.4 South Auckland Volcanic Field

The SAVF is located throughout the Manukau Lowlands covering an area of 300 $km^2$ (Schofield, 1958a; Rafferty & Heming, 1979; Weaver & Smith, 1989) across the Bombay-Tuakau-Pukekawa-Onewhero regions (Briggs *et al.*, 1994) (Fig. 2.3). Like most continental intraplate volcanics, the SAVF is situated in an extensional tectonic environment (Turcotte & Oxburgh, 1978) around 160 km behind the active volcanic front of the TVZ, and is considered to represent an intraplate association developed on the Australian Plate behind the currently active plate boundary (Briggs *et al.*, 1994). Two contrasting styles of volcanism occurred when the field was active between 1.59-0.51 Ma, with two peaks of activity at 1.3 and 0.6 Ma before abruptly ending at 0.5 Ma (Briggs *et al.*, 1994).The two types

are: magmatic, producing scoria cones and lava flows, and second, phreatomagmatic, producing tuff rings and maar craters (Briggs *et al.*, 1994). Recent studies have investigated the volcanic evolution of several centres throughout the SAVF including the Kellyville volcanic complex, Onewhero tuff ring, Bombay volcanic complex (Gibson, 2011), and Barriball road tuff ring (Ilanko, 2010). The tuff rings vary in diameter ranging from 0.5-2.5 km with occasional scoria cones nested inside the tuff ring (Rosenberg 1991). Rafferty (1977) proposed that the formation of these intra-tuff ring cones was from Strombolian or Hawaiian activity following phreatomagmatic eruptions.

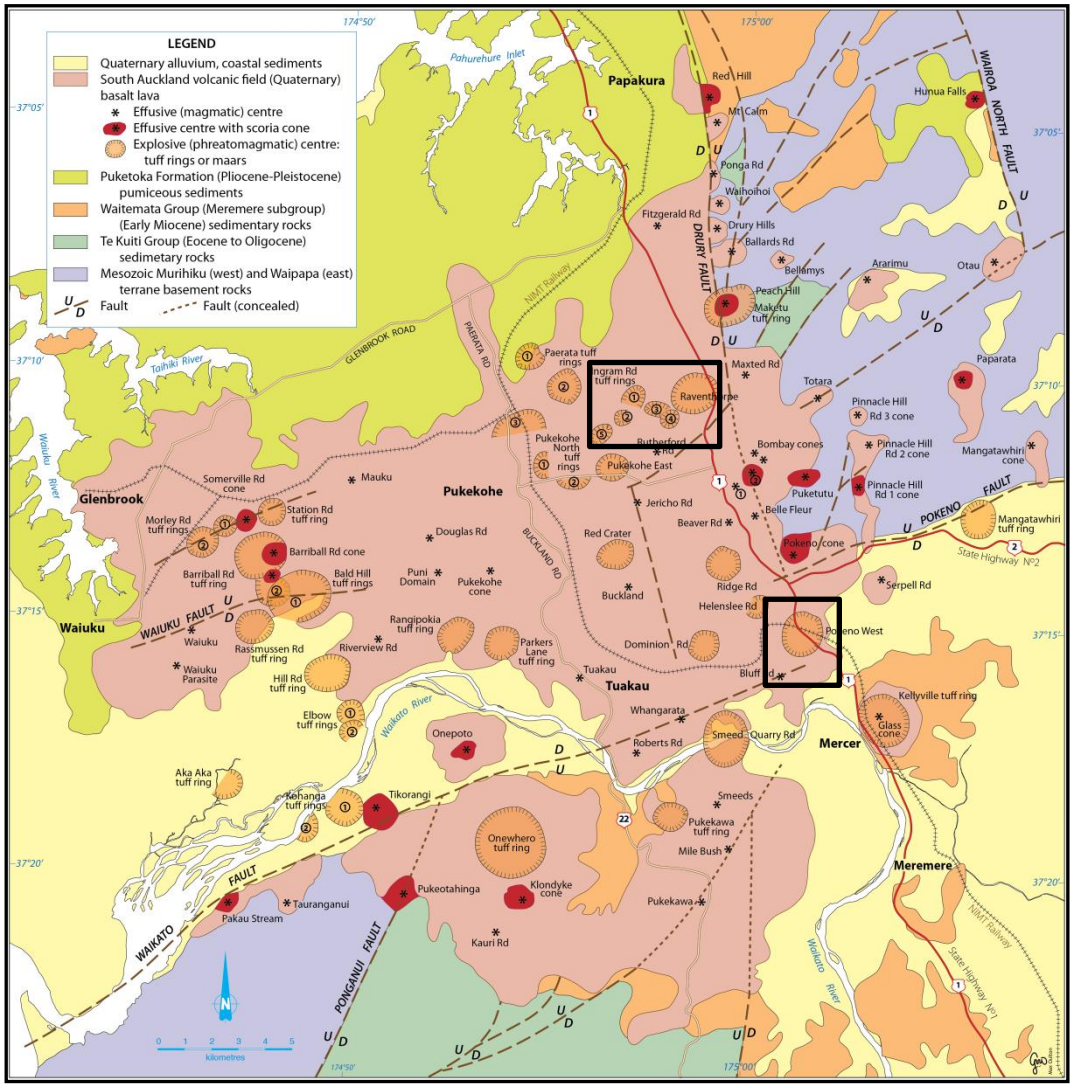


**Figure 2.3:** Distribution of volcanic centres and underlying geology of the SAVF. The two study areas are shown (Briggs *et al.* in prep.).

Early studies of the SAVF counted 97 volcanic centres (Rafferty, 1977). Today it is accepted the field contains ~82 volcanic centres (R. Briggs pers. com. Sept. 6,

2010). Magmatic volcanism has been dominant forming ~59 centres as scoria cones and lava flows, while phreatomagmatic activity has formed 38 maars or tuff rings (Rosenberg, 1991). Many of the eruptive centres throughout the SAVF are located directly over faults or fault extensions, likely providing the easiest pathway for magma to ascend through the crust (Raffery, 1977; Briggs *et al.*, 1994). Rosenberg (1991) noted the fault controls on the SAVF as more evident compared to the AVF, the modern analogue of the SAVF.

No systematic age pattern within the field exists, although younger volcanics are more common in the centre of the field where clusters occur (Briggs et al 1994). Several older volcanic centres exist in the northeast, however these are exceptions and overall the older volcanics have an isolated distribution (Briggs *et al.*, 1994). The centre of the field has been covered by thick layers of basalt lava which have hidden any structural controls that might have existed during volcanism (Briggs *et al.*, 1994). This also may have biased the distribution of older volcanics as seen today, by covering them with younger ones. Alternatively this could demonstrate that the early onset of volcanism was widespread and become more confined to the centre through the fields' evolution (Briggs *et al.*, 1994). Cassidy and Locke (2011) cite a number of reasons for the absence of a consistent pattern of vent alignments in the AVF, including the lack of known faults through the immediate vicinity of the field. Cassidy and Locke (2011) considered that the relatively weak Miocene cover rocks may be altering the ascending magmas course in the top-most crust, disrupting any spatial pattern that might have otherwise been observed.

Rafferty (1977) identified two different magma types within the SAVF, an alkalic group and a subalkalic group. Rafferty and Heming (1979) considered the alkalic magmas to be older, and being higher in volatiles, they produced violent, small volume eruptions. Rafferty and Heming (1979) divided the basalts of the SAVF into two groups based on their geochemical differences. The two types are referred to as group A and B basalts (Rafferty & Heming, 1979), and while this distinction can be made through geochemistry and petrography, they cannot be separated spatially or temporally (Briggs *et al.*, 1994). Group A basalts are hypersthene normative subalkaline basalts that are silica undersaturated with low total alkalis, while the group B basalts are a nepheline normative alkaline group, strongly silica undersaturated with high total alkalis (Cook *et al.*, 2005).

Intraplate volcanic fields, despite their widespread geographical distribution, commonly display ocean island basalt (OIB)-like characteristics. The South Auckland basalts are no exception, with the two basalt groups comparing well to other continental intraplate volcanic fields (Cook *et al.*, 2005). The two groups of basalts have evolved independently of each another, display slight variations in abundances of large ion lithophile elements (LILE), high field strength elements (HFSE), rare earth elements (REE), and isotope compositions (Cook *et al.*, 2005).

Rafferty and Heming (1979) proposed a theory for the origin of the magmas throughout the Auckland Volcanic Province, proposing that a rising diapir with partial melting occurring at different depths could be the source for the magmas. Briggs *et al.* (1994) however, state there is no time related trend in magma compositions within fields, proving this early theory unlikely. A number of recent studies have proposed origins for the Auckland Volcanic Province magmas (Huang *et al.*, 1997; Hoernle *et al.*, 2006; Sprung *et al.*, 2007).

Cook *et al.* (2005) proposed a model involving a heterogeneous mantle with three components: an enriched subcontinental lithospheric mantle derived from Mesozoic subduction of Gondwana, remnant Mesozoic plumes, and a depleted asthenospheric mantle. They concluded that group A magmas were generated by melting of a mantle-enriched shallow spinel peridotite, while group B magmas were generated by melting of a mantle-enriched garnet peridotite. The spatial and temporal randomness of eruptives from both groups indicates that magma generation for each group was occurring simultaneously in their respective source locations, and that contemporaneous ascent of magmas must also have occurred. No monogenetic field other than the AVF is known to have had contemporaneous eruptions at distant and structurally unrelated localities (Cassidy, 2006).

Sprung *et al.* (2007) showed that a similar model to that of Cook *et al.* (2005) is generally applicable to New Zealand intraplate fields, with asthenospheric mantle dominating the plume signature due to extension. Hoernle *et al.* (2006) however attributed melting to the removal of the lower lithosphere and corresponding decomposition in the upwelling asthenosphere, instead of extension and plume related activity. The model proposes that alkalic magmas are sourced at depths

consistent with the fossil plume influence and small degrees of partial melting, while subalkalic magmas are from a shallow source and have been enriched by the lithosphere with higher degrees of partial melting.

## 2.5 The Geological Setting of South Auckland

The South Auckland region is characterised by block faulting and consists of uplifted Mesozoic greywacke, argillite, and conglomerate basement rocks (Greig, 1989). These rocks formed on the eastern margin of Gondwana and have subsequently been faulted and folded; they are termed the Murihiku Terrane to the west, and Waipapa Terrane to the east (Greig, 1989: Edbrooke, 2001) (Fig. 2.3). To the west of the Drury fault, magmas have erupted through the Waipapa Terrane basement, commonly along faults or inferred fault extensions (Cook *et al.*, 2005).

These basement terranes are unconformably overlain by transgressive sequences of Late Eocene to Early Oligocene age Te Kuiti Group, including the Waikato Coal Measures, sandstones, mudstones, and limestones (White & Waterhouse, 1993) (Table 2.1). During the Miocene, siltstones, sandstones, and limestones of the Waitemata Group were deposited, over the Te Kuiti Group (Table 2.1), and consisted of the transgressive shallow marine Warkworth and Meremere Subgroups (Hayward & Brook, 1984). The Warkworth Subgroup comprises the Pakiri, and the East Coast Bays Formation, while the Meremere Subgroup includes the Waikawau Sandstone (Hayward & Brook, 1984). These subgroups overlie bathyal flysch sequences recognised as the Kawau Subgroup, comprising the Cape Rodney Formation, Tipakuri Sandstone, and the Papakura Limestone (Hayward & Brook, 1984).

Through the Late Miocene remobilisation of old faults or a period of increased normal faulting occurred in the region (Edbrooke, 2001). Significant faults in the region include the north-northwest trending Drury Fault (Nixon, 1977) upthrown to the east. The southern end of the Drury Fault connects with the east-northeast trending Pokeno Fault (Edbrooke, 2001) which is, upthrown to the north and producing the Hunua Ranges. To the west the Waikato Fault (Hochstein & Nunns,

1976) trends east-northeast on a similar orientation to the Pokeno Fault, however it is a reverse fault and downthrown to the north (Hochstein & Nunns, 1976: Edbrooke, 2001) producing the Manukau Lowlands bounded by the Manukau Harbour (Viljevac *et al.*, 2002).

**Table 2.1:** Generalised stratigraphic column for the South Auckland region. No scale is inferred. Empty row indicates a break in the geological record. After Edbrooke (2001).

| | Geological Unit | | |
|---|---|---|---|
| **Epoch** | **Primary** | **Secondary** | **Tertiary** |
| **Holocene** | Recent alluvial and coastal sediments | Tauranga Group | |
| **Late Pleistocene** | Hinuera Formation | Puketoka Formation | Tauranga Group |
| **Early Pleistocene** | South Auckland Volcanic Field | | |
| **Late Pliocene** | Puketoka Formation | Tauranga Group | |
| **Early Pliocene** | Kaawa Formation | | |
| **Late Miocene** | Tauranga Group | | |
| **Early Miocene** | Waitemata Group | Waitakere Group | |
| **Late Eocene** | Te Kuiti Group | | |
| **Jurassic** | Murihiku Supergroup | Waipapa Terrane | |

The down-faulted blocks of the Waitemata and Te Kuiti Groups in the Manukau Lowlands are infilled with Pliocene age marine, and estuarine sands and sandstones known as the Kaawa Formation (Greig, 1989). The Kaawa Formation represents a significant and important aquifer to the lowlands and many studies have been undertaken to investigate the characteristics of the aquifer (Hollis, 1986; Hadfield, 1988; Greig 1989; Viljevac *et al.*, 2002). Hollis (1986) identified four units within the formation: a basalt conglomerate, shelly sands, shell bed, and upper sands. Greig (1989) described the formation as comprising of an upper sand sequence and lower shell gravel sequence, also noting that the contacts between the sand and gravel units could be sharp or gradational, interbedding the two facies over few tens of meters. Hadfield (1988) described the main unit in the formation as a fine, well sorted, greenish-grey sand, comprised of rounded lithics, feldspars, and quartz.

Greig (1989) indicated that the thickness of the Kaawa Formation ranges from less than 50 m in the north to over 150 m in the south based on borehole data. These data were better confined by Viljevac *et al.* (2002) demonstrating that to the south, the formation reaches a maximum thickness of 300 m, while to the

southwest thicknesses of up to 200 m are recorded. Greig (1989) and Viljevac *et al.* (2002) noted the thickness distribution of the formation is consistent with the basement topography.

Greig (1989) described the Kaawa Formation as petrographically distinct, with highly fossiliferous lower units. Hollis (1986) summarised the formation componentry as dominated by sedimentary and less common igneous rock fragments, with quartz, plagioclase, ferromagnesian minerals, and less abundant authigenic minerals. The deposits that overlie the Kaawa Formation are locally variable consisting of the Quaternary Tauranga Group, and Seagrove Formation, (Hadfield, 1988), with the local variation a response to non-marine deposition (Jukić, 1995). The sediments within the Tauranga Group were deposited prior to, and concurrently with, Pleistocene volcanism in the TVZ. The sedimentary sequences of the Seagrove Formation overlie the Kaawa Formation across the Manukau Lowlands (Greig, 1989). The formation comprises of pumiceous and rhyolitic sands, silts, clays, and peats of varying distribution (Hadfield, 1988).

## 2.6 Previous Work: Raventhorpe Volcanic Complex

The Raventhorpe tuff ring is one of the larger tuff rings in the SAVF and has subsequently been included in both large and small scale studies (Schofield, 1958a; Rafferty, 1977; Rosenberg, 1991; Briggs *et al.*, 1994; Cook, 2002; Cook *et al.*, 2005). Early work was undertaken by Schofield (1958a) mapping the field and making distinctions on the types of basalts observed across this region. He discussed the relationship of volcanism and the structural controls that allowed inception of the field, and the observed distribution of centres. Rafferty (1977) also mapped the field and discussed many aspects of the volcanism throughout the region. Rosenberg (1991) while studying several individual centres in depth, included the Raventhorpe tuff ring, and concluded that no relationship exists between style of volcanism and age of the centre. Rather, the type of volcanism was controlled by other factors such as the hydrology and lithology of the underlying strata, and inferred that these controls have been present throughout the duration of activity in the SAVF.

Schofield (1958a) interpreted the Raventhorpe outcrop as a pseudo-dike remaining after erosion. Rafferty (1977) described the complex as consisting of five centres, with the first and largest centre, Raventhorpe, successively followed by smaller tuff rings (Ingram Road tuff rings), and interpreted this clustering to be related to a single magmatic event. Rosenberg (1991) interpreted the 200 m wide, north trending outcrop as an exposure along a ring fault produced by subsurface collapse of a diatreme. Rosenberg (1991) went on to describe the petrography of the deposit as vitric-lapilli-tuff in addition to matrix material, and the facies as planar bedded, dominated by several sequences of surges. Rosenberg (1991) cited the sequence of events at the tuff ring to have incorporated pyroclasts from the Ingram Road tuff rings, indicating that at least one, if not all were present during the evolution of Raventhorpe, in contrast to Rafferty (1977).

Rosenberg (1991) interpreted the controls on the observed clustering of the complex as explosive interaction of magma and groundwater due to the presence of the St. Stevens Fault allowing magma ascent. He states that the depth of the maar would have been a minimum of 300 m, based on observations by Rafferty (1977) who recorded Waitemata Group flysch, known to be present at this depth in the area from Greig's (1989) borehole study.

The available water source for phreatomagmatic volcanism has been proposed as the Kaawa Formation throughout the Manukau Lowlands (Waterhouse, 1978; Hadfield, 1988; Greig, 1989, Rosenberg, 1991, Gibson, 2011). Evidence for this is present in the petrography of the tuffs, with many xenocrysts observed and identified (Rosenberg, 1991; Gibson, 2011). Previous studies on the basalts exposed on Ambush Road by Briggs *et al.* (1994) have been dated to 0.73 Ma ± 0.13 Ma. Rosenberg (1991) considered this as an upper age limit for the tuff ring as texturally similar basalt lithics were found in the tuff. Rosenberg (1991) inferred that Raventhorpe was one of the last phreatomagmatic centres to erupt before effusion of lava commenced from the Rutherford Road cone. Briggs *et al.* (1994) dated the lavas of the Rutherford Road cone at 0.65 Ma, adding evidence to Rosenberg's (1991) interpretation.

Geochemical analyses by Cook *et al.* (2005) identified olivine-tholeiitic basalts and alkali olivine-basalts within the tuff at Raventhorpe. Geochemical analysis

revealed that both A and B group lavas occurred in the tuff as bombs or blocks (Cook, 2002). Rosenberg (1991) identified the juvenile clasts from the Raventhorpe tuff ring through petrography, identifying basalts with hawaiite, nepheline hawaiite, nephelinite, and basanite compositions.

## 2.7 Previous Work: Pokeno West Volcanic Complex

While the geology of the Pokeno District has been described previously by Cox (1877, 1882), Bartrum and Branch (1936), Battey (1949), Schofield (1958a, b), Kear (1960), and Rafferty (1977), few studies mention the tuff rings in this area. The Pokeno West tuff ring, although included on many maps (Rafferty, 1977; Rosenberg, 1991; Briggs *et al.*, 1994, Cook *et al.*, 2005), has never been studied in detail.

Battey (1949) described the geology immediately to the south of the Pokeno West tuff ring, identifying lava outcrops over a small area on a south facing slope at the head of Cole Road. To the north of this lava exposure, Battey (1949) described ash deposits, composed almost entirely of small basaltic lapilli forming a line of north-facing, east-west trending bluffs around half a kilometre in length.

Rafferty (1977) documented the relative chronology of the tuff rings and magmatic cones at Pokeno West, inferring relationships and limit intervals of eruptives. He considered the Pokeno West tuff ring to be an isolated centre, not occurring in conjunction with other magmatic cones or tuff rings in the area. The interpreted chronological history of the SAVF by Rafferty (1977) places the eruption of the Pokeno West tuff ring during the middle of the field's life, sometime between 1.24-1.08 Ma, based on morphology and ages from other previously dated volcanic centres throughout the SAVF. The tuff ring was later flooded with lavas from the volcanic centres of the Bombay hills (Rafferty, 1977). The lavas of the Bombay hills have been dated by Briggs *et al.* (1994) to be 0.59 ± 0.03 Ma.

To the southwest of the Pokeno West tuff ring a magmatic centre, the Bluff Road cone, occurs, which Battey (1949) described as outcropping lavas. Briggs *et al.*

(1994) dated lavas to the south of Pokeno Road at 0.64 Ma, with the nearest likely source the Bluff Road cone. Cook (2002) determined the lavas of the Bluff Road cone to be of alkali olivine-basalt composition.

# Chapter Three

# Geomorphology and Stratigraphy

## 3.1 Introduction

The volcanic centres within the SAVF are poorly exposed with in situ outcrops rare. The volcanic complexes of both Raventhorpe and Pokeno West are exposed as thin, often highly weathered tuffaceous successions. These successions occur as rings which are characterised by low angle, inward and outward dipping beds, rather than cones with much steeper outer slopes (Cas & Wright, 1987). The geomorphology, field stratigraphy and facies of the two volcanic complexes are presented in this chapter (Fig. 3.1).

## 3.2 Raventhorpe Volcanic Complex

The Raventhorpe Volcanic Complex is located in the central region of the SAVF 10 km to the east of Pukekohe, and is comprised of the Raventhorpe tuff ring and the five Ingram Road tuff rings. The volcanic complex association is based on the overlapping relationship of the 6 interconnected tuff rings. On the western rim of the Raventhorpe tuff ring, a north-south trending outcrop >200 m long is exposed. From the outcrop, the eastern rim is visible along State Highway One. To the west are the Ingram Road tuff rings, consisting of five interconnected rings (Fig. 3.1). The complex occurs between the Drury Fault trending north-south (Fig. 3.2) and upthrown to the east, and the St. Stevens Fault trending northeast-southwest upthrown to the south. A magmatic centre, the Rutherford Road cone, is located directly to the south of the complex and has produced extensive lava flows in the area, which in some cases breach the southern rims of several of the Ingram Road tuff rings. The southern (and northern) rim of the Raventhorpe tuff ring has also been breached; but unlikely by lava flows of the Rutherford Road cone, which will be discussed in later chapters. The Pukekohe East tuff ring while included on several maps is not considered part of the Raventhorpe

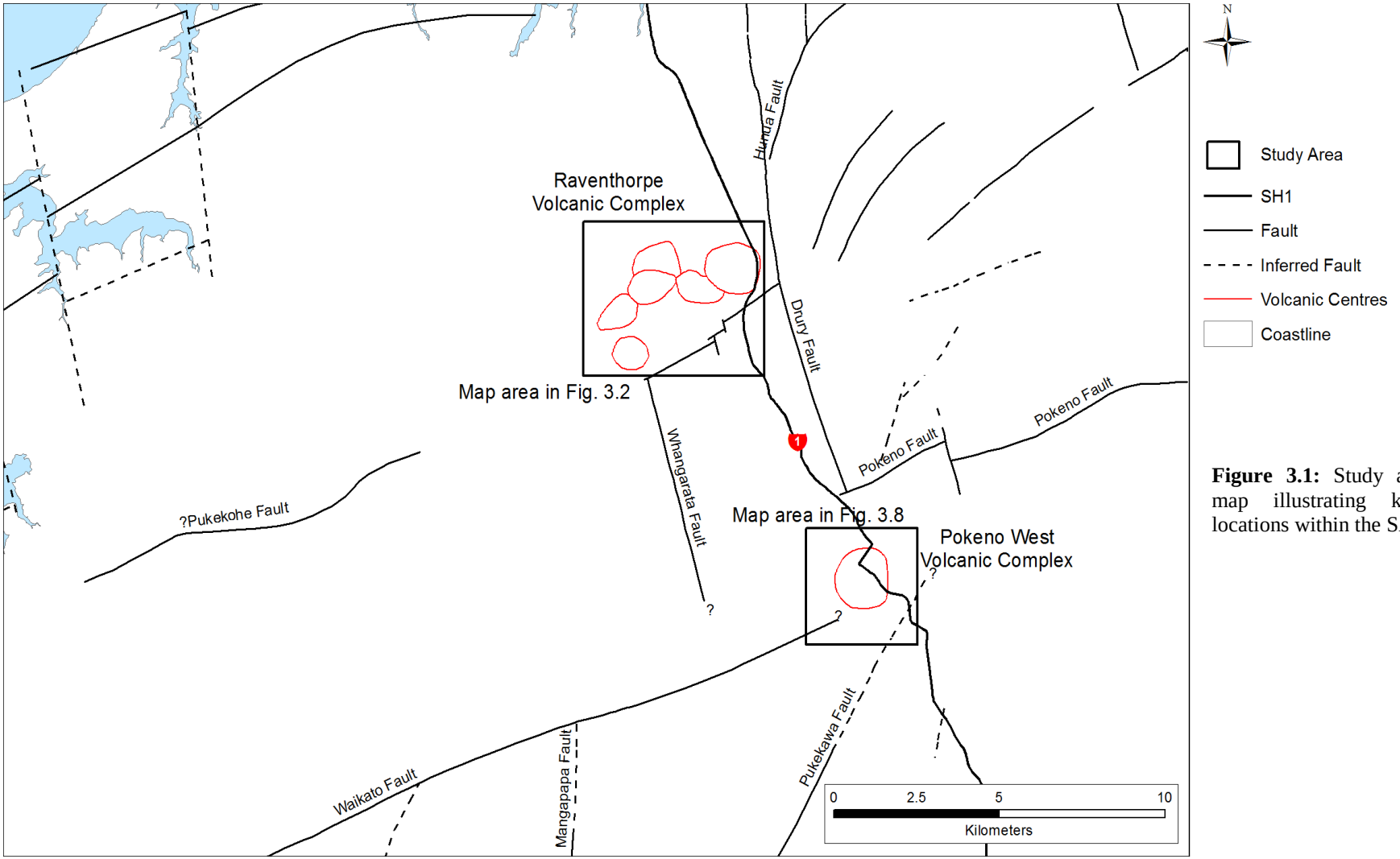


**Figure 3.1:** Study area location map illustrating known fault locations within the SAVF

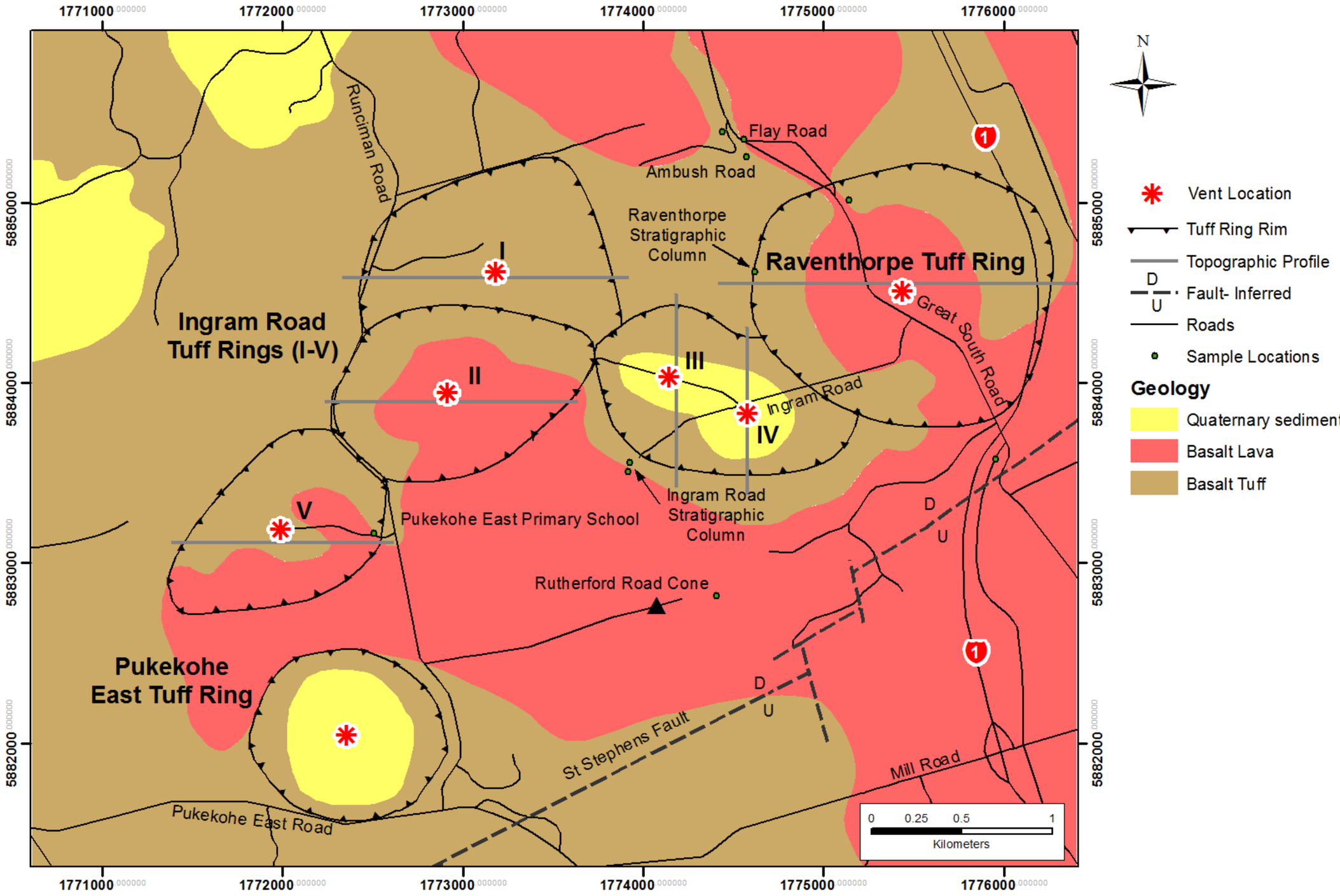


**Figure 3.2:** Map of the Raventhorpe volcanic complex, surrounding lava flows, faults, and the closely located Pukekohe East tuff ring.

volcanic complex. Several of the lava flows outcropping in the surrounding area, and at the complex have been sampled to attempt correlation between distant locations. Several lava flows to the east of Raventhorpe tuff ring outcrop with thicknesses >4 m. West of the Raventhorpe tuff ring the lavas are more weathered and occur commonly as boulder fields with exposures rare. There are no exposures of any country rock in the study area or its immediate surrounds.

The thicknesses and diameters of the tuff ring centres at the Raventhorpe volcanic complex are presented in Table 3.1. Excavation widths and depths have been disregarded as determination of these is impossible to be done with any accuracy as Rosenberg (1991) described.

**Table 3.1:** Maximum vertical thickness, maximum diameter, and mean ring slope angle of the Raventhorpe and Ingram Road tuff rings. Calculated in ArcGIS from raster images and topographic profiles measured from the highest topographic point of the rim to the lowest internal topographic point (often assumed the vent in this study).

| Tuff Ring | Thickness (m) | Diameter (km) | Mean Angle (°) | |
|---|---|---|---|---|
| | | | Internal | External |
| Raventhorpe Tuff Ring | 50 | 1.7 | 9 | 7 |
| Ingram Road Tuff Ring I | 10 | 1.4 | 4 | 4 |
| Ingram Road Tuff Ring II | 22 | 1.3 | 4 | 3 |
| Ingram Road Tuff Ring III | 45 | 0.8 | 4 | 7 |
| Ingram Road Tuff Ring IV | 47 | 0.7 | 5 | 8 |
| Ingram Road Tuff Ring V | 46 | 1.3 | 8 | 8 |

### 3.2.1 Topographic Expression of the Raventhorpe Tuff Ring

The transect running west to east across the Raventhorpe tuff ring illustrates the preserved topographic expression of the volcanic centre (Fig. 3.3). The thickness, diameter and slope angles illustrated by the profiles presented in this chapter should be regarded as a minimum due to the effects of weathering and erosion over the last 0.5 Ma as such processes must have altered the original structures. The data are of use when comparing the effects of erosion and weathering over time, that is where such fields are analogous to presently active volcanic fields.

The steeply sloping western rim of the Raventhorpe tuff ring, where the single north-south trending 200 m wide outcrop is exposed, consists of a 50 m high tuff ring rim. To the east the rim is comparably much flatter (Fig. 3.4), consisting of a 30 m high rim on which State Highway One has been built and thus modified. The

rim to the north and south is eroded with few observable features. The tuff ring is however, circular, therefore the best orientation for a topographic profile is west to east.

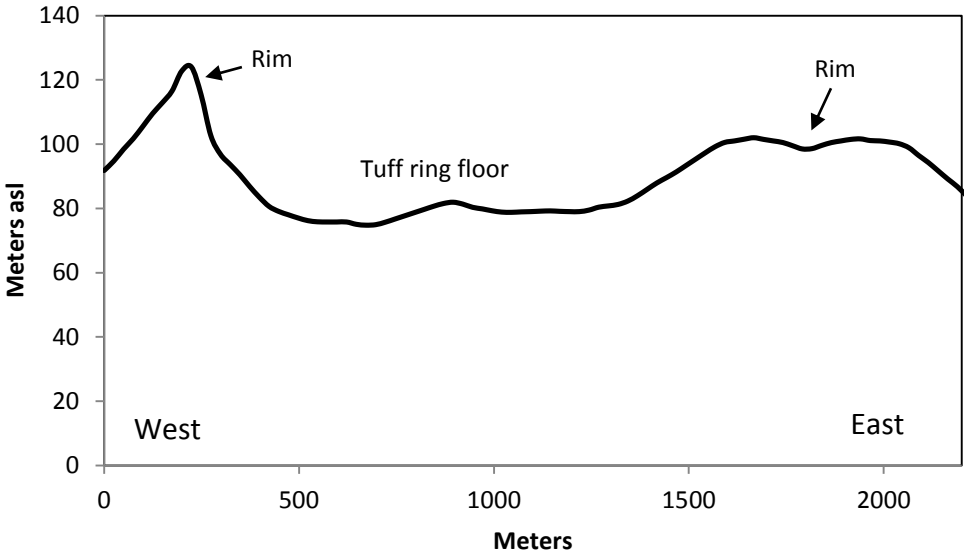


**Figure 3.3:** Topographic profile running from west to east over Raventhorpe. VE = 8.3.

**Figure 3.4**: Looking over to the eastern rim of the Raventhorpe tuff ring indicated by arrows on which the Hamilton-Auckland Motorway (SH1) passes across. The houses in the centre are located near the vent.

### 3.2.2 Topographic Expression of the Ingram Road Tuff Rings

Transects of each tuff ring are displayed in Figure 3.5 with the rims of the tuff rings marked by an arrow. The Ingram Road tuff rings are overall poorly exposed at both small and large scales as they are substantially weathered and eroded. Only a single outcrop of Ingram Road tuff ring III was located to sample. The profiles through these tuffs show a general concave trend, although in some instances the rims are hard if not impossible to distinguish.

Ingram Road tuff ring I has a very flat profile, running west to east. The western rim is most apparent with no clear expression of an eastern rim. Ingram Road tuff ring II shows a much more concave profile with high, well expressed rims. The vent location occurs at the topographic low, approximately half the diameter of the inferred rims. The lowest topographic point, and most central point were used as the basis for defining vent location. The profile of Ingram Road tuff ring III runs from north to south. The topographic expression shows a clear, 45 m high southern rim with a much lower rim evident to the north. This can be observed in the field (Fig. 3.6). Tuff ring IV also has a north-south topographic profile. Both rims are clearly expressed, although slightly less so to the north. The profile illustrates that ring IV is the highest of the Ingram Road tuff rings at 47 m. The last tuff ring, ring V runs from the west to the east. There is a steeply sloping rim on the eastern side with no observable features to the west. Tuff ring V, like tuff ring IV is also high, around 46 m.

The Ingram Road tuff rings are predominantly elliptical in shape (Fig. 3.2). Tuff ring I is squarely circular (rounded corners) with two relatively straight rims on the northern and eastern side (Fig. 3.2). Tuff ring II is strongly elliptical in an east-northeast orientation, overlapping tuff ring I (Fig. 3.2). Tuff rings III and IV are both circular, however there is no present day rim between the two to define each rings extent (Fig. 3.2); they are also the smallest of the five tuff rings. Tuff ring V connects to tuff ring II on the south eastern rim expressing an elongate morphology orientated northeast (Fig. 3.2).

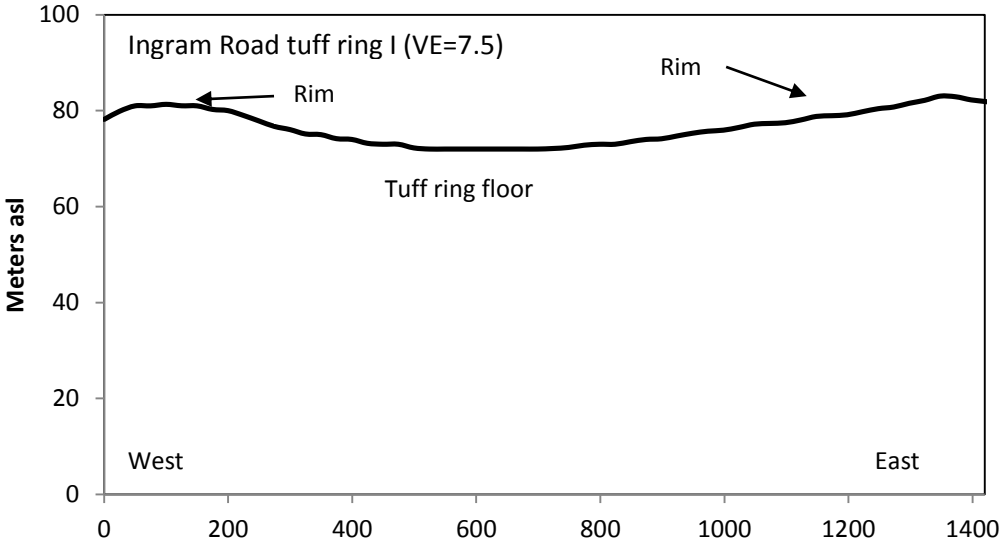
Ingram Road tuff ring I (VE=7.5)
Rim
Rim
Tuff ring floor
Meters asl
West
East
100
80
60
40
20
0
0
200
400
600
800
1000
1200
1400

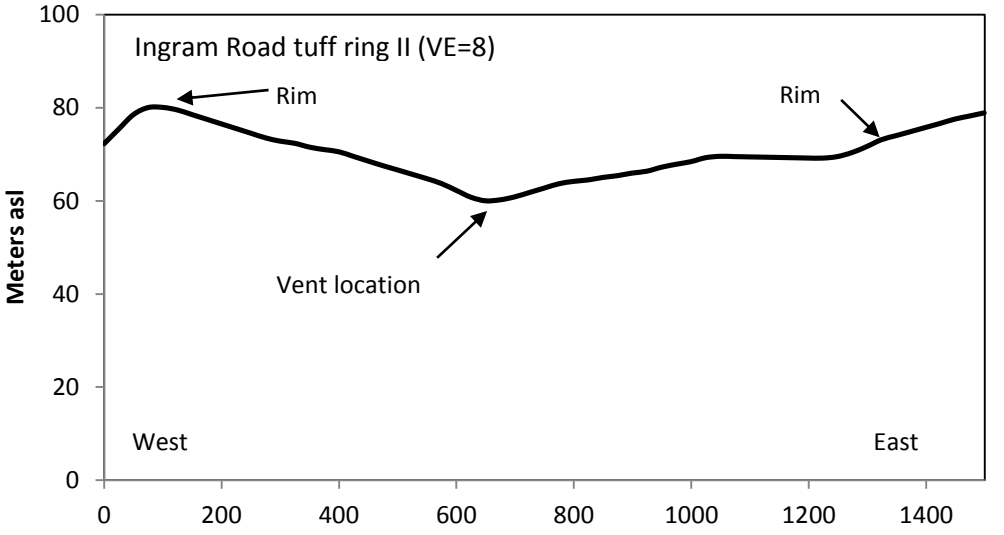
Ingram Road tuff ring II (VE=8)
Rim
Rim
Vent location
Meters asl
West
East
100
80
60
40
20
0
0
200
400
600
800
1000
1200
1400

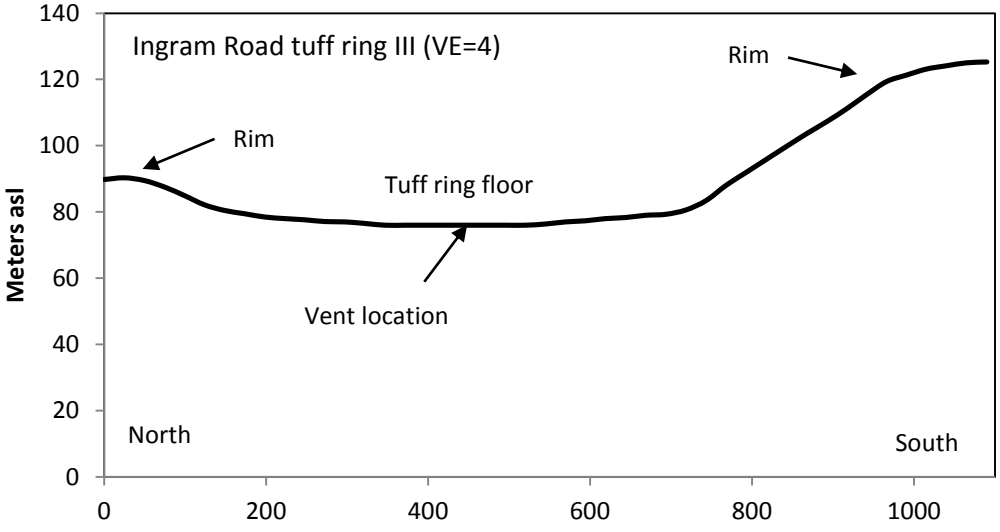
Ingram Road tuff ring III (VE=4)
Rim
Rim
Tuff ring floor
Vent location
Meters asl
North
South
140
120
100
80
60
40
20
0
0
200
400
600
800
1000

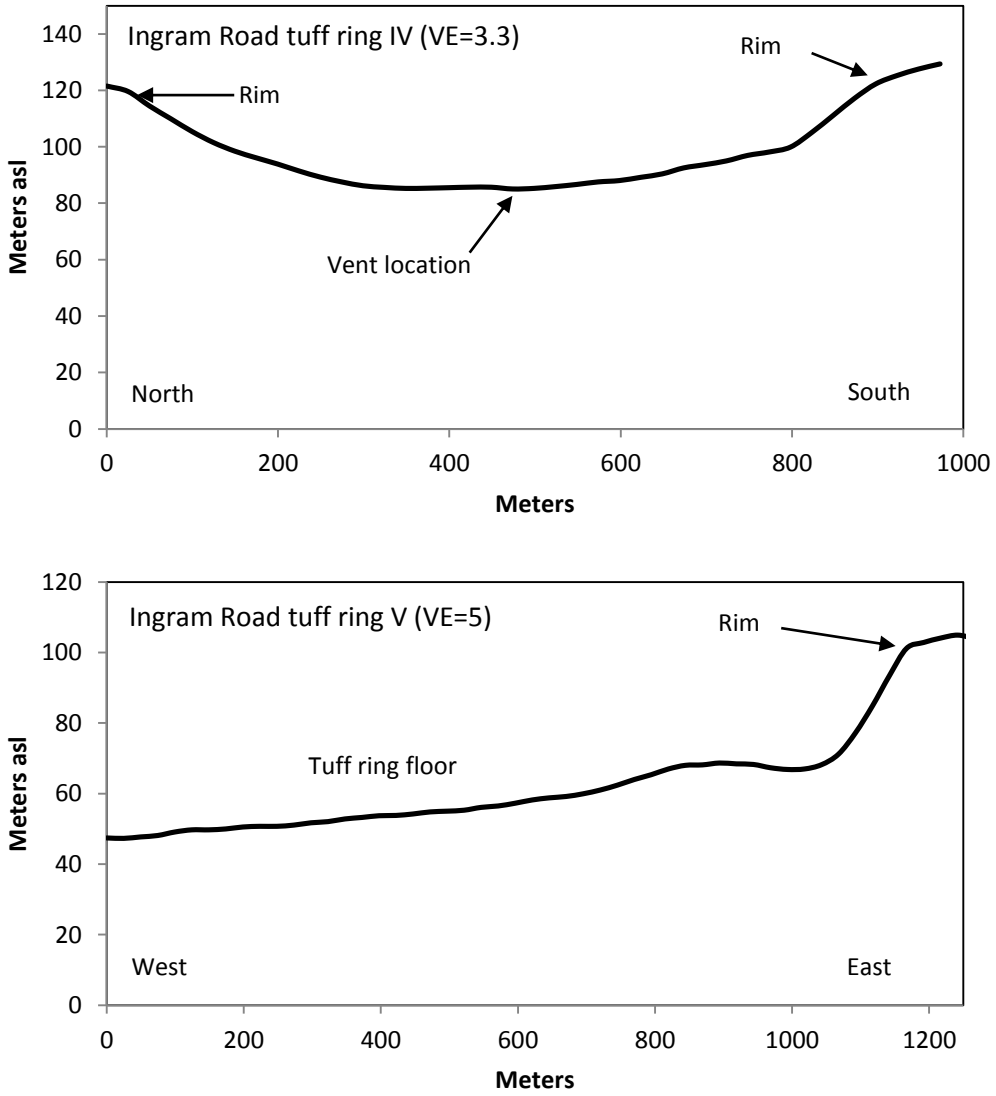


**Figure 3.5:** Topographic profiles of the Ingram Road tuff rings I-V with labels indicating the tuff ring rims, floor and vent location where apparent. Measurements are taken every 5 meters.

The most apparent feature occurring throughout the Ingram Road tuff ring cluster is the presence of thick rims to the south and south-east of the complex, regardless of the profile orientation. Towards the north and northwest there is very little evidence of the tuff ring rims. Where rims are present, thicknesses are at maximum, half that of what occurs to the south and southeast.


**Figure 3.6**: The rim of Ingram Road tuff ring III (A) looking north and (B) directly south. The locations of Raventhorpe tuff ring and Ingram Road tuff ring I have been labelled.

## 3.3 Pokeno West Volcanic Complex

The Pokeno West volcanic complex comprises a single tuff ring (Pokeno West) and magmatic cone (Bluff Road) and is better exposed than the Raventhorpe volcanic complex with three tuff ring outcrops and two boulder fields. All three outcrops are located on the southern and south-eastern rim of the tuff ring and range in stratigraphic thickness from 4 to 14 m. The exposures are predominantly highly indurated tuff that have maintained their structural features. One exposure only exists due to a large land-slip that occurred in 2008 (Fig. 3.7).

**Figure 3.7:** Current land surface after a slip removed much of the hill exposing the tuff to the east (left in picture) and the underlying thick ignimbrite sequence. Scale bar is ~5 vertical meters.

The Pokeno West tuff ring is located 10 km southeast of Pukekohe and 6 km south of the Bombay Hills. The ring has a diameter of 1.7 km and a thickness of 36 m in a predominantly circular morphology (Fig. 3.8). The Waikato Fault (Fig. 3.1) is located to the southwest, trending east-northeast along the orientation which the 0.65 Ma Bluff Road cone has erupted (Fig. 3.8). The Pukekawa Fault lies directly to the south of the complex and strikes northeast-southwest but is concealed (Figs. 3.1, 8).

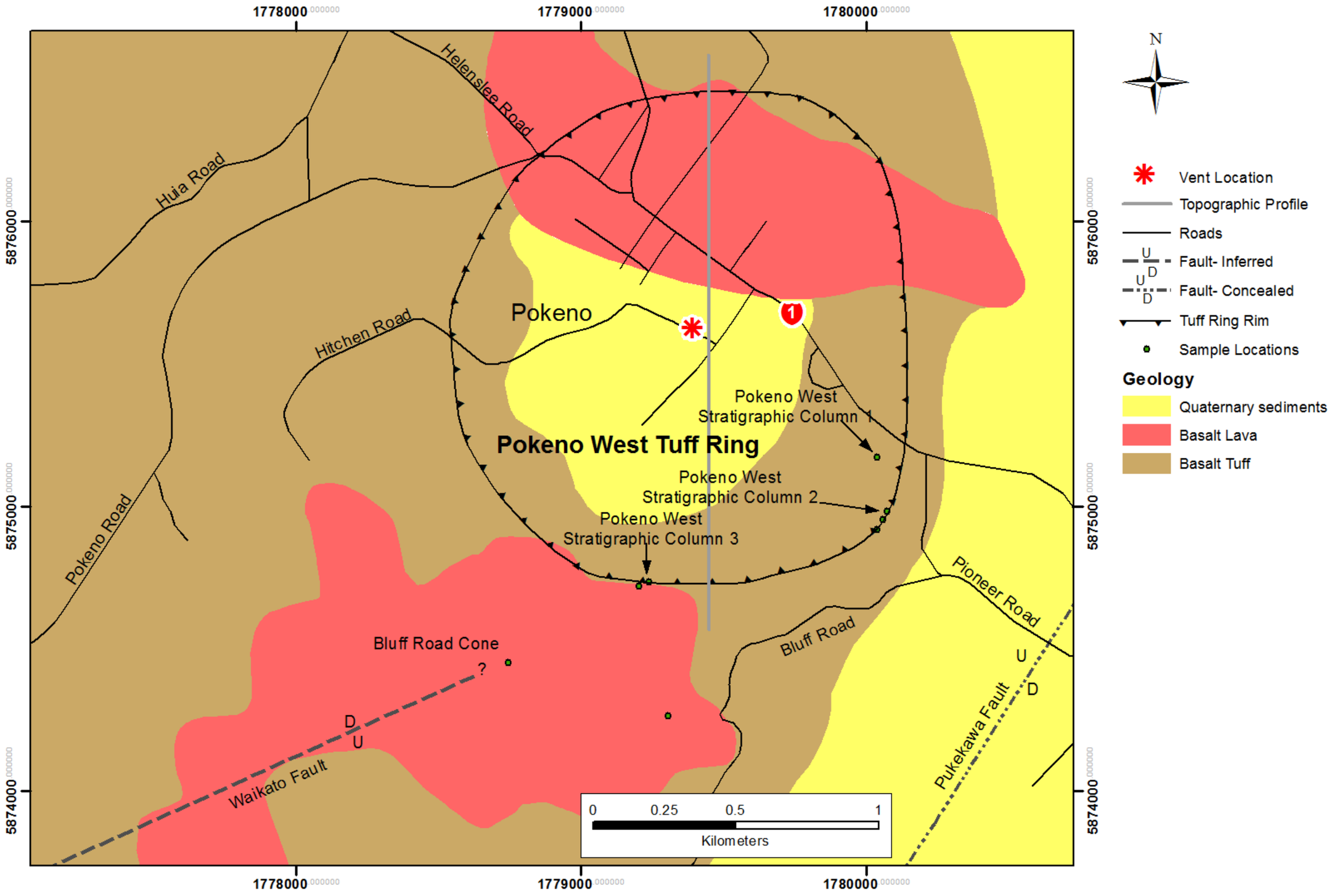


**Figure 3.8:** Map of the Pokeno West volcanic complex, the surrounding lava flows, and the Waikato and Pukekawa faults.

Similar to the Raventhorpe volcanic complex there are no exposures of country rock in the Pokeno West volcanic complex, except for a very fine-grained ignimbrite which occurs in the field area of the Pokeno West tuff ring. The ignimbrite is known to be the Kidnappers Ignimbrite (V. Moon pers. com. Nov. 11, 2010) and lies below the tuff ring sequence with contacts clearly evident in the field (Figs. 3.7, 9). The 1.0 Ma Kidnappers Ignimbrite erupted from the TVZ and has been correlated for >385 km from source representing the most widespread ignimbrite known (Wilson *et al.*, 1995). The thickness of the ignimbrite exposed in this area is at least 9 m, but the base was not observed. Correlation of the Kidnappers Ignimbrite across the landscape is made extremely difficult as it is overlain by basaltic tuff and lava, and Quaternary deposits. The contact however allows for a stratigraphic age constraint on the eruption of the Pokeno West tuff ring.

**Figure 3.9:** Contact between the soft, fine grained Kidnappers Ignimbrite and the overlying Pokeno West tuff ring sequence. Tuff beds are dipping at 19° into the tuff ring. Scale bar is 2 vertical meters.

### 3.3.1 Topographic Expression of Pokeno West Tuff Ring

The topographic transect across the Pokeno West tuff ring presents two apparent rims to the south and to the north (Fig. 3.10). The tuff ring diameter is ~1.7 km with the thickest succession occurring along the southern rim with a maximum thickness of ~60 m. Few other structural rim features exist, all occurring to the southwest with low angle slopes and thin successions. The three exposures sampled all occurred between the southeast and southwest rim.

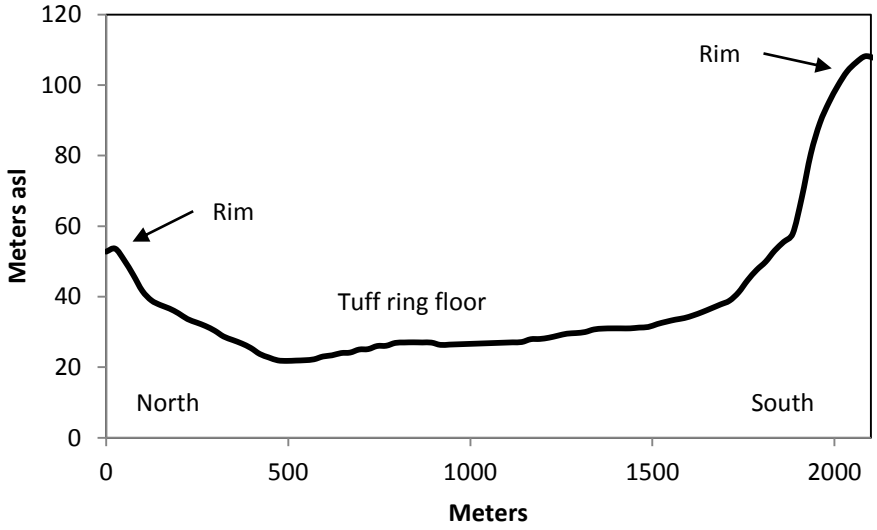


**Figure 3.10:** Topographic profile running south to north over Pokeno West tuff ring. VE=10.

## 3.4 Facies and Stratigraphy

Rosenberg (1991) employed a facies concept to document the characteristics of distinctive recurring associations in the stratigraphic successions observed throughout the SAVF. This concept was adopted for this study as a methodical approach to record the characteristics and changes in eruptive style of the successions observed throughout the two complexes.

The tuffaceous succession was divided into units comprising several similar beds or individual beds containing uniform distinctive features. The parameters used to classify the facies types included (1) grainsize, (2) physical components (field and petrographical observation), (3) degree of sorting, and (4) bedding structures.

These aspects of the componentry, and textural, and structural properties provide data to interpret eruption dynamics and style.

### 3.4.1 Raventhorpe Volcanic Complex

The stratigraphic sequence observed at the Raventhorpe volcanic complex can be divided into five facies within the 11 m thick succession (Fig. 3.11):

(1) facies one is a laminated to thinly bedded, well sorted, coarse ash to fine lapilli unit, which occurs from 0-0.7 m and again at 5.5-10.2 m;
(2) facies two occurs at 0.7-1.1 m, and is a wavy bedded, moderately to well sorted, coarse ash to fine lapilli;
(3) facies three is a massive, poorly to moderately sorted, medium lapilli and block and bomb bed, which occurs from 1.1-1.4 m;
(4) facies four occurs from 1.4-2 m and repeats again from 3.65-5.5 m. It comprises a planar bedded, moderately sorted, coarse ash to coarse lapilli, and occurs both above and below facies five; and
(5) facies five consisting of a crudely bedded, moderately to poorly sorted, medium ash to medium lapilli from 2.0-3.65 m.

The exposure of the Raventhorpe tuff ring shows much variation within the deposit throughout the 10 m sequence (Fig. 3.11). Facies one through five successively comprise the lower 3 m of the deposit, reverting to facies four over the following 2 m, before facies one comprises the final 5 m (Fig. 3.11). Finer grained ash units dominate the middle and upper sections while the blocks and bombs only occur in the lower to middle section of the stratigraphic column. The observable trend shows a decrease in grainsize with an increase in stratigraphic height (Fig. 3.11). Vesicularity values show a large range from 2-40% (Fig. 3.11). The data show a decreasing trend (mean vesicularity) with increasing stratigraphic height, except for a slight increase measured at one sample location in the middle of the exposure. Componentry data have been divided into two groups: juvenile components, i.e. basalt clasts and crystals; and accessory or accidental components, i.e. lithics and xenocrysts. The juvenile components dominate, comprising 20-55% of the tuff with juvenile basalt clasts ranging from 10-50% of that. The accidental/accessory components comprise a maximum of 11%, with sedimentary lithics more common than igneous lithics or xenocrysts, and are discussed in chapter 4.

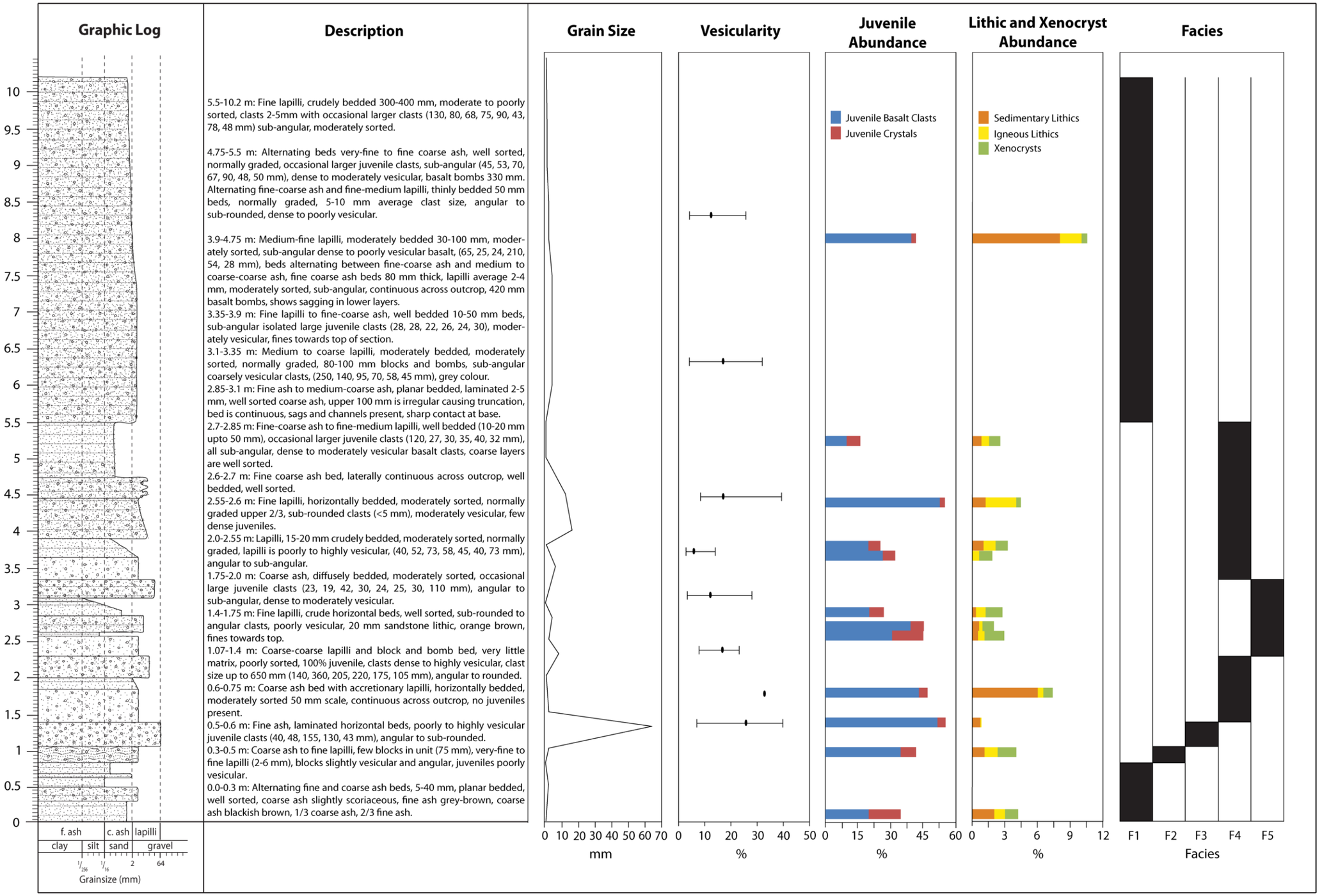


**Figure 3.11:** Stratigraphic variation of the of the Raventhorpe tuff ring. Data presented from left to right includes grainsize, vesicularity, juvenile abundance, lithic and xenocryst abundance, and facies occurrence.

### 3.4.2 Facies

## Facies One - Laminated to thinly bedded, well sorted, coarse ash to fine lapilli

Facies one (Fig. 3.12) consists of planar beds dominated by coarse ash with few lapilli present (maximum clast, Mc: 48 mm) and very occasional blocks (maximum block, Mb: 155 mm), especially in the upper section of the facies. The beds alternate on a fine scale of 5-30 mm but can be as thick as 50 mm in the lower section. Occasionally pinch and swell bedforms are observed, however these are not cross bedded. Fine to coarse ash dominates all layers including the fine lapilli layers (abundance 20-39 %). The coarser beds, although few, are generally continuous across the outcrop. Juvenile lapilli clasts are predominantly angular but also occur as blocky clasts, ranging in vesicularity from poorly vesicular to highly vesicular based on descriptions taken in the field. Of note, a thin layer of accretionary lapilli was encountered in the lower section of this facies and these ranged in size from 2-3 mm. No ballistics were encountered. Lithics were not observed or recorded throughout any of the section in the field but were noted in hand specimen and as ash sized fragments in thin section (abundance 5-16 %).


**Figure 3.12:** Sample of Raventhorpe tuff ring facies one deposits with few fine lapilli and very fine lithics within planar bedded coarse ash.

## Facies Two - Wavy bedded, moderately to well sorted, coarse ash to fine lapilli

Facies two consists of a coarse ash dominated, wavy bedded unit (Fig. 3.13) with few fine lapilli present (Mc: 50 mm; abundance ~20 %). Cross bedding is present, as is truncation of the beds from pinch and swell layering. The unit is continuous across the outcrop. The larger juvenile scoria clasts are poorly to moderately vesicular, commonly sub-angular with others sub-rounded. Many ballistic bombsags are present in the upper section of the unit and have been derived from facies three so have not been included in this description. There is no field evidence for any lithics present, but they are known to occur in thin section (abundance ~4 %). Sorting is variable throughout the unit ranging from moderate, which dominates, to well sorted within the thinly bedded layers. Channel features and slumps are visible throughout the unit's exposure.

**Figure 3.13:** Example of facies two as seen in the field.

## Facies Three - Massive, Poorly to moderately sorted, medium lapilli to block and bomb bed

Facies three is a massive coarse block and bomb layer that comprises a large range of grainsizes (Fig. 3.14). There is very little matrix in the unit with the dominant grainsize being a very coarse lapilli (Mc: 64 mm) with many larger blocks and bombs present (Mb: 650 mm) (Fig. 3.15). The unit is almost 100% juvenile. Lapilli and blocks and bombs range from non-vesicular to highly vesicular (Fig. 3.15) with sub-rounded and sub-angular clasts most common. Lithics are uncommon (abundance ~ 1%) and are predominantly fine lapilli size (Maximum lithic, Ml: 3 mm). They are light grey to cream coloured, siltstones

and mudstones. The unit is continuous across the outcrop and is stratigraphically higher to the south than at the north indicating the dipping nature of the outcrop. The maximum angle of dip is 12°.

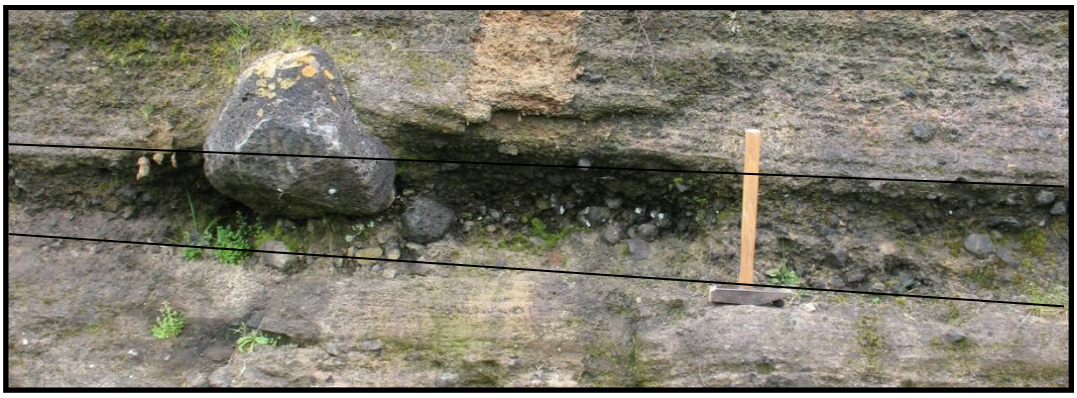

**Figure 3.14:** Facies three as observed in the field. Note the large range of clast sizes.

**Figure 3.15:** The largest recorded basalt bomb from facies three measuring 650 mm. Note the abundance of vesicles.

## Facies Four - Planar bedded, moderately sorted, coarse ash to coarse lapilli

Facies four is a coarse ash to coarse lapilli dominated unit, although coarse ash is slightly more common, and comprises many different grainsize classes (Fig. 3.16). The moderate degree of sorting throughout this horizontally bedded unit helps to distinguish it from other facies along with the presence of normal grading. The unit occurs within the final six meters of the tuff succession and is therefore exposed as horizontal beds perpendicular to the vent. The unit is continuous across the exposed section. Coarse ash dominates the upper layers while the larger

lapilli clasts (Mc: 42 mm) and rare blocks (Mb: 420 mm) are more common in the lower sections. Commonly the larger bombs show sagging into the ash layers below, with the bedform layering maintaining its features. There is no cross bedding but some truncation of thin ash beds does occur. Lapilli are sub-rounded to sub-angular as is common at Raventhorpe and range in abundance from 9-52 %. The vesicularity of juvenile clasts when observed in the field ranges from poor to highly vesicular with the former more common. Medium lapilli-sized lithics were observed as orange-brown sandstones (Ml: 20 mm). Lithics are also present in thin section with abundance ranging from 1-7 %. Sags and channels are present in some ash units within the facies sequence.

**Figure 3.16:** Hand specimen of facies four with common fine lapilli within in an ash matrix. The unit is coarser at the base and is normally graded.

## Facies Five - Crudely bedded, moderately to poorly sorted, medium ash to medium lapilli

Facies five ranges from medium ash to medium lapilli size grains and clasts with coarse ash dominating. The bedding structures are crudely horizontal (Fig. 3.17) due to the position in the final meters of the tuff ring succession in which they occur. There are occasional standalone laminated beds present. Beds are generally poorly sorted with few exceptions occurring over very small tens of millimetres scale. The boundaries of the beds are generally diffuse and gradational with some showing normal grading. There are no cross beds evident. Lapilli clasts commonly show a large size (Mc: 58 mm) and abundance (A: 20-40 %) range throughout the entire section of the facies. Occasional blocks and bombs are also

present (Mb: 360 mm) (Fig. 3.18). The juvenile pyroclasts are commonly very vesicular with few slightly vesicular, and are predominantly sub-angular with few sub-rounded clasts. Lithics are observed as cream coloured siltstones and yellow-brown sandstones (Ml: 15 mm). The unit can be observed across the entire exposure.


**Figure 3.17:** Example of facies five as it appears in the tuff sequence at Raventhorpe.

**Figure 3.18:** Large bombsag into facies four from facies five. Note the difference between the two basalt bombs in terms of vesicularity.

### 3.4.3 Ingram Road Tuff Ring III

The stratigraphic sequence of the Ingram Road tuff ring III can be divided into two facies units within the 4.8 m thick exposure.

(1) Facies one is similar to facies one at Raventhorpe and is a laminated to thinly bedded, moderately to well sorted, coarse ash to medium lapilli, occurring from 0-1.6 m and recurring from 3.2-4.8 m.
(2) Facies two comprises a graded, planar bedded, well sorted, coarse ash to fine lapilli unit that has been divided into two sub-facies occurring from 1.6-3.2 m:
    (a) facies 2.1 which is a normally graded unit occurring from 1.6-2.2 m; and
    (b) facies 2.2, a reversely graded unit from 2.2-3.2 m.

The sampled outcrop of the Ingram Road tuff ring III shows wide variation within the deposit throughout the short 4.8 m sequence (Fig. 3.19). Facies one through facies 2.2 comprise the lower 3 m, with the final 1.8 m of the section comprising facies one (Fig. 3.19). Variations in grainsize are observable with fine to medium ash dominating the record. Fine lapilli only occur through the middle and upper sections of the stratigraphy. As the sequence is short, the general trend is of a fine grainsize that may be increasing slightly towards the top of the section, but this is difficult to confirm because of the poor exposure. As there were very few lapilli, and those present were very fine, no vesicularity measurements were able to be made. Juveniles dominate the componentry with an abundance of 8-55%. The juvenile basaltic clasts further dominate this ranging from 5-50% abundance. Accessory igneous lithics are more common (abundance 0-9%) than sedimentary lithics or xenocrysts. The overall accidental/accessory components of the Ingram Road tuff ring III tuff ranges from 2-11% with the higher abundances occurring in the upper sections where the grainsize increases.

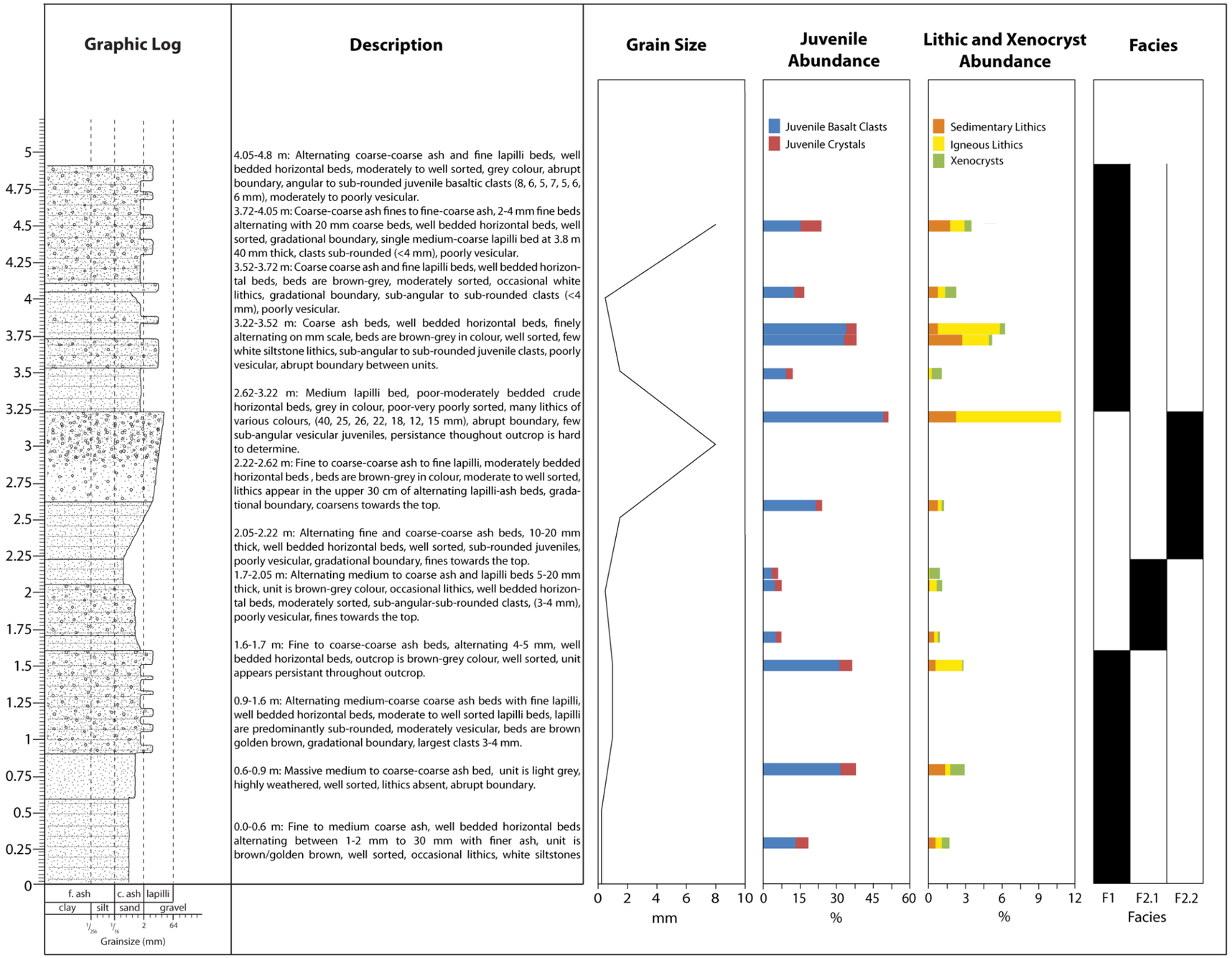


**Figure 3.19:** Stratigraphic variation of the of the Ingram Road tuff ring III. Data presented from left to right includes grainsize, juvenile abundance, lithic and xenocryst abundance, and facies occurrence.

### 3.4.4 Facies

## Facies One - Laminated to thinly bedded, moderately to well sorted, coarse ash to medium lapilli

Facies one consists of planar beds dominated by coarse ash with few lapilli present (Mc: 5 mm) (Fig. 3.20). The beds alternate on a thickness of 5-25 mm but can be as thick as 40 mm in the upper 1.6 m of section. Some ash beds are truncated and pinch out, while the lapilli-rich bed sets appear more continuous across the outcrop, although their greater extent is hard to gauge as the exposure is poor. Very fine lapilli are present in thin section with an abundance ranging from 8-30 %. There were no ballistics observed. Lapilli range from sub-angular to sub-rounded and from poor to incipiently vesicular. Accretionary lapilli were absent. Lithic abundance ranges from 1-10%, averaging 4 mm with a maximum of 7 mm. Lithics were most commonly a white-cream siltstone. Yellow sandstones were present, but less common.


**Figure 3.20:** Facies one at Ingram Road tuff ring III.

## Facies 2.1 - Normally graded, planar bedded, well sorted, coarse ash to fine lapilli

Facies 2.1 consists of planar bedded coarse ash and fine lapilli, well sorted and normally graded (Fig. 3.21). Similar to facies one, the persistence of the facies is difficult to determine due to the limited exposure. The ash beds generally alternate similar to facies one on a scale of 4-20 mm. Medium ash is most common and

dominates the section, with fewer lapilli layers (Mc: 4 mm) occurring at the base of units. The normally graded, moderately sorted ash and lapilli beds present at the base of a unit fine upwards to thinner, well sorted, planar bedded, coarse ash bedforms. This sequence of normal grading is repeatable over the 0.8 m thickness of the facies. Lapilli abundances range from 3-28 %. Juvenile clasts range from sub-angular to sub-rounded and are moderately vesicular. No ballistics were observed. Accretionary lapilli are present throughout a 100 mm thick section as seen in Fig. 3.21. Lithics are present (Ml: 6 mm) although rare (Al: 0-4 %), and occur as white-cream siltstones. Juvenile crystal abundance ranges from 2-5 % and is dominantly fine grained.

**Figure 3.21:** Example of facies 2.1 in hand specimen showing accretionary lapilli and white siltstone lithics amongst a coarse ash matrix. Due to size of the sample the grading cannot be observed. Scale bar is 2 cm.

## Facies 2.2 - Reversely graded, planar bedded, well sorted, coarse ash to fine lapilli

Similar to facies one and facies 2.1, facies 2.2 differs due to the presence of reverse grading (Fig. 3.22). The facies is planar bedded consisting of coarse ash which dominates and fine lapilli clasts (Mc: 10 mm). No truncation of bedforms or pinching and swelling of beds were observed. Cross bedding is absent. The facies is generally well sorted but reversely graded, coarsening towards the top of each bed. Fine coarse ash coarsens to moderately sorted fine or medium lapilli. Juvenile basalt clasts are moderately vesicular and sub-rounded with abundances

ranging from 19-43 %. Few accretionary lapilli were present in this unit, however no ballistics occurred throughout the facies. The coarser upper unit is primarily due to the increased lithic abundance 3-13 %, and increased lithic size (Ml: 40 mm), where many lithics of various colours are present. These accessory lithics are: igneous lithics consisting of closely related juvenile basalt, differentiated by the groundmass, and sedimentary lithics, a cream siltstone. Facies 2.1 has less juvenile crystal abundance than facies 2.2, ranging from 0.5-2 % and are fine grained (Fig. 3.19).

**Figure 3.22:** Facies 2.2 as seen in hand specimen showing accretionary lapilli and cream siltstones within an ash matrix, coarsening slightly towards the top. The presence of reverse grading can be observed from the finer planar beds at the base coarsening upwards. Scale bar is 2 cm.

### 3.4.5 Pokeno West Volcanic Complex

Three stratigraphic columns (Figs 3.23, 24, 25) were recorded at the Pokeno West volcanic complex and the sequences observed can be classified into five facies units. Heights at which each facies occurs are not given here, however are discussed in a subsequent chapter.

(1) Facies one comprises laminated to thinly bedded, moderately to well sorted, coarse ash to medium lapilli, occurring commonly at all three column locations;
(2) facies two is a normally graded, planar bedded, moderately to well sorted, coarse ash to fine lapilli unit;
(3) facies three consists of a laminated to thinly bedded, moderately to well sorted, coarse ash and lapilli;
(4) facies four is a massive, poorly sorted, medium lapilli unit, and occurs most commonly as single bedforms; and

(5) facies five is a cross bedded, poorly to moderately sorted, coarse ash, which occurs only at one location.

The data collected at the three outcrops sampled at Pokeno West tuff ring are presented below. The first stratigraphic section (Fig. 3.23) is a 9 m thick succession with 4 m of missing exposure. The first section of the succession comprises facies one, and briefly facies two for the first 6 m (Fig. 3.23). Facies three and four briefly alternate with facies one for the following two meters (Fig. 3.23). The final meter of the succession comprises facies two and facies three (Fig. 3.23). The grainsize data is highly variable throughout. The juvenile abundance of basalt and crystals ranges from 10-55%, with basaltic clasts dominating. Juvenile crystal abundance reaches 6% (Fig. 3.23). Lithics and xenocrysts (up to 3%) are most abundant in the upper section of the sequence with sedimentary lithics comprising 9% total (Fig. 3.23). A single layer records the only accessory igneous lithic throughout the sequence at 1% total abundance (Fig. 3.23).

The second stratigraphic sequence sampled (Fig. 3.24) is a short 4 m section that was exposed during a landslip event in 2008. The succession starts with facies one exposed for the first half meter before facies three comprises the following meter (Fig. 3.24). The facies then successively decrease starting with thin occurrences of facies five, four, and three, before facies two comprises the following two meters (Fig. 3.24). The final 20 cm comprises facies one. The grainsize data indicates that the sequence is coarsening upwards. Juvenile components are low when compared to all other locations at Pokeno West tuff ring, with a maximum of 38% total abundance with juvenile basalt up to 36% and juvenile crystals up to 5% throughout the entire sequence. Sedimentary lithics dominate the lithic component with abundances up to 7.5%. Accessory igneous lithic abundance is recorded at 0.3% and was found in a single sample.

The third stratigraphic sequence (Fig. 3.25) is the highest exposure at 14 m with 3 m missing. The facies associations at this location are complex. Facies one, four, and then three comprise the first 1.5 m of the succession before facies one and two alternate, comprising the lower 6 m (Fig. 3.25). Facies three then dominates the following 3 m, with 3 m of missing section (Fig. 3.25). The final two meters consist of facies four and facies one (Fig. 3.25). The grainsize data shows a general fining upwards with two much coarser sections within the stratigraphy at

6 m and 12.5 m. The vesicularity data shows no trend with values ranging between 10-56% with means between 15-30%. Abundance of juvenile components ranges from 20-62% with juvenile basalt most common. Abundance of sedimentary lithics is at maximum 6.5%, with igneous lithics more common ranging up to 4% and occurring in 9 of 13 samples analysed. Xenocrysts are present in all but one sample.

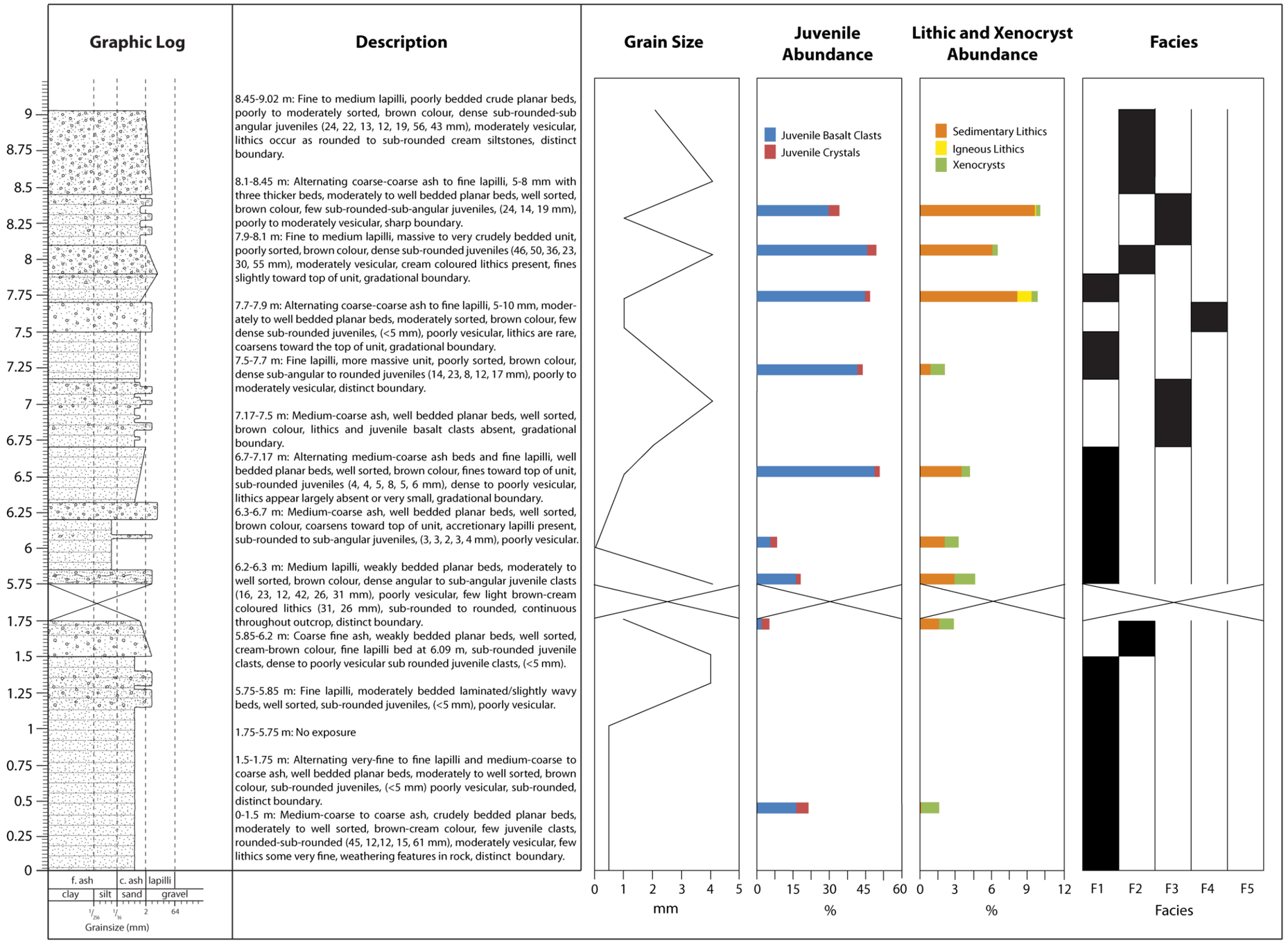


**Figure 3.23:** Stratigraphic variation of the Pokeno West tuff ring at location one. Data presented from left to right includes grainsize, juvenile abundance, lithic and xenocryst abundance, and facies occurrence.

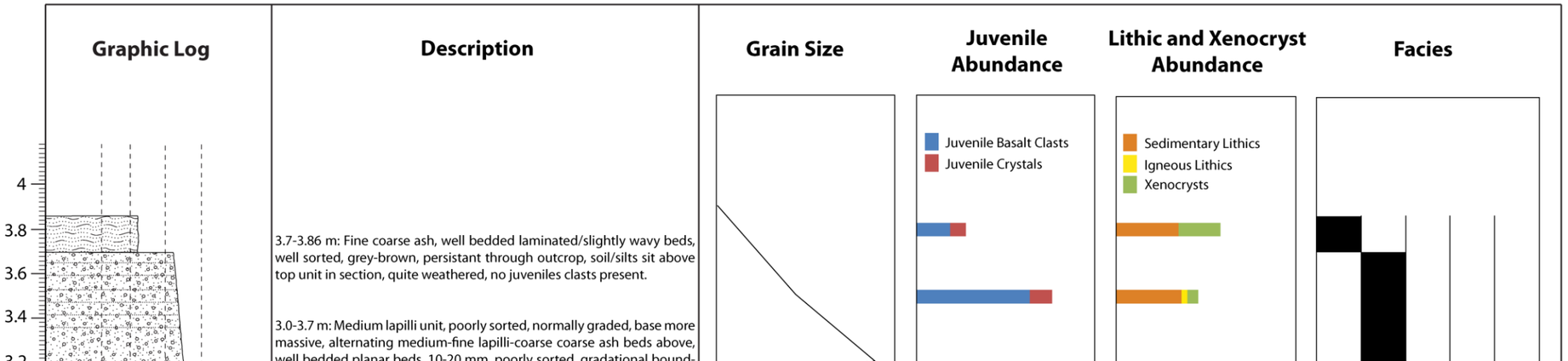


**Figure 3.24:** Stratigraphic variation of the Pokeno West tuff ring at location two. Data presented from left to right includes grainsize, juvenile abundance, lithic and xenocryst abundance, and facies occurrence.

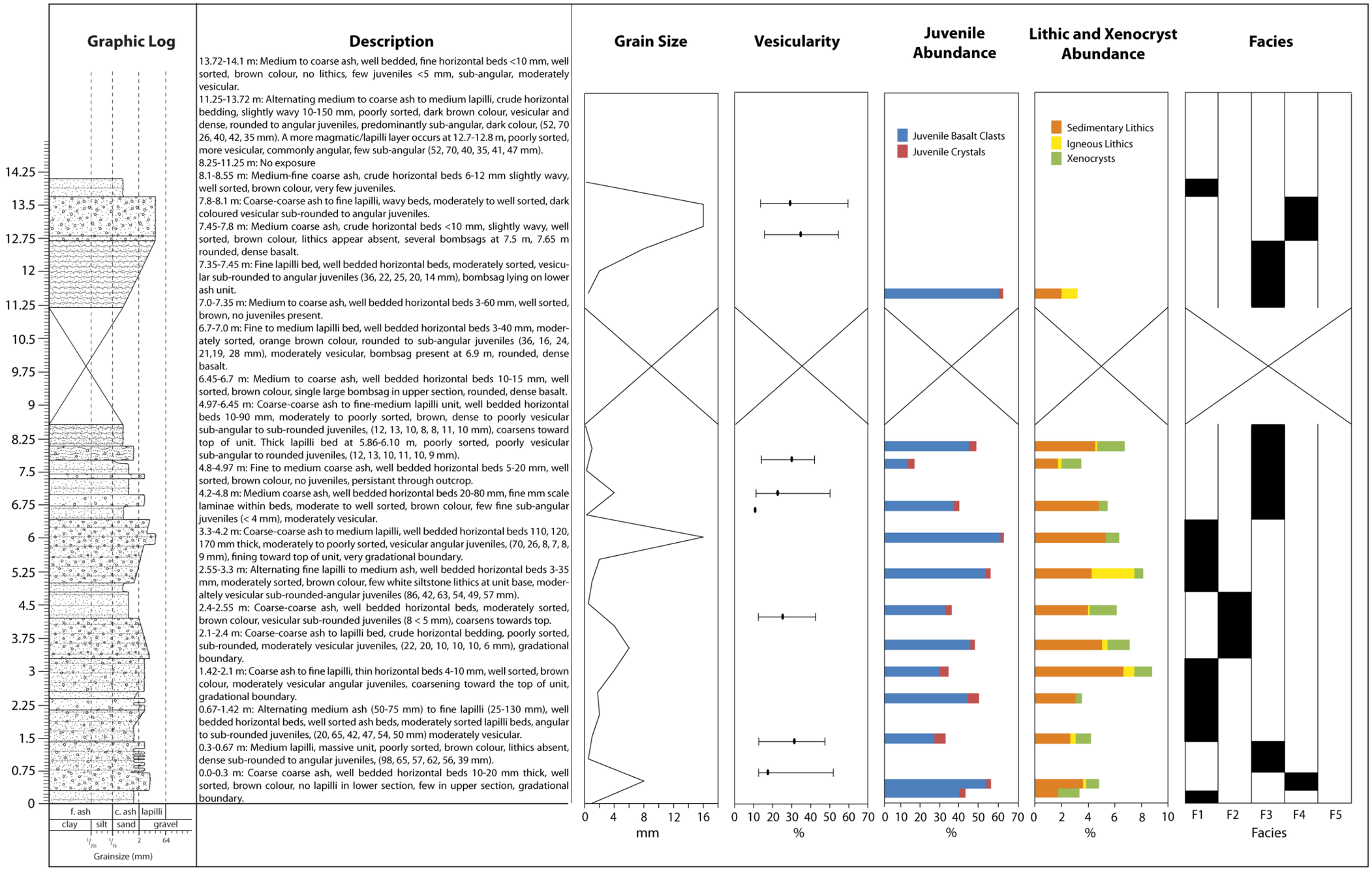


**Figure 3.25:** Stratigraphic variation of the Pokeno West tuff ring at location three. Data presented from left to right includes grainsize, juvenile abundance, lithic and xenocryst abundance, and facies occurrence.

### 3.4.6 Facies

Facies One – Laminated to thinly bedded, moderately to well sorted, coarse ash to medium lapilli

Facies one consists of planar laminated beds dominated by coarse ash, less common lapilli (abundance 3-57 %) and very occasional blocks and bombs ($Mb^3$*: 98 mm), sometimes with bombsags (Fig. 3.26). There were no cross beds present at any location, however some pinching out of bedforms were observed. Facies one is most common in all three columns with persistence sometimes difficult to determine at each location, however is generally continuous. It is dominated by ash packages which are generally better sorted and laminated than the finely planar bedded lapilli. Juvenile lapilli clasts ($Mc^1$: 61 mm; $Mc^3$: 62 mm) are predominantly angular but range from sub-angular to sub-rounded. They are commonly moderate to highly vesicular, especially at location three where highly vesicular juveniles dominate. There were no noticeable lithics observed or recorded at location two, however did occur as ash sized fragments in thin section with an overall abundance in between 0-16 %. White-cream siltstones and light sandstones were observed in the outcrop at locations one and three ($Ml^1$: 31 mm; $Ml^3$: 57 mm).


**Figure 3.26:** Field example of facies one showing laminated bedding of coarse ash lying beneath a massive layer with a ballistic bomb.

* Denotes stratigraphic column location

## Facies Two - Normally graded, planar bedded, moderately to well sorted, fine lapilli to coarse ash

Facies two is planar bedded (sometimes crudely) comprising of moderately to poorly sorted fine lapilli ($Mc^1$: 55 mm; $Mc^2$: 36 mm; $Mc^3$: 26 mm) which often grades into a coarse ash (Fig. 3.27). Some layers truncate and display a lensoidal character. Cross bedding is absent. Small basalt blocks and bombs ($Mb^2$: 142 mm; $Mb^3$: 70 mm) are present with some of the larger occurring as bombsags over the planar beds (Fig. 3.26). Lapilli range from rounded to angular, but are most commonly sub-angular. Juvenile basalt abundance ranges from 1-42 % while vesicularity of basaltic juveniles ranges from dense non-vesicular to highly vesicular basalt, with a more intermediate vesicularity most common. Lithics ($Ml^2$: 31 mm; $Ml^3$: 86 mm; 3-16 %) were observed at two of the sample locations, but have been observed in all thin sections. Lithics observed in the outcrop were a white siltstone and are most likely Waitemata Group. Accessory igneous lithics were present in thin section.

**Figure 3.27:** Facies two; moderately sorted fine lapilli beds grading into well sorted, planar bedded, coarse ash layers within a coarse ash matrix. Few lithics are observable grey siltstones. Scale bar is 2 cm.

## Facies Three - Laminated to thinly bedded, moderately to well sorted, coarse ash and lapilli

The third facies is the second most common facies unit after facies one. It comprises planar bedded alternating coarse ash and lapilli, moderately to well sorted (Fig. 3.28). Cross beds and wavy bedforms are absent. Medium-coarse and coarse-coarse ash dominates the facies, occasionally alternating with fine lapilli beds ($Mc^1$: 8 mm; $Mc^2$: 5 mm; $Mc^3$: 54 mm). The coarser, fine lapilli layers are generally continuous across the outcrop at locations one and three. Lapilli range from rounded to angular with sub-rounded most common. Abundance ranged from 12-44 %. Juvenile basalt clasts were occasionally non-vesicular or poorly vesicular, with the majority moderately vesicular. Many juvenile clasts were highly weathered and fractured into many smaller pieces when removed from the outcrop. Ballistic blocks and bombs are mainly absent, except for some small occasional bombsags at one location. Similarly lithics were unusually absent in the field from all locations throughout this facies. However, they were observed in thin sections (abundance: 4-42 %) as accessory igneous lithics and small siltstones and sandstones, potentially derived from the underlying Waitemata Group.

**Figure 3.28:** Facies three; planar bedded ash and lapilli, with occasional bombs. Scale bar is 10 cm.

## Facies Four – Massive, poorly sorted, medium lapilli

Poorly sorted lapilli (Fig. 3.29) dominate this unit with a matrix of fine ash. The facies is massive with occasional thin, coarse planar beds. Coarse lapilli are common (abundance: 37-57 %) along with occasional slightly larger blocks and bombs. The juvenile lapilli ($Mc^1$: 23 mm; $Mc^2$: 6 mm; $Mc^3$: 52 mm) are dominantly sub-angular to angular and are generally denser than the larger more vesicular sub-rounded to rounded basalts. Blocks and bombs ($Mb^1$: 102 mm; $Mb^3$: 114 mm) are present as dense basalt and are most abundant at location three where the outcrop is best exposed. Lithics are absent but have been observed in thin section as both accessory sedimentary and cognate lithics (Abundance: 2-3 %). The facies is stratigraphically continuous across the outcrop when present.


**Figure 3.29:** Facies four, moderately to poorly sorted, massive, fine to medium lapilli with a fine ash matrix.

## Facies Five - Cross bedded, poorly to moderately sorted, coarse ash

Facies five occurs only at one location (stratigraphic column two, Fig. 3.24) over a total thickness of 24 cm. The presence of cross bedded ash that can be traced across the outcrop and pinches out to lensoidal layers is unique when compared to the overall planar bedded and occasionally massive nature of the sequences

observed at the three locations (Fig. 3.8). The facies comprises a coarse ash with fine lapilli ($Mc^2$: 4 mm) poorly sorted in the lower section with better sorting towards the top of the sequence. Coarse ash dominates overall abundance. The juvenile basalt abundance is ~7 % with the majority of these sub-rounded to rounded, and of moderate vesicularity. Ballistics were absent from the facies. No lithic clasts were observable in the field but had a similar abundance to the juvenile basalt of ~7 % in thin section.

# Chapter Four

# Petrography

## 4.1 Introduction

This chapter describes the petrography of the pyroclastic deposits within the two study areas. Individual pyroclasts, lava and tuff were sampled throughout the two locations and were examined in thin section. Distinction between A (subalkalic, low, high field strength element (HFSE) abundances) and B (alkalic, high HFSE abundances) group basalts are based on bulk geochemical analyses and defined for each rock type. Classifications are based on CIPW normative compositions (see appendix 2), according to the classification scheme used by Cook (2002). Petrography of the tuff and its components: matrix, crystals, and lithic material are described separately and have been compiled from representative samples and modal analysis (see appendix 3).

Throughout this chapter terminology such as fine and coarse grained is used. This implies grainsize divisions of phenocrysts within the fine grained basalts. Microphenocrysts and megacrysts are defined as notably smaller and larger in size respectively, relative to the size of the majority of phenocrysts. Vesicularity ranges are based on the classification by Houghton and Wilson (1989) (Table 4.1) (see appendix 4).

**Table 4.1:** Classification of vesiculation characteristics. From Houghton and Wilson (1989).

| % Vesicularity | Description |
|---|---|
| 0-5 | Non-vesicular |
| 5-20 | Incipiently vesicular |
| 20-40 | Poorly vesicular |
| 40-60 | Moderately vesicular |
| 60-80 | Highly vesicular |
| >80 | Extremely vesicular |

## 4.2 Basalt Lava - Group A

### 4.2.1 Alkali olivine-basalt

The alkali olivine-basalts of group A range from relatively coarse to fine grained and have porphyritic and glomeroporphyritic textures. All samples are non-vesicular, with typically 1-2% vesicles. They are commonly holocrystalline consisting of olivine, clinopyroxene, and plagioclase phenocrysts.

#### Phenocrysts

Olivine is the dominant phase (Table 4.2) and ranges from irregular, to anhedral, to euhedral, and may be resorbed (showing embayments) (Figs. 4.1, 2). Olivine is commonly iddingsitised around the rims, and some olivine contains inclusions, possibly chromite. Light brown clinopyroxene phenocrysts are often subhedral or irregular and may exhibit darker brown rims. Clinopyroxene sometimes occurs as glomeroporphyritic clusters (Fig. 4.1). Plagioclase is present as a phenocryst and microphenocryst, although it was not observed in all samples (Table 4.2); it displays a tabular or lath shape when present. Phenocryst size ranges from small microphenocrysts (0.5 to ~1 mm) (commonly clinopyroxene) to much larger olivine megacrysts (>2.5 mm). Phenocryst abundance is typically 10-23% (Table 4.2). Cook *et al.* (2005) observed disequilibrium textures of some of the larger megacrysts displaying reaction rims of pyroxene and kink-banded metamorphic textures. Cook *et al.* (2005) attributed this to xenolith disaggregation, however no such textures were observed in this study.

#### Groundmass

The groundmass is dominated by plagioclase with less common clinopyroxene, typically comprising 75-90% of the rock (Table 4.2; Figs. 4.1, 2). Olivine and less common titanomagnetite occur as additional groundmass phases, within the fine to medium grained intergranular groundmass texture (Table 4.2). Cook *et al.* (2005) cited the presence of these phases plus ilmenite, apatite, chlorite and smectite, none of which were observed in this study. Plagioclase occurs as laths, commonly densely packed around irregular clinopyroxene and olivine.

Plagioclase often exhibits clustering and are the largest groundmass phase (~200 µm) with the other phases generally much smaller (50-100 µm).

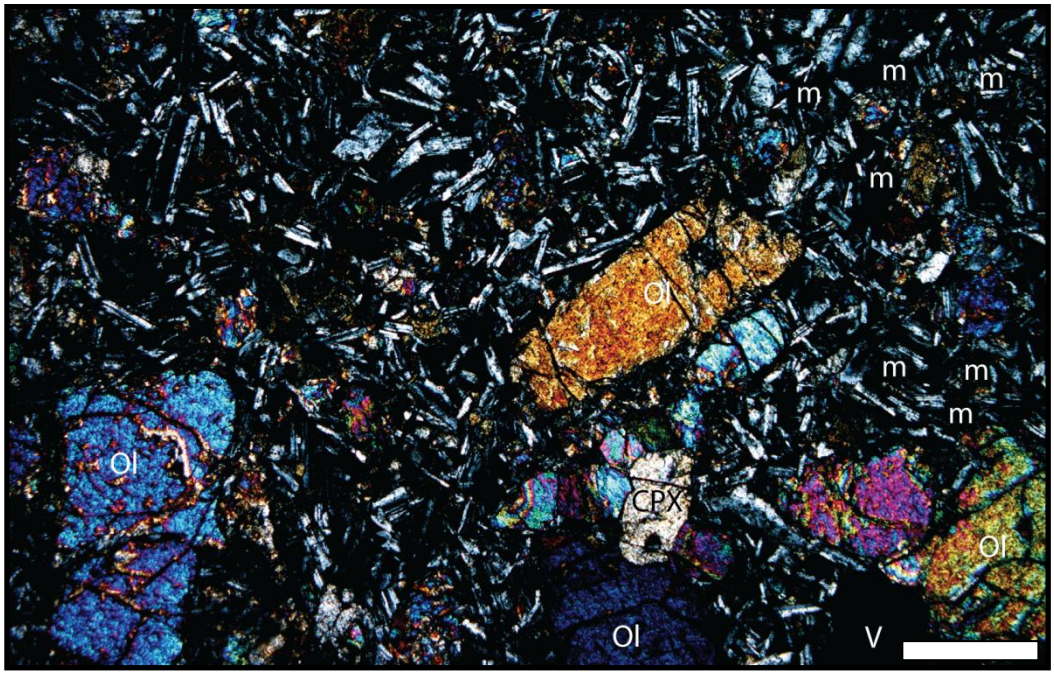


**Figure 4.1:** Photomicrograph of a group A alkali olivine-basalt (BF5S1), showing holocrystalline, porphyritic, coarse grained and non-vesicular textures. Phenocrysts of subhedral olivine (Ol), subhedral clinopyroxene microphenocrysts (CPX), and small grains of titanomagnetite (m), are set in a medium grained intergranular groundmass. The groundmass comprises of plagioclase laths and granular clinopyroxene with lesser amounts of olivine and fine titanomagnetite grains. XPL. Scale is 500 µm.

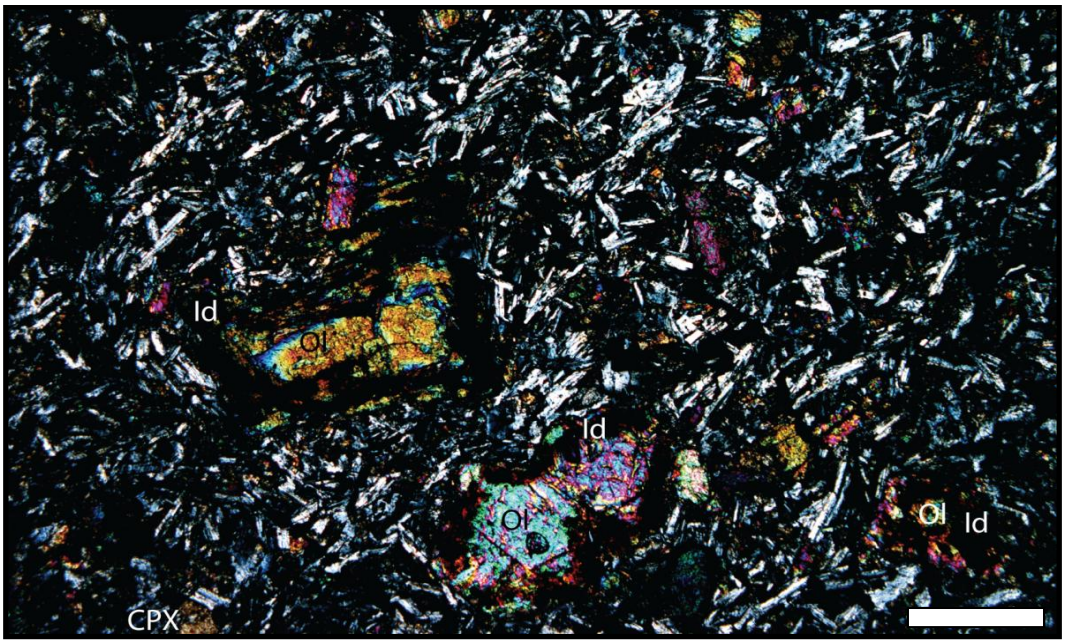


**Figure 4.2:** Photomicrograph of a holocrystalline, porphyritic, coarse grained, and non-vesicular group A alkali olivine-basalt (HS1). Phenocrysts of euhedral and subhedral olivine (Ol), some displaying iddingsite alteration (Id), and a single anhedral clinopyroxene microphenocryst (CPX), are set in an intergranular groundmass. The groundmass comprises plagioclase laths and clinopyroxene, with lesser amounts of olivine and fine titanomagnetite grains. XPL. Scale is 500 µm.

**Table 4.2:** Modal abundances of phenocrysts and groundmass phases of group A alkali olivine-basalts. Abundances based on counting 300 points. Values are in %.

| Sample | HS1.1 | HS1.2 | BF1S1 | AL1.1 | AL1.2 | BF5S1.1 | BF5S1.2 |
|---|---|---|---|---|---|---|---|
| **Rock Classification** | Alkali olivine-basalt | | | | | | |
| **Phenocrysts** | | | | | | | |
| **Olivine** | 8.7 | 12.3 | 12.3 | 15.3 | 17.7 | 15.7 | 11.7 |
| **Clinopyroxene** | 2.0 | 2.3 | 3.0 | 5.0 | 4.7 | 2.3 | 7.7 |
| **Plagioclase** | - | - | - | - | 1.0 | 1.7 | 0.7 |
| **Titanomagnetite** | - | - | - | - | - | - | 0.3 |
| **Total Phenocrysts** | 10.7 | 14.7 | 15.3 | 20.3 | 23.3 | 19.7 | 20.3 |
| **Groundmass** | | | | | | | |
| **Vesicles** | - | 0.7 | - | 2.0 | 1.7 | - | 1.0 |
| **Groundmass** | 89.3 | 84.7 | 84.7 | 77.7 | 75.0 | 80.3 | 78.7 |
| **Plagioclase** | 63.7 | 61.0 | 62.7 | 57.7 | 57.3 | 64.0 | 60.3 |
| **Clinopyroxene** | 19.7 | 19.3 | 15.7 | 14.3 | 13.3 | 13.0 | 15.3 |
| **Olivine** | 4.0 | 3.3 | 4.3 | 3.7 | 3.3 | 2.7 | 2.3 |
| **Titanomagnetite** | 2.0 | 1.0 | 2.0 | 2.0 | 1.0 | 0.7 | 0.7 |
| **Glass** | - | - | - | - | - | - | - |
| **Total (%)** | 100 | 100 | 100 | 100 | 100 | 100 | 100 |

### 4.2.2 Olivine-tholeiitic basalt

The olivine-tholeiitic basalts of group A are porphyritic and range from fine to medium grained. Vesicularity ranges from non-vesicular (0%) to poorly vesicular (33%) (Table 4.3). The basalts are holocrystalline with mineral assemblages dominated by olivine, less common plagioclase, and brown to yellow-brown clinopyroxene. Titanomagnetite also occurs as a phenocryst phase as noticeably larger blocky grains. The phenocryst and microphenocryst phases are set in an intergranular groundmass dominated by plagioclase laths.

#### Phenocrysts

Olivine is the major phenocryst and microphenocryst phase (Table 4.3) occurring in subhedral or irregular form, commonly with thick reddish to dark brown iddingsite rims (Figs. 4.3, 4). Cook *et al.* (2005) described olivine of group A basalts to be predominantly subhedral, as is observed throughout the alkali olivine-basalts and the olivine-tholeiitic basalts. Olivine crystals range in size from small microphenocrysts (>0.4 mm) to larger phenocrysts (>1 mm). Brown rimmed clinopyroxene are dominantly anhedral but also occur in subhedral form. Clinopyroxene phenocrysts are relatively uncommon (Table 4.3) and generally occur as microphenocrysts, ranging up to 0.5 mm. Phenocrysts of plagioclase are uncommon, and occur more abundantly as tabular or lath shaped microphenocrysts (<0.6 mm). Titanomagnetite are small (~50 μm) and irregular.

Olivine megacrysts (up to 2.3 mm) are rare. Total phenocryst abundance is typically 10-15% (Table 4.3).

## Groundmass

The groundmass is medium grained, intergranular, with abundant irregularly orientated tabular or lath shaped plagioclase, and less common yellowish-brown anhedral clinopyroxene (Figs. 4.3, 4). Olivine is variable throughout the samples (Table 4.3). Titanomagnetite occurs as an additional groundmass phase as small (<5-10 μm) irregular grains. Total groundmass abundance is typically 56-85% of the rock.

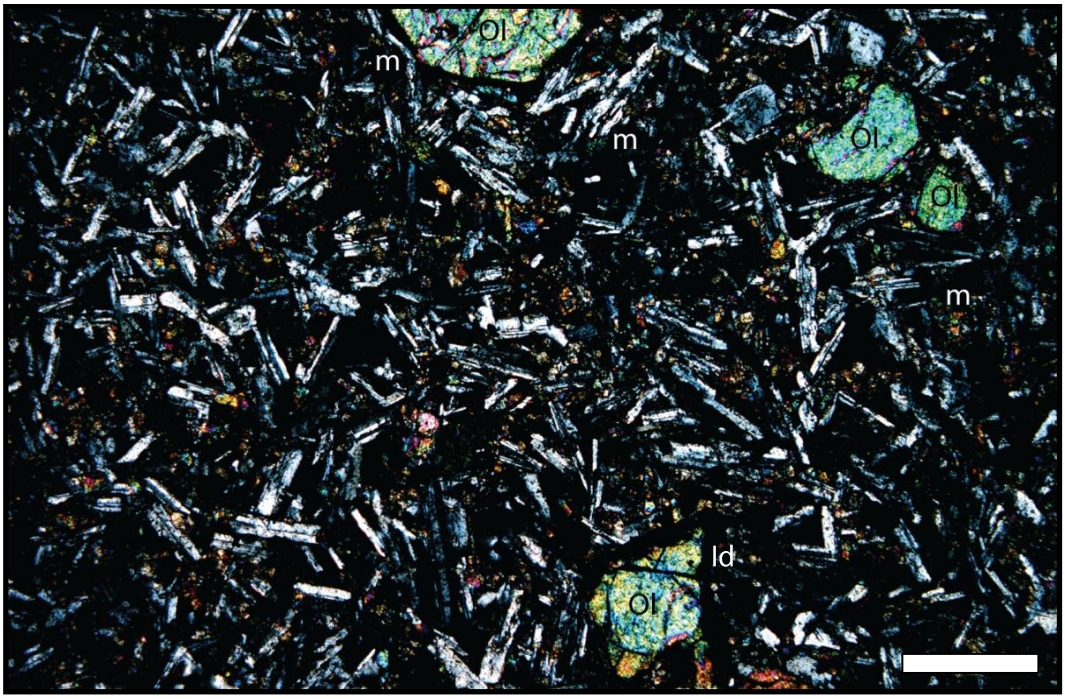


**Figure 4.3:** Photomicrograph of a group A olivine-tholeiitic basalt (BF4S1), showing a holocrystalline, porphyritic, medium grained, and non-vesicular texture. Phenocrysts of euhedral and subhedral olivine (Ol), with thick dark rims of iddingsite (Id), and small grains of titanomagnetite (m) are set in a coarse, intergranular groundmass. The groundmass comprises plagioclase laths and less common clinopyroxene, olivine, and small titanomagnetite grains. XPL. Scale is 500 μm.

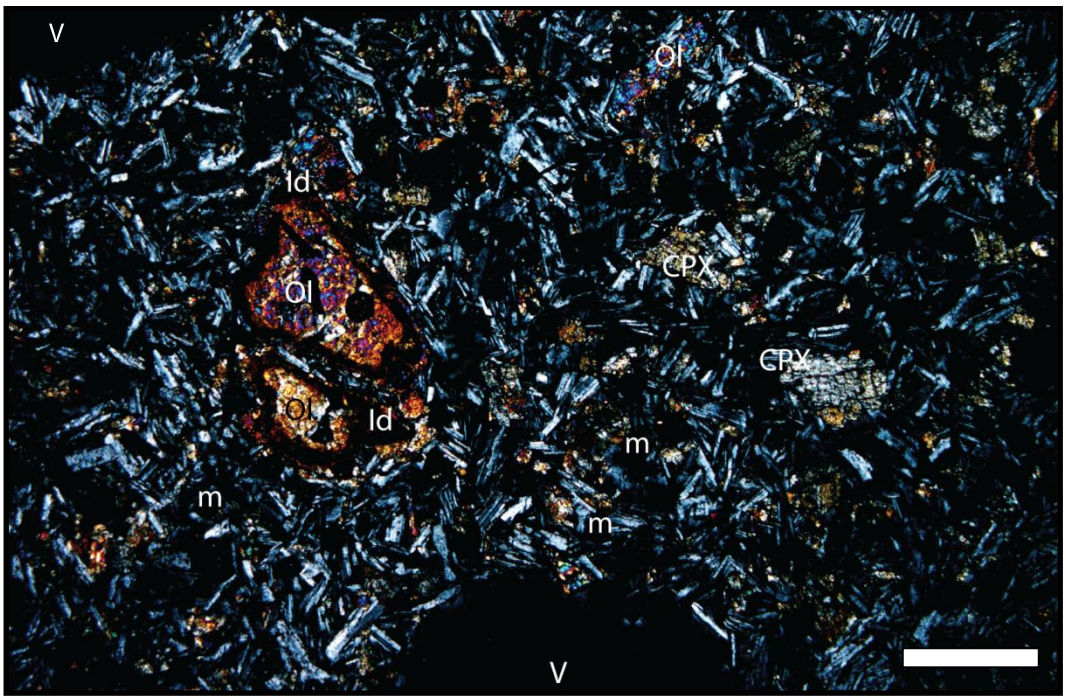


**Figure 4.4:** Photomicrograph of a group A olivine-tholeiitic basalt (HS3), showing a holocrystalline, porphyritic, medium to coarse grained, and poorly vesicular texture. Phenocrysts of subhedral olivine (Ol), with strong, thick, dark reddish-brown rims of iddingsite (Id) alteration, anhedral clinopyroxene microphenocrysts (CPX), and small grains of titanomagnetite (m) are set in a coarse grained intergranular groundmass. Plagioclase laths dominate the groundmass with clinopyroxene, olivine and small irregular titanomagnetite grains. Vesicles are denoted (V). XPL. Scale is 500 µm.

**Table 4.3:** Modal abundances of phenocrysts and groundmass phases of group A olivine-tholeiitic basalts. Abundances based on counting 300 points. Values are in %.

| **Sample** | HS3 | BF4S1.1 | BF4S1.2 |
|---|---|---|---|
| **Rock Classification** | Olivine-tholeiitic basalt | | |
| | | | |
| **Phenocrysts** | | | |
| **Olivine** | 7.7 | 10.3 | 8.7 |
| **Clinopyroxene** | 2.3 | 1.3 | 1.0 |
| **Plagioclase** | - | 2.3 | 1.7 |
| **Titanomagnetite** | 0.7 | 0.3 | 0.3 |
| | | | |
| **Total Phenocrysts** | 10.7 | 14.3 | 11.7 |
| | | | |
| **Groundmass** | | | |
| **Vesicles** | 33.3 | - | 2.7 |
| **Groundmass** | 56.0 | 85.7 | 85.7 |
| | | | |
| **Plagioclase** | 52.0 | 69.0 | 70.3 |
| **Clinopyroxene** | 3.7 | 12.0 | 10.3 |
| **Olivine** | 0.3 | 2. 7 | 2.3 |
| **Titanomagnetite** | - | 2 | 2. 7 |
| **Glass** | - | - | - |
| | | | |
| **Total (%)** | 100 | 100 | 100 |

## 4.3 Basalt Lava Group B

### 4.3.1 Basanite

The basanites of the group B basalts are predominantly fine grained, and display porphyritic or glomeroporphyritic textures. They are hypocrystalline, comprising variable amounts of glass (6-10%) in the groundmass and are non-vesicular or incipiently vesicular with values ranging from 1-10% (Table 4.4). Phenocrysts are mainly subhedral or euhedral olivine with lesser amounts of titaniferous clinopyroxene, and rare plagioclase. Total phenocryst abundance is typically 16-25%. The groundmass textures are most commonly intersertal comprising 65-82% of the rock.

#### Phenocrysts

The megacryst (>1.6 mm), phenocryst (0.5-1.4 mm), and microphenocryst (<0.4 mm) phases of the basanites are limited to olivine and titaniferous clinopyroxene (Table 4.4). Olivine is commonly euhedral or subhedral in shape, sometimes displaying glomeroporphyritic textures (Fig. 4.5) with occasional inclusions. Cook *et al.* (2005) cited small inclusions within the subhedral to euhedral olivine as common. Reddish to brown iddingsite alteration is present around olivine rims. Clinopyroxene is titaniferous and purplish-brown to light brown in colour, and occurs in euhedral and subhedral form, occasionally displaying resorbed textures. Cook *et al.* (2005) noted the presence of dark purplish-pink rims of high-Ca titanaugite or diopside, however no such rims were observed in this study. Cook *et al.* (2005) also cited the dominance of clinopyroxene in the basanites commonly as the main phase with olivine subordinate.

#### Groundmass

The groundmass is intersertal and consists of plagioclase and purple-brown titaniferous clinopyroxene (Fig. 4.5). Plagioclase is the dominant groundmass phase occurring with olivine as an additional phase as fine anhedral grains (Table 4.4). Clustering of grains is absent. Plagioclase laths are the largest phase (up to 150 μm) and are abundant along with fine grained clinopyroxene, occurring commonly as euhedral crystals (although sometimes are more irregular in shape).

Cook *et al.* (2005) observed the presence of other additional groundmass phases including titanomagnetite and ilmenite.

## Xenoliths

One feature of interest in this group of basalts is the inclusion of quartz xenoliths, typically consisting of interlocking quartz grains with a moderately thick reaction rim of irregularly orientated, prismatic titaniferous clinopyroxene crystals (Fig. 4.6). Rosenberg (1991), Cook (2002), and Cook *et al.* (2005) also observed the presence of quartz and feldspar xenoliths, and xenocrysts within the group B basalts, occurring with a reaction rim of clinopyroxene. The quartz grains can display resorbed textures and embayments occasionally filled with extremely fine grained crystals. These quartzite xenoliths are possibly derived from quartz veins in the underlying Mesozoic greywacke basement.

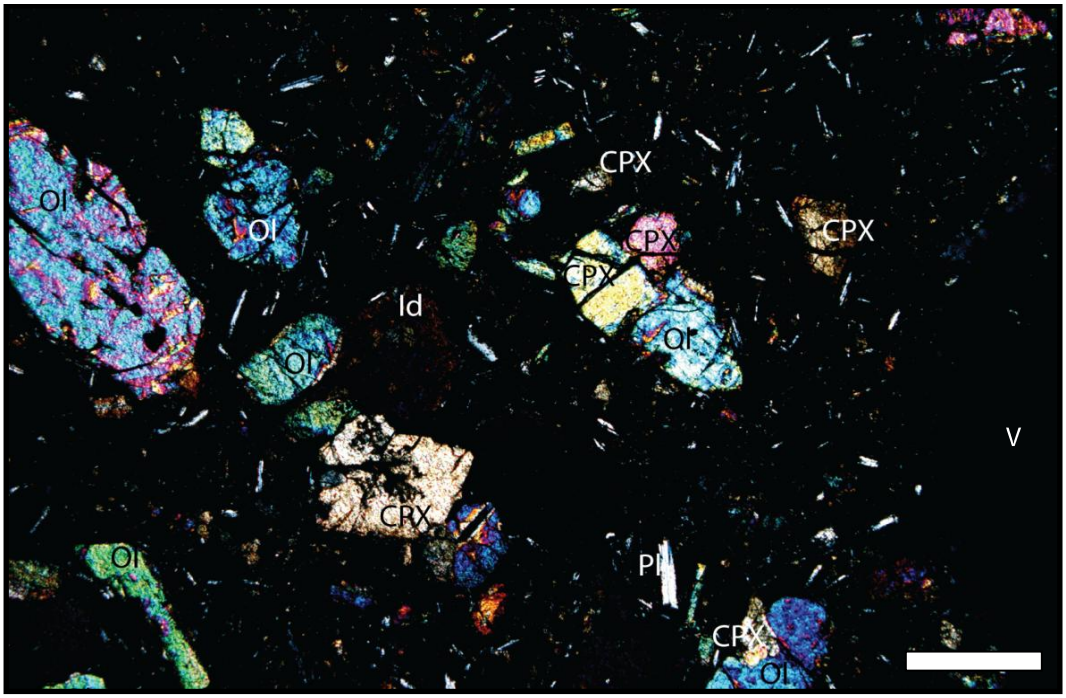


**Figure 4.5:** Photomicrograph of a group B basanite (BF3S1). Megacrysts (left) and phenocrysts of subhedral olivine (Ol), with moderately thick, dark rims of iddingsite, (Id), subhedral phenocrysts and microphenocrysts of clinopyroxene (CPX), and small tabular plagioclase microphenocrysts (Pl) are set in a fine grained intersertal groundmass dominated by plagioclase laths and clinopyroxene. Less common olivine grains and glass are also present. Vesicles are denoted (V). XPL. Scale is 500 µm.

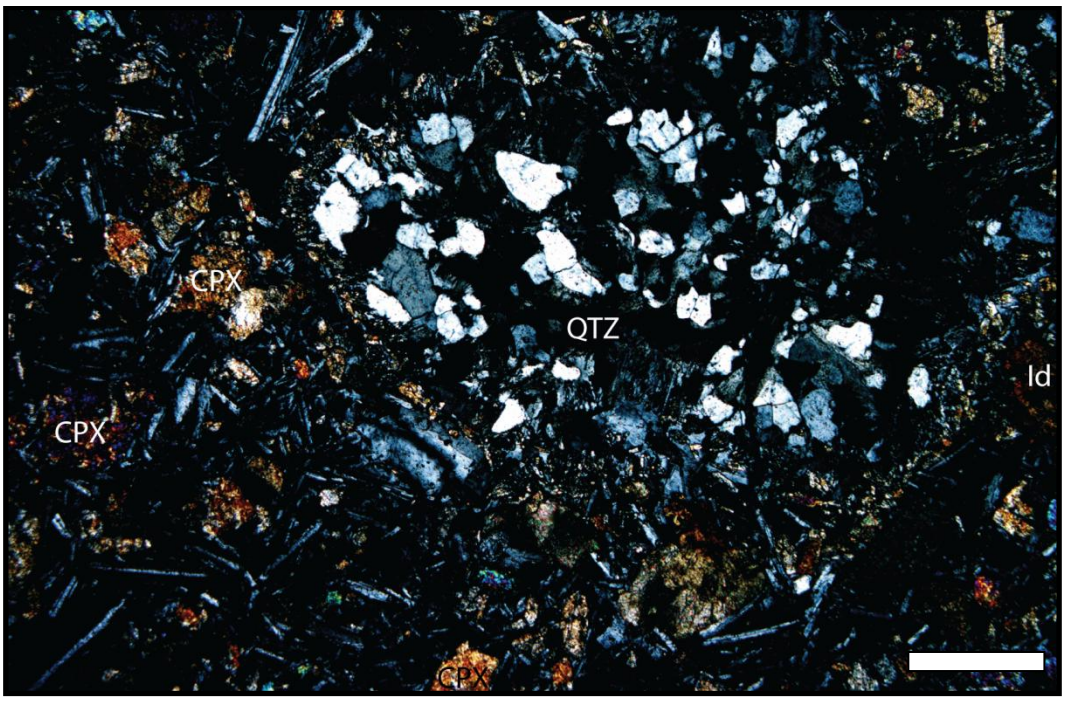


**Figure 4.6:** Photomicrograph of a group B basanite (BF7S1). Fine grained irregularly orientated titaniferous clinopyroxene (CPX) crystals have formed a reaction rim around a quartz xenolith (QTZ). Some iddingsite (Id) alteration of olivine is evident. Groundmass is intersertal comprising plagioclase laths, clinopyroxene, and olivine. XPL. Scale is 500 µm.

**Table 4.4:** Modal abundances of phenocrysts and groundmass phases of group B basanites. Abundances based on counting 300 points. Values are in %.

| **Sample** | BF3S3.1 | BF3S1 | BF3S3.2 | BF7S1.1 | BF7S1.2 |
|---|---|---|---|---|---|
| **Rock Classification** | | | Basanite | | |
| | | | | | |
| **Phenocrysts** | | | | | |
| **Olivine** | 19.7 | 15.0 | 9.7 | 6.7 | 11.7 |
| **Clinopyroxene** | 5.3 | 8.3 | 7.3 | 8.7 | 4.0 |
| **Plagioclase** | - | - | - | 1.0 | 0.7 |
| **Titanomagnetite** | - | - | - | - | - |
| | | | | | |
| **Total Phenocrysts** | 25.0 | 23.3 | 17.0 | 16.3 | 16.3 |
| | | | | | |
| **Groundmass** | | | | | |
| **Vesicles** | 9.0 | 2.7 | - | 0.7 | 2.0 |
| **Total Groundmass** | 65.3 | 74.0 | 82.3 | 81.3 | 80.0 |
| | | | | | |
| **Plagioclase** | 34.7 | 38.0 | 42.3 | 47.7 | 45.7 |
| **Clinopyroxene** | 20.3 | 21.3 | 32.0 | 20.7 | 23.7 |
| **Olivine** | 1.0 | 1.3 | 1.7 | 2.7 | 3.0 |
| **Titanomagnetite** | - | - | - | - | - |
| **Glass** | 9.3 | 13.3 | 6.3 | 10.3 | 7.7 |
| | | | | | |
| **Quartz Xenoliths** | 0.7 | - | 0.7 | 1.7 | 1.7 |
| | | | | | |
| **Total (%)** | 100 | 100 | 100 | 100 | 100 |

### 4.3.2 Alkali olivine-basalt

Similar to the group A alkali olivine-basalts, the group B alkali olivine-basalts are porphyritic, coarse grained, and consist of olivine, clinopyroxene, and plagioclase phenocrysts, but no other similarities to group A exist. Samples are hypocrystalline and are non-vesicular (1%) to incipiently vesicular (8%) (Table 4.5). The basalts comprise common megacrysts, phenocrysts, and microphenocrysts of olivine, and phenocrysts and microphenocrysts of titaniferous clinopyroxene, plagioclase, and titanomagnetite.

#### Phenocrysts

Olivine (up to 2.5 mm) ranges from subhedral to anhedral, and occasionally prismatic. They occasionally occur in small clusters displaying glomeroporphyritic textures (Fig. 4.7) and have rims commonly altered to iddingsite. Phenocrysts and microphenocrysts of titaniferous purplish-brown clinopyroxene (<1 mm) are present in subhedral or irregular habits, and sometimes display glomeroporphyritic textures (Fig. 4.7). Plagioclase microphenocrysts are fine grained (<1.1 mm), lath shaped or tabular. Fine grained irregular titanomagnetite are generally rare but can be more abundant in some samples (Table 4.5). Total phenocryst abundance typically ranges from 15-25%.

#### Groundmass

The groundmass is medium to coarse grained and intersertal, comprising plagioclase, titaniferous clinopyroxene, olivine and glass (4-8%) (Table 4.5; Fig. 4.7). Plagioclase is abundant (Table 4.5), occurring as laths (up to 300 µm). Finer grained euhedral to anhedral titaniferous clinopyroxene (<150 µm) is common (Table 4.5); olivine is less common and are finer grained, consisting of anhedral or irregular grains (<100 µm). The total groundmass abundance ranges from 75-83%.

#### Xenoliths and Xenocrysts

Large quartzose xenoliths (up to 4 mm) are also present in this type of rock (Table 4.5) (Fig. 4.8). Very fine grained, moderately thick reaction rims of titaniferous clinopyroxene surround these interlocking granular textured quartzose xenoliths. The clustering of grains frequently display recrystallised textures forming

interstices, occasionally filled by tabular titaniferous clinopyroxene. These quartzite xenoliths are probably derived from Mesozoic basement quartz veins in low grade metagreywackes.

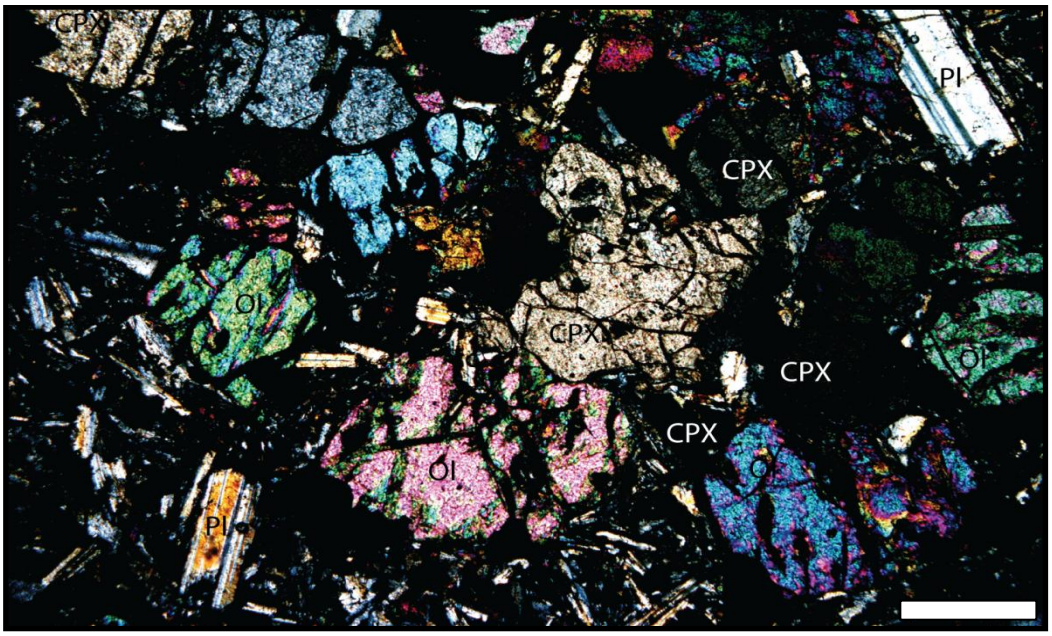


**Figure 4.7:** Photomicrograph of a group B alkali olivine-basalt (BF2S1), showing a hypocrystalline, glomeroporphyritic, coarse grained, and poorly vesicular texture. Phenocrysts of subhedral olivine (Ol), anhedral clinopyroxene (CPX), and tabular plagioclase (Pl) are set in a groundmass of plagioclase laths, titaniferous clinopyroxene, olivine, granular titanomagnetite grains and glass. XPL. Scale is 500 µm.

**Table 4.5:** Modal abundances of phenocrysts and groundmass phases of group B alkali olivine-basalts. Abundances based on counting 300 points. Values are in %.

| **Sample** | BF2S1.1 | BF2S1.2 | BF6S1.1 | BF6S1.2 |
|---|---|---|---|---|
| **Rock Classification** | Alkali Olivine-basalt | | | |
| | | | | |
| **Phenocrysts** | | | | |
| **Olivine** | 16.7 | 15.3 | 6.0 | 7.0 |
| **Clinopyroxene** | 5.3 | 6.0 | 6.3 | 3.3 |
| **Plagioclase** | 3.0 | 2.3 | 2.0 | 2.7 |
| **Titanomagnetite** | 0.3 | - | 0.7 | 1.7 |
| | | | | |
| **Total Phenocrysts** | 25.3 | 23.7 | 15.0 | 14.7 |
| | | | | |
| **Groundmass** | | | | |
| **Vesicles** | - | 0.3 | 2.3 | 8.0 |
| **Total Groundmass** | 74.7 | 76.0 | 82.7 | 76.0 |
| | | | | |
| **Plagioclase** | 35.7 | 42.0 | 40.3 | 38.0 |
| **Clinopyroxene** | 26.0 | 23.3 | 29.7 | 25.7 |
| **Olivine** | 4.7 | 5.0 | 6.3 | 5.3 |
| **Titanomagnetite** | - | - | - | - |
| **Glass** | 8.0 | 4.3 | 6.3 | 6.7 |
| | | | | |
| **Quartz Xenoliths** | - | - | - | 1.3 |
| | | | | |
| **Total %** | 100 | 100 | 100 | 100 |

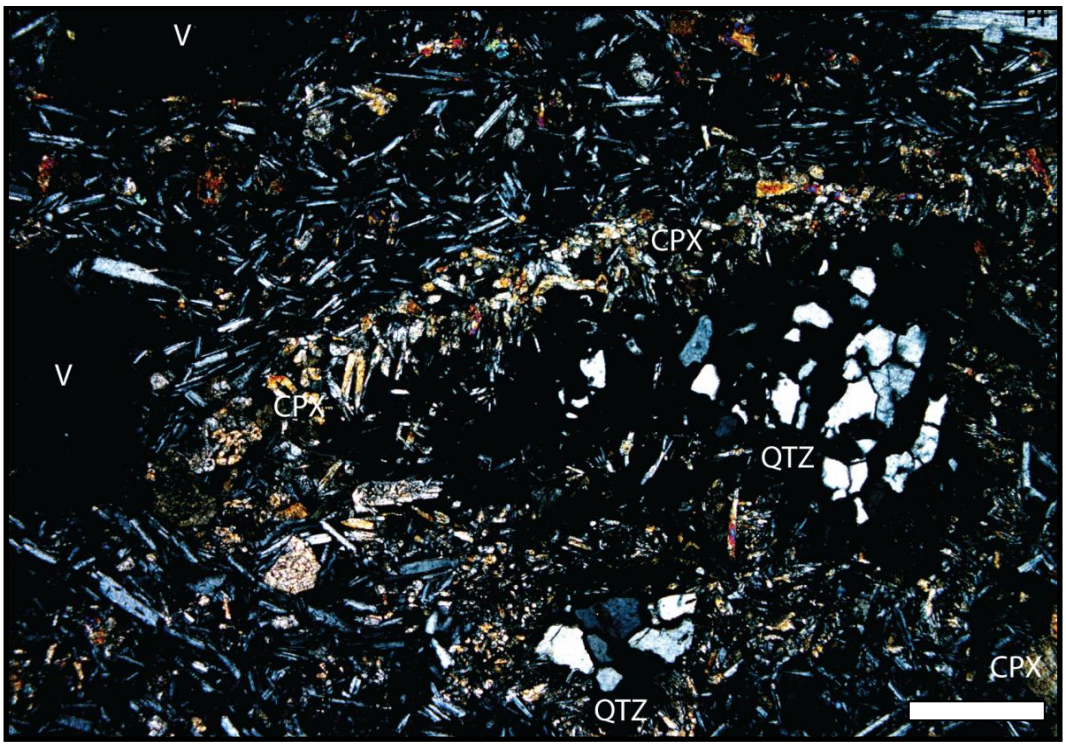


**Figure 4.8:** Photomicrograph of a group B alkali olivine-basalt (BF6S1). Irregular titaniferous clinopyroxene (CPX) crystals have formed a reaction rim around a quartz xenolith (QTZ). Groundmass comprises plagioclase laths, clinopyroxene, olivine, and glass. Vesicles are denoted (V). XPL. Scale is 500 µm.

## 4.4 Basalt Lava – Andesite

This unusual rock was sampled near the Rutherford Road cone and is a very weathered, and poorly vesicular (25-27%, Table 4.6) rock. Petrographically it is similar to the trachydacite and is medium to coarse grained, vitrophyric, and hypocrystalline. It is unique due to its vitrophyric nature and that the crystal abundance is significantly less than what is observed in other samples (Table 4.6). Olivine and clinopyroxene are the only phenocrysts observed and occur as microphenocrysts along with small plagioclase. The groundmass texture is vitrophyric, comprised solely of glass (~64%) (Table 4.6; Fig. 4.9).

### Phenocrysts

Olivine phenocrysts (>1 mm) ranged from euhedral to anhedral and are uncommon when compared to microphenocrysts. Iddingsite alteration is effectively complete with each crystal totally altered (Fig. 4.9). Subhedral to anhedral phenocrysts of clinopyroxene are generally larger than those of olivine

(>1.2 mm), although microphenocrysts are more abundant. Plagioclase are fine grained and occur as microphenocrysts (<0.5 mm) and wispy thin laths. Total phenocryst abundance is ~10% (Table 4.6).

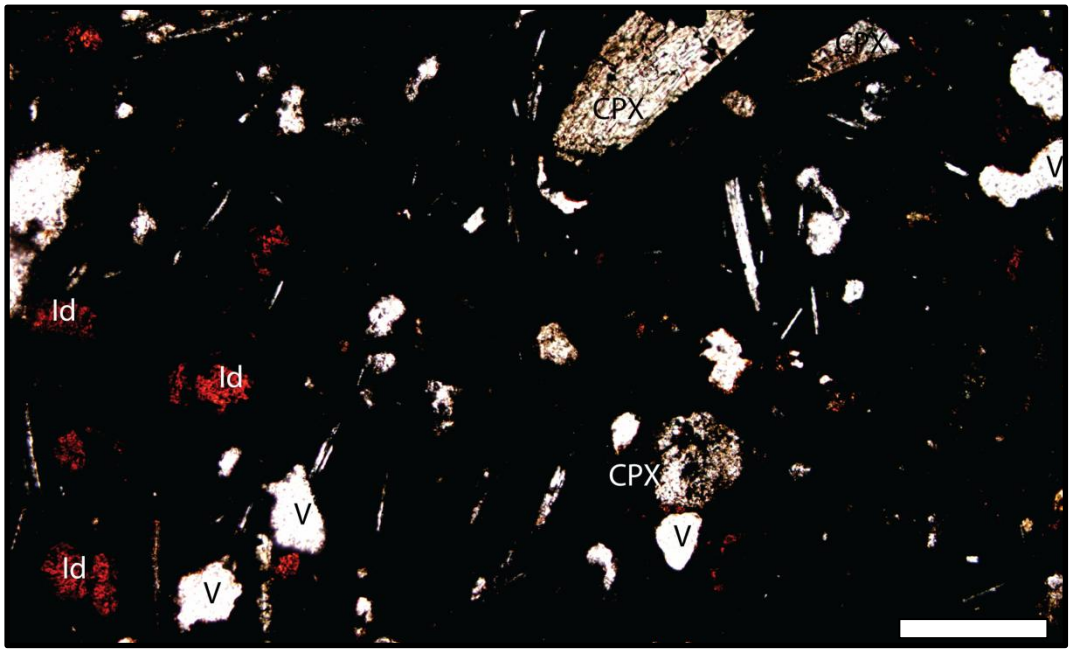


**Figure 4.9:** Photomicrograph of the andesite (BF3S2). Phenocrysts of subhedral and irregular clinopyroxene (CPX), with olivine microphenocrysts strongly iddingsitised (Id), and lath shaped plagioclase microphenocrysts (Pl), are set in a vitrophyric groundmass. PPL. Scale is 500 µm.

**Table 4.6:** Modal abundance for the andesite. Abundances based on counting 300 points. Values are in %.

| **Sample** | BF3S2.1 | BF3S2.2 |
|---|---|---|
| **Rock Classification** | Andesite | |
| | | |
| **Phenocrysts** | | |
| **Olivine** | 4.3 | 5.7 |
| **Clinopyroxene** | 4.0 | 4.3 |
| **Plagioclase** | 1.3 | 0.7 |
| **Titanomagnetite** | - | - |
| | | |
| **Total Phenocrysts** | 9.7 | 10.7 |
| | | |
| **Groundmass** | | |
| **Vesicles** | 27.0 | 25.3 |
| **Total Groundmass** | 63.3 | 64.0 |
| | | |
| **Plagioclase** | - | - |
| **Clinopyroxene** | - | - |
| **Olivine** | - | - |
| **Titanomagnetite** | - | - |
| **Glass** | 63.3 | 64.0 |
| | | |
| **Quartz Xenoliths** | - | - |
| | | |
| **Total %** | 100 | 100 |

## 4.5 Tuff Ring Deposits

Basalt tuff requires different petrographic parameters to be described as they have a pyroclastic or fragmental texture; rather than a coherent texture as of the basalt lava. Tuffs contain significant amounts of foreign derived components including lithic fragments and free xenocrysts important in determining eruption processes. The description of the tuff given here is divided into three parts:

(1) juvenile components, this includes free crystals derived from basalt magma and basalt clasts ranging from coarse ash to block and bomb size;
(2) accretionary lapilli, not strictly juvenile or lithic material so are discussed in a separate category;
(3) alteration products of the matrix, including the various alteration products and morphology of glass shards; and
(4) accidental components, including all accidentally derived lithic fragments and material from underlying geological formations, including lithics from previously erupted lavas, and xenocrysts.

Tuffaceous rock is best classified using the scheme of Le Maitre (1989) based on the relative abundance of glass to crystals to lithics (Fig. 4.10). Crystals in this classification are defined as xenocrysts and juvenile crystals. Lithics are defined as accidental sedimentary and igneous lithic fragments. The tuffs at Raventhorpe and Pokeno West are both vitric tuffs. This is in agreement with the findings of Rosenberg (1991) and Ilanko (2010) who described tuff rings of Barriball Road, Aka Aka, Maketu, Raventhorpe, and Smeed Quarry also as vitric tuffs

.

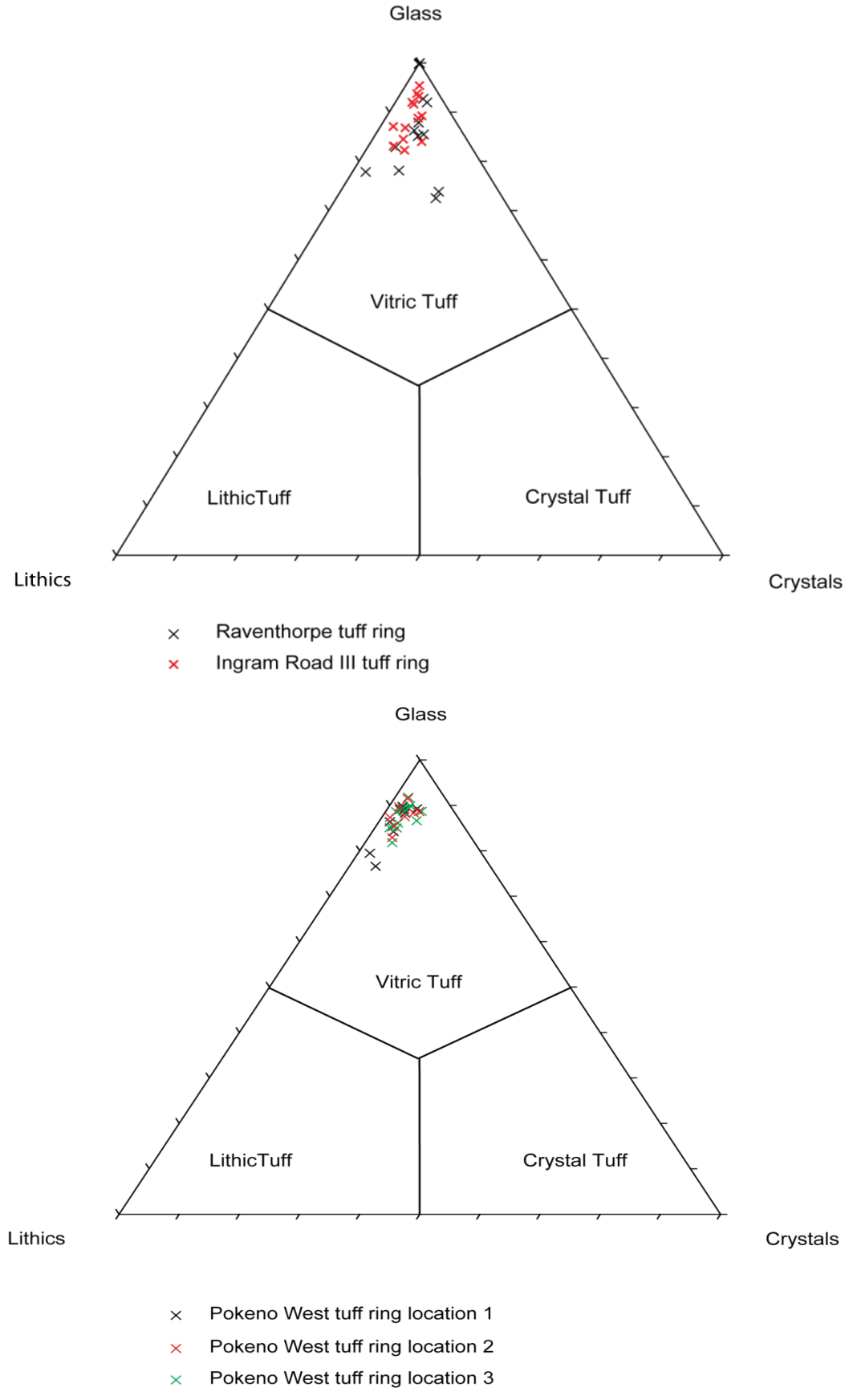


**Figure 4.10:** Ternary plot showing proportions of vitrics, crystals, and lithics of samples from Raventhorpe, Ingram Road tuff ring III, and Pokeno West tuff rings. Classification is after Le Maitre (1989). Percentages have been recalculated to exclude vesicles

### 4.5.1 Juvenile Components

Crystals and basaltic clasts are described in this section including the sample identified as a trachydacite (P3S2) from Pokeno West tuff ring.

#### Crystals

Crystals constitute between 2.3 to 20.3% of the tuff composition (Tables 4.7, 4.8). This includes crystals of juvenile and accidental origin, with the latter discussed in a subsequent section. Crystals of juvenile origin are olivine, clinopyroxene, and plagioclase (Tables 4.7, 4.8) (Figs. 4.11, 12). Crystals often exhibit very irregular shapes (Figs. 4.11, 12) and often appear to have been torn and broken during fragmentation and deposition. Larger crystals on occasion have a thin layer of devitrified glass surrounding them.

One final mechanism deserving of consideration is the separation of large, slowly cooled crystals from underlying basaltic rock. Such accessory crystals could be considered juvenile in origin if they are similar in size to the other phenocrysts. Unless they exhibit different petrographical properties or features, i.e. resorption textures, they might not be distinguished. Plagioclase interpreted as juvenile are smaller than the less calcic, larger oligoclase to andesine composition xenocrysts.

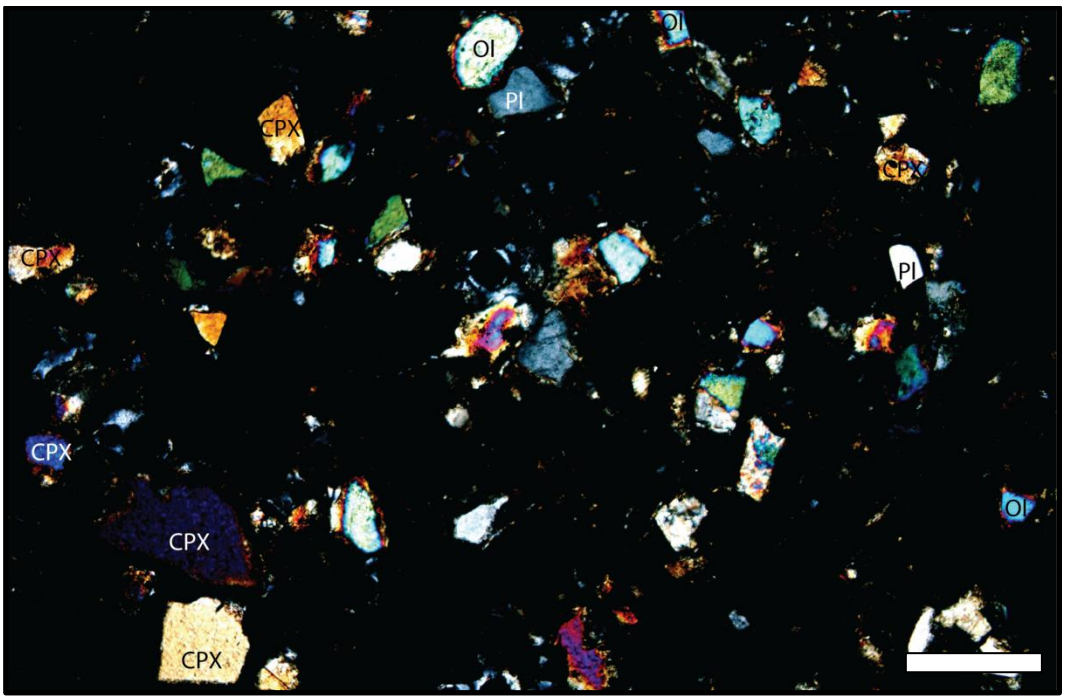


**Figure 4.11:** Photomicrograph of a typical tuff sample from Pokeno West tuff ring (P3S15). Irregular titaniferous clinopyroxene (CPX) crystals display purplish-brown colours, with olivine crystals (Ol), and few plagioclase microphenocrysts (Pl). The matrix is fine grained, brown, gel palagonite. XPL. Scale is 500 µm.

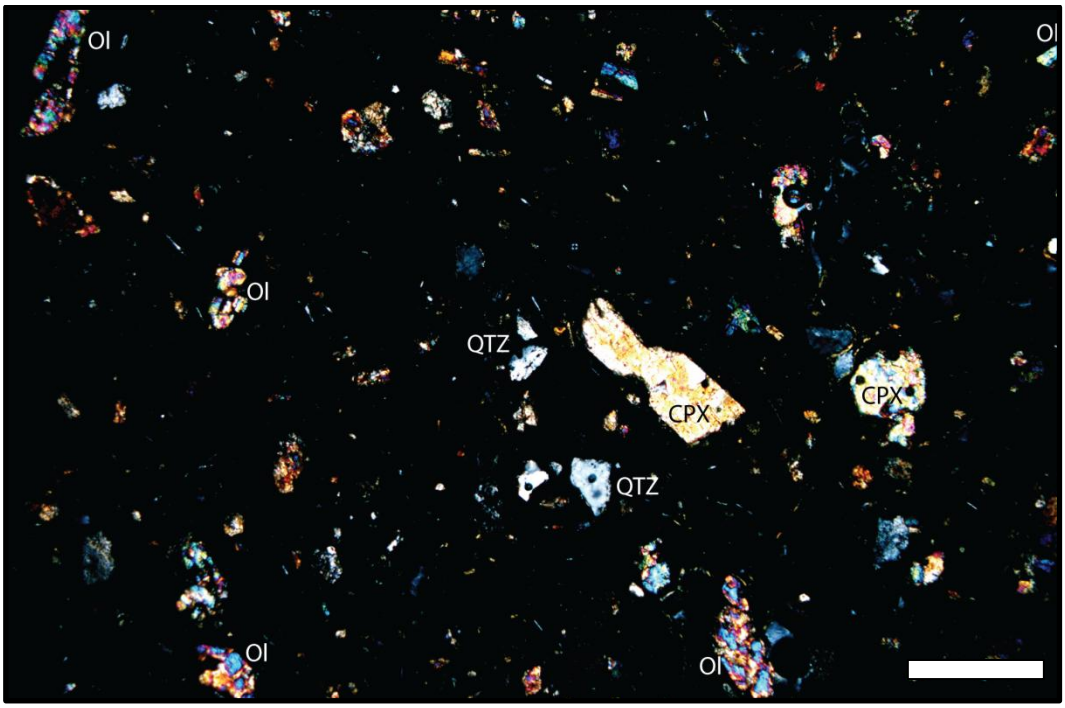


**Figure 4.12:** Photomicrograph of a typical tuff sample from Raventhorpe tuff ring (R6). Irregularly shaped clinopyroxene crystals (CPX) display dull brown colours, with olivine crystals (Ol), and few quartz xenocrysts (QTZ). Matrix is fine grained, brown, gel palagonite. XPL. Scale is 500 µm.

**Table 4.7:** Summary of modal analyses of the components in the tuffs at Raventhorpe and Pokeno West tuff rings, including crystals, lithics, juvenile basalt, vesicles, and palagonite matrix. Minimum (Min) and maximum (Max) ranges are given for each component within each facies group for each of the volcanic centres. Individual values are from a single sample analysis that recorded the highest or lowest value for that particular facies. Values are in %.

| **Volcanic Centre** | **Raventhorpe** | | | | | | | | **Pokeno West** | | | | | | | | | |
|---|---|---|---|---|---|---|---|---|---|---|---|---|---|---|---|---|---|---|
| **Facies Group** | Facies 1 | | Facies 2 | | Facies 4 | | Facies 5 | | Facies 1 | | Facies 2 | | Facies 3 | | Facies 4 | | Facies 5 | |
| | Min | Max | Min | Max | Min | Max | Min | Max | Min | Max | Min | Max | Min | Max | Min | Max | Min | Max |
| **Total Crystal Abundance**[1] | 3.7 | 18.7 | 12.7 | 12.7 | 3.7 | 20.3 | 9.5 | 11.8 | 4.2 | 9.3 | 2.7 | 8.2 | 3.0 | 8.7 | 5.0 | 6.0 | 8.0 | 8.0 |
| **Olivine** | 0.7 | 10.0 | 5.3 | 5.3 | 1.0 | 8.7 | 3.3 | 4.7 | 0.0 | 2.7 | 0.0 | 3.0 | 0.7 | 2.3 | 0.0 | 1.0 | 1.7 | 1.7 |
| **Clinopyroxene** | 0.0 | 6.0 | 1.3 | 1.3 | 0.3 | 4.7 | 0.6 | 4.3 | 0.3 | 0.6 | 0.0 | 6.0 | 0.3 | 5.3 | 0.3 | 3.7 | 2.0 | 2.0 |
| **Plagioclase** | 0.0 | 1.0 | 0.3 | 0.3 | 0.0 | 0.7 | 0.0 | 0.3 | 0.0 | 1.0 | 0.0 | 0.3 | 0.0 | 0.0 | 0.0 | 0.0 | 0.0 | 0.0 |
| **Plagioclase**[2] | 0.0 | 0.0 | 0.0 | 0.0 | 0.0 | 0.7 | 0.0 | 1.7 | 0.0 | 1.3 | 0.0 | 0.7 | 0.0 | 1.0 | 0.0 | 1.0 | 0.0 | 0.0 |
| **Hornblende**[2] | 0.0 | 1.0 | 0.0 | 0.0 | 0.0 | 0.7 | 0.0 | 1.7 | 0.0 | 0.7 | 0.0 | 0.3 | 0.0 | 0.7 | 0.0 | 0.0 | 0.0 | 0.0 |
| **Quartz**[2] | 1.0 | 4.3 | 5.7 | 5.7 | 0.0 | 5.7 | 2.3 | 4.7 | 0.3 | 5.3 | 0.7 | 5.7 | 0.0 | 5.7 | 2.0 | 3.7 | 4.3 | 4.3 |
| **Hypersthene**[2] | 0.0 | 1.0 | 0.0 | 0.3 | 0.0 | 0.3 | 0.0 | 0.7 | 0.0 | 0.0 | 0.0 | 0.3 | 0.0 | 0.3 | 0.0 | 0.7 | 0.0 | 0.3 |
| **Total Lithic Abundance** | 4.7 | 22.3 | 7.7 | 7.7 | 1.7 | 15.7 | 1.0 | 2.7 | 0.0 | 22.0 | 2.7 | 19.0 | 2.0 | 8.3 | 2.0 | 3.0 | 7.7 | 7.7 |
| **Sedimentary Lithics** | 3.0 | 17.0 | 3.7 | 3.7 | 0.0 | 12.7 | 0.0 | 1.7 | 0.0 | 22.0 | 2.7 | 19.0 | 2.0 | 8.3 | 2.0 | 3.0 | 7.7 | 7.7 |
| **Igneous Lithics** | 1.3 | 2.0 | 4.0 | 4.0 | 0.0 | 6.7 | 0.3 | 1.7 | 0.0 | 8.0 | 0.0 | 4.0 | 0.0 | 1.0 | 0.0 | 0.0 | 7.0 | 7.0 |
| **Total Juvenile Basalt Abundance** | 20.0 | 39.5 | 7.0 | 7.0 | 9.6 | 52.5 | 20.1 | 39.1 | 3.0 | 57.6 | 1.5 | 42.6 | 11.5 | 43.3 | 37.0 | 57.0 | 7.3 | 7.3 |
| **Total Vesicularity**[3] | 5.0 | 12.7 | 7.0 | 7.0 | 3.7 | 17.0 | 3.3 | 26.7 | 3.3 | 18.0 | 3.0 | 18.0 | 2.0 | 13.3 | 8.7 | 12.0 | 8.3 | 8.3 |
| **Palagonite Matrix** | 31.7 | 52.0 | 38.0 | 38.0 | 21.3 | 72.0 | 19.3 | 70.0 | 21.3 | 80.7 | 28.7 | 72.3 | 34.0 | 76.0 | 29.0 | 42.0 | 68.7 | 68.7 |

1/ Total crystal abundance includes all (xenocrysts and juvenile) free crystals within the tuff matrix.

2/ Denotes crystals identified as xenocrysts.

3/ Total vesicularity refers to pore space in the matrix.

**Table 4.8:** Summary of modal analyses of the components of the tuff samples for Ingram Road tuff ring III, including crystals, lithics, juvenile basalt, vesicles, and palagonite matrix. Minimum (Min) and maximum (Max) ranges are given for each component within each facies group for each of the volcanic centres. Individual values are from a single sample analysis that recorded the highest or lowest value for that particular facies. Values are in %.

| **Volcanic Centre** | Ingram Road | | | | | |
|---|---|---|---|---|---|---|
| **Facies Group** | Facies 1 | | Facies 2.1 | | Facies 2.2 | |
| | Min | Max | Min | Max | Min | Max |
| **Total Crystal Abundance**[1] | 5.0 | 9.7 | 2.3 | 5.3 | 3.0 | 3.7 |
| **Olivine** | 1.0 | 7.3 | 0.7 | 5.3 | 0.0 | 3.7 |
| **Clinopyroxene** | 0.3 | 4.3 | 0.0 | 1.3 | 0.0 | 0.0 |
| **Plagioclase** | 0.0 | 0.7 | 0.0 | 0.0 | 0.0 | 0.0 |
| **Plagioclase**[2] | 0.0 | 0.7 | 0.0 | 0.3 | 0.0 | 0.3 |
| **Hornblende**[2] | 0.0 | 0.7 | 0.0 | 0.7 | 0.0 | 0.0 |
| **Quartz**[2] | 0.3 | 2.3 | 0.3 | 3.0 | 0.0 | 0.3 |
| **Hypersthene**[2] | 0.0 | 0.7 | 0.0 | 0.7 | 0.0 | 0.3 |
| **Total Lithic Abundance** | 1.0 | 14.7 | 0.0 | 8.7 | 3.3 | 14.0 |
| **Sedimentary Lithics** | 0.0 | 6.6 | 0.0 | 1.7 | 0.7 | 5.3 |
| **Igneous Lithics** | 0.3 | 13.7 | 0.0 | 7.0 | 0.7 | 13.3 |
| **Total Juvenile basalt Abundance** | 8.3 | 30.3 | 3.0 | 28.0 | 19.0 | 42.5 |
| **Total vesicularity** | 8.7 | 19.3 | 12.7 | 24.7 | 12.7 | 18.3 |
| **Palagonite Matrix** | 40.7 | 64.3 | 45.0 | 80.0 | 22.3 | 57.7 |

1/ Total crystal abundance includes all (xenocrysts and juvenile) free crystals within the tuff matrix.

2/ Denotes crystals identified as xenocrysts.

3/ Total vesicularity refers to pore space in the matrix.

## Basaltic clasts

Three types of basaltic clasts or fragments occur in the tuff rings of Raventhorpe and Pokeno West. The first type is tan to light yellow-brown palagonite, the second a black, almost isotropic sideromelane, and the third, a black, crystal rich holocrystalline or hypocrystalline type with a groundmass and are considered to be accessory in origin, and will be discussed in section 4.5.3. The following descriptions document the basalt clasts in the finer grained (ash) fraction of the tuff ring deposits.

The first type of clast generally occurs as a tan or pale yellow-brown palagonite (Fig. 4.13). They have a higher crystal abundance than the sideromelane dark isotropic type and crystals are almost exclusively very small clinopyroxene with an irregular or occasionally prismatic shape. Olivine and plagioclase are rare. The clasts are generally non-vesicular, however some moderately to highly vesicular clasts have been observed at Pokeno West tuff ring.

The second type of clast is much darker, almost isotropic in thin section, and is comprised of sideromelane. They are also hypocrystalline and are often highly

vesicular (Fig. 4.13). Olivine is the dominant phenocryst in this type of clast with iddingsite alteration common. Clinopyroxene phenocrysts are also present although they are often a little smaller than olivine phenocrysts (Fig. 4.14). Overall both types accounted for between 3 and 57% of the tuff (Tables 4.7, 8). The two types of clast occur together within the tuff and rare clasts comprised of both palagonite and sideromelane were observed at Raventhorpe, indicating incomplete alteration of basaltic glass (Fig. 4.14).

Thin sections of individual basalt clasts in the coarser grained fraction of the tuff, including basalt lapilli and block and bombs were also produced (Table 4.9). These clasts are slightly different to the finer ash sized clasts previously described. They are commonly hypocrystalline (with up to 60% glass, Table 4.9), fine grained, non-vesicular to poorly vesicular with a fine grained plagioclase groundmass (0-78%, Table 4.9). Vesicle abundance ranges from 0-30% (Table 4.9). Phenocryst abundance ranges from 9-30% (Table 4.9). These clasts contain many inclusions including tuff, sedimentary, igneous, and quartzite lithics, indicating juvenile origin, typically 0-5% (Table 4.9).

**Table 4.9:** Summary of modal analyses of the basalt lapilli, and blocks and bombs in the tuffs at Raventhorpe and Pokeno West tuff rings. Values are in %.

| Sample | R4 | R7 | R10 | R10 | R13 | R13 | R18 | R19 | P12 | P3S2 | P3S2 | P3S18 | P3S18 | P3S22 | P3S22 | P3S23 | P3S23 |
|---|---|---|---|---|---|---|---|---|---|---|---|---|---|---|---|---|---|
| **Group** | A | | | | | | | | B | | | | | | | | |
| **Phenocrysts** | | | | | | | | | | | | | | | | | |
| **Olivine** | 22.7 | 7.3 | 5.3 | 7.0 | 10.7 | 12.3 | 7.3 | 15.3 | 5.0 | 5.3 | 6.0 | 8.0 | 7.0 | 7.7 | 8.0 | 12.0 | 8.0 |
| **Clinopyroxene** | 0.0 | 1.0 | 6.0 | 6.7 | 6.7 | 8.7 | 4.3 | 3.0 | 2.0 | 4.3 | 2.7 | 3.0 | 3.3 | 4.0 | 5.3 | 10.0 | 5.0 |
| **Plagioclase** | 2.0 | 1.7 | 0.0 | 0.0 | 1.3 | 0.7 | 0.3 | 0.0 | 9.7 | 0.7 | 0.3 | 1.3 | 0.0 | 0.0 | 0.0 | 8.7 | 0.0 |
| **Total Phenocrysts** | 24.7 | 10.0 | 11.3 | 13.7 | 18.7 | 21.7 | 12.0 | 18.3 | 16.7 | 10.3 | 9.0 | 12.3 | 10.3 | 11.7 | 13.3 | 30.7 | 13.0 |
| **Groundmass** | | | | | | | | | | | | | | | | | |
| **Vesicles** | 12.7 | 16.7 | 11.3 | 15.3 | 23.0 | 20.3 | 1.3 | 1.0 | 0.0 | 27.7 | 30.3 | 20.7 | 14.7 | 19.3 | 28.3 | 1.7 | 20.7 |
| **Total Groundmass** | 62.7 | 68.7 | 75.4 | 70.0 | 55.7 | 58.0 | 86.7 | 80.7 | 80.4 | 60.0 | 58.3 | 66.7 | 75.0 | 68.0 | 57.7 | 67.7 | 66.3 |
| **Plagioclase** | 48.3 | 46.7 | 61.0 | 58.7 | 51.7 | 52.3 | 78.7 | 76.3 | 71.7 | 0.0 | 0.0 | 53.0 | 55.3 | 62.3 | 55.3 | 63.7 | 60.7 |
| **Clinopyroxene** | 6.3 | 4.0 | 9.7 | 8.3 | 3.7 | 4.7 | 4.0 | 1.3 | 7.7 | 0.0 | 0.0 | 5.3 | 4.3 | 4.6 | 1.0 | 3.7 | 4.0 |
| **Olivine** | 1.7 | 0.7 | 1.3 | 0.0 | 0.3 | 0.7 | 0.7 | 0.0 | 0.7 | 0.0 | 0.0 | 1.3 | 1.3 | 0.3 | 0.7 | 0.3 | 1.7 |
| **Glass** | 6.3 | 17.3 | 3.3 | 3.0 | 0.0 | 0.3 | 3.3 | 3.0 | 0.3 | 60.0 | 58.3 | 7.3 | 14.0 | 0.7 | 0.7 | 0.0 | 0.0 |
| **Lithics** | | | | | | | | | | | | | | | | | |
| **Tuff** | 0.0 | 4.7 | 1.7 | 1.0 | 2.7 | 0.0 | 0.0 | 0.0 | 0.3 | 1.3 | 1.0 | 0.3 | 0.0 | 1.0 | 0.7 | 0.0 | 0.0 |
| **Sedimentary** | 0.0 | 0.0 | 0.3 | 0.0 | 0.0 | 0.0 | 0.0 | 0.0 | 0.0 | 0.7 | 1.3 | 0.0 | 0.0 | 0.0 | 0.0 | 0.0 | 0.0 |
| **Igneous** | 0.0 | 0.0 | 0.0 | 0.0 | 0.0 | 0.0 | 0.0 | 0.0 | 2.7 | 0.0 | 0.0 | 0.0 | 0.0 | 0.0 | 0.0 | 0.0 | 0.0 |
| **Quartz** | 0.0 | 0.0 | 0.0 | 0.0 | 0.0 | 0.0 | 0.0 | 0.0 | 0.0 | 0.0 | 0.0 | 0.0 | 0.0 | 0.0 | 0.0 | 2.0 | 0.0 |
| **Total Lithics** | 0.0 | 4.7 | 2.0 | 1.0 | 2.7 | 0.0 | 0.0 | 0.0 | 3.0 | 2.0 | 2.3 | 0.3 | 0.0 | 1.0 | 0.7 | 2.0 | 0.0 |
| **Totals** | 100.0 | 100.0 | 100.0 | 100.0 | 100.0 | 100.0 | 100.0 | 100.0 | 100.0 | 100.0 | 100.0 | 100.0 | 100.0 | 100.0 | 100.0 | 100.0 | 100.0 |

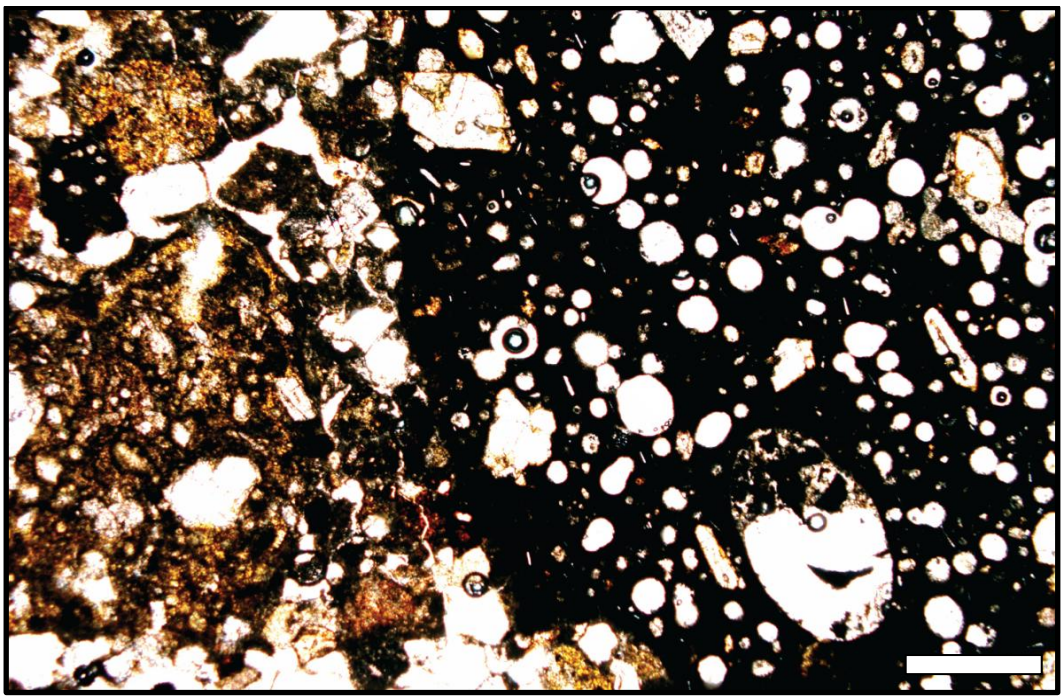

**Figure 4.13:** Photomicrograph of typical basalt clasts from the Raventhorpe tuff ring (R6). The smaller yellow and brown palagonite clasts (left) next to the black, highly vesicular sideromelane clast (right). PPL. Scale is 500 µm.

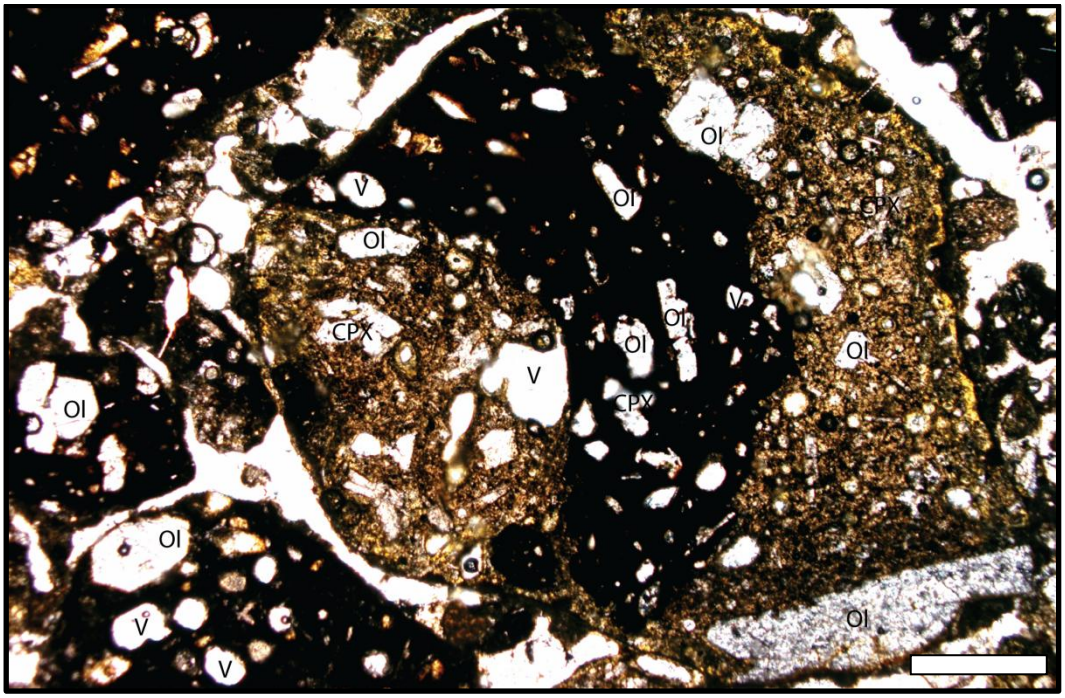


**Figure 4.14:** Photomicrograph of a basalt clast from the Raventhorpe tuff ring (R1). The vesicular black sideromelane clasts (lower left) include olivine. The clast in the centre predominantly comprised of palagonite, displays banding of sideromelane through the middle indicating variable amounts of alteration. PPL. Scale is 500 µm.

The SEM was used to study the microvesicular textures of the juvenile basalt clasts (Fig. 4.15). Vesicle size ranges from ~10-500 µm in diameter (Fig. 4.15). Small <100 µm vesicles are common with larger vesicles rarer. Voids are predominantly elliptical with some slightly irregular, especially in the larger size vesicles (Fig. 4.15). Vesicles are most commonly surrounded by glass and rarely seen contacting the sides of phenocrysts. Distribution appears to be relatively uniform regardless of vesicle size, however no preferred direction of elliptical elongation is observed (Fig. 4.15).

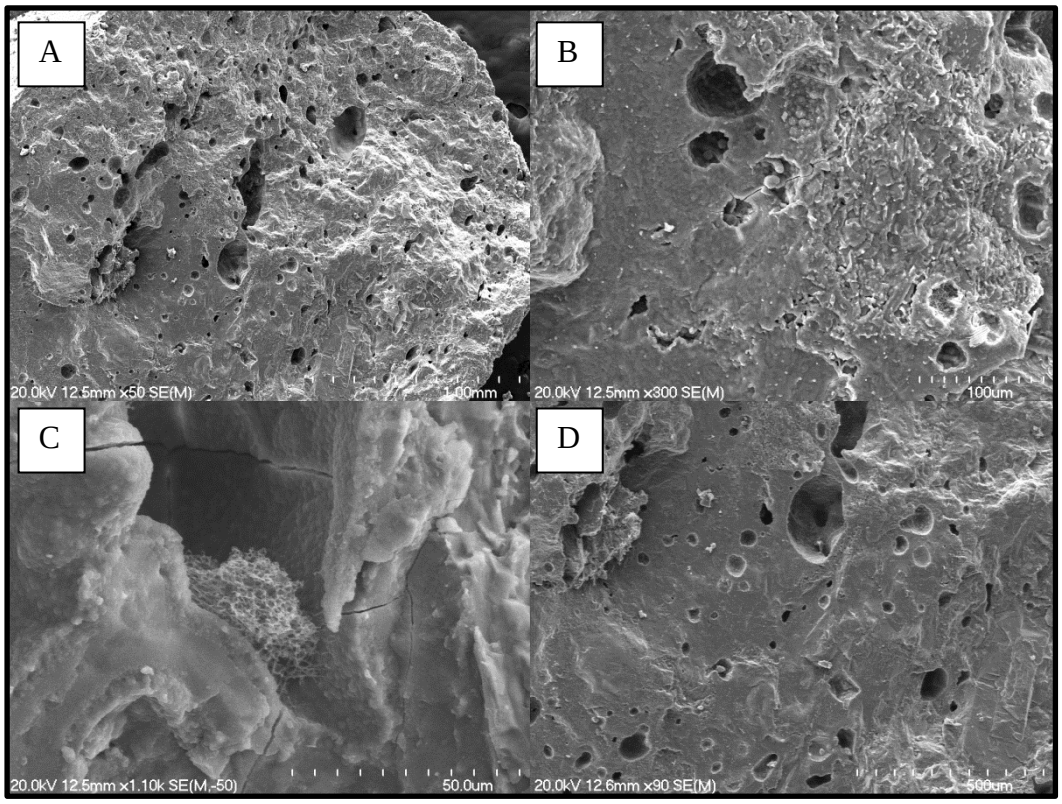


**Figure 4.15:** SEM images of juvenile basalt clasts. (A) delicate angular and vesicular pyroclast (Raventhorpe), (B) smooth mossy pyroclast (Pokeno West), (C) an elliptical vesicle lined with fine grained granular alteration minerals (Raventhorpe), (D) circular vesicles exposed along a fractured surface of a pyroclast (Pokeno West), note the phenocryst in the lower right.

The vesicularity data obtained from the method of Houghton and Wilson (1989) (Fig. 4.16) returned results that were comparable to those obtained for the pycnometer study using the method of Formenti and Druitt (2003) (Figs. 4.17, 18) (see appendix 4). These data display a bimodal distribution with two ranges (10-20% and 30-45%) accounting for the majority of clasts measured (Fig. 4.16).

Many values >40%, and few >50% vesicularity were observed using the Houghton and Wilson (1989) method (Fig. 4.16). Only several clasts recorded vesicularities >40% using the method of Formenti and Druitt (2003) (Figs. 4.17, 18). This could be due to the difficulty of coring brittle, weathered scoriaceous samples for analysis in the pycnometer, or the lack of larger, vesicular samples collected. Similarly to the data presented in Fig. 4.16, the data presented in Figs. 4.17 and 18 has very few recorded samples for the vesicularity range of 20-30%.

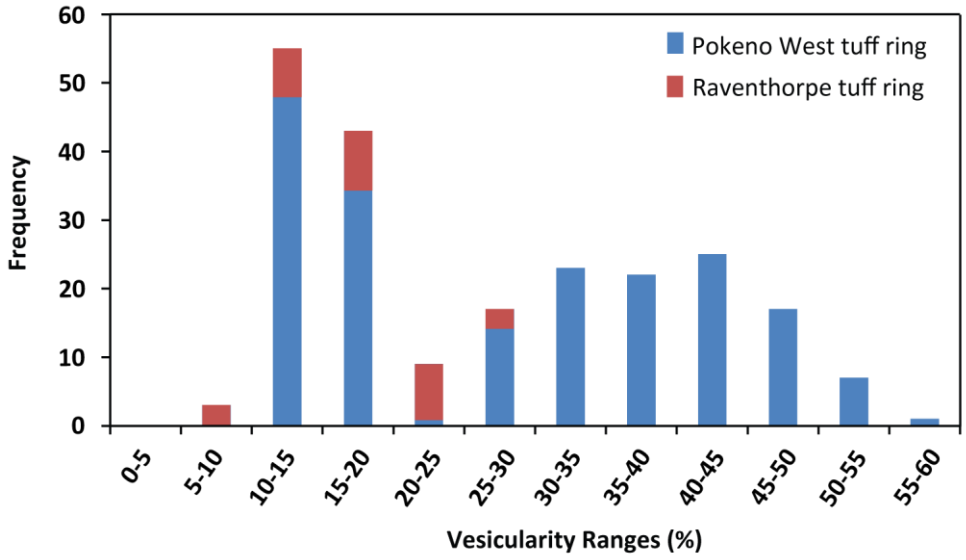


**Figure 4.16:** Vesicularities of juvenile basalt clasts picked from the Raventhorpe and Pokeno West tuff rings: 192 clasts from the Pokeno tuff ring, 30 clasts from the Raventhorpe tuff ring. Vesicularity was calculated using the method of Houghton and Wilson (1989).

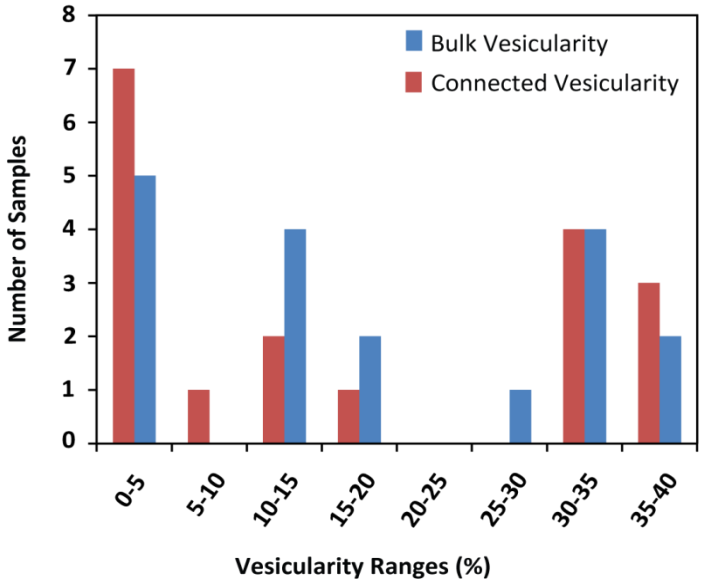


**Figure 4.17:** Frequency of vesicularity ranges for bulk and connected vesicularities from 1.5" pycnometer cores measured from Raventhorpe and Pokeno West tuff rings.

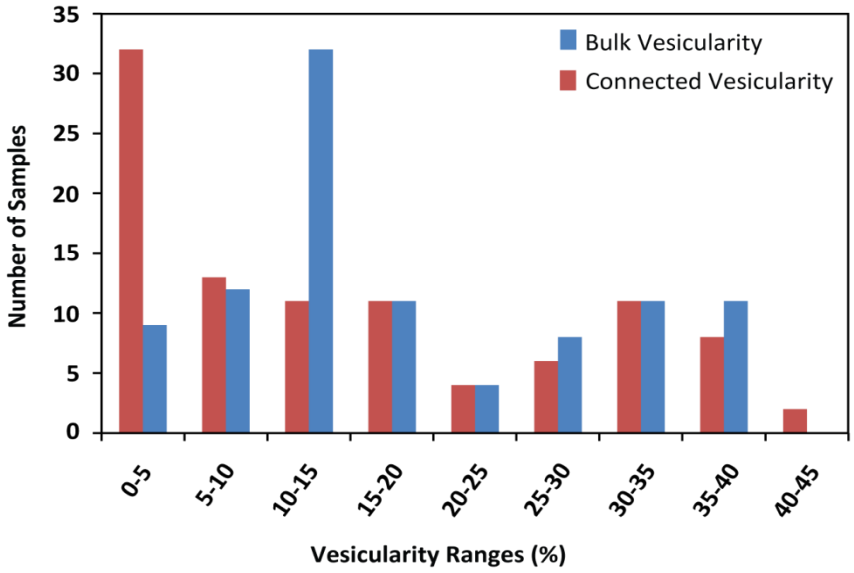


**Figure 4.18:** Frequency of vesicularity ranges for bulk and connected vesicularities from 1" pycnometer cores measured from Raventhorpe and Pokeno West tuff rings.

Plotting the connected and bulk vesicularity data with a linear trendline illustrates how interconnected the vesicles are (Formenti & Druitt, 2003). Points that plot above the trendline indicate the vesicles are interconnected. Data that plot below the line indicate the presence of isolated vesicles. The data observed for the large core samples is sporadic and no trend can be concluded from the data (Fig. 4.19).

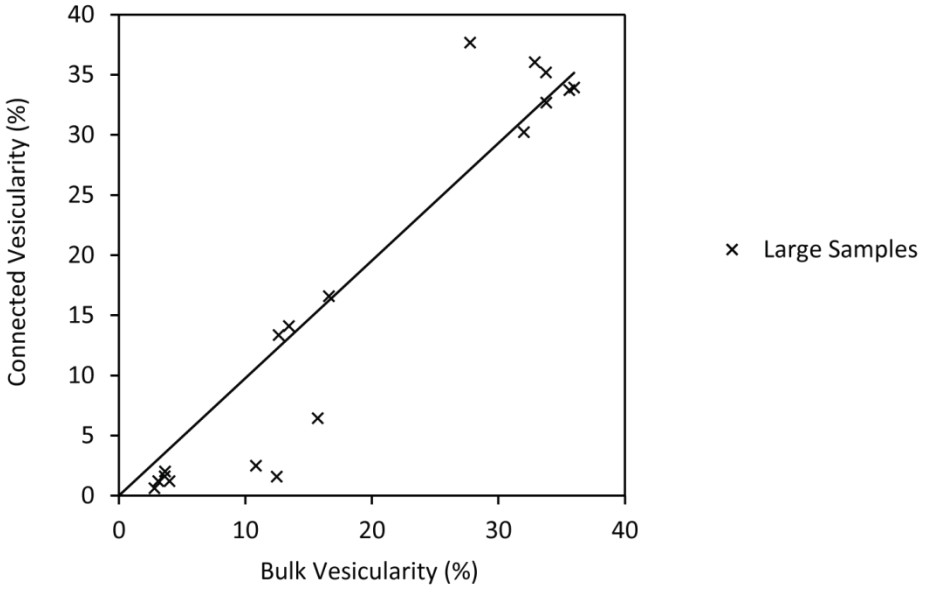


**Figure 4.19:** Connected vesicularity versus bulk vesicularity for 1.5" pycnometer core samples of juvenile basalt from Raventhorpe and Pokeno West tuff rings.

The data presented in Fig. 4.20 is more comprehensive due to the large sample population for the two study locations. Data from this study indicate the dense, low vesicular clasts have more isolated vesicles than the less dense, more vesicular clasts (Fig. 4.20). These less dense clasts appear unable to hold gas due to the effective total interconnectivity of the vesicles.

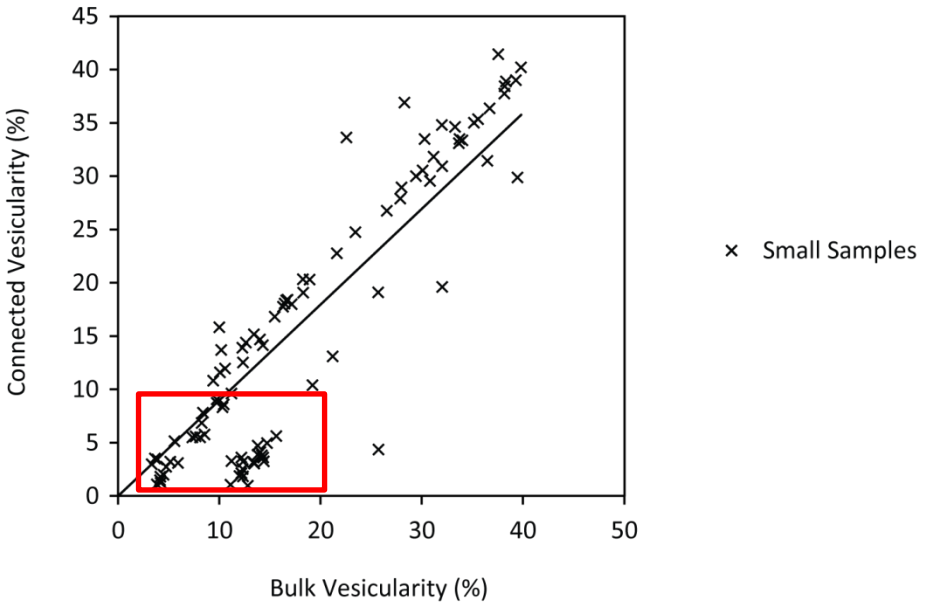


**Figure 4.20:** Connected vesicularity versus bulk vesicularity for 1" pycnometer core samples of juvenile basalt from Raventhorpe and Pokeno West tuff rings. The red box indicates dense, low vesicular samples with isolated vesicles.

## Trachydacite

Only one sample of this type was identified geochemically (see chapter 5) (due to the high $SiO_2$ and alkali values), and occurred as a brittle, weathered, scoriaceous clast (Fig. 4.21) picked out of the tuff at Pokeno West tuff ring, believed to be juvenile in origin. The sample is light and glassy in hand specimen (Fig. 4.21) and petrographically in part it resembles the andesite described earlier. It is fine grained, vitrophyric, hypocrystalline and poorly vesicular (Table 4.9).

Olivines, clinopyroxenes and rare plagioclase were the only phenocryst and microphenocryst phases observed.

**Figure 4.21:** Hand specimen of trachydacite sample (P3 S2), displaying a slightly scoriaceous, angular brittle texture.

Anhedral olivine crystals are completely altered to iddingsite (Fig. 4.22). Clinopyroxene crystals are small, and like olivine they are irregularly shaped. Plagioclase crystals are rare and occur as singular thin laths. No clustering was observed.

The high geochemical values of $SiO_2$ and alkalis obtained in this sample could perhaps be due to the inclusion of many lithics from the underlying Pleistocene gravels, and the high glass content of the rock observable in fig. 4.23.

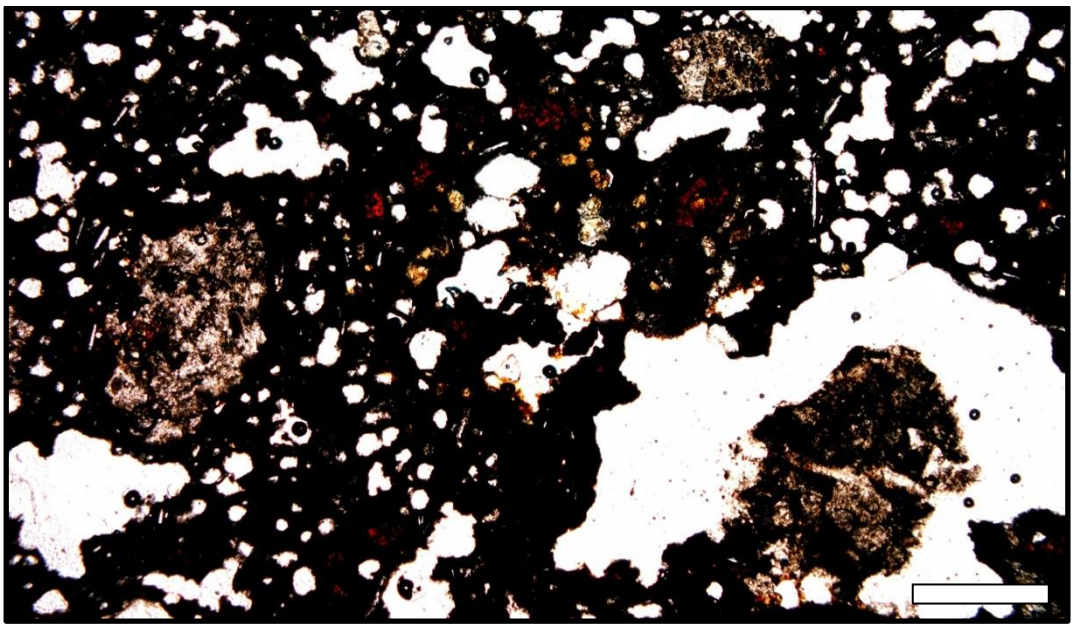

**Figure 4.22:** Photomicrograph of the trachydacite sample (P3S2). Sample is vitrophyric, hypocrystalline, fine grained, and highly vesicular. Olivine crystals are completely altered to iddingsite. Note the three xenoliths occurring in the lower right, middle left, and upper middle. Such xenoliths are common in this sample. PPL. Scale is 500 µm.

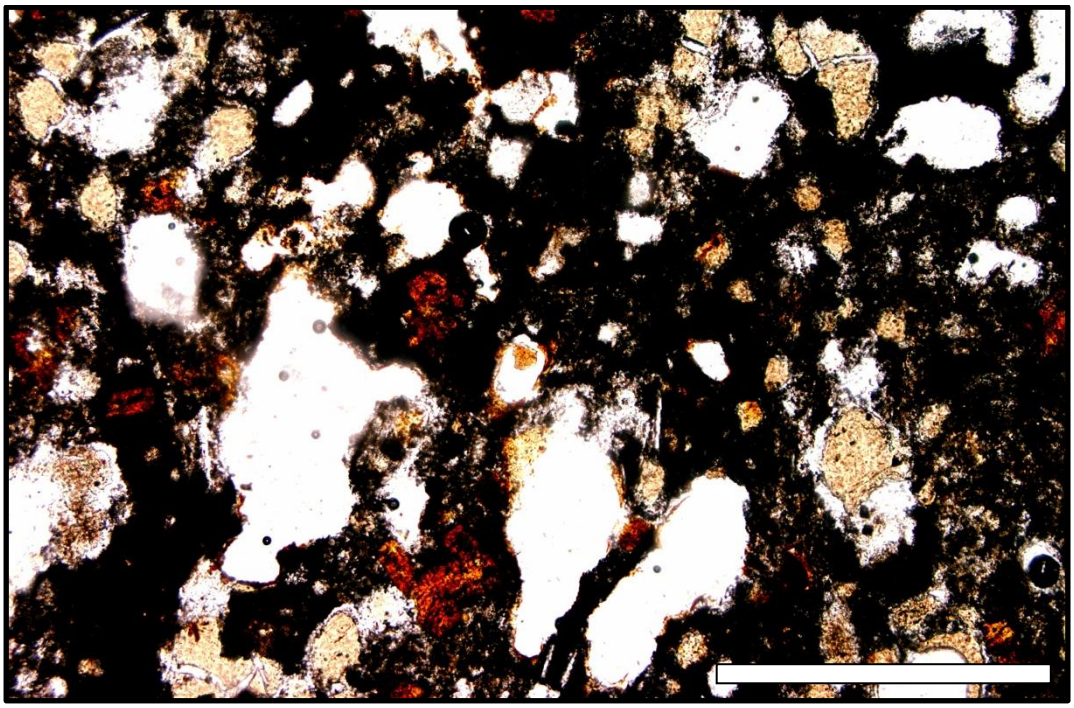

**Figure 4.23:** Photomicrograph of the trachydacite sample (P3S2). Olivine phenocrysts are completely altered to iddingsite. Note the blocky pale brown glass shards infilling or lining the vesicle walls. PPL. Scale is 500 µm.

### 4.5.2 Accretionary Lapilli

Accretionary lapilli were observed and recorded from the Raventhorpe and Ingram Road III tuff rings. They are apparent in hand specimen, but were not observed in thin section. Rosenberg (1991) noted the presence of accretionary lapilli in the field and in thin section at several centres, but concluded that despite their abundance in the deposits they are not always obvious or present in thin section. Rosenberg (1991) described accretionary lapilli in thin section broadly as small spherical clasts of fine lapilli size (2-4 mm), predominantly light brown to brown in colour, consisting of a fine ash core encased by slightly coarser ash. From hand specimen and observation under hand lens, a few of these features can be observed including the colour, spherical shape, and the thin slightly coarser ash rim (Fig 4.24). No accretionary lapilli were observed at Pokeno West tuff ring.

**Figure 4.24:** Hand specimen from the Ingram Road tuff ring III tuff ring. The presence of accretionary lapilli is evident from the thin ash rinds surrounding the ash centres in various shades of browns and light yellows. Scale is 10 mm.

### 4.5.3 Alteration Products of the Matrix

The matrix of the tuff rings in the SAVF consist of alteration products derived from basaltic glass shards. The fine ash matrix has a light brown, occasionally pale yellow colouration with no observable shard morphology evident in thin section. Throughout all samples at Raventhorpe, Ingram Road, and Pokeno West tuff rings, palagonite was the only alteration product observed. Rosenberg (1991) observed several other secondary mineral phases petrographically, including smectite, zeolite, calcite, and chlorite. None of these were identified in this study.

Palagonite is a highly variable (especially in colour and structure) secondary alteration product that occurs from the interaction between water and volcanic glass (Michalski, *et al.*, 2005). It is the first stable product of this interaction (Stroncik & Schminke, 2002). Palagonatisation can also occur via the slow weathering of basalt lava (Michalski, *et al.*, 2005). The different colours and shades observed in this study, indicate different structures and degrees of weathering (Stroncik & Schminke, 2002).

Two types of palagonite occur. The first, known as gel-palagonite, consists of smooth, banded material, ranging from clear to isotropic. The second fibropalagonite, is anisotropic, commonly birefringent, consisting of a fibrous or lath-like structure (Stroncik & Schminke, 2002). The tuff samples from the three tuff rings exhibit the features, colouration, and structure resembling gel palagonite (Fig. 4.25). These can be observed as the pale colouration and overall consistent smooth texture of the tuff.

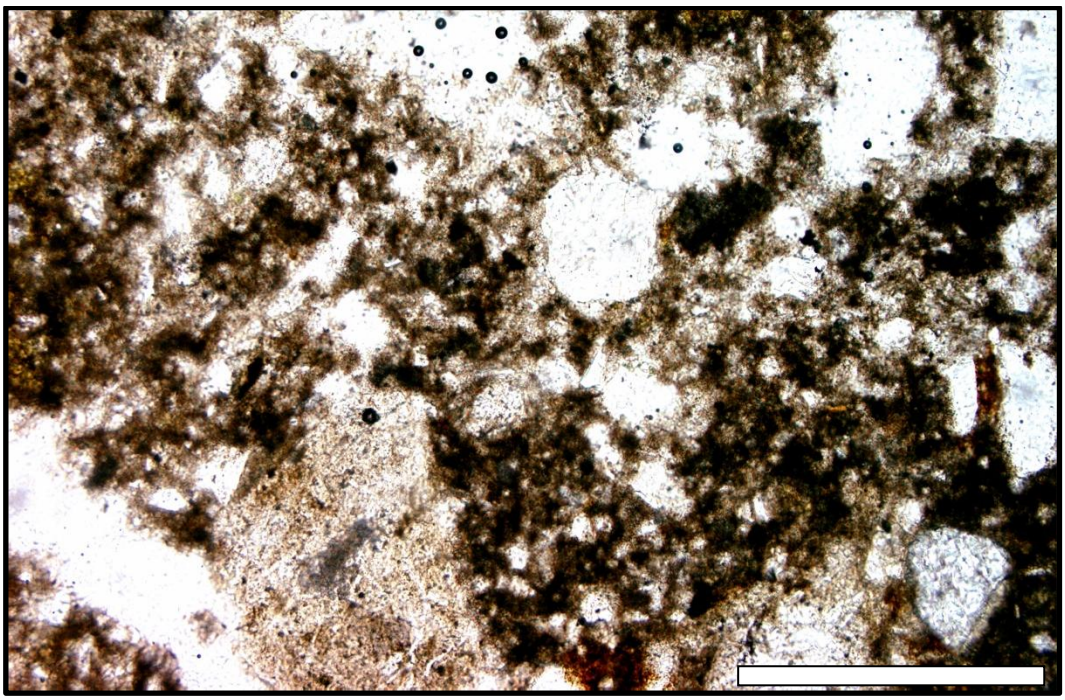

**Figure 4.25:** Photomicrograph of the altered tuff ring matrix from the Ingram Road tuff ring III tuff ring (I9). Several crystals are set in the light brown palagonite. PPL. Scale is 500 µm.

The matrix components of the tuff were investigated using the SEM (Fig. 4.26). Whole grains, commonly ~200 µm, of fine basalt clasts, lithics and crystals were observed. Crystals commonly display sharp faces distinguishing themselves from sub-rounded to sub-angular basalt clasts of similar size (Fig. 4.26B, D). Crystal size ranges greatly, however the majority are ~80 µm with prismatic or irregular habits (Fig. 4.26A, B, D). Closer observation of the grains reveals palagonite alteration products commonly showing cracks (Fig. 4.26C), likely produced by "pull-apart" of hydrated skin (Wohletz & Krinsley, 1982). Strongly defined, angular faces exist within the palagonite where crystals or blocky glass shards protrude (Fig. 4.26D). The presence of small particles (likely of juvenile origin) and modern biological material, commonly string-like, occurs throughout the tuff samples studied (Fig. 4.26).

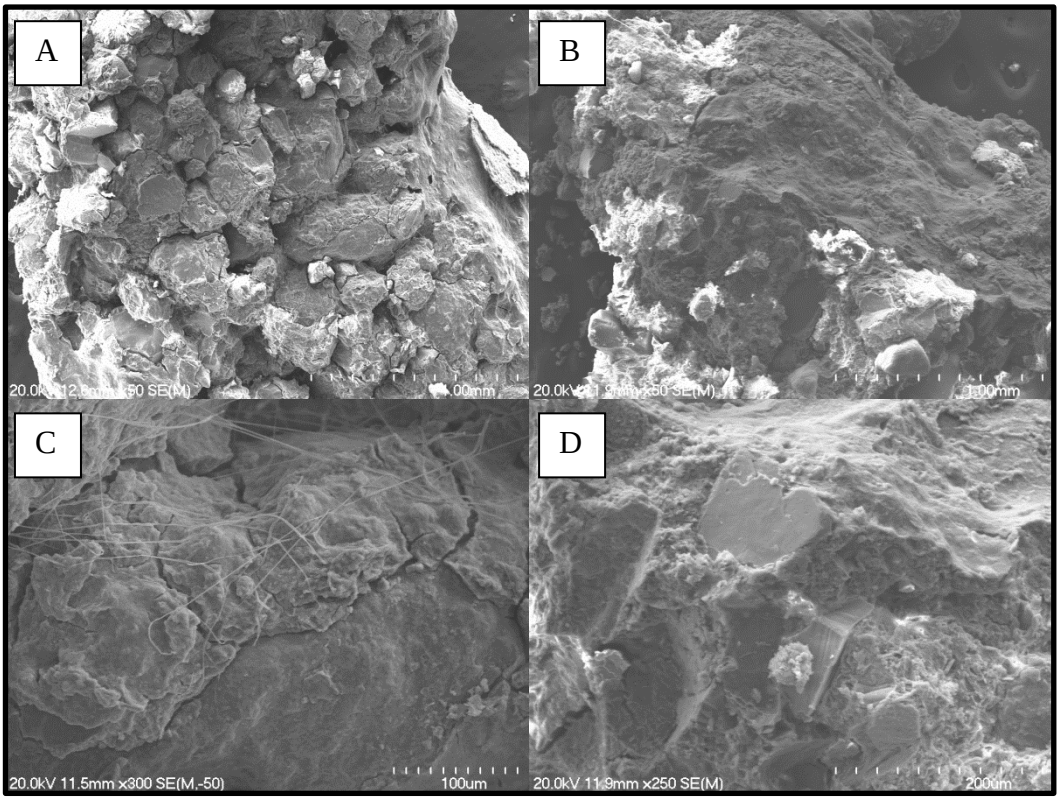


**Figure 4.26:** SEM images of the tuff matrix and alteration products. (A) component grains comprising the matrix (B) smooth mossy surface of alteration products of the matrix, (C) alteration products of the matrix showing palagonite cracks, likely produced by pull apart (note: fibre represents modern biological material), (D) fine grained matrix alteration products and prismatic, blocky crystal faces.

### 4.5.4 Accidental Components

The foreign material that partly comprises the tuff, consists of accessory sedimentary and igneous lithics, and xenocrysts derived from the underlying geological units. These lithic components are an important constituent of the tuff and range in abundance from 0-22% (Tables 4.7, 8).

#### Sedimentary Accessory Lithics

Determination of the units and formations which were involved in the eruption can help constrain eruption dynamics based on the units' physical and hydrological parameters. Accessory lithics represent the underlying geological units implicated in the eruption sequence. These formations have been previously described by Kear (1957), Kear and Schofield (1978), and Gibson (2011). Lithics include the Koheroa Siltstone, a well sorted fine grained calcareous rock mineralogically comprising of fine quartz and plagioclase feldspars, and calcite. Otaian in age (Kear & Schofield, 1978), it contains many benthic foraminifera

representative of the late-mid Miocene (Gibson, 2011) and in some areas in the Manukau Lowlands can reach thicknesses of up to 75 meters (Edbrooke, 2001).

Sedimentary lithics of various shapes (rounded to irregular) and sizes (0.4-20 mm) are evident throughout the three tuff ring locations sampled, in the field and in thin section. These lithics included: calcareous, light grey to off-white coloured siltstones (likely Waitemata Group), pale yellow, well sorted, medium sandstones (likely Kaawa Formation), and other sedimentary rocks. Correlation between these lithics and the formations from which they were derived are sometimes possible.

## Igneous Accessory Lithics

Igneous accessory lithics in the tuff rings of the SAVF consist of fragments of pre-existing basalt which has been incorporated by ascending magma or derived from wall collapse during vent widening before being deposited.

The presence of accessory basalt lithics from previous eruptives can be distinguished from the abundant juvenile basalt clasts within the tuff from their texture and composition (Fig. 4.27). Igneous accessory lithics can be hypocrystalline or hypercrystalline containing large, often iddingsitised olivine, clinopyroxene, and plagioclase phenocrysts set in an intergranular or intersertal plagioclase groundmass. This is contrasting to the crystal poor, often vesicular, glass rich hypocrystalline groundmass observed in the juvenile basalt clasts. The lithics have originated as pre-existing lava flows to become incorporated into the tuff during the eruption. Such lithics are evident and quite common in thin section throughout all samples, and as blocks within the tuff.

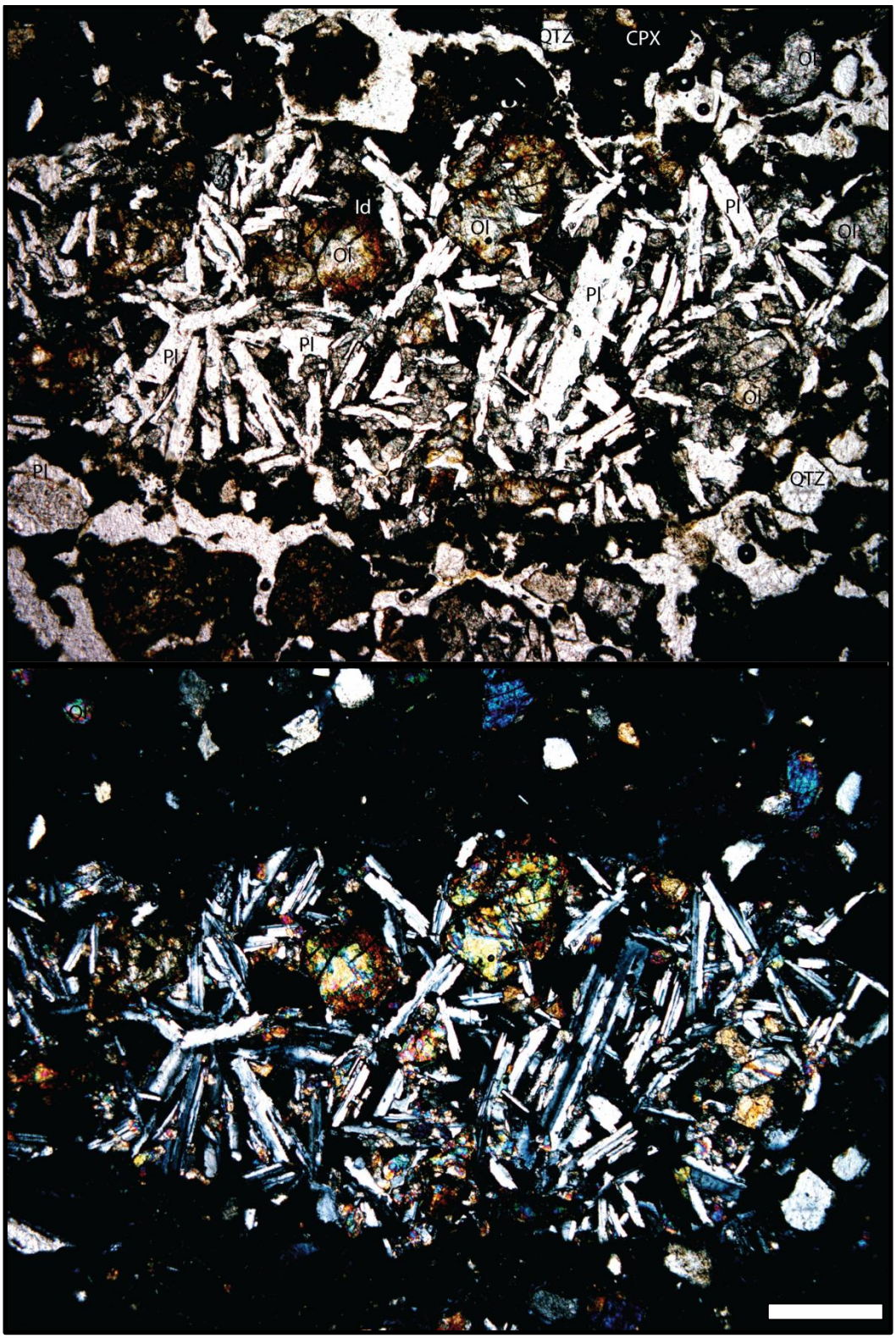


**Figure 4.27:** Accessory igneous basalt lithic observed in the tuff at Raventhorpe tuff ring (R1). These types of cognate lithics are common. All comprise of a plagioclase groundmass in which olivine, and clinopyroxene phenocrysts and microphenocrysts are set. PPL (above), XPL (below). Scale is 500 µm.

## Xenocrysts

Many different free crystals occurring in the tuff are observable in thin section. Several of these minerals are incompatible in basaltic melts and therefore must be derived from another source. Xenocrysts observed in the tuff at Raventhorpe, Ingram Road tuff ring III, and Pokeno West tuff rings include: hornblende, quartz, plagioclase, and hypersthene (Fig. 4.28A, B, C). Identification of plagioclase as a xenocryst is based primarily on size and texture. Juvenile phenocrysts are irregular or lath-like and smaller, whereas xenocrysts occur as larger, smooth, and well-rounded in blocky habits (Fig. 4.28B). In addition glauconite pellets were observed (Fig. 4.28) throughout the tuff ring deposits and are especially abundant within the tuff at Raventhorpe. The xenocrysts are likely derived from underlying

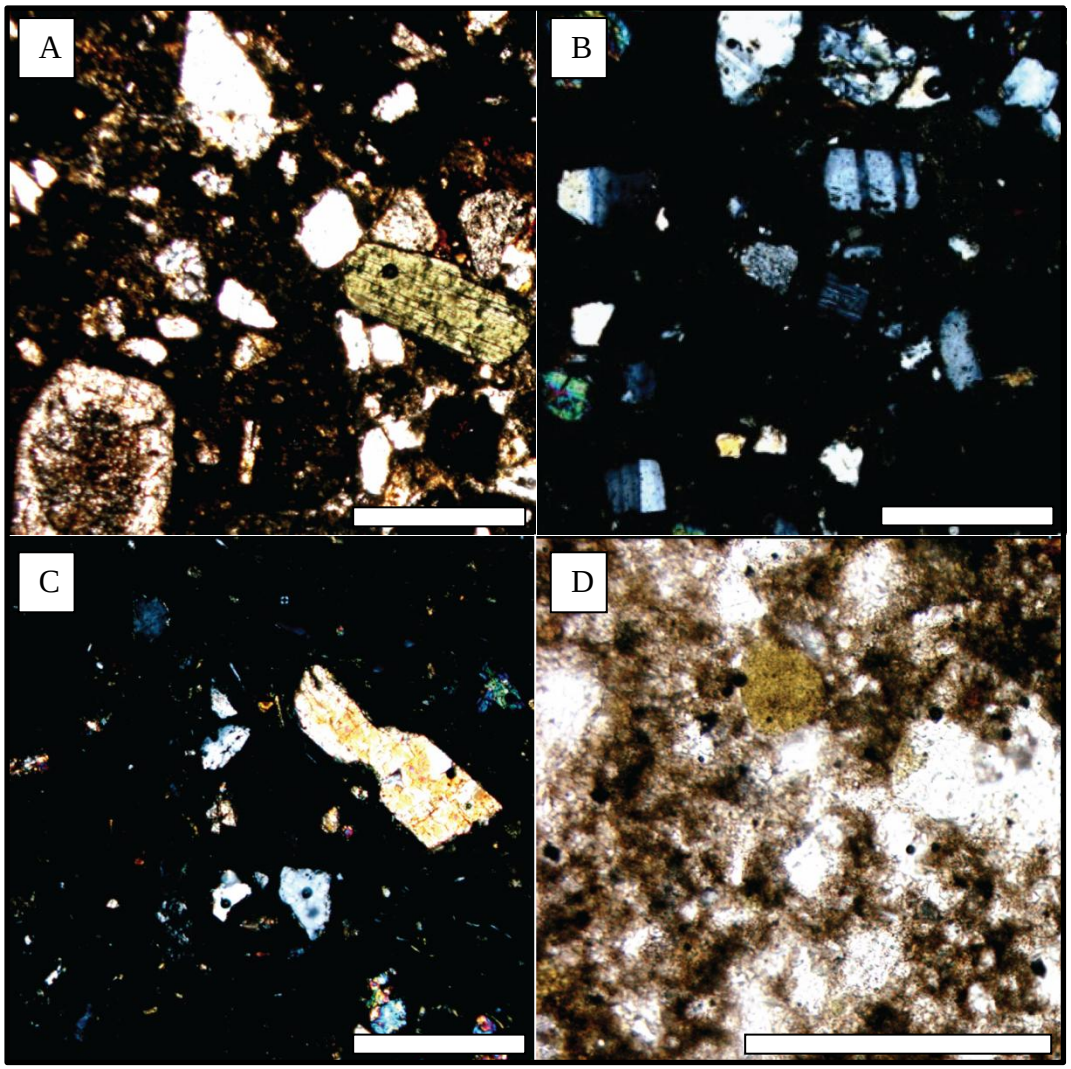


**Figure 4.28:** Photomicrograph of selected xenocrysts and a glauconite pellet from the Raventhorpe and Pokeno West tuff rings. A/ hornblende, PPL (Raventhorpe, R2), B/ plagioclase, XPL (Raventhorpe, R6), C/ quartz, XPL (Ingram Road tuff ring III, I4), D/ glauconite pellet, PPL (Raventhorpe, R1). Scales are 500 µm.

sedimentary sequences such as the Pliocene Kaawa Formation, or are present due to the widespread nature of silicic volcanism occurring in the Coromandel Volcanic Zone and during the early onset of the TVZ at the time the SAVF was active. These are most notable in the facies 1, 2, and 5 at Raventhorpe, and facies 1, 2, and 3 at Pokeno West.

On rare occasion, extremely large (2-5 mm) crystals of olivine and rarer pyroxene (Fig. 4.29) were observed within the tuff samples from the three locations. The crystals are several times larger than the juvenile megacrysts occurring in the sample and display different petrographic textures and properties to the phenocrysts and megacrysts. Resorbed crystal margins displaying rounded or embayed textures from contact with the host melt is evidence for xenocrystal origin (Sanders, 1994). Xenocrysts observed in this study occur in subhedral, elongate, or irregular forms, with often embayed, rounded or corroded rims. Olivine xenocrysts occasionally show parallel fractures, possibly due to peridotite wall-rock being hydraulically fractured by ascending magmas (Nicholas, 1986; Wilshire & Kirby, 1989; Klűgel, 1997). Pyroxene crystals occasionally have a reaction rim ~20-50 µm thick of irregularly orientated clinopyroxene crystals.

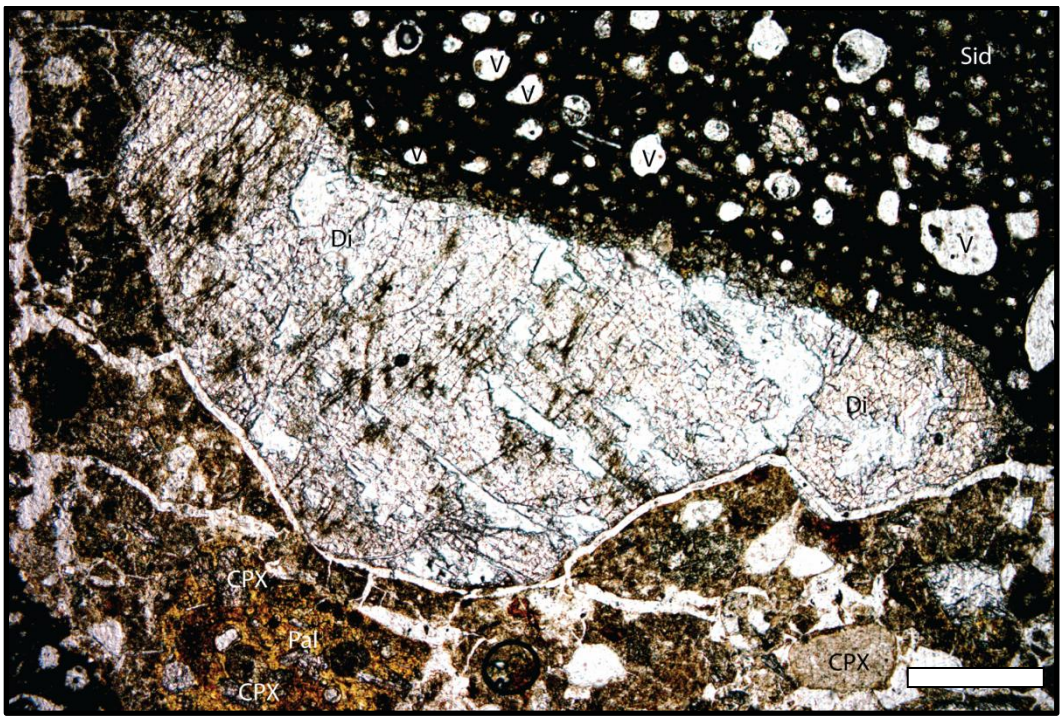


**Figure 4.29:** Photomicrograph of a diopside, mantle derived xenocryst occurring in the tuff at Raventhorpe (R1). The large diopside (Di) xenocryst is attached to the vesicular, black sideromelane (Sid) clast. A reaction rim around the clast is present. Selected clinopyroxene (CPX), olivine (Ol), palagonite (Pal), and vesicles (V), are identified. PPL. Scale is 500 µm.

# Chapter Five

# Geochemistry

## 5.1 Introduction

Two types of basalts occur in the SAVF and are divided by Rafferty and Heming (1979) based on their differences in geochemical composition. Rafferty and Heming (1979) identified basalts with subalkalic and alkalic compositions, terming the basalts group A and B respectively. The relationships between the two groups and between rock types are described with particular importance in terms of whole rock major and trace elements, and microprobe data on minerals (see appendix 5). Samples analysed include individual juvenile pyroclasts, lavas, and basaltic boulders, and were categorised based on the methodology of chapter 4 (Petrography), according to the classification used by Cook (2002).

## 5.2 Identification

The CIPW normative classification identified four basalts in this study: basanites, alkali olivine-basalts, transitional basalts, and olivine-tholeiitic basalts (Tables 5.1, 5.2). Two samples were classified as andesite and trachydacite based on their $SiO_2$ weight percent, 61.96% and 66.3% respectively, and so have been excluded from many of the results; their origin is discussed later.

Based on Cook (2002) and Cook *et al.* (2005) discrimination of group A and B basalts is best determined from abundances of HFSE, i.e. Nb and Zr. Subalkaline group A basalts have low HFSE abundances of Nb (9-29 ppm), and Zr (97-219 ppm), while group B basalts are comparatively much higher (Nb 35-102 ppm) (Zr 194-491 ppm).

**Table 5.1:** Major elements and rock type classification of lava and juvenile basalt samples from the two study areas in the SAVF.

| **Rock Type** | Basanite | | Transitional Basalt | Olivine-tholeiitic basalt | | | Alkali olivine-basalt | | | | Andesite | Trachydacite |
|---|---|---|---|---|---|---|---|---|---|---|---|---|
| **Basalt Group** | B | | A | A | | | A | | B | | - | |
| **Sample** | BF3S1 | BF7S1 | R19 | BF4S1 | HS3 | R4 | HS1 | BF5S1 | BF6S1 | BF2S1 | BF3S2 | P3S2 |
| **Location** | Rutherford Road cone | | Raventhorpe tuff ring | Pukekohe East School | Great South Road | Raventhorpe tuff ring | Great South Road | Ambush Road | Pokeno West tuff ring | Ingram Road | Rutherford Road | Pokeno West tuff ring |
| **$SiO_2$** | 42.45 | 46.30 | 48.69 | 47.77 | 45.06 | 47.32 | 47.76 | 45.26 | 45.44 | 46.49 | 61.69 | 66.30 |
| **$TiO_2$** | 2.85 | 2.68 | 2.11 | 1.60 | 2.09 | 2.12 | 2.28 | 2.82 | 1.93 | 2.86 | 0.81 | 0.65 |
| **$Al_2O_3$** | 12.35 | 14.28 | 13.55 | 13.30 | 16.10 | 14.14 | 14.28 | 14.29 | 14.76 | 14.29 | 16.52 | 15.68 |
| **$Fe_2O_3$** | 14.38 | 13.90 | 13.50 | 13.46 | 14.26 | 14.00 | 13.24 | 14.35 | 13.61 | 14.07 | 6.41 | 4.88 |
| **MnO** | 0.19 | 0.21 | 0.16 | 0.18 | 0.17 | 0.16 | 0.14 | 0.20 | 0.17 | 0.17 | 0.09 | 0.06 |
| **MgO** | 10.82 | 7.35 | 7.77 | 7.51 | 8.60 | 7.35 | 7.73 | 6.56 | 8.09 | 7.29 | 2.61 | 1.4 |
| **CaO** | 9.76 | 8.18 | 8.80 | 7.75 | 6.71 | 8.55 | 7.95 | 8.14 | 7.18 | 8.37 | 2.83 | 1.94 |
| **$Na_2O$** | 2.68 | 4.08 | 3.29 | 3.03 | 2.50 | 3.20 | 3.73 | 3.39 | 3.69 | 3.25 | 3.70 | 6.12 |
| **$K_2O$** | 1.18 | 1.55 | 0.48 | 0.38 | 0.30 | 0.30 | 0.97 | 1.48 | 0.4 | 1.07 | 2.69 | 2.04 |
| **$P_2O_5$** | 0.60 | 0.61 | 0.27 | 0.14 | 0.29 | 0.44 | 0.40 | 0.57 | 0.26 | 0.46 | 0.19 | 0.16 |
| **LOI** | 2.06 | 0.58 | 0.76 | 1.44 | 5.14 | 2.11 | 1.62 | 2.34 | 2.59 | 1.07 | 2.72 | 2.62 |
| **Total** | 99.32 | 99.72 | 99.39 | 96.56 | 101.22 | 99.68 | 100.11 | 99.41 | 98.11 | 99.39 | 99.98 | 101.85 |

**Table 5.2:** Trace elements and rock type classification of lava and juvenile basalt samples from the two study areas in the SAVF.

| **Rock Type** | Basanite | | Transitional Basalt | Olivine-tholeiitic basalt | | | Alkali olivine-basalt | | | | Andesite | Trachydacite |
|---|---|---|---|---|---|---|---|---|---|---|---|---|
| **Basalt Group** | B | | A | A | | | A | | B | | - | |
| **Sample** | BF3S1 | BF7S1 | R19 | BF4S1 | HS3 | R4 | HS1 | BF5S1 | BF6S1 | BF2S1 | BF3S2 | P3S2 |
| **Location** | Rutherford Road cone | | Raventhorpe tuff ring | Pukekohe East School | Great South Road | Raventhorpe tuff ring | Great South Road | Ambush Road | Pokeno West tuff ring | Ingram Road | Rutherford Road | Pokeno West tuff ring |
| **S** | 215 | 159 | 135 | 87 | 232 | 110 | 92 | 88 | 212 | 91 | 527 | 120 |
| **Cl** | 57 | 91 | 50 | 58 | 2836 | 52 | 54 | 75 | 88 | 36 | 62 | 62 |
| **V** | 263 | 185 | 216 | 233 | 202 | 262 | 190 | 195 | 201 | 196 | 154 | 95 |
| **Cr** | 377 | 202 | 325 | 293 | 276 | 303 | 237 | 231 | 219 | 182 | 77 | 36 |
| **Co** | 101 | 82 | 82 | 106 | 101 | 84 | 86 | 80 | 73 | 82 | 37 | 25 |
| **Ni** | 286 | 129 | 232 | 200 | 190 | 242 | 175 | 165 | 148 | 175 | 33 | 16.2 |
| **Cu** | 74 | 51 | 60 | 87 | 59 | 70 | 36 | 61 | 58 | 43 | 27 | 18.4 |
| **Zn** | 112 | 107 | 132 | 115 | 129 | 128 | 120 | 114 | 126 | 125 | 89 | 77 |
| **Ga** | 22 | 23 | 21 | 21 | 25 | 24 | 24 | 25 | 25 | 25 | 20 | 17.9 |
| **Ge** | - | - | 1 | 1.1 | 0.9 | - | 0.6 | 0.9 | 0.7 | 0.7 | 1.1 | 1 |
| **As** | - | - | - | - | - | 0.8 | - | - | - | - | 6.6 | 5.7 |
| **Se** | - | 0.4 | 0.4 | 0.5 | 0.4 | - | 0.3 | 0.4 | 0.4 | - | 1.1 | 0.8 |
| **Br** | 1.8 | 0.7 | 0.9 | 2.5 | 3.9 | 0.6 | 0.4 | 2.2 | 2.2 | 1.3 | 0.4 | 0.2 |
| **Rb** | 21 | 22 | 5.6 | 7.9 | 2.9 | 3.3 | 18.9 | 5.8 | 20 | 19.9 | 92 | 57 |
| **Sr** | 607 | 708 | 314 | 196 | 230 | 346 | 422 | 278 | 713 | 495 | 493 | 397 |
| **Y** | 23 | 24 | 25 | 111 | 21 | 30 | 29 | 22 | 24 | 25 | 30 | 29 |
| **Zr** | 262 | 295 | 142 | 106 | 155 | 146 | 175 | 148 | 317 | 196 | 192 | 184 |
| **Nb** | 54 | 47 | 16.9 | 10.1 | 16.5 | 18 | 24 | 15.6 | 51 | 30 | 9.3 | 7.9 |
| **Mo** | 4.8 | 5.2 | 2.8 | 2.4 | 2.4 | 2.6 | 2.6 | 2.4 | 4.5 | 3 | 2.2 | 1.4 |
| **Sn** | 1 | 1.6 | 0.6 | - | 0.8 | 1.1 | 0.8 | 0.9 | 1.5 | 0.9 | 2.3 | 2 |
| **Sb** | - | - | - | 0.4 | - | - | - | - | - | - | 1.2 | 1.3 |
| **Te** | - | - | - | - | - | - | - | - | - | - | 2 | 2.5 |
| **Ba** | 224 | 220 | 128 | 70 | 249 | 141 | 213 | 164 | 288 | 202 | 557 | 645 |
| **La** | 26 | 27 | 8.2 | 111 | 5.8 | 17.7 | 17.9 | 7 | 26 | 16.8 | 50 | 45 |
| **Ce** | 62 | 63 | 21 | 25 | 20 | 24 | 33 | 25 | 63 | 42 | 77 | 78 |
| **Nd** | 29 | 23 | 16.2 | 60 | 9.9 | 15.2 | 19.9 | - | 26 | 19.1 | 61 | 43 |
| **Hf** | 6.3 | 5.8 | 5.1 | 5.5 | 4.7 | - | 5 | 3.2 | 5.9 | 4.4 | 8.1 | 6.9 |
| **Ta** | - | 7.2 | - | - | - | - | - | - | 8.4 | - | 6.9 | 4.2 |
| **Tl** | 1.4 | 1.5 | 1.4 | 1.1 | 0.9 | 1.2 | 0.8 | 1 | 1.3 | 0.9 | 1.9 | 2.2 |
| **Pb** | 4.2 | 5.1 | 3.3 | 2.9 | 4.1 | 3.6 | 61 | 4.5 | 5.8 | 4 | 15.4 | 20.3 |
| **Bi** | - | - | - | 1.1 | - | - | - | 0.8 | 0.8 | - | 0.9 | 1.5 |
| **Th** | 5.8 | 6.3 | 3.3 | 3 | 4 | 3.9 | 5.2 | 4.1 | 6.3 | 4.9 | 14.5 | 13.7 |
| **U** | 6.5 | 5.3 | 5.8 | 6.7 | 5.9 | 3.6 | 5 | 6.4 | 6 | 6.3 | 5.9 | 5.7 |

Samples were also classified based on their total alkalis versus silica (TAS) abundance (Fig. 5.1). With the exception of two samples plotting as an andesite and a trachydacite, all samples plotted in the basalt, basanites, and trachybasalt regions. Furthermore some discrimination of group A and B basalts can be made from Fig. 5.1. Group A basalts dominantly plotting in the subalkaline field, and group B plotting in the alkaline field. Basalts of group A comprise the alkali olivine-basalts, and olivine-tholeiitic basalts while those of group B comprise basanites and alkali olivine-basalts (Tables 5.1, 5.2).

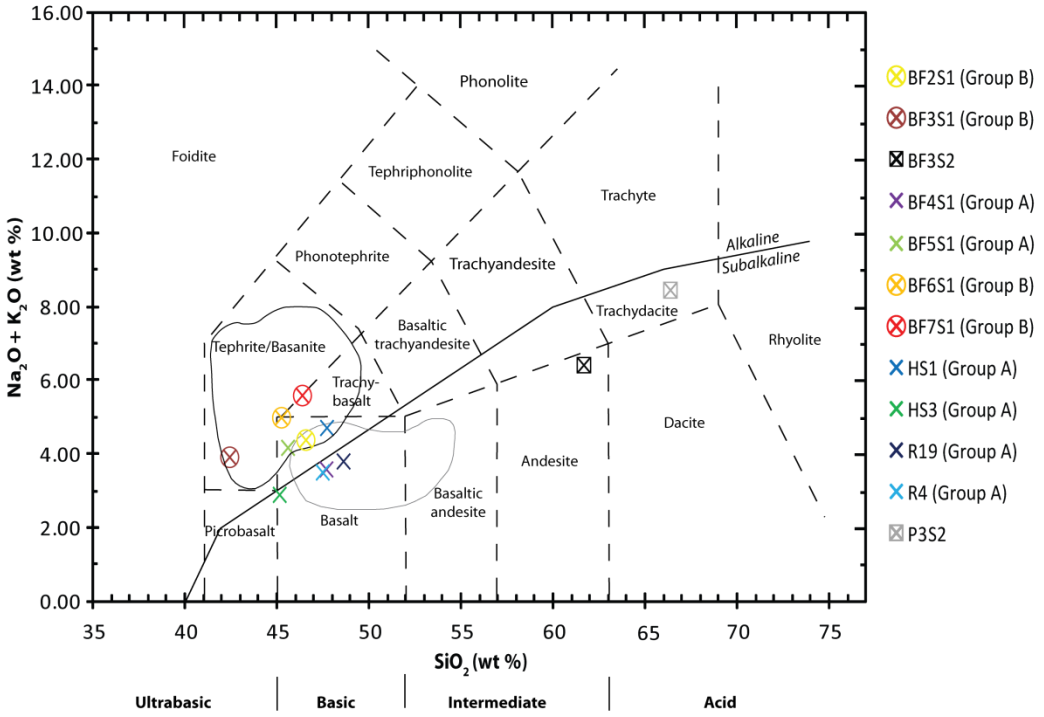


**Figure 5.1:** Total alkalis versus $SiO_2$ plot for basalt samples throughout the two study areas. The light grey outline indicates the range of values for subalkalic (group A) basalts while the black outline indicates the range of values for the alkali (group B) basalts in the SAVF from Cook (2002). The two outliers (BF3S2 and P3S2) are assigned a cross surrounded with a box.

## 5.3 Major Element Geochemistry

The data (Table 5.1) are generally in agreement with the range of expected results for the SAVF as obtained by Cook (2002), except for the samples of BF3S2 (andesite) and P3S2 (trachydacite). The data indicate several trends across the four major elements plotted against MgO ($SiO_2$, $TiO_2$, $Al_2O_3$, and $Fe_2O_3$) (Fig 5.2).

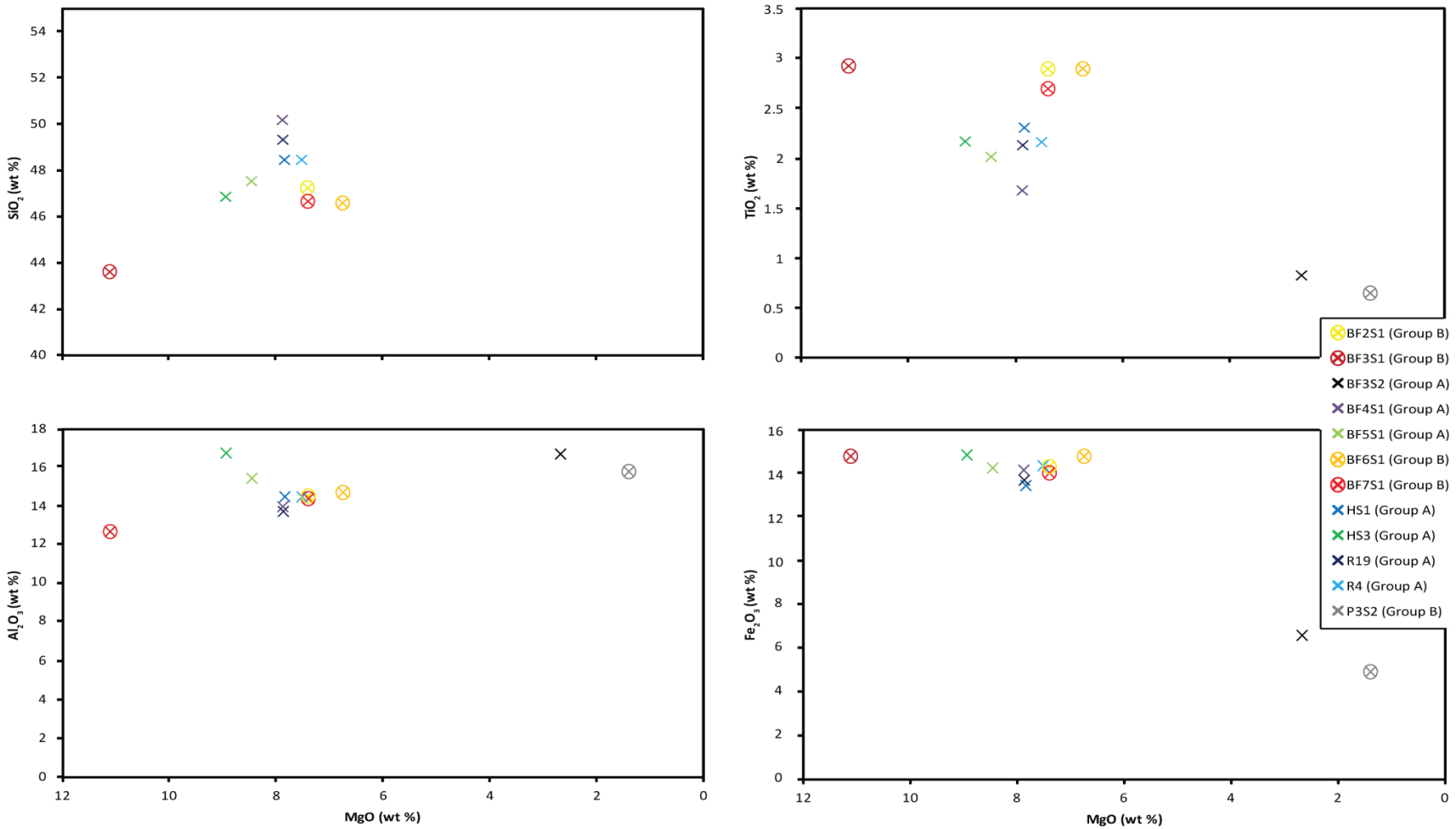


**Figure 5.2:** Variation diagram of selected major element abundances for samples collected from the two study areas. Data are plotted against MgO (wt %). Group B basalts are differentiated by circles with a cross.

The $SiO_2$ abundance of group A basalts is higher than the basalts of group B, although no trend exists within either group or rock type. There is a weak trend of decreasing $TiO_2$ with decreasing MgO wt%, and $Al_2O_3$ and $Fe_2O_3$ show flat trends. No relationship between $SiO_2$ and MgO wt% exists.

The exceptions to these trends are samples P3S2 and BF3S2. Both are very glassy samples containing abundant lithic inclusions and have high $SiO_2$ contents. Both of these rocks are interpreted as glassy basalts with abundant accidental lithic fragments derived from underlying Pleistocene gravels.

## 5.4 Trace Element Geochemistry

Six selected trace elements (Sr, Zr, Cr, Nb, Ni, V) were plotted against MgO weight percent (Fig 5.3). The samples classified as olivine-tholeiitic basalts, and alkali olivine-basalts generally plot in accordance with the findings of Cook (2002). All trace elements are clustered and show no clear trends.

## 5.5 Mineral Geochemistry

The main crystals occurring within the tuff sequences at Raventhorpe and Pokeno West tuff rings are olivine and clinopyroxene. Juvenile plagioclase crystals were less common and also exist as xenocrysts. Determination between juvenile crystals and xenocrysts is described with more detail in previous chapters; however distinction is based primarily on size and texture. Plagioclase xenocrysts occur as larger, stumpy, well rounded, block-like crystals, while the juvenile crystals exist as smaller crystals in tabular and lath shapes.

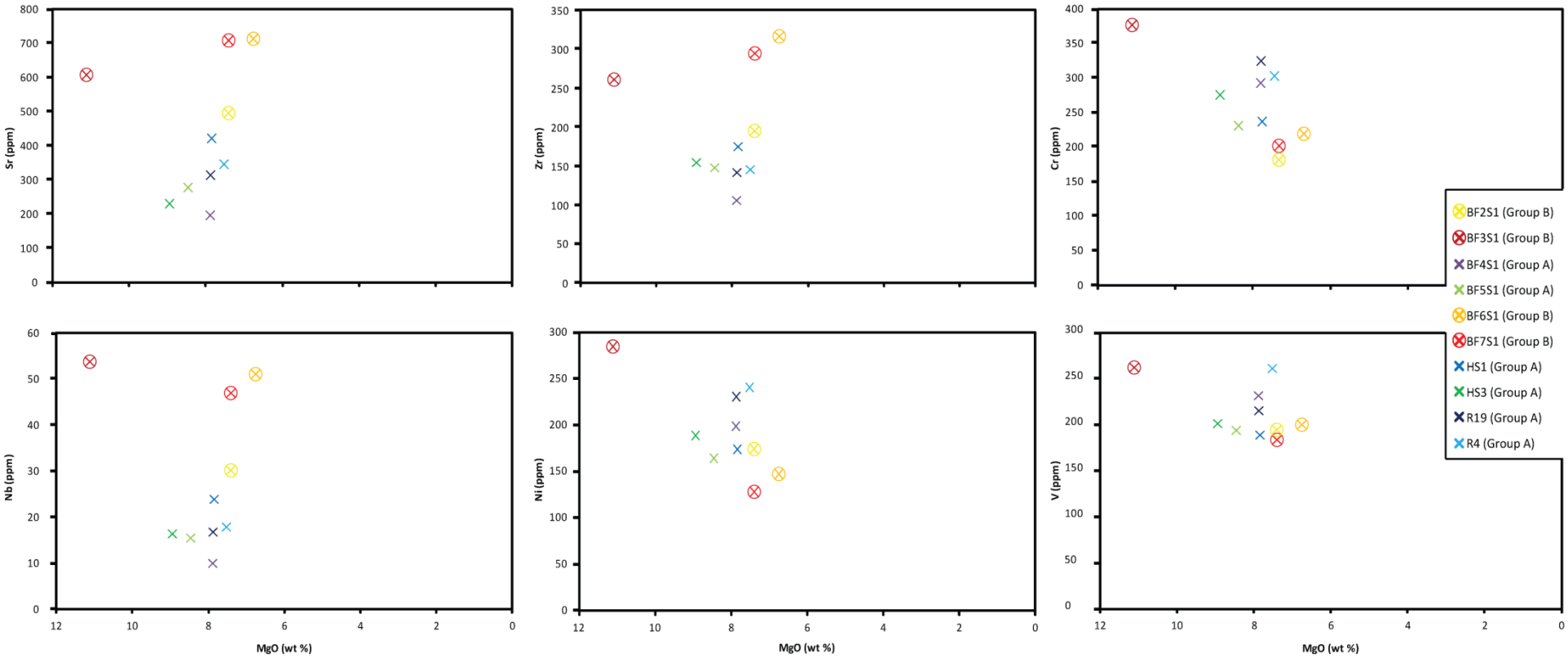


**Figure 5.3:** Selected trace element abundances for samples collected from the two study areas. Data are plotted against MgO (wt %). Group B basalts are differentiated by circles with a cross. Elements Sr, Nb, and Zr are incompatible while Ni, Cr, and V are compatible.

### 5.5.1 Juvenile Crystals

## Olivine

Olivine is the second most dominant phenocryst and groundmass phase in all SAVF lava samples with abundance ranging significantly between rock types. It is also abundant as discrete crystals throughout all tuff rings sampled. Overall compositions ranged from $Fo_{91.7}$ to $Fo_{73.0}$ (Table 5.3). The same compositional range occurs with samples from Raventhorpe tuff ring, while compositions from Pokeno West tuff ring range from $Fo_{89.9}$ to $Fo_{87.3}$ (Fig. 5.4).

Olivine compositions are in broad agreement with those determined by Cook (2002) and Cook *et al.* (2005) plotting olivine compositions with Fo values ranging from 68.1-91.8, slightly less than is presented here (Fig. 5.4).

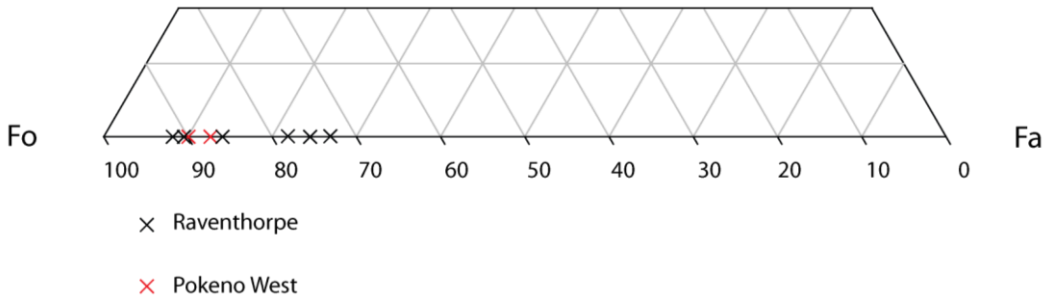


**Figure 5.4:** Olivine compositions for discrete free crystals in the tuff rings of Raventhorpe and Pokeno West, SAVF. Compositions are in mol. %.

## Clinopyroxene

Clinopyroxene is a dominant crystal in all tuff samples after olivine. Abundance varies significantly between rock types and its composition varies between groups within the SAVF lavas (Cook, 2002) and likely the tuffs also. Of the two rock groups for the SAVF lavas, the group A clinopyroxene displays the most diverse range of phenocryst compositions plotting as diopside, augite, and pigeonite (Cook, 2002) but is most commonly augite with low $TiO_2$ contents (Table 5.3) (Cook *et al.*, 2005). The single clinopyroxene probed in this study plots as an augite based on end member compositions in agreement with Cook *et al.*, (2005) (Table 5.3). Clinopyroxenes from group B basalts are more consistent in composition and occur most commonly as diopside with less common augite

**Table 5.3:** Electron microprobe analyses of discrete free crystals from tuff samples of olivines and a single clinopyroxene (far right) from Raventhorpe (group A) and Pokeno West (group B) tuff rings in the SAVF.

| **Location** | Raventhorpe | | | | | | Pokeno West | | Raventhorpe |
|---|---|---|---|---|---|---|---|---|---|
| **Group** | A | | | | | | B | | A |
| **Sample** | R14 | | | | R1 | | P11 | | R14 |
| **Phase** | Olivine | | | | Olivine | | Olivine | | Clinopyroxene |
| **Analysis** | ID=3677 | ID = 3689 | ID = 3685 | ID = 3687 | ID = 3701 | ID = 3703 | ID = 3665 | ID = 3669 | ID=3681 |
| **$SiO_2$** | 38.53 | 40.85 | 41.85 | 54.02 | 41.52 | 39.4 | 41.15 | 41.3 | 51.18 |
| **$TiO_2$** | - | - | - | 0.39 | - | - | - | - | 1.2 |
| **$Al_2O_3$** | - | - | - | 0.98 | - | - | - | - | 1.91 |
| **$Cr_2O_3$** | - | - | - | - | - | - | 0.15 | - | 0.11 |
| **FeO** | 22.07 | 13.38 | 8.08 | 16.69 | 9.28 | 20.32 | 9.67 | 12.18 | 9.51 |
| **MnO** | 0.16 | 0.26 | 0.09 | 0.36 | 0.21 | 0.29 | 0.13 | 0.22 | 0.18 |
| **MgO** | 38.15 | 45.72 | 50.68 | 25.41 | 49.47 | 40.67 | 48.49 | 47.05 | 14.38 |
| **CaO** | 0.18 | 0.24 | 0.13 | 1.32 | 0.04 | 0.15 | 0.09 | 0.08 | 20.18 |
| **$Na_2O$** | 0.17 | 0.15 | 0.38 | 0.11 | 0.13 | 0.13 | - | - | 0.28 |
| **TOTAL** | **99.09** | **100.45** | **100.83** | **98.78** | **100.52** | **100.83** | **99.53** | **100.83** | **99.25** |
| **End Member Compositions** | | | | | | | | | |
| **Fo** | 75.49 | 87.32 | 75.49 | 91.79 | 85.89 | 90.48 | 73.07 | 78.10 | |
| **Fe** | 24.51 | 12.68 | 24.51 | 8.21 | 14.11 | 9.52 | 26.93 | 21.90 | |

| | |
|---|---|
| **Wo** | 42.39 |
| **En** | 42.01 |
| **Fs** | 15.59 |

(Cook *et al.*, 2005). Clinopyroxenes of Group B are also more enriched in $TiO_2$, MgO and $Al_2O_3$ (Cook *et al.*, 2005).

## Plagioclase

Plagioclase occurs throughout the tuff samples in many different crystal shapes. The samples probed were all of juvenile origin as their tabular and lath-like shapes and small size suggests. A total of five plagioclase feldspars were analysed at the Raventhorpe and Pokeno West tuff ring centres, residing as discrete free crystals in the tuff and occurred as labradorite and andesine (Fig 5.4) based on their end member compositions (Table 5.4). These results are consistent with the data presented by Cook (2002) and Cook *et al.* (2005) for group A and B basalts.

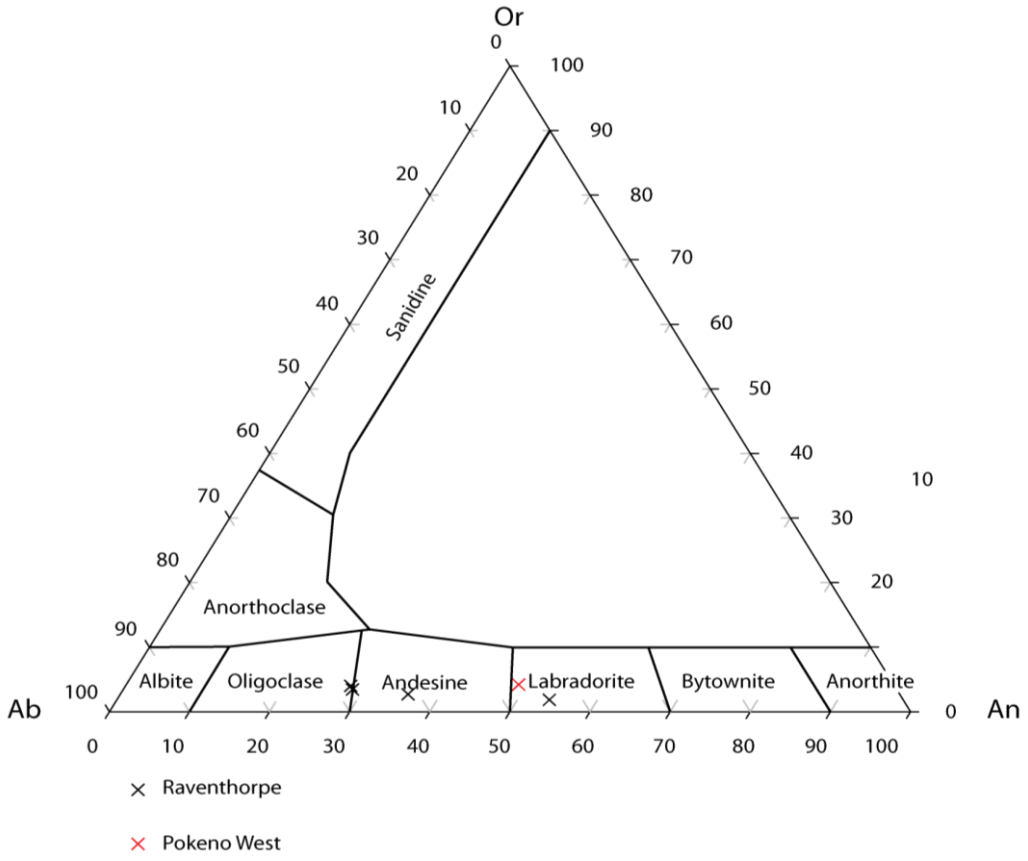


**Figure 5.5:** Feldspar compositions for discrete free crystals occurring in the Raventhorpe and Pokeno West tuff rings, SAVF. Compositions are in mol. %

**Table 5.4:** Electron microprobe analyses of discrete free plagioclase crystals from tuff samples from Raventhorpe (group A) and Pokeno West (group B) tuff rings in the SAVF.

| **Location** | Raventhorpe | | | | Pokeno West |
|---|---|---|---|---|---|
| **Group** | A | | | | B |
| **Sample** | R1 | | | | P11 |
| **Analysis** | ID = 3691 | ID = 3697 | ID = 3693 | ID = 3705 | ID = 3661 |
| **$SiO_2$** | 58.55 | 54.57 | 61.34 | 60.26 | 56.92 |
| **$TiO_2$** | 0.07 | 0.11 | 0.19 | 0.19 | 0.04 |
| **$Al_2O_3$** | 25.26 | 28.74 | 23.63 | 23.84 | 26.23 |
| **FeO** | 0.29 | 0.2 | 0.21 | 0.27 | 0.48 |
| **MgO** | - | - | - | - | - |
| **CaO** | 7.43 | 11.13 | 5.71 | 5.96 | 9.63 |
| **$Na_2O$** | 6.98 | 5.02 | 7.6 | 7.77 | 5.07 |
| **$K_20$** | 0.45 | 0.31 | 0.67 | 0.6 | 0.68 |
| **TOTAL** | **99.03** | **100.11** | **99.3** | **98.86** | **99.02** |
| **End Member Compositions** | | | | | |
| **An** | 36.07 | 54.07 | 28.18 | 28.74 | 49.10 |
| **Ab** | 61.33 | 44.13 | 67.88 | 67.81 | 46.78 |
| **Or** | 2.60 | 1.79 | 3.94 | 3.45 | 4.13 |

### 5.5.2 Xenocrysts

Petrographic analysis of the tuff revealed the incorporation of foreign material including crystals. Throughout all samples, plagioclase, quartz, and hornblende were all common while to a lesser extent, but still present, hypersthene and glauconite pellets were observed. Table 5.5 summarises the major element compositions and identifies some of the xenocryst minerals that have been observed in thin section. Conclusive determination of these minerals as xenocrysts occurring within the tuff at Raventhorpe and Pokeno West tuff rings will be used to help mineralogically constrain important underlying geological units that could have had significant implications in the eruption.

**Table 5.5:** Summary of electron microprobe analyses of major element compositions of xenocrysts for Raventhorpe and Pokeno West tuff rings in the SAVF. HB = hornblende, G = glauconite pellet, Qtz = quartz.

| **Location** | Raventhorpe | | | | | | | | Pokeno West | | | | |
|---|---|---|---|---|---|---|---|---|---|---|---|---|---|
| **Sample** | R1 | | | | | R14 | | | P11 | | | | |
| **Analysis ID** | 3695 | 3699 | 3707 | 3709 | 3711 | 3675 | 3679 | 3683 | 3655 | 3659 | 3673 | 3663 | 3667 |
| **$SiO_2$** | 45.13 | 46.11 | 48.45 | 49.42 | 97.06 | 45.62 | 45.42 | 46.49 | 40.86 | 98.14 | 40.86 | 49.33 | 50.27 |
| **$TiO_2$** | 1.02 | 2.42 | 1.63 | - | - | 2.2 | 1.93 | 1.96 | 5.09 | - | 4.98 | - | 0.23 |
| **$Al_2O_3$** | 10.51 | 8.57 | 7.79 | 7.58 | - | 8.64 | 8.29 | 7.69 | 13.66 | - | 13.99 | 6.82 | 10.48 |
| **FeO** | 17.12 | 13.89 | 7.27 | 22.39 | - | 14.02 | 14.7 | 14.34 | 10.07 | - | 9.22 | 22.45 | 18.34 |
| **MnO** | 0.45 | 0.34 | 0.1 | - | - | 0.19 | 0.15 | 0.18 | 0.14 | - | - | - | - |
| **MgO** | 11.77 | 13.93 | 14.44 | 3.34 | - | 13.74 | 13.08 | 13.76 | 13.37 | - | 13.74 | 3.31 | 3.72 |
| **CaO** | 9.7 | 11.01 | 17.91 | 0.23 | - | 10.7 | 10.77 | 10.49 | 10.41 | - | 10.64 | 0.12 | 0.28 |
| **$Na_2O$** | 1.28 | 1.79 | 0.84 | 0.17 | - | 1.8 | 1.79 | 1.52 | 2.81 | - | 2.41 | - | - |
| **$K_2O$** | 0.48 | 0.58 | 0.03 | 8 | 0.11 | 0.49 | 0.48 | 0.41 | 1.84 | - | 1.9 | 8.04 | 7.34 |
| **TOTAL** | **97.46** | **98.64** | **98.46** | **91.13** | **97.17** | **97.4** | **96.61** | **96.84** | **98.25** | **98.14** | **97.74** | **90.07** | **90.66** |
| **Identified** | HB | HB | HB | G | Qtz | HB | HB | HB | HB | Qtz | HB | G | G |

# Chapter Six

# Spatial and Temporal Analysis

## 6.1 Introduction

Volcanic centres in monogenetic volcanic fields commonly display a random distribution and indicate little by way of spatial and temporal relationships (Rapela *et al.*, 1987; Condit & Connor, 1996; Magill *et al.*, 2005; Weller *et al.*, 2006). Spatial and temporal studies on the SAVF (Briggs *et al.*, 1994) and AVF (Magill, 2005; Cassidy & Locke, 2011) have previously concluded that no relationships exist. This chapter describes the spatial and temporal analysis and relationships of the volcanic centres within the SAVF. Slope analysis data are also presented for the two field areas, while age, and control relationships are described for the whole SAVF.

## 6.2 Slope Analysis

Extinct volcanic fields, or those not well preserved can make identification of volcanic structures difficult, especially when centres are nested within each other or are overlapping such as the Raventhorpe volcanic complex. Slope analysis can identify crater rim or cone structures. A high slope index indicates a central topographic feature that if hollow and circular can be interpreted as a tuff ring, or if circular, a scoria cone. The slope analyses presented at the two study locations match well with the volcanic centre interpretations derived from field study and stereoscopic imagery.

Slope analysis of the Raventhorpe volcanic complex defines much of the rim structure of the Raventhorpe and Ingram Road tuff rings (Fig. 6.1). The rim along the 200 m north-trending exposure at Raventhorpe is well defined by the high slope values presented (Fig. 6.1). The Ingram Road tuff rings are substantially eroded and indicate little by way of tuff ring structures as defined by the slope

analysis (Fig. 6.1). The rims of the Ingram Road tuff rings are best defined to the south, where they appear slightly more preserved (Fig. 6.1). Pukekohe East tuff ring, although not considered part of the Raventhorpe volcanic complex is situated nearby and so is included on the maps of the area. The Pukekohe East tuff ring displays a strong correlation between the mapped location which was determined by stereoscopic imagery, and previous studies (Rafferty, 1977) and the location of the tuff ring as determined by the slope analysis (Fig. 6.1).

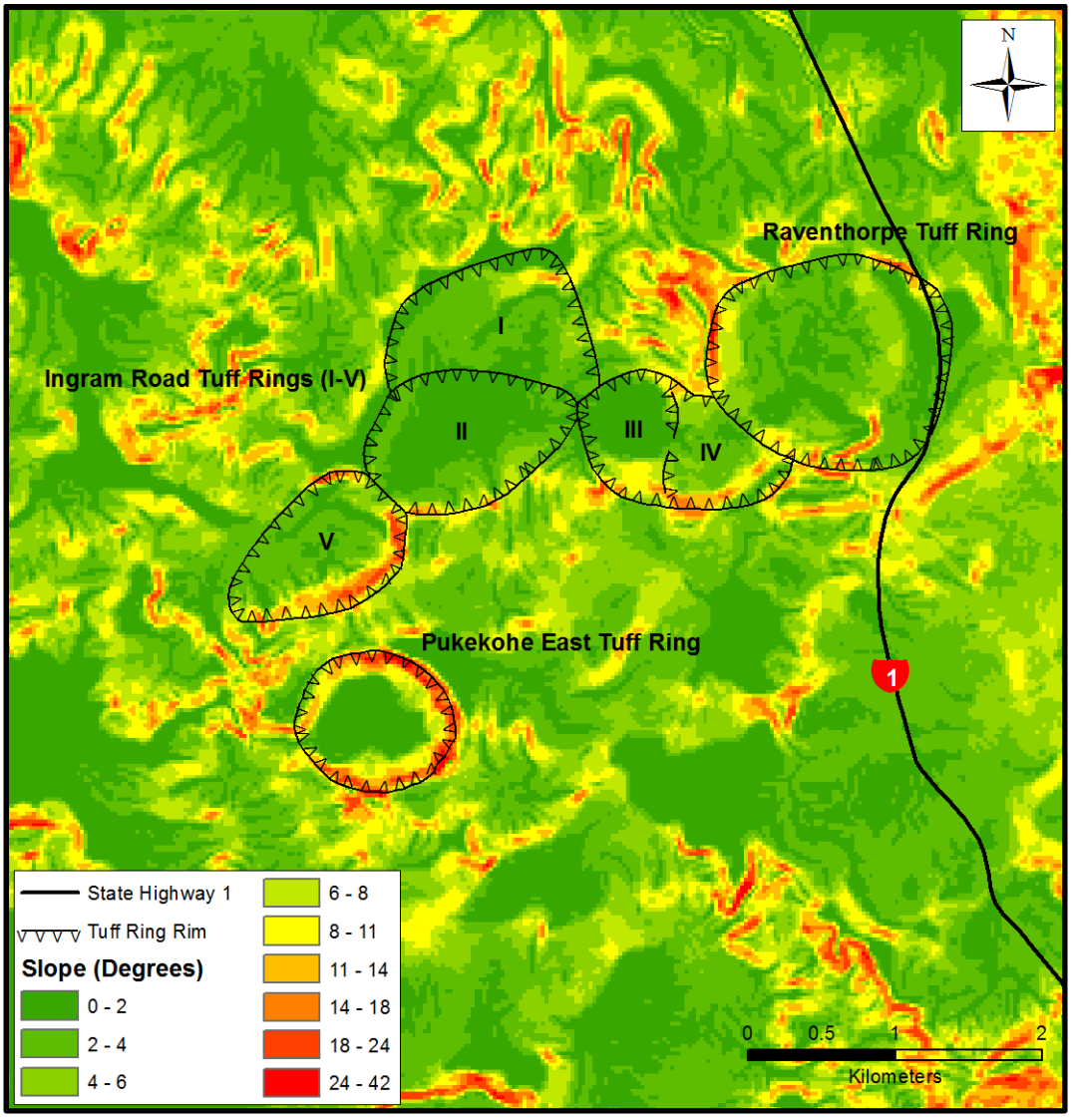


**Figure 6.1:** Slope analysis of the Raventhorpe volcanic complex overlain with the tuff rings identified from field survey and stereoscopic imagery.

The Pokeno West volcanic complex occurs in an area dominated by undulating and hilly topography, most notably to the south (Fig. 6.2). This is likely a result of the various lava flows in the area from the Bluff Road cone, present to the southwest. The southern and south-eastern rim of the tuff ring is the most clearly

defined feature. The output displays higher slope values to the west and the north within a broadly topographical flat area, suggesting possible preservation of the tuff ring rim.

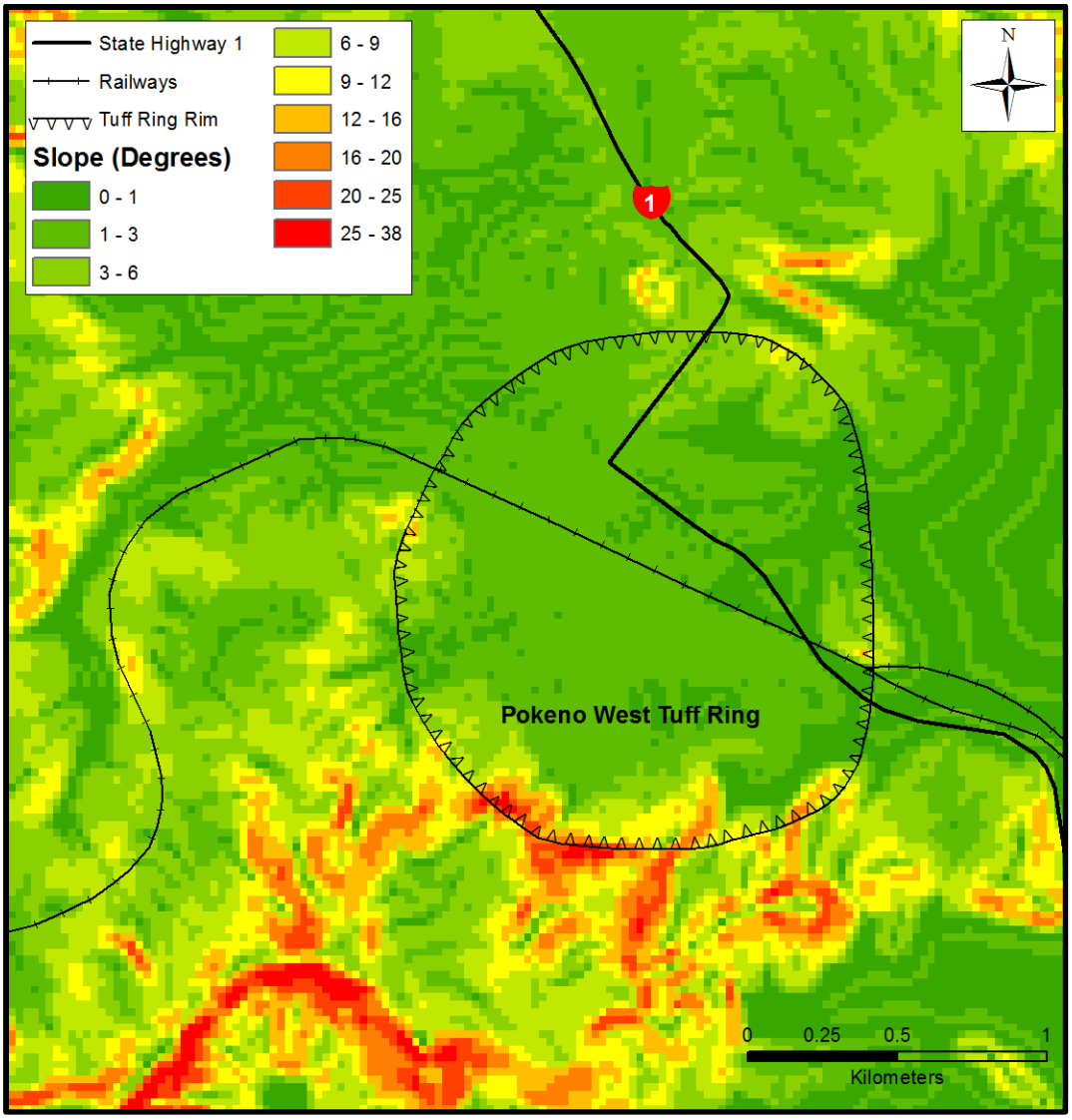


**Figure 6.2:** Slope analysis of the Pokeno West volcanic complex overlain with the identified tuff ring from field survey and stereoscopic imagery. The Bluff Road cone is beyond extent to the southwest. The lavas from the Bluff Road cone are seen in the lower left.

## 6.3 Spatial Relationships of the South Auckland Volcanic Field

The volcanic centres of the SAVF display a random distribution between both basalt groups, A and B, and eruption mechanism, i.e. magmatic or phreatomagmatic. Magmatic centres are most common throughout the field,

accounting for 53 of the 90 centres defined in the spatial analysis of this study. Although ~82 centres are now recognised, phreatomagmatic centres with intra-tuff ring cones are recognised as two centres in this spatial analysis.

Table 6.1 summarises the occurrence between the style of volcanism and the resulting basalt group. Group A basalts are slightly less common than basalts of group B, and also occur more commonly as phreatomagmatic centres. This statistic may be bias by the phreatomagmatic centres that are unclassified or "ungrouped" of which there are 18. Six group A basalts occur in the north to the East of the Drury Fault amongst 16 group B centres to the east of the Drury Fault and north of the Pokeno Fault (Fig 6.3). This indicates some degree of clustering may be occurring to the east of the Drury Fault, although, several centres are unclassified as they lack exposure, or are too eroded to sample.

Eroded centres are most often phreatomagmatic, commonly occurring in isolation west of the Drury Fault in the Manukau Lowlands (Fig. 6.3). Throughout the regions of Pukekohe and Bombay, there appears to be clusters of volcanic centres occurring around the St. Stevens and Pukekohe Faults. Unclassified centres throughout the SAVF account for just over one quarter of all the centres (Table 6.1).

**Table 6.1:** Occurrence and percentage of group A and B basalts and magmatic and phreatomagmatic volcanism throughout the SAVF. No. denotes number.

| Volcanic Centre | No. Group A | % of Field | No. Group B | % of Field | % Total | No. Unknown | % of Field |
|---|---|---|---|---|---|---|---|
| Magmatic | 19 | 21.1 | 28 | 31.2 | 52.2 | 6 | 6.6 |
| Phreatomagmatic | 12 | 13.3 | 7 | 7.8 | 21.2 | 18 | 20.0 |
| Total | 31 | 34.4 | 35 | 39.0 | 73.4 | 24 | 26.6 |

Magmatic and phreatomagmatic centres can broadly be differentiated spatially with the latter predominantly occurring east of the Drury Fault and north of the Waikato Fault. This coincides with the extent of the Kaawa Formation over the Manukau Lowlands through the centre of the field (Fig 6.4) and the Pleistocene sediments of the Waikato River valley south. These sediments have high permeability, porosity, and transmissivity that have provided suitable hydrological

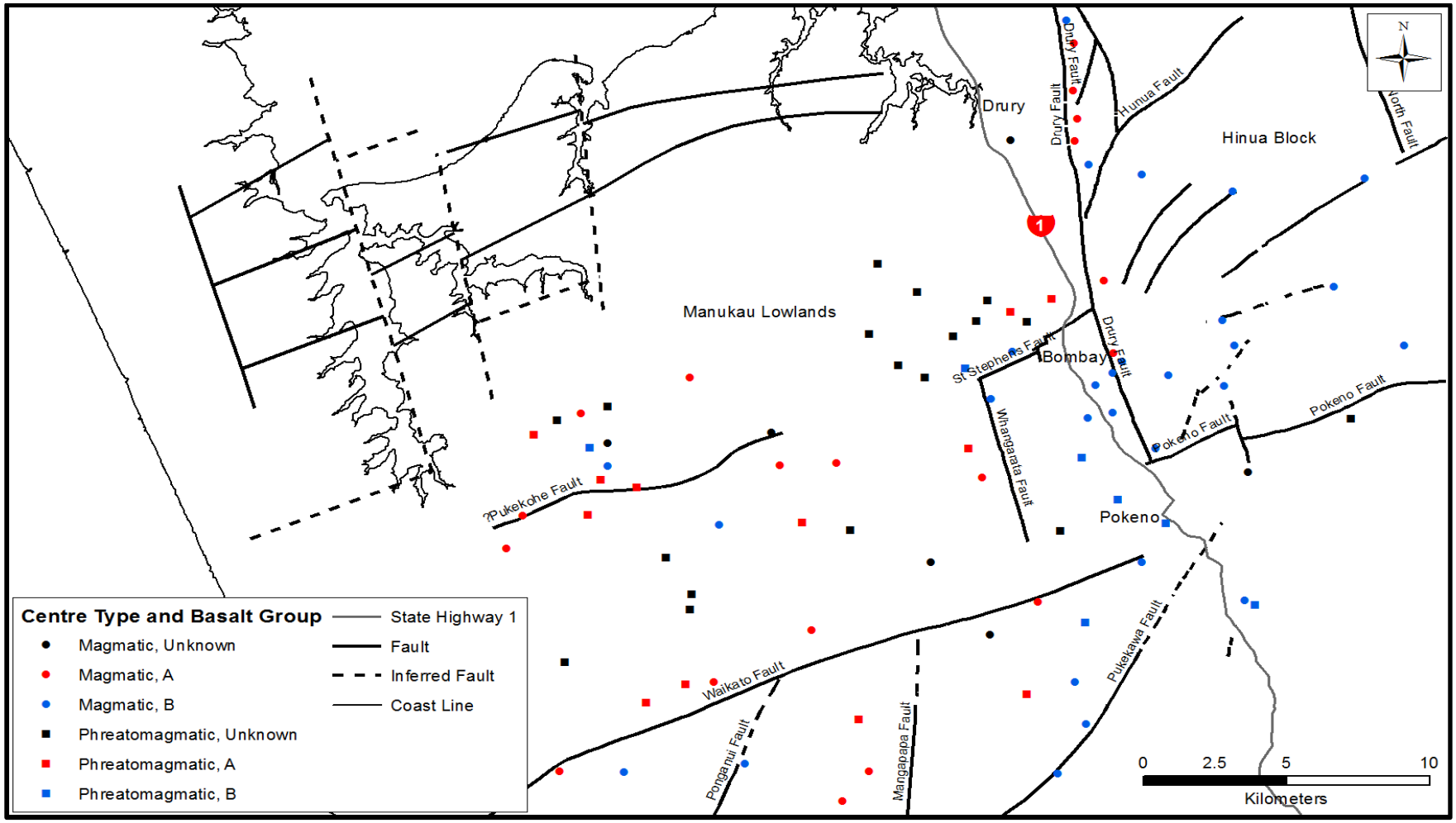


**Figure 6.3:** Occurrence of group A and B, magmatic and phreatomagmatic centres in the SAVF.

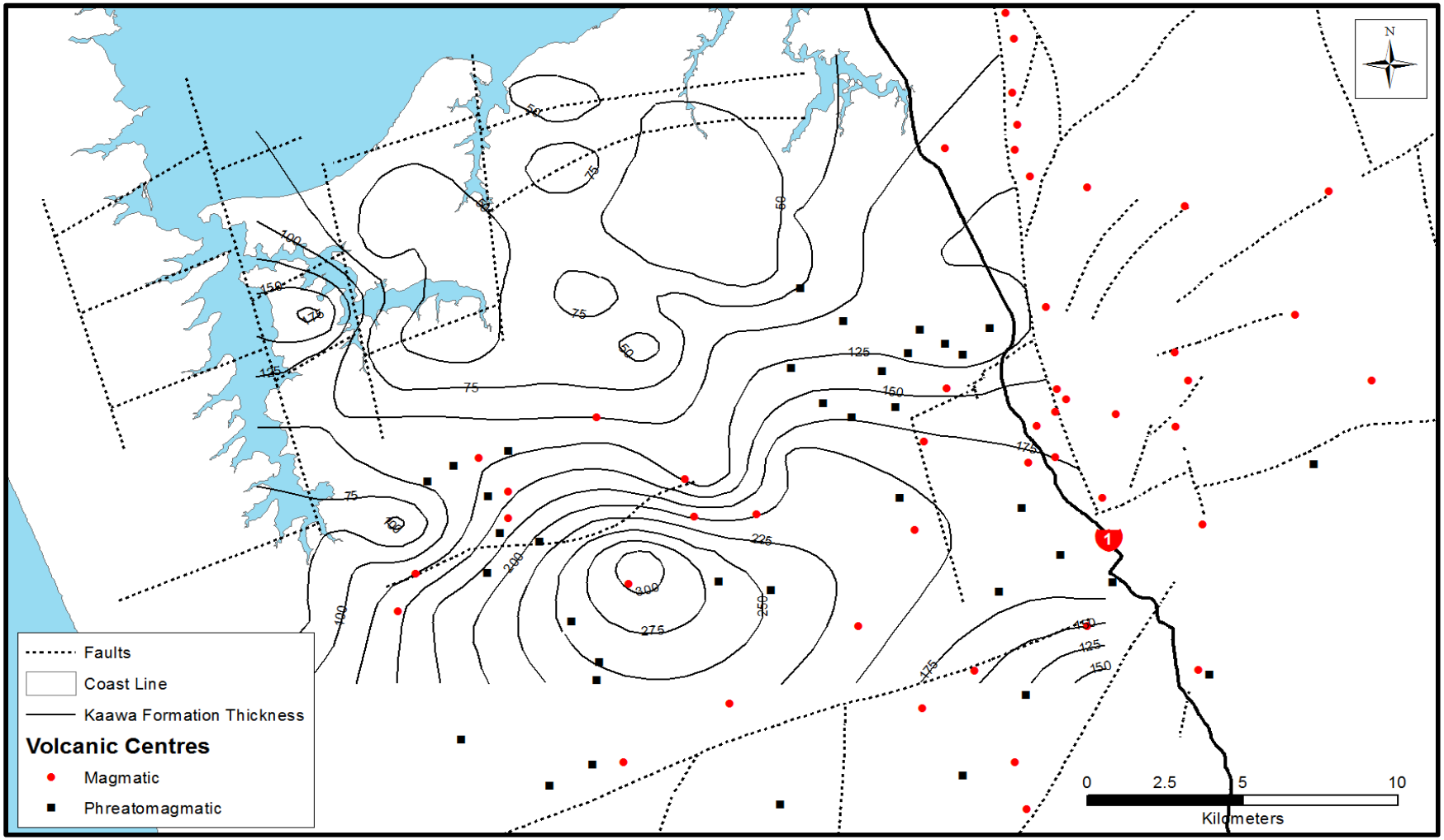


**Figure 6.4:** Isopach map of the Kaawa Formation in relation to the distribution of volcanic centres, SAVF. After Greig, (1989), and Viljevac *et al.* (2002).

conditions for explosive magma-water interactions to construct tuff rings and maars (Briggs *et al.*, 2010).

Magmatic centres are virtually exclusive in the east of the field where several major faults, i.e. Drury and Pokeno Faults occur along with other smaller faults (Fig. 6.3). Three phreatomagmatic centres, however occur south of the Pokeno Fault, in the Waikato River valley. Volcanic centres confined to the uplifted Hunua Block are solely magmatic.

### 6.3.1 Age

Briggs *et al.* (1994) considered there was no age relationship between volcanic centres within the field, except for several older volcanic centres that occur to the northeast, although younger volcanics occurred through the centre of the field and older volcanics are peripheral, isolated, and dispersed. The younger ages observed through the central and eastern regions of the field occur within a 0.2 Ma period, from 0.76-0.56 Ma with the centres displaying a general clustering. 16 centres occur within this age period, with the remaining 16 dated centres spanning a 1.57-0.77 Ma period (Table 6.2). One outlying centre occurring on the Drury Fault to the north, recorded an age of 2.09 Ma (Table 6.2; Fig. 6.5). Some of the older volcanic centres in the field could be buried by more recent eruptives as Gibson (2011) illustrated in Bombay Quarry, and Greig (1989) described from borehole data. Centres that have been dated are most commonly magmatic (Table 6.2).

**Table 6.2:** Occurrence of magmatic and phreatomagmatic volcanic centres through 0.1 Ma intervals for the SAVF. No. denotes number.

| Age Interval (Ma) | No. Magmatic Centres | No. Phreatomagmatic Centres | Total No. Centres |
|---|---|---|---|
| 0.56-0.66 | 11 | 0 | 11 |
| 0.67-0.76 | 3 | 2 | 5 |
| 0.77-0.86 | 2 | 0 | 2 |
| 0.87-0.96 | 0 | 3 | 3 |
| 0.97-1.06 | 0 | 2 | 2 |
| 1.07-1.16 | 1 | 0 | 1 |
| 1.17-1.26 | 1 | 0 | 1 |
| 1.27-1.36 | 1 | 0 | 1 |
| 1.37-1.46 | 2 | 0 | 2 |
| 1.47-1.56 | 0 | 1 | 1 |
| 1.57-2.09 | 2 | 1 | 3 |

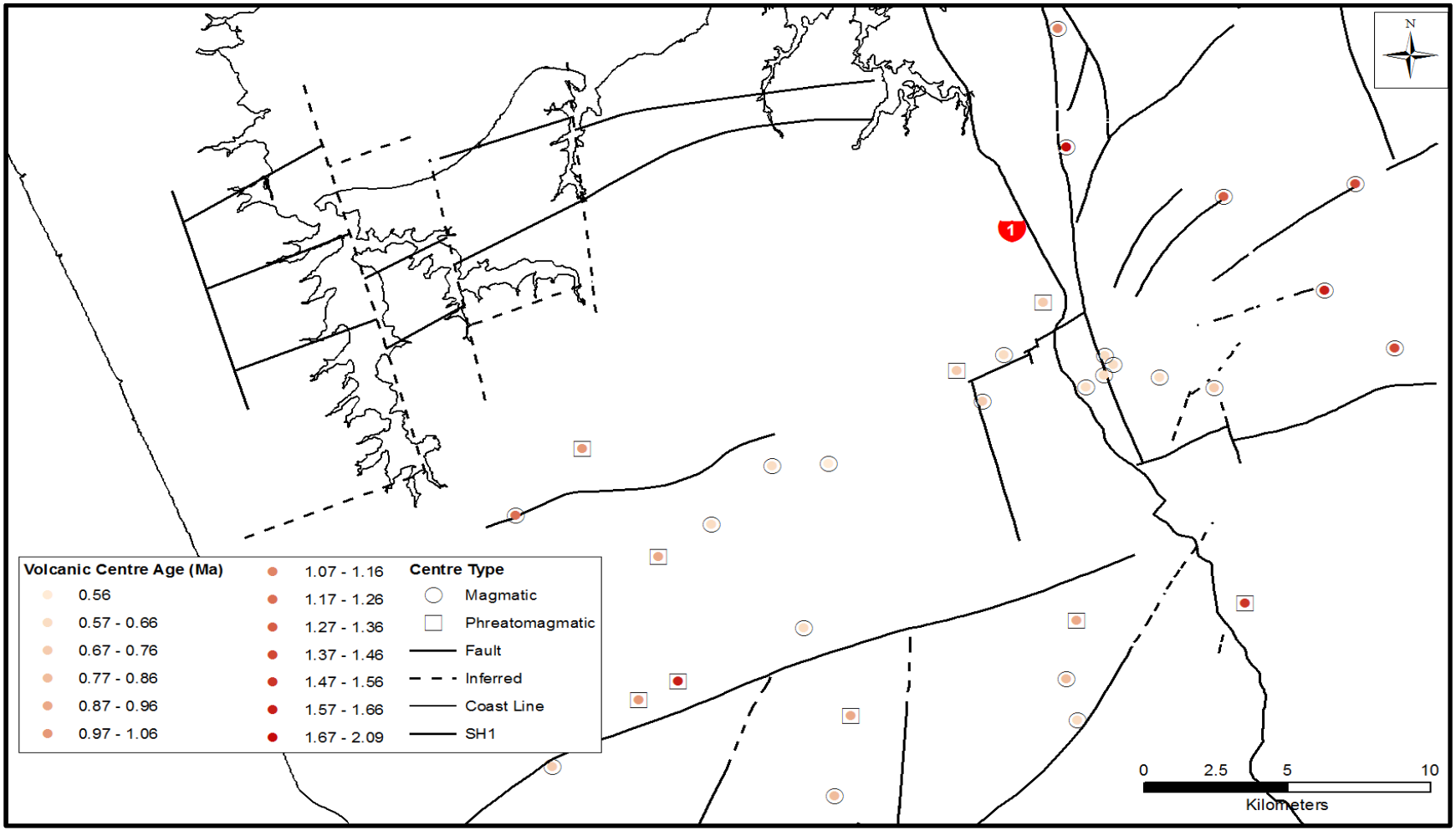


**Figure 6.5:** Ages and occurrence of dated, magmatic and phreatomagmatic volcanic centres throughout the SAVF.

Statistical analyses were conducted using a Geographic Information System (GIS) for the available age data of centres within the SAVF. Table 6.3 presents the observed scores for the statistical tests used to analyse the spatial distribution and age data for the SAVF.

**Table 6.3:** Results of the two statistical analyses of age and spatial distribution for dated volcanic centres throughout the SAVF.

| Analysis | Z-Score | P-Value |
|---|---|---|
| Getis-Ord General G | -1.119684 | 0.262849 |
| Average Nearest Neighbour | -1.299837 | 0.193657 |

The null hypothesis for these statistical tests was complete spatial randomness. The P value represents the probability that the observed spatial pattern was created by a random process (ESRI, 2011). A small p-value indicates it is very unlikely that the observed spatial pattern is the result of random processes (Fig. 6.6). Z-scores are standard deviations from the geographical mean. High (positive) or low (negative) z-scores, associated with small probability values, are found in the tails of the normal distribution indicating it is unlikely that the observed spatial pattern is a result of random distribution (ESRI, 2011). From the results obtained for this study (Table 6.3) the null hypothesis cannot be rejected. The apparent age and spatial distribution of volcanic centres throughout the SAVF produce a normal distribution, indicating the observed features are random (Fig. 6.6).

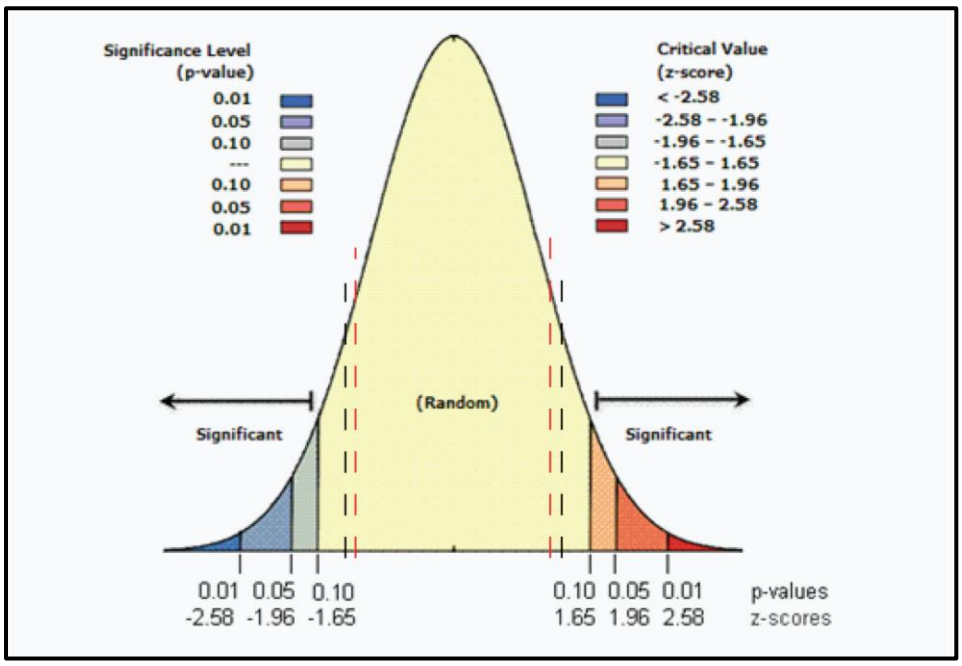


**Figure 6.6:** Normal distribution curve indicating P-values and Z-scores. Black dashed lines indicate the results for the Average Nearest Neighbour analysis. Red dashed lines indicate the results for the Getis-Ord General G analysis. Analyses completed using the hotspot analysis and cluster analysis tools (ESRI, 2011). Figure modified from ESRI (2011).

### 6.3.2 Controls on Volcanism

Schofield (1976) noted the close relationship between eruptive centres and controls such as faulting. Rosenberg (1991) also cited that faulting was a dominant control on the volcanism of the SAVF and that faults likely provided the easiest path for magma ascent. These statements appear correct as 33.6% of all SAVF volcanic centres occur within 500 m of known or inferred faults (Table 6.4). Cumulatively 49.2% and 66.5% of all centres occur within 500-1000 m, and 1000-1500 m of faults respectively (Table 6.4).

**Table 6.4:** Occurrence of magmatic and phreatomagmatic centres in relation to fault proximity throughout the SAVF.

| Proximity to Fault (m) | No. Mag. Centres | (%) | No. Phre. Centres | (%) | Combined (%) | Accumulative (%) |
|---|---|---|---|---|---|---|
| 0-500 | 27 | 30.3 | 3 | 3.3 | 33.6 | 33.6 |
| 500-1000 | 9 | 10.0 | 5 | 5.6 | 15.6 | 49.2 |
| 1000-1500 | 10 | 10.7 | 6 | 6.6 | 17.3 | 66.5 |
| 1500-2000 | 2 | 2.2 | 6 | 6.6 | 8.8 | 75.3 |
| >2000 | 5 | 5.6 | 17 | 19.1 | 24.7 | 100.0 |

There are three general areas where faulting occurs in the SAVF: the northwest, just south of the Manukau Harbour; to the east where the Drury and Pokeno Faults uplift the Hunua block, and to the south of the Waikato Fault. The association between location of the volcanic centre and fault control is clear, with the alignment of many volcanic centres along the north trending Drury Fault and east-northeast trending Pokeno Fault (Fig. 6.7). Volcanic centres also occur within the uplifted Hunua Block and along the faults occurring within. The closely located St. Stevens and Whangarata Faults in the eastern-central region of the field are surrounded by several small groupings of predominantly phreatomagmatic centres (Fig. 6.7). To the south, the Waikato and Pukekawa Faults are located near many of the more southern volcanic centres which are a fairly even distribution of magmatic and phreatomagmatic volcanoes.

Rosenberg (1991) stated that the type and style of volcanism was primarily controlled by the hydrology of the shallow 100-200 m thick aquifers. The dominant aquifers within the South Auckland region and Manukau Lowlands are basalt lavas, basaltic tuff, and the Pliocene age Kaawa Formation (Viljevac *et al.*, 2002). The basalt aquifers have limited spatial distribution due to the basalt flows which occurred during the life of the SAVF. Basaltic tuff is highly porous with low permeability (ARC, 1996; Viljevac, 1998) and is also limited spatially. The Pliocene and Pleistocene sediments are variable throughout the Manukau Lowlands and form a regional aquatard that confines the widely dispersed Kaawa Formation (Hadfield, 1988; Viljevac *et al.*, 2002).

Using borehole data produced by Greig (1989) and better confined by Viljevac *et al.* (2002), the thickness of the Kaawa Formation has been calculated (Fig. 6.7). There are 37 phreatomagmatic centres occurring within the SAVF, of which 29 (78%) occur within the mapped extent of the Kaawa Formation (Table 6.5) which is bounded to the south by the Waikato Fault (Viljevac *et al.*, 2002). There would likely be a further three phreatomagmatic centres that have ascended through the Kaawa Formation included to this number, however the data from Greig (1989) and Viljevac *et al.* (2002) limits the maximum possible extent of the formation able to be mapped. The remaining five centres occur to the south of the Pokeno and Waikato Faults and are likely the result of abundant water present within the Waikato River valley.

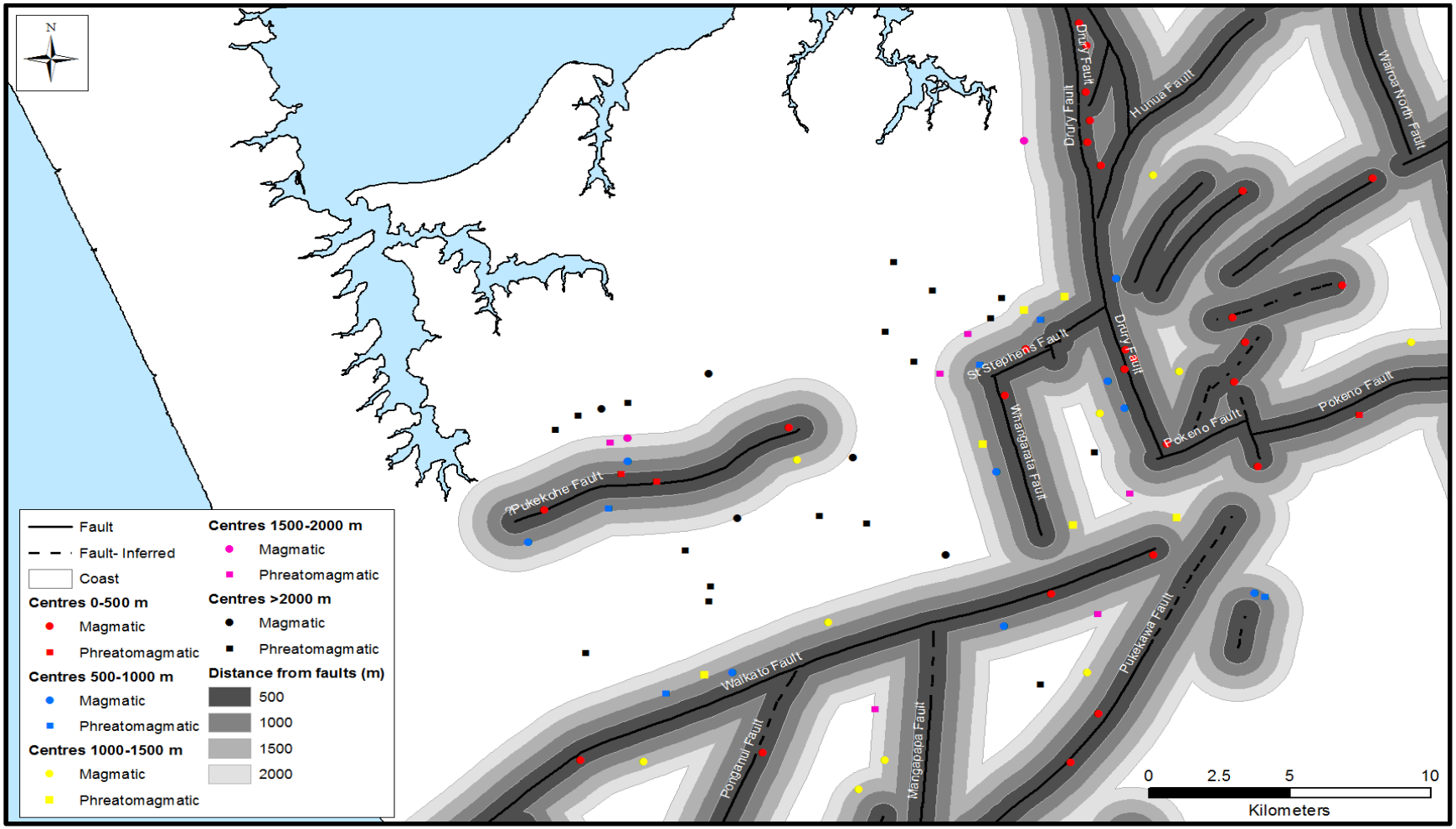


**Figure 6.7:** Distribution of magmatic and phreatomagmatic centres, and their proximity to faults throughout the SAVF.

Magmatic centres also occur throughout the Manukau Lowlands, but are however less common than phreatomagmatic centres, accounting for 21 occurrences, or 23.5% of all volcanic centres. The presence of these magmatic centres could indicate possible hidden faults. Over 50% of the volcanic centres in the field occur over the mapped extent of the Kaawa Formation (Table 6.5).

**Table 6.5:** Thickness of the mapped extent of the Kaawa Formation (data from Greig, 1989 and Viljevac *et al.*, 2002) versus the occurrence of magmatic and phreatomagmatic volcanic centres throughout the SAVF. No. denotes number.

| Thickness of Kaawa Formation (m) | No. Phreatomagmatic Centres | No. Magmatic Centres |
|---|---|---|
| 75-100 | 1 | 1 |
| 100-125 | 10 | 3 |
| 125-150 | 3 | 4 |
| 150-175 | 4 | 6 |
| 175-200 | 5 | 4 |
| 200-225 | 2 | 2 |
| 225-250 | 2 | 0 |
| 250-275 | 2 | 0 |
| 275-300 | 0 | 0 |
| >300 | 0 | 1 |
| **Total** | **29** | **21** |
| **Total Field %** | **31.4** | **23.5** |
| Outside Data Limits | 8 | 32 |

### 6.3.3 Cross Sections of the South Auckland Volcanic Field

Five geological cross sections were produced, orientated west-east across the extent of the Kaawa Formation through the SAVF (Figs. 6.8, 9). These cross-sections were produced using a digital elevation model and elevation raster images of the Kaawa and Waitemata Group topographic surfaces. These surfaces were interpolated using a line interpolation tool across the same transect. Once constructed, the faults and points of interest were added, and geological interpretation was conducted to produce fault offsets. For this reason the fault offsets are considered to be an approximation. The data sets used to construct the elevation raster images were based on the borehole data of Greig (1989), and Viljevac *et al.* (2002).

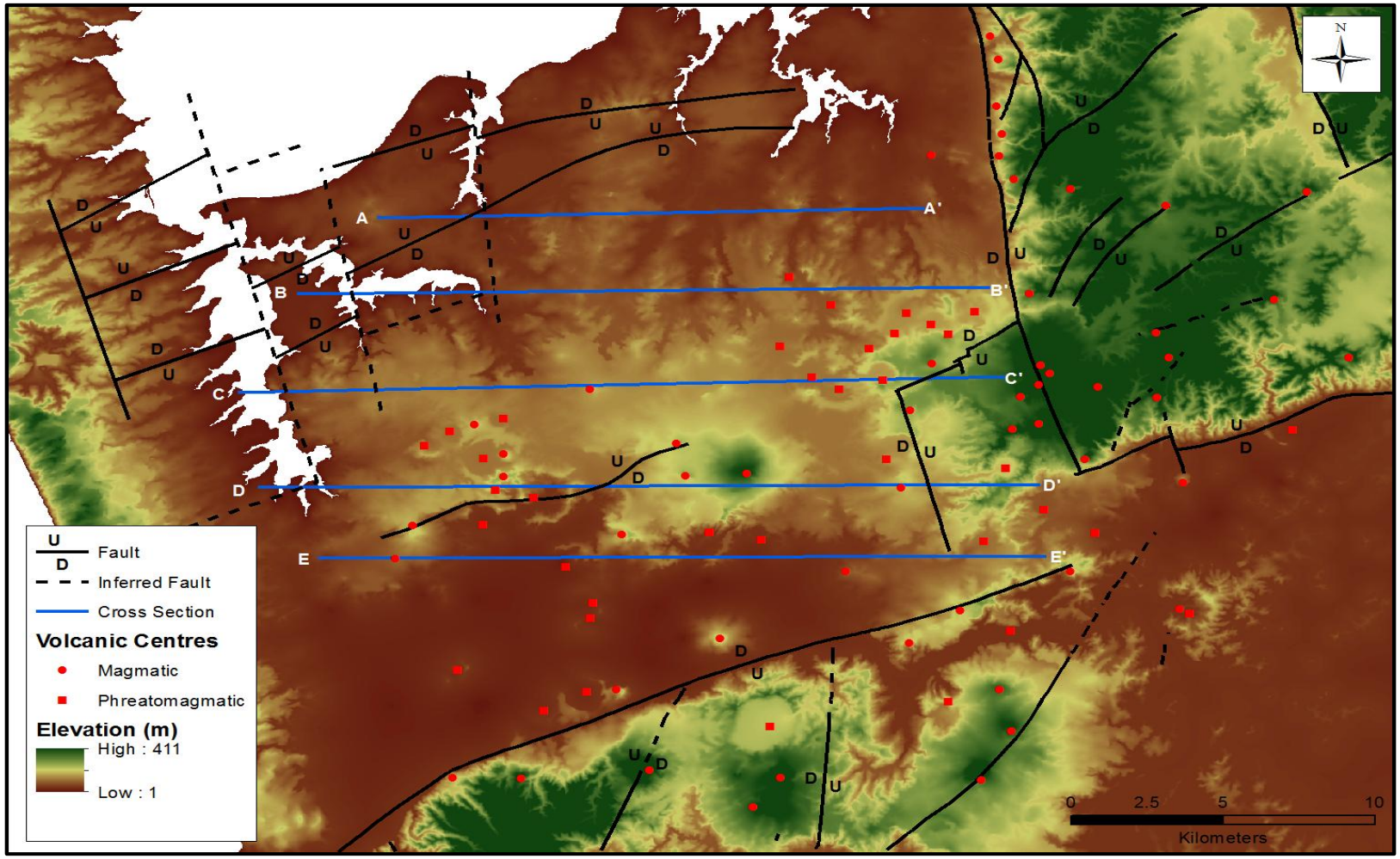


**Figure 6.8:** Faulting and cross section locations, and distribution of volcanic centres throughout the SAVF.

These five cross sections produced illustrate several aspects or relationships that relate to the Kaawa Formation:

(1) the thickness of the Kaawa formation, especially south where thicknesses >250 m occur;
(2) the relationship between the topography of the Kaawa Formation surface and the topography of the Waitemata Group surface;
(3) the presence of faulting displaying observable changes in the topography and thickness of the Waitemata Group and Kaawa Formation; and
(4) the observable volcanic features, i.e. cones and tuff rings, and their relationships to faults and/or Kaawa Formation thickness.

Cross-section (A-A') is the shortest due to the extent constraints of the Kaawa Formation and Waitemata Group topographic surfaces. Two faults occur in the west of the Manukau Lowlands (Fig. 6.8), one of which is an inferred fault, and dissect the cross-section several hundred meters apart (Fig. 6.9). To the west of these faults, the Kaawa Formation thickness is at most 20 m, while to the east this increases to >60 m (Fig. 6.9). The upper surface of the Waitemata Group is irregular and in places 20-30 m below mean sea level. The overlying Pleistocene sediments are very thick in this northern area and topography is irregular.

Progressing southward, cross-section B-B' extends over 23 km from the east of the Waiuku River to the Drury Fault (Fig. 6.8). This section crosses two inferred faults that occur in the west of the field ~5 km apart. The Kaawa Formation to the west has a thickness of ~120 m, and the thickness pinches out to a maximum of 60 m across 10 km to the east before the thickness increases again across the final 8 km towards the Drury Fault (Fig. 6.9). The maximum thickness of the Kaawa Formation (150 m) occurs in the east, three kilometres west of the Drury Fault. The upper topographic surface of the Kaawa Formation broadly mirrors the topographic surface of the Waitemata Group, possibly constrained by faulting (Fig. 6.9). To the east near the Drury Fault, Pleistocene sediments and basalt eruptives (likely dominant) are up to 130 m thick, infilling a local depression over a few kilometres, likely produced by the Drury Fault. The location of Paerata tuff ring III is proposed (Fig. 6.9).

Cross-section C-C' extends over 25 km from the western side of the Waiuku River across to the Drury Fault (Fig. 6.8). The cross-section encounters three

faults, two to the west which are inferred, and the St. Stevens Fault, several kilometres to the west of the Drury Fault (Fig. 6.9). The topography of the Kaawa Formation and Waitemata Group demonstrates that 100-200 m of displacement has occurred along this fault (Fig. 6.9). The Kaawa Formation thickness through this section is reasonably consistent (~100 m) and broadly mimics the topographic surface of the Waitemata Group (Fig. 6.9). Thicknesses of up to 225 m however occur in the east. The Waiuku River, Mauku scoria cone, Pukekohe North, and Pukekohe East tuff rings have been identified (Fig. 6.9). Both tuff rings occur directly above the thickest sections of the Kaawa Formation (Fig. 6.9).

The fourth cross-section, D-D', covers >25 km from the western side of the lower reaches of the Waiuku River, east to the Drury Fault (Fig 6.8). Topography of the land surface is highly irregular partly due to the presence of several tuff rings, volcanic cones, lava flows, and faults (Fig. 6.9). The Waiuku River, Bald Hill tuff rings, Pukekohe, and Buckland cones, and the Pukekohe and Whangarata faults are all identified (Fig. 6.9). The thickness of the Kaawa Formation is highly variable across this section due to the highly irregular topography of the underlying Waitemata Group which appears to have been significantly faulted (up to 300 m) in several areas (Fig. 6.9). As a consequence of this the thickness of the Kaawa Formation ranges from 50-270 m for the most part across the profile (Fig. 6.9). To the east of the north-northwest trending Whangarata Fault the Waitemata Group is upthrown and the Kaawa Formation pinches out to ~10 m below the Pleistocene sediments and eruptives, most likely the lavas from the Pokeno and Bombay cones (Fig. 6.9).

The final most southern cross-section, E-E', extends from the south of Waiuku township to the south of Pokeno township (Fig. 6.8). The cross section extends >23 km over a broadly consistent, and flat, land surface (Fig. 6.9). The Kaawa Formation is however highly variable with the thickest occurrences (up to 150 m) to the west, before thinning out from ~12 km west to ~20 m (Fig. 6.9). The upper topographic surface of the Kaawa Formation strongly resembles the upper topographic surface of the Waitemata Group which appears to have undergone considerable faulting (Fig. 6.9). The Waiuku cone, Hill Road tuff ring, and Whangarata Fault are identified (Fig. 6.9).

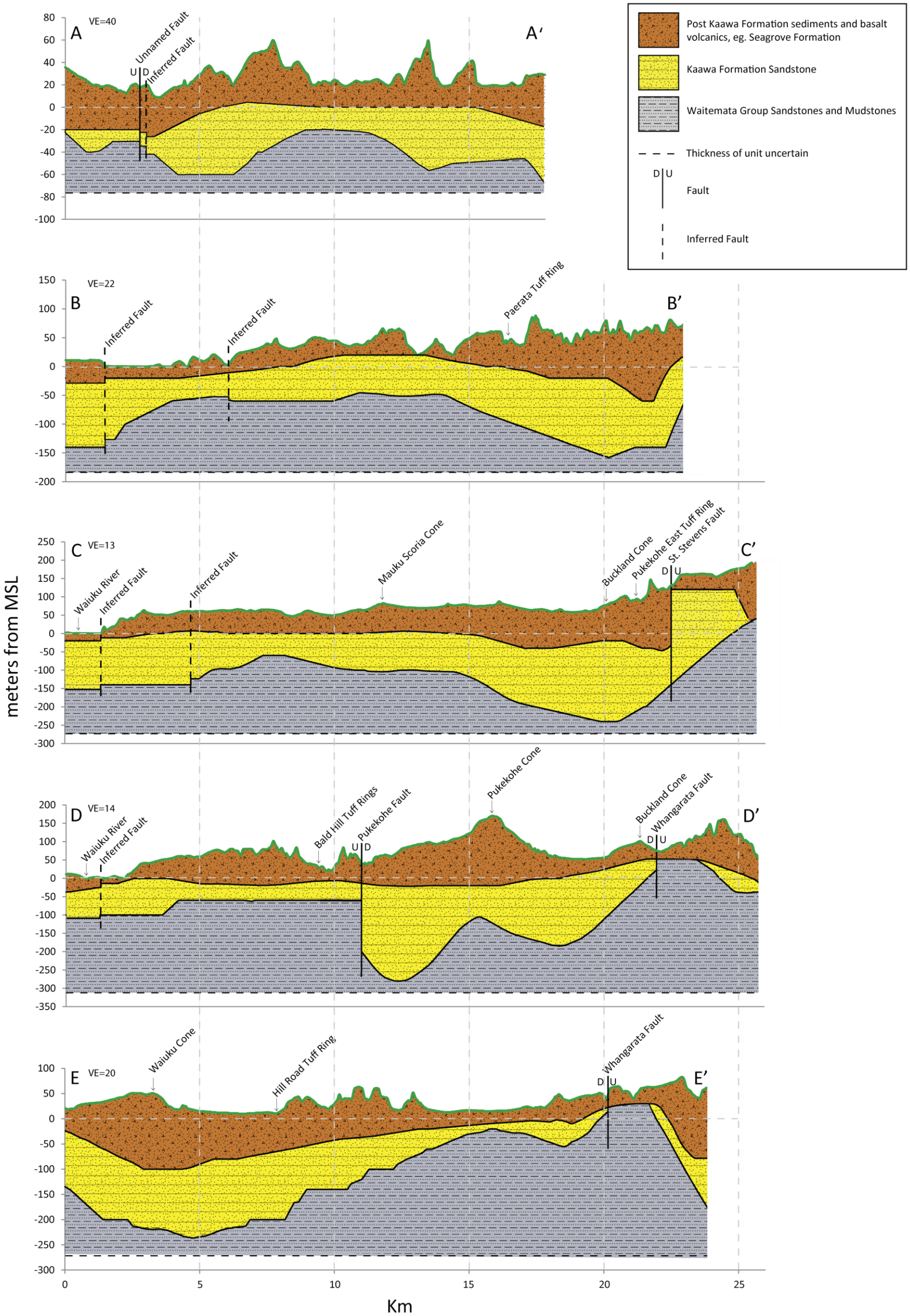


**Figure 6.9:** West-east trending cross sections of the Kaawa Formation and Waitemata Group through the SAVF. Faults and points of interest are indicated.

# Chapter Seven

# Discussion

## 7.1 Introduction

Phreatomagmatic volcanism across the SAVF has formed many tuff rings and/or maar craters. Studies such as Rosenberg (1991), Ilanko (2010), and Gibson (2011) have described and interpreted the volcanology and eruptive history of several phreatomagmatic (and magmatic) centres throughout the SAVF. This study builds on these previous studies, and discusses the classification of each centre as a tuff ring or maar crater, the eruption styles, phreatomagmatic processes, and emplacement mechanisms of each centre, along with spatial and temporal relationships throughout the SAVF.

## 7.2 Classification of Raventhorpe, Ingram Road and Pokeno West Tuff Rings

Tuff rings and maar craters both form by phreatomagmatic activity, generally by way of Surtseyan eruptions when magma contacts water (Houghton *et al.*, 2000). Tuff ring eruptions are generally more explosive than tuff cone eruptions (Francis & Oppenheimer, 2004) and comprise of more surge deposits than fall (Cas & Wright, 1987). Tuff rings generally display positive relief and higher profiles than maar craters (Cas, 1989). Juvenile material is abundant in tuff rings, whereas maar craters are generally juvenile poor (Cas & Wright, 1987).

Morphologically tuff rings have inner floor levels equal with, or higher than the surrounding land elevation (Cas & Wright, 1987). They have equally steep inner and outer slopes (Cas & Wright, 1987). Maar craters are characterised by inner floors that are lower than surrounding ground level elevation (negative relief), with low rims and steep internal slopes exposing the underlying country rock (Cas

& Wright, 1987). Maar craters generally have lower profiles than tuff rings and relatively flat outer slopes. Maar craters can be between 10-500 m deep (Lorenz, 2003; Francis & Oppenheimer, 2004) while tuff rings can form deposits up to 100 m thick (Cas & Wright, 1987).

Using a similar method to Kereszturi (2010), the land surfaces surrounding the tuff rings at each study location were calculated. The Raventhorpe volcanic centre has an inner floor that is approximately 21 m higher than the surrounding land surface, and the rim has a thickness of 50 m, which is considered a minimum of the original deposit due to erosion. The inner and outer (where present) slopes are steep, calculated from slope analysis in GIS. The deposit, while containing many lithics, is dominated by juvenile fragments and predominantly emplaced by surge processes. This suggests the Raventhorpe volcanic centre is a tuff ring.

The Ingram Road III volcanic centre, like all Ingram Road tuff rings, has undergone significant erosion since its formation. The volcanic centre has an inner floor that is approximately 9 m higher than the surrounding land surface, with a maximum thickness of the southern rim around 45 m. The slopes are moderately steep and only the southern rim is well defined. The deposit is dominated by finely fragmented juvenile pyroclasts, although a lapilli layer rich in lithics exists. This is an exception and the only bed in the outcrop observed. These data suggest Ingram Road volcanic centre III is a tuff ring. It is also likely that based on slope angles and floor elevation with respect to the surrounding land elevation, the four unexposed Ingram Road volcanic centres are also tuff rings.

The Pokeno West volcanic centre has an inner floor 7 m above the surrounding land surface. The centre has a maximum total thickness of 80 m from the lowest point to the highest point on the southern rim. The slope analysis displays steep slopes on the south, and south-western rim. The deposit is extremely high in juvenile components, much of it finely fragmented, indicating the Pokeno West volcanic centre is a tuff ring.

## 7.3 Spatial and Temporal Controls on Volcanism in the South Auckland Volcanic Field

The relationship between faulting and volcanic centres in the SAVF has been recognised previously by Bartrum and Branch (1936), Schofield (1958a), Rosenberg (1991), and Briggs *et al.* (1994). While this relationship has been recognised, statistics detailing the occurrence of volcanic centres in relation to fault proximity has never been presented. Faults are considered to have provided the path of least resistance for magma ascent (Rosenberg, 1991), with several centres located directly on faults (e.g. Bald Hill Tuff Ring) or are aligned parallel to the fault such as the magmatic centres to the north along the Drury Fault.

The relationship between the age of the volcanic centres and their distribution has previously been presented by Briggs *et al.* (1994). The statistical analysis for this study presented values representing a random distribution with respect to age. These values, although characterising the volcanic distribution as random, was nearer the tails of the normal distribution than would be expected. This could suggest that a larger data set might statistically yield a relationship, as Briggs *et al.* (1994) observed several older centres occurring to the northeast, and a small clustering of younger aged centres in the central-eastern region of the field. Briggs *et al.* (1994) suggested the SAVF volcanoes might have become more centrally located as the field developed. If such a relationship existed between age and location, it is possible that the younger volcanic centres and lava flows, especially in the centre of the field, have hidden the older centres from the geological record (Briggs *et al.*, 1994). Greig's (1989) study of borehole data revealed sediments between basalt eruptives, indicating that lavas and possibly other volcanic centres may be hidden and buried.

The interaction between ascending magma and water has had large implications in the eruptions, and hence the deposits of the SAVF (cf. Németh *et al.*, 2001; Németh & White, 2003). The presence of suitable, permeable strata, containing abundant water is therefore required to explain the presence of many of the volcanoes and their deposits throughout the SAVF. The aquifers' ability to continuously supply water during the eruptions, producing the explosive

interaction, is demonstrated at each outcrop (Houghton *et al.*, 2000). The aquifers throughout the extent of the SAVF and Manukau Lowlands consist of basalt (lavas and tuff), Pleistocene sediments, Kaawa Formation, and Waitemata Group.

The Pleistocene sediments are low-yielding aquifers with gravels providing locally high transmissivity (Greig, 1989). The sediments are found at shallow levels, and based on the stratigraphic analysis and interpretations the magma-water interaction was occurring much deeper, indicating that the Pleistocene sediments are not responsible for the water availability at the centres studied, and likely throughout most of the SAVF.

The thickness, petrographic evidence, and well known aquifer properties of the Kaawa Formation throughout the Manukau Lowlands indicates it provided the water for the phreatomagmatic volcanism that occurred. Stratigraphic evidence that water was encountered deeper (>250 m) suggests a source origin from the Te Kuiti or Waitemata Group. However, the aquifers within the Waitemata Group have a transmissivity of around 20-60 $m^2$/day, in comparison to 30-500 $m^2$/day from the Kaawa Formation (Greig, 1989).

## 7.4 Eruption and Emplacement Processes

Tuff rings are small monogenetic volcanoes produced through explosive interaction of magma with surficial or ground water (Cough & Sohn, 1990). They are most commonly emplaced by pyroclastic surges originating from collapsing eruption columns (Cough & Sohn, 1990). The eruption and emplacement processes, associated with each of the facies types identified at the three tuff ring centres studied (chapter 3) are presented here, and summarised in Table 7.1.

### 7.4.1 Raventhorpe Tuff Ring

Facies one (laminated to thinly bedded, well sorted, coarse ash to fine lapilli) represents pulses of highly fragmented material and occurs at the top and bottom of the stratigraphic column indicating surge beds with occasional fallout. The laminated to thinly bedded deposit of finely fragmented juvenile and lithic

material indicates the magma is interacting with abundant water (Houghton *et al.*, 2000). The presence of accretionary lapilli, vesiculated tuff, and gentle deformation of beds from bombsags indicates a wet depositional environment during transportation, possibly from condensation of steam (Németh *et al.*, 2001; Németh & White, 2003). This could indicate a near source origin (Németh & White, 2003).

These deposits are likely related, as the fall layers have settled out from the surge cloud (Németh *et al.*, 2001). The occasional pinch and swell bedforms indicate unsteady flow conditions (Allen *et al.*, 1996). The presence of different lithic types including igneous and sedimentary (Waitemata Group), represents subsurface explosions and/or unstable conduit conditions during eruptions (Németh & White, 2003). The high abundance of quartzofeldspathic crystals implies the Kaawa Formation was very important in the deposition of this facies.

The trajectories of bombsags appear to be directed into the outcrop at an orientation similar to interpreted flow directions, perpendicular to the vent and indicated by surge channels in the outcrop. The size range, angular to blocky clast shape, and vesicularities observed in juvenile clasts represents phreatomagmatic fragmentation of a non-homogenous magma with respect to bubble distribution (Németh & White, 2003). In the upper section of the stratigraphic column, lithics are more abundant and have been identified as Waitemata Group siltstones, representing an increase in water availability (or decrease in magma ascent rates) and hence a more explosive phase of the eruption (cf. Németh *et al.*, 2001). This indicates the vent was not stable during this phase, and that the fragmentation depth would have likely been >300 m based on the observed Waitemata Group lithics.

Facies two (wavy bedded, moderately to well sorted, coarse ash to fine lapilli) represents variable pulses of highly fragmented material across a thin succession within the outcrop. The wavy bedforms indicate an unsteady surge, whereas the high juvenile abundance and low lithic abundance indicates the eruption phase was dryer than the underlying beds of facies one (Houghton & Schminke, 1989; Allen *et al.*, 1996). The low lithic abundance indicates there was a decrease in fragmentation energy, at least with respect to the strength of the country rock at

the locus of fragmentation (Németh & White, 2003). This would suggest a decrease in the efficiency of the fuel coolant interaction occurring (White, 1996) and indicates that the vent was relatively stable during this phase (Németh *et al.*, 2008). The low angle undulations represent lower-regime to transitional bedforms produced by a relatively low concentration base surge (Sohn & Chough, 1989). They also suggest the bedforms did not involve flow separation, and maximum sediment deposition was on lee surfaces (Chough & Sohn, 1990).

The prevalence of sideromelane or its alteration product (palagonite), coupled with the variation in vesicularity, and angular to sub-rounded shape, suggests phreatomagmatic processes were important in forming these deposits (cf. Németh & White, 2003). The variably vesicular sideromelane implies sudden chilling and magma fragmentation upon contact with groundwater (Németh & White, 2003). Many quartzofeldspathic crystals were observed within this facies derived from the Kaawa Formation. Slumps are present and represent deformation of beds after deposition of a drying phase of the eruption.

Facies three, represented by massive, poorly to moderately sorted, medium lapilli to block and bomb bed with rare lithics, occurs as a thin succession within the outcrop, and represents explosive magmatic fallout. The presence of juvenile basalt clasts of different sizes, shapes, and vesicularities, represents fragmentation of a magma with uneven bubble distribution (Németh & White, 2003), or recycling of clasts as a result of repeated explosions (Houghton & Smith, 1993).

Many impact sags in the underlying facies indicate the depositional environment was still wet (or perhaps soft) during this time, even though the eruption was drying out (Németh *et al.*, 2001). The bed is likely an outcome of increased magma ascent rates, subsequently reducing the water to magma ratio, and resulting in a less explosive, dryer phase of the eruption (Houghton & Schminke, 1989). The reduced magma-water interaction resulted in less fragmentation energy, represented by the apparent lack of accessory lithics (Németh & White, 2003). This indicates the vent was stable through this phase, although a few white Waitemata Group siltstones were observed and were scavenged from at least 200 m deep where the surface of the Waitemata Group occurs. The coarse grainsize, wide vesicularity range, and rounded to angular shape of juvenile basalt clasts,

indicates that phreatomagmatic processes were occurring throughout this Strombolian style eruption (cf. Németh & White, 2003). The rate of magma ascent therefore must have been too large to allow for efficient fuel coolant type interaction (White, 1996).

Facies four, represented by planar bedded, moderately sorted, coarse ash to coarse lapilli represents variable explosive fall and surge phases of variably fragmented material. The low abundance of fine ash, planar bedding, and little topographic infilling indicates fallout as the dominant mechanism (Allen *et al.*, 1996). The sub-rounded to sub-angular shapes of the basalt clasts and moderate degree of sorting, likely represents phreatomagmatic fragmentation of magma with uneven bubble distribution (Németh & White, 2003).

Facies four occurs twice within the outcrop and comprises coarse ash, accessory lithics, and poorly to moderately vesicular scoriaceous lapilli. The increased presence of lithics, finely fragmented juvenile lapilli, and vesicularity range indicates there was an increase in the efficiency of fragmentation from fuel-coolant interactions (White & Houghton, 2000), likely due to increased water supply (Németh *et al.*, 2001; Németh & White, 2003; Németh *et al.*, 2008). This is likely a result of a decrease in magma ascent rates rather than an increase in water supply rates based on juvenile abundance (Németh *et al.*, 2001). The vent during this phase was therefore being excavated deeper and wider, based on the ratio of accessory basaltic igneous (surface) and sedimentary (deeper derived) lithics (Németh *et al.*, 2001). The moderate degree of sorting reflects the water available during the stage of the eruption, causing fine material from the plume, or surge cloud, to collide and amalgamate, forming ash aggregates that have a similar terminal velocity as the larger fall material (Houghton *et al.*, 2000).

Evidence for occasional surge deposits are present from some fine truncation of beds, and small scale channels. Some crude stratification of alternating ash and lapilli layers are also present, and indicate some tractional transport has occurred modifying the fall deposit (cf. Allen *et al.*, 1996). A slight grainsize decrease occurs upwards and could be attributed to a reduction in flow concentration (Allen *et al.*, 1996), or represent a continuous period of activity (Houghton *et al.*, 2000).

Rare impact sags have softly deformed the underlying bed sets indicating the depositional environment and eruption phase is wet (Németh *et al.*, 2001).

Facies five (crudely bedded, moderately to poorly sorted, medium ash to medium lapilli) represents an explosive fall phase in the eruption. The moderately sorted juveniles vary widely in vesicularity and are crudely bedded, indicating rapid deposition from fallout (Németh & White, 2003). Accessory lithic abundance is consistently low compared with other facies. This likely represents the vent becoming increasingly more stable, and suggests limited fragmentation energy (Németh & White, 2003). The juvenile clast abundance is high, inferring a reduction in the water-magma ratio (Allen *et al.*, 1996), either a result of a decline in water availability, reducing fuel coolant interaction efficiency, or due to an increase in magma supply. Bombsags occurring at the base of the unit, and sub-rounded to rounded voids within the tuff, where bombs have weathered out, are present throughout the facies.

The grainsize variations throughout the succession of coarse ash to coarse lapilli could represent fluctuating fragmentation energy, perhaps due to variations in available water. This is demonstrated in the large range of observed vesicularities (cf. Allen *et al.*, 1996). The presence of massive units within the crudely bedded succession represents relatively sustained periods during the eruption phase with the poor sorting a measure of the variable hydrological conditions (Houghton *et al.*, 2000). This would infer magma ascent rates were relatively constant. This increased magmatic explosivity may represent a drying out of the system (Németh *et al.*, 2001).

### 7.4.2 Ingram Road Tuff Ring III

Facies one is present in the lower 1.5 m of section, and in the final 2 m of section and represents varying pulses of highly fragmented material and explosive activity, depositing material as surges and fall. Laminated to thin bed sets occasionally truncate and pinch out, representative of many thin surge layers (Carmona *et al.*, 2011). The low lithic abundance indicates that fragmentation energy was limited (Németh, *et al.*, 2001), and that the vent was reasonably stable (Németh & White, 2003). The fine grainsize, and sub-angular to sub-rounded nature of the juveniles,

indicates that fragmentation however limited, was efficient enough to finely fragment the magma but not large volumes of country rock (Allen *et al.*, 1996).

In the upper two meters of section, both accessory lithic abundance and grainsize increases substantially, indicating more explosive activity (Németh *et al.*, 2001). The increase in large accessory lithics suggests excavation of the vent during this phase (Németh *et al.*, 2001). The moderately to well sorted nature, and presence of alternating ash and fine lapilli beds, is an indication of varying fragmentation energy throughout this part of the succession, and represents the interaction of magma with a reasonably constant supply of water (Allen *et al.*, 1996; Houghton *et al.*, 2000; Németh *et al.*, 2001). The variably vesicular, juvenile sideromelane and fragments of palagonite, infer sudden chilling, and magma fragmentation due to groundwater contact (Németh & White, 2003). Quartzofeldspathic debris are evident and implicate the Kaawa Formation as an important underlying strata in the dynamics of the Ingram Road tuff ring III eruption.

Facies two (graded, planar bedded, well sorted, coarse ash to fine lapilli) represents varying explosive pulses of predominantly highly fragmented material. The fine grainsize, sub-angular to sub-rounded shape, and well sorted nature of the beds indicate that fragmentation energy was fairly constant, and magma-water interaction was stable with only occasional fluctuations (Allen *et al.*, 1996; Houghton *et al.*, 2000; Németh *et al.*, 2001). Within the succession many quartzofeldspathic crystals were observed.

Accessory lithics are uncommon in the lower normally graded succession, however increase in size and abundance in the reversely graded upper succession, representing an increased explosive phase (cf. Németh *et al.*, 2001). It is probable during this phase that the vent deepened, indicated by the increase of deeper derived accidental lithics (Waitemata Group, and basement?), either by the downward migration of the fragmentation front, or from vent widening (Németh *et al.*, 2001). This indicates the vent was stable during the deposition of the normally graded lower succession, becoming less stable with time.

The normally graded beds are derived from sustained eruptions (Houghton *et al.*, 2000). The reversely graded section of facies two might be caused by decreases in

flow concentration with time, hindering settling, buoyancy, and/or dispersive pressure (Allen *et al.*, 1996). The presence of accretionary lapilli in the lower succession of the facies suggests a moisture rich environment during transportation, probably resulting from condensation of steam, and suggests a near source origin (Németh & White, 2003). No erosion channels were observed so it is unlikely that this facies has been reworked (Allen *et al.*, 1996).

### 7.4.3 Pokeno West Tuff Ring

Facies one (laminated to thinly bedded, moderately to well sorted, coarse ash to medium lapilli) represents varying explosive activity of moderate to highly fragmented material and infers vent clearing stages in the eruption. The planar laminated bedding, fine grained character, and moderate to well sorted nature of the deposit suggest primary fall origin with occasional surges (Allen *et al.*, 1996). Lithic abundance is moderate throughout this facies representing the consistent removal of country rock from the vent walls. The presence of deeply-seated lithics are evidence that the explosion locus was excavating the vent during this time (Németh *et al.*, 2001) at depths >250 m, based on the depth of the Waitemata Group surface. The occurrence of quartzofeldspathic debris is evidence for the Kaawa Formation. The predominantly angular character and variable vesicularity of the juvenile clasts indicates phreatomagmatic fragmentation of a non-homogenous magma (Németh & White, 2003).

The variable grainsize and sorting throughout the facies indicates changing water availability to the fuel-coolant type interaction fragmentation process (Németh *et al.*, 2001; Németh & White, 2003). The coarser bed sets within the facies likely represent the fall deposits and are more lithic rich than the laminated, more fragmented (fine-grained) beds of the surge deposits. Ballistic blocks and bombs from overlying units are occasionally present and gently deform the underlying laminated surge beds implying a damp or soft depositional environment (cf. Németh *et al.*, 2001).

Facies two (normally graded, planar bedded, moderately to well sorted, coarse ash to fine lapilli) represents pulsing of moderately fragmented material with increasing fragmentation energy. The variable size range and vesicularity of the

juvenile basalt clasts indicate the increasing fragmentation energy during the deposition of this facies (Németh & White, 1993). The juvenile basalt clasts also indicate fragmentation of a non-homogenously vesiculated magma (Németh & White, 2003). The moderate to well sorted nature of the deposit and laminated to thinly bedded structure indicates fall (Allen *et al.*, 1996). Lithic size and abundance throughout this facies succession is comparably high and infers increased fragmentation energy occurring at the explosion locus, likely >250 m, and suggests a large influx of water (Németh *et al.*, 2001). This is supported by the low juvenile abundance observed.

The normally graded nature of the deposit indicates the eruption stage was continuous, with the grading likely a response to gravity settling in surge layers (Allen *et al.*, 1996). Truncation and lensoidal beds are common, and indicate multiple surges occurring (Allen *et al.*, 1996). The overlying coarser lapilli and ballistic layers observed have occasionally deformed the underlying bed sets indicating a soft environment at the time of deposition (Németh *et al.*, 2001).

Facies three comprises laminated to thinly bedded, moderately to well sorted, coarse ash and lapilli, and represents varying explosive activity and less frequent pulses of highly fragmented material. The planar bedded nature of the deposit indicates fallout was the dominant mechanism, likely related to co-surge ash clouds (Allen *et al.*, 1996; Németh *et al.*, 2001). The well sorted, rounded to angular shape, size, and vesicularity of the juvenile clasts indicates consistent fragmentation energy of a non-homogenous melt (Allen *et al.*, 1996). This suggests a stable incoming flux of water (Houghton *et al.*, 2000). Many quartzofeldspathic crystals and debris are present in this facies implicating the Kaawa Formation, along with accessory igneous and sedimentary lithics. This suggests the vent is widening due to the abundant water and explosive activity produced during this phase. Bombsags are rare, and represent efficient fragmentation, gently distorting the underlying bedsets due to compaction in a damp environment (Németh *et al.*, 2001).

Facies four consisting of a massive, poorly sorted, medium lapilli, represents steady explosive activity of relatively unfragmented magma. The massive nature of the deposit indicates a continuous phase of the eruption (Houghton *et al.*, 2000).

The high concentration of scoriaceous juveniles represent a change in the water-magma ratio by either a reduction in available water, or an increase in magma ascent rate (Németh *et al.*, 2001). The wide range of vesicularities might suggest some stagnation and ponding of magma at the vent enabling degassing, while more gas rich magma exploded through the degassed crust (Allen *et al.*, 1996). The sub-angular to sub-rounded shape, and size of the lapilli, with the relative lack of accessory lithic materials, suggests that phreatomagmatic fragmentation energy from the fuel coolant interaction process was limited (Allen *et al.*, 1996; Németh & White, 2003). Throughout the succession, large blocks and bombs have weathered out of the tuff producing voids. Commonly the finer underlying beds are deformed due to the weight of the overlying lapilli. This indicates a damp or soft environment at the start of deposition (Németh *et al.*, 2001) with this phase likely representing a drying out, and fairly quick deposition (Houghton *et al.*, 2000; Németh & White, 2003).

Facies five (cross bedded, poorly to moderately sorted, coarse ash) represents varying pulses of highly fragmented material. The cross bedding observed is attributed to stoss-erosional dune formation, deposited from a sediment starved decelerating surge (Allen *et al.*, 1996). The dune-antidune structures and fine grained cross beds indicate a series of dry surges (Németh et al, 2001). This is also inferred from lensoidal layers indicating multiple surges (Allen *et al.*, 1996). The poor sorting in the lower section of the succession may perhaps be due to surge modification of underlying beds, incorporating material. The low juvenile abundance indicates fragmentation energy was high (Allen *et al.*, 1996), supported by fine grained accessory sedimentary lithics occurring in thin section. The variably vesicular, sub-rounded to rounded nature of the sideromelane dominated juvenile clasts indicates that phreatomagmatic processes were important in the deposition of this facies (Németh & White, 2003), and that fragmentation likely occurred in an unevenly vesicular magma (Németh *et al.*, 2001).

**Table 7.1:** Summary of facies, depositional interpretation and environment.

| Tuff Ring | Facies | Description | Depositional Interpretation | Environment | Eruption Style |
|---|---|---|---|---|---|
| Raventhorpe | 1 | Laminated to thinly bedded, well sorted, coarse ash to fine lapilli | Surge | Wet | Phreatomagmatic |
| Raventhorpe | 2 | Wavy bedded, moderately to well sorted, coarse ash to fine lapilli | Surge | Drying | Phreatomagmatic |
| Raventhorpe | 3 | Massive, poorly to moderately sorted, medium lapilli to block and bomb bed | Fall | Dry | Strombolian |
| Raventhorpe | 4 | Planar bedded, moderately sorted, coarse ash to coarse lapilli | Fall and surge | Wet | Phreatomagmatic |
| Raventhorpe | 5 | Crudely bedded, moderately to poorly sorted, medium ash to medium lapilli | Fall | Drying | Phreatomagmatic |
| Ingram Road | 1 | Laminated to thinly bedded, moderately to well sorted, coarse ash to medium lapilli | Surge | Wet | Phreatomagmatic |
| Ingram Road | 2 | Graded, planar bedded, well sorted, coarse ash to fine lapilli | Surge and fall | Wet | Phreatomagmatic |
| Pokeno West | 1 | Laminated to thinly bedded, moderately to well sorted, coarse ash to medium lapilli | Fall and surge | Wet | Phreatomagmatic |
| Pokeno West | 2 | Normally graded, planar bedded, moderately to well sorted, coarse ash to fine lapilli | Fall and surge | Wet | Phreatomagmatic |
| Pokeno West | 3 | Laminated to thinly bedded, moderately to well sorted, coarse ash and lapilli | Fall and occasional surge | Wet | Phreatomagmatic |
| Pokeno West | 4 | Massive, poorly sorted, medium lapilli | Fall | Dry | Strombolian |
| Pokeno West | 5 | Cross bedded, poorly to moderately sorted, coarse ash | Surge | Drying | Phreatomagmatic |

## 7.5 Petrography and Geochemistry

Magmatic (lava flows) and phreatomagmatic (tuff ring) deposits were analysed petrographically and geochemically with the implications to magmatic processes based on descriptions, modal analysis, bulk rock geochemistry, and mineral geochemistry.

### 7.5.1 Magmatic Deposits

Plagioclase feldspars exist predominantly as labradorite with less common andesine. Feldspars are commonly intersertal, or intergranular, but also occur as a comparatively rare phenocryst phase. Clinopyroxene phenocrysts most commonly occur as augite and are present in a variety of textures from glomeroporphyritic to subhedral to anhedral. These glomeroporphyritic textures could indicate the presence of cognate xenoliths (Cook *et al*., 2005) and have implications for petrogenesis. Commonly clinopyroxene phenocrysts display resorption textures representing melt disequilibrium (Cook *et al.*, 2005) and could indicate xenocrysts of mantle origin (Cook, 2002) and therefore fast magma ascent rates. However glass, when present, occurs in small amounts indicating that lavas of the SAVF likely ascended at rates satisfactory for near total crystallisation to occur (Cook, 2002).

The CIPW normative values returned for geochemical analyses of SAVF basalts, indicated high volumes of plagioclase, olivine, and clinopyroxene (as diopside), with lesser amounts of orthoclase, nepheline, ilmenite, magnetite, and apatite. Modal ilmenite, magnetite, and apatite are known to occur within the basalts from previous studies, often occurring in rarer rock types, i.e. mugearites (Rafferty & Heming, 1979; Rosenberg, 1991; Cook *et al.*, 2005). These data along with those from Cook (2002), indicate the basalts of the SAVF represent a diverse and heterogeneous group of basaltic magmas. Geochemical compositions of the SAVF basalts also display a similar range to basaltic magmas from the Northland Volcanic Province (Weaver *et al.*, 1989; Cook 2002).

Within both rock types (basanite, alkali olivine-basalt) of group B basalts sampled, quartzose xenoliths were observed. Texturally they display a recrystallised texture and indicate that they have undergone some degree of metamorphism. Searle (1962a, b) described very similar quartzose xenoliths in the AVF, and concluded their origin was most likely derived from quartz veins in the greywacke basement. It is likely the origins of both AVF and SAVF quartzites are the same. Their presence infers that high silica material has been incorporated into the melt. High $SiO_2$ values were determined from XRF analysis, indicating quartz normative CIPW values. Calculated Mg# values based on bulk geochemical analyses of the basalts produced a range of 49 to 61, in agreement with Cook (2002) and indicate a range of magma compositions that have likely evolved from fractional crystallisation processes (Cook *et al*., 2005).

One sample was classified a trachydacite and was interpreted as comprising an aggregation of accessory lithics from underlying Pleistocene gravels. Other examples were observed in lavas sampled from the SAVF containing large lithics.

### 7.5.2 Phreatomagmatic Deposits

The phreatomagmatic deposits of the Raventhorpe, Ingram Road, and Pokeno West tuff rings in the SAVF are composed of vitric tuff. The tuffs comprise of juvenile basalt clasts and crystals, rare accretionary lapilli, accessory lithics (both igneous and sedimentary), foreign crystals, and palagonite.

Two distinct types of juvenile basalt clast occur throughout the SAVF (Rosenberg, 1991), and comprise a dark sideromelane, and a yellow-brown palagonite. Crystalline basalt clasts are generally larger, non-vesicular, and have much higher phenocryst abundances, and are therefore considered to be accessory lithics from earlier basalt eruptives. The low phenocryst content of the sideromelane and palagonite clasts indicate residence time within the magma chamber was short (Houghton *et al*., 2000).

The sideromelane and palagonite clasts are variably vesicular, however, the sideromelane clasts are generally the more vesicular. The degree of vesicularity these two clasts display indicates that phreatomagmatic processes were important

in their formation (Németh & White, 2003) and indicate variable fragmentation energy throughout different eruption phases (Allen *et al.*, 1996). Higher vesicularities indicate complex interactions between magma and water, boosted by rapid vesiculation of a non-homogenous foam (Houghton *et al*., 2000), resulting in isolated vesicles (Wohletz & McQueen, 1984; Formenti & Druitt, 2003). More magmatic phases are characterised by the essentially total vesicle interconnectedness due to easy gas escape from permeable magma (Formenti & Druitt, 2003). The variably vesicular sideromelane and palagonite therefore indicate different water flux rates and hence variable degrees of alteration. The variable amounts of alteration occurring are evident from rare samples that comprise banding of sideromelane and palagonite, and suggests that recycling of altered basaltic glass was a mechanism involved with the formation of these clasts (cf. Németh *et al.*, 2001).

Data from this study indicates that the magma was not homogenous based on the broad vesicularity ranges obtained (Németh *et al.*, 2001; Formenti & Druitt, 2003; Németh & White, 2003). In many cases values of >30% to near 50% were measured, and represents magma that was already at various stages of vesiculation or degassing (Houghton & Schminke, 1989). The tuff deposits are all vesicular to some degree. The vesicularity of the tuff ranges 3% to 26% at Raventhorpe, 8% to 24% at Ingram Road tuff ring III, and 3% to 18% at Pokeno West.

Juvenile crystals occurring within the tuffs are predominantly olivine, clinopyroxene, and plagioclase. Discrimination of group A or B basalts can be made from observable clinopyroxene colours, with group B basalts displaying purple colours indicating large titanium contents. Phenocryst assemblages are respective of source depths. Group A basalts were generated by a shallow spinel peridotite source, while group B basalts were much deeper derived from a garnet peridotite (Cook *et al*., 2005).

Plagioclase composition is predominantly labradorite with a few in the calcic andesine field. This is in contrast to the xenocryst plagioclase which occurs as larger tabular crystals and would likely occupy the oligoclase field. Many other foreign quartz and plagioclase crystals are observed in the tuffs, and were derived from poorly consolidated sands and sandstones which served as aquifers that were

intersected by the ascending magma. Hornblende, hypersthene, and quartz are incompatible in alkali basalts and must therefore be exotic. Authigenic glauconite pellets were also observed, the nature of which forms in a marine environment. The Kaawa Formation comprises quartz, plagioclase, hornblende, hypersthene and glauconite (Hollis, 1986: Hadfield 1988; Greig, 1989), and was deposited in a marine environment, confirming this strata as the source of the xenocrysts.

Foreign accessory lithics comprise a significant volume of material within the tuffs. Accessory lithics are present throughout the tuff successions as: (1) accessory igneous basaltic lithics, which occur near surface from previous SAVF eruptives, (2) alluvium-derived Pleistocene gravels, also occurring near surface, (3) deeper-seated accessory sedimentary lithics comprising the Waitemata Group, and (4) basement rocks. These accessory lithics suggest changing vent dynamics, including vent clearing phases, widening (shallow derived lithics) and/or deepening (deeper derived lithics) (Németh *et al.*, 2001; Németh & White, 2003; Carmona *et al.*, 2011). The variable abundance (and size) of these accessory sedimentary lithics, indicates variable fragmentation energy available, and hence explosivity of the eruption (Allen *et al.*, 1996; Németh *et al.*, 2001; Németh & White, 2003; Németh *et al.*, 2008). There may have been magma-water interactions prior to the eruption as indicated by the presence of armoured accessory sedimentary lithics occurring as inclusions within pyroclasts, and could be derived from the aquifers of the Te Kuiti Group (if present), or the Waitemata Group.

Efficient fragmentation in a wet environment is indicated by the presence of accretionary lapilli (Németh & White, 2003). They comprise a core of ash surrounded by a thin film of fine ash and indicate the eruption cloud or column carried sufficient steam for the ash to nucleate and accumulate before deposition. They may also imply near source origins (Németh & White, 2003).

Mantle xenocrysts are present within the tuff at Raventhorpe, and can be used as a measure of magma ascent rate. Cook *et al.* (2002) also noted the presence of mantle xenocrysts in the lavas of the SAVF, using their presence to partly constrain a model for their generation. The presence of mantle xenocrysts indicates rapid magma ascent from the mantle, as they have not been resorbed or

reincorporated into the melt. The reaction rims that these crystals display indicates they are not stable in a surface environment. A magma ascending from 50 km depth, as proposed by Cook *et al.* (2005) as the lower limit for group A magmas, traveling at an ascent rate of 0.5 m/s (1.8 km/hr) (Wilson & Head, 1981; Serpa, 1984) requires 27 hours to reach the surface and have formed reaction rims (Righter & Carmichael, 1993). The thin reaction rims surrounding the pyroxene xenocrysts indicate magma ascent was slower than this, likely several days, allowing time for the reaction to occur. Cook (2002) also concludes the SAVF lavas ascended at a rate sufficient for near total crystallisation to occur, this however cannot be true of the tuff rings in the SAVF.

Alteration products of basaltic glass (palagonite) throughout the tuff, indicates that phreatomagmatic fragmentation had a large role in the three tuff ring deposits studied, and the wider SAVF (Rafferty, 1977; Rosenberg, 1991; Ilanko, 2010; Gibson, 2011). On rare occasion relict basalt shards are evident and appear in irregular blocky shapes. Wohletz (1983) described similar fragments which represent brittle deformation of magma during quenching in water. The presence of glass and its alteration products indicate the ascent rates of the magma producing the tuff rings and maars were insufficient for total crystallisation to occur and thus must have been highly variable compared to those producing the SAVF lavas. The rate and variability of magma ascent is likely controlling the type of centre that occurs throughout the Manukau Lowlands.

## 7.6 Eruption History

The magmas erupting at the Raventhorpe and Ingram Road tuff rings have been determined to be group A, and at Pokeno West tuff ring, group B. Cook *et al.* (2005) illustrates a model for the genesis of the magma which erupted throughout the SAVF. The model identifies partial melting of a metasomatised enriched mantle derived from an ancient Gondwanaland subduction zone as the origin of the magma (Cook *et al.*, 2005). The group A magmas were produced at shallow depths in a spinel peridotite source, while the group B magmas were derived from a much deeper source, >60 km, and were generated in the sub-continental lithosphere (Cook *et al.*, 2005). Cook *et al.* (2005) states that the two magmas

evolved simultaneously in their respective source regions, and would have likely ascended contemporaneously.

### 7.6.1 Raventhorpe tuff ring

The Raventhorpe tuff ring has been dated to 0.73 Ma (Briggs *et al.*, 1994), in an eruption that likely lasted weeks to months, or possibly years. The Raventhorpe tuff ring is a phreatomagmatic deposit that has formed as a result of basaltic magma intruding into basement. It has then likely ascended along the St. Stevens Fault which might have provided the least resistance, before intruding into Waitemata Group sediments which have been observed and identified (Rafferty, 1977) within the tuff. Magma has then encountered large volumes of groundwater within the Kaawa Formation, becoming highly explosive and establishing a vent. As the final 10 m in the tuff ring succession is exposed, the early eruption stages are unknown and can only be speculated.

During the early stages of the eruption the vent would have likely been unstable, such as Gibson (2011), Rout *et al.* (1993), Németh *et al.* (2001), Németh and White (1993), and Németh *et al.* (2008) have illustrated. Large lithic blocks would have been removed from the vent walls due to the early explosive encounters of the magma and water interaction. This first phase of the eruption likely built the outer tuff ring and would have been predominantly fall derived, with intermittent surges. As the vent began to stabilise different rates of magma ascent and water interaction would have produced a variation of falls and surges, with variable amounts and sizes of lithic material. Fluctuating eruption energy and intensity produced a combination of wet fall deposits, likely the result of Surtseyan style eruptions (Houghton *et al.*, 2000).

As the eruption progressed, surges modified slightly by fallout have occurred (Fig. 7.1A). The variable supply of magma contacting abundant water resulted in fine fragmentation, and deposition in a damp environment (Németh *et al.*, 2001). Variable magma ascent rates and water availability inferred from bombsags, grainsize, and lithic abundance, have likely caused the eruption to pulsate (Houghton *et al.*, 2000). This produced discrete phreatomagmatic explosions generating surges.

Wavy bedforms during this phase indicate that surge concentrations were relatively low, while the high juvenile abundance, and low lithic abundance, indicates this phase was drier than the previous (Németh *et al.*, 2001). The dryer environment suggests either: magma ascent rates increased, or water availability decreased.

The drying out of a system has been demonstrated by Houghton and Schminke (1989), and Németh *et al.* (2001), to be the result of increased magma ascent rates. The block and bomb bed would have resulted from Strombolian ballistic fallout (Fig. 7.1B), similar to that observed by Houghton and Schminke (1989), derived from an increased rate of magma ascent reducing the magma to water ratio (Houghton *et al.*, 2000; Németh *et al.*, 2001). The underlying surge deposit could have been formed during the last of the phreatomagmatic phase before the rate of magma ascent overwhelmed the available water.

The rate of magma ascent, and hence dry phase in the eruption would not have lasted long based on the 40 cm thickness of the deposit. The subsequent phases of volcanism saw the system revert back to its previous phreatomagmatic and Surtseyan styles. The succession is characterised by variable explosive phases with fallout dominating, modified with pulsing surges of highly fragmented magma (Fig. 7.1C). While the system reverted back to a phreatomagmatic dynamic, it is likely this sequence is the result of a more Surtseyan type style of volcanism (Allen *et al.*, 1996), and can be observed from facies five, which displays solely fall characteristics over a short succession. An increase in lithic abundance occurs through this succession indicating increased eruption and fragmentation energy, and the destabilisation of the vent (Houghton *et al.*, 2000).

The final stage in the eruption produced a very thick deposit of coarse ash and lapilli. This has been interpreted as surges with occasional fall deposits (Fig. 7.1D). Throughout the final five meters of the column, the grainsize decreased, suggesting the eruption energy waned before terminating.

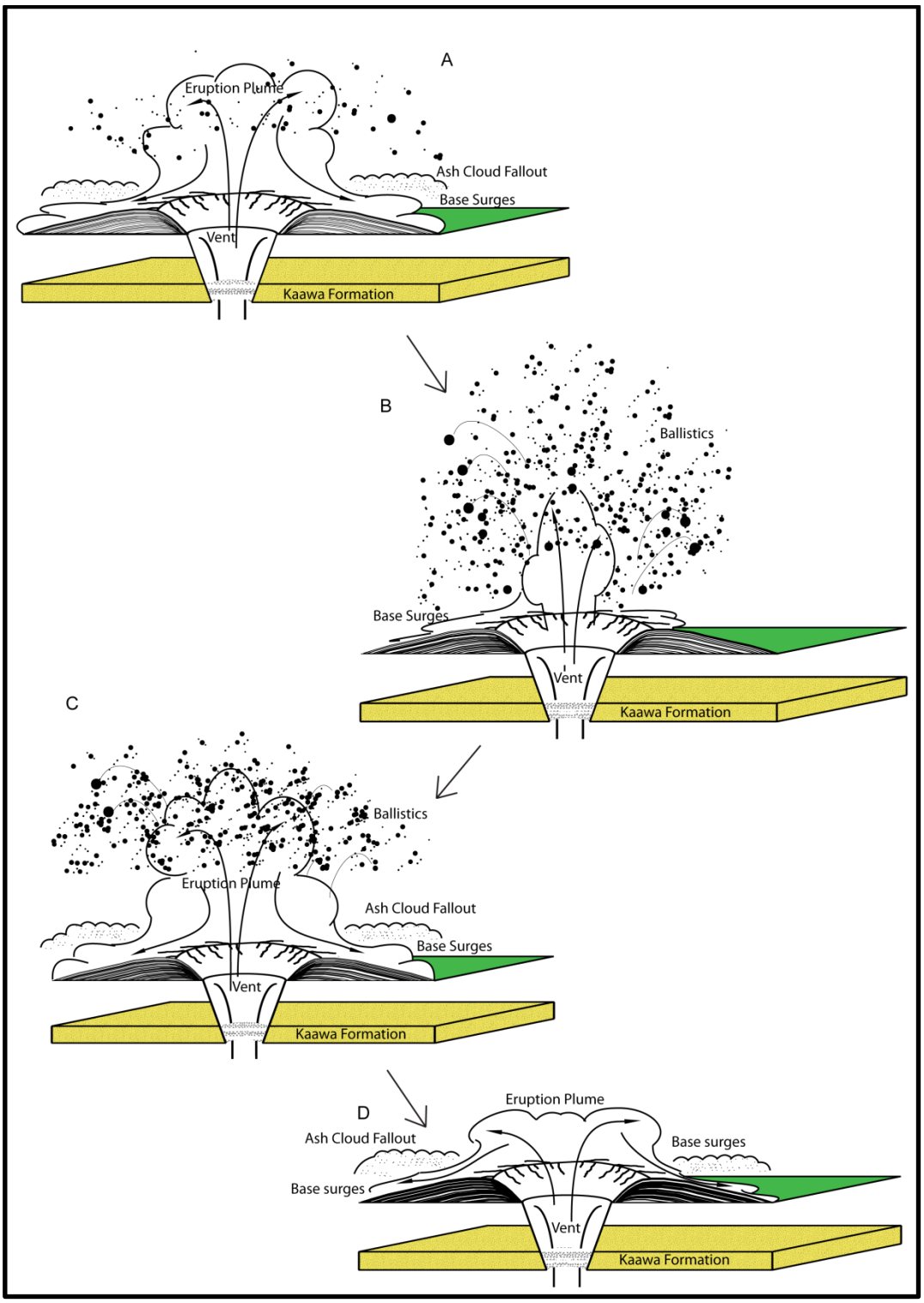


**Figure 7.1:** Eruption model for Raventhorpe tuff ring. (A) Surges modified by fall. (B) Dry phase depositing low concentration dry surges and block and bomb bed. (C) Fall modified by surges. (D) final stage surges before eruption ended, occasional fall deposits.

The succeeding events to the eruption have seen lavas breach the southern rim of the Raventhorpe tuff ring. Rosenberg (1991) suggested these lavas were derived from one of the several Bombay centres. A lava flow occurs to the north of the Raventhorpe tuff ring on which a stream flows, and could have preceded the tuff

ring eruption, or be related to the breach of the southern wall. Petrographic analysis indicates that the lava is very similar. Briggs *et al.* (1994) dated the Bombay cones at 0.59 ± 0.03 Ma, inferring they were one of the last centres in the field to erupt. This evidence suggests the lavas breaching the southern rim of the Raventhorpe tuff ring, and flowing out to the north, were derived from the Bombay cones erupting after the Raventhorpe tuff ring.

### 7.6.2 Ingram Road tuff ring III

The tuff ring of Ingram Road III has previously not been studied, and relative age has only been inferred from overlapping relationships (Rosenberg, 1991). Much like Raventhorpe tuff ring, the Ingram Road tuff ring III exposure comprises a short succession near what is now the top of the tuff ring rim. The highly eroded nature of the tuff ring and short succession offers little in terms of truly understanding the evolution of the centre. However, the short stratigraphic sequence infers that the dominant eruption style is phreatomagmatic with occasional Surtseyan phases based on the surge and occasional fall deposits observed.

Ingram Road tuff ring III has formed under similar conditions to that of the Raventhorpe tuff ring. The basaltic magma has likely ascended along the St. Stevens Fault before encountering large volumes of groundwater within the Kaawa Formation and establishing a vent. The early eruption processes are unknown.

The earliest indication of the eruption dynamics occurring at Ingram Road tuff ring III are represented by deposits characteristic of variable explosive fall and surges (Fig. 7.2A). The eruption during this phase was phreatomagmatic, and while fragmentation energy was limited, it was however still efficient enough to finely fragment the magma. The truncating layers are indicative of many thin surges, and likely pulses of activity due to an unsteady supply of magma and water, possibly from collapses in country rock (Houghton *et al.*, 2000).

As the eruption progressed, a thin sequence of solely surge derived material was deposited from phreatomagmatic activity (Fig. 7.2B). The characteristics of the

bed sets, the normally graded nature of the package, and the componentry data indicate fragmentation energy was quite constant throughout deposition during this phase. The lack of lithics throughout the entire lower section of the deposit, and evidence of apparent vent stability, suggests previous phases were more explosive (7.2C).

The eruption likely moved to an increased explosive phase (Fig. 7.2D). The increased lithic content indicates fragmentation energy was higher, however an increase in the juvenile abundance also indicates rates of magma ascent had increased (Németh *et al.*, 2001). Unstable vent dynamics would cause the collapse of country rock, and hence alter the rates of water availability producing variable eruptions (Houghton et al, 2000). After a relatively short period of increased explosive activity, the energy in the system began to decrease, as indicated by the reduction in grainsize and the decline in lithic abundance.

The final stage in the eruption sequence at Ingram Road tuff ring III was phreatomagmatic producing surge and fall deposits. This was likely due to a reduction in magma ascent as the eruption waned, indicated by the high fragmentation energy determined from the lithic content. A general decrease in lithic content indicates vent stabilising conditions, and waning energy in the final stages.

The subsequent events have seen the southern rim of the tuff ring breached by a lava flow that has not flowed into the tuff ring crater. This lava flow was likely produced by an eruption from the Rutherford Road cone. Geochemically, basalt lava samples taken from the Rutherford Road cone, and near the Ingram Road tuff ring III, are very similar and plot out in the same basalt field. Petrographically they are also very similar, suggesting the lava breaching the rim of the Ingram Road tuff ring III cone was derived from the Rutherford Road cone, erupting 0.65 Ma (Briggs *et al.*, 1994). This would indicate the age of the Ingram Road tuff ring III to be older than 0.65 Ma.

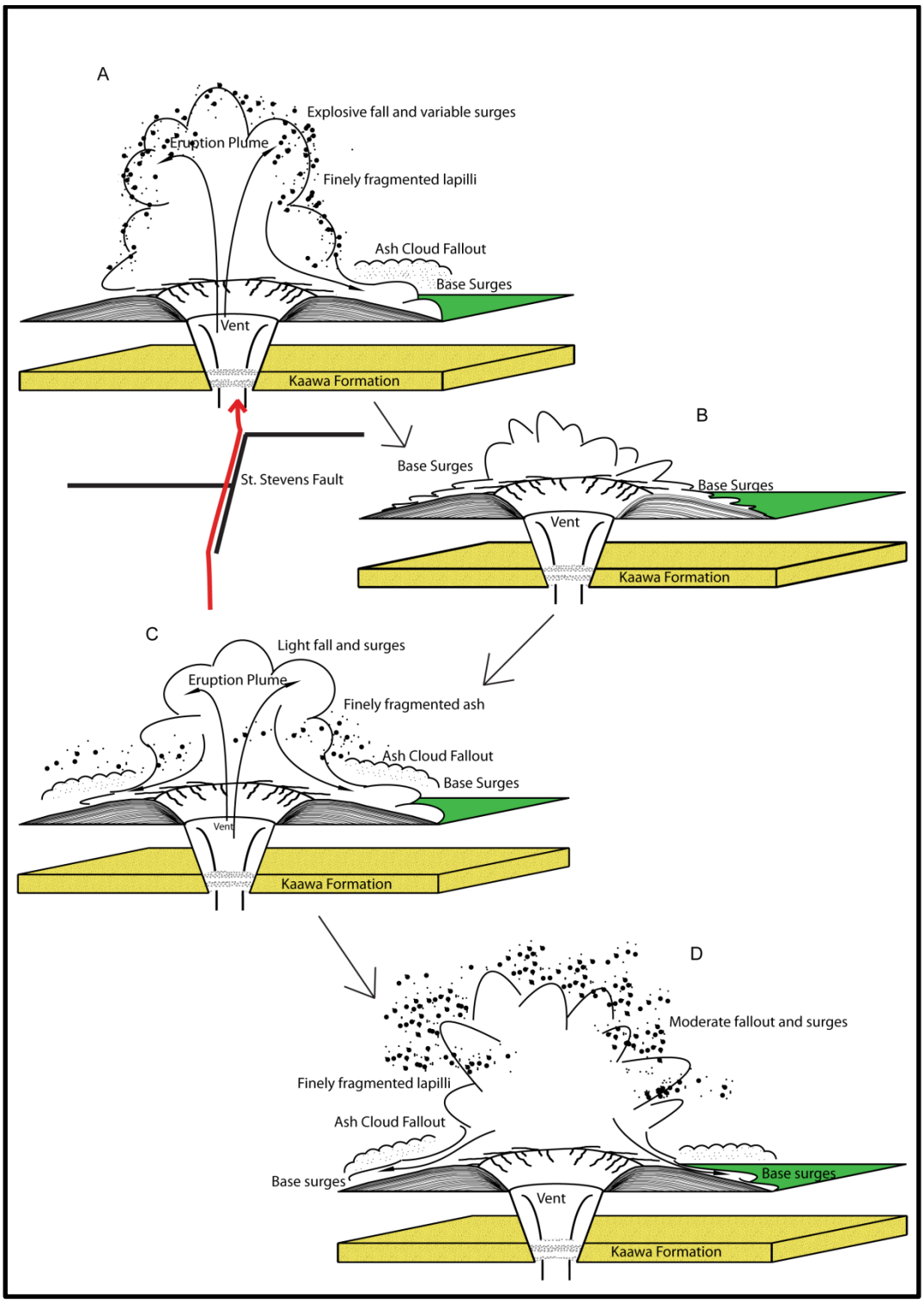


**Figure 7.2:** Eruption model for Ingram Road tuff ring III. (A) Finely fragmented fall and surge deposits. (B) Solely surge phase. (C) Decreasing energy-light fallout and surges. (D) Explosive fallout and surges.

### 7.6.3 Raventhorpe Volcanic Complex

Only two of the six interconnected tuff rings at the Raventhorpe volcanic complex have an adequate exposure to study. The sequence of volcanic events which produced the cluster can be speculated. The overlapping relationships are evidence on which the relative eruptive timing is inferred. The Raventhorpe tuff ring, and Ingram Road tuff ring III have been identified as group A magmas. It is possible the entire complex is group A magma and erupted at similar times, based on magma ascent along the St. Stevens Fault and into different, yet closely spaced, feeder dykes when one became inaccessible.

The overlapping relationship of the tuff rings suggest Ingram Road tuff ring I erupted first, followed by Ingram Road tuff ring II. The following eruption was either Ingram Road tuff ring III or V, although tuff ring V could have erupted at any time before 0.65 Ma based on lavas of the Rutherford Road cone breaching the tuff ring. Ingram Road tuff ring IV was the last of the Ingram Road tuff rings to erupt before the Raventhorpe eruption (0.73 Ma; Briggs *et al.*, 1994) overlapping Ingram Road tuff ring IV. Rosenberg (1991) observed accessory tuff lithics from Ingram Road tuff ring within the Raventhorpe tuff ring succession, indicating their presence prior to that of Raventhorpe. The entire tuff ring complex can therefore be constrained to an age older than 0.73 Ma.

### 7.6.4 Pokeno West tuff ring

The Pokeno West tuff ring is the thickest tuff succession in this study, and is the best stratigraphically exposed outcrop. The tuff ring has never previously been studied in detail. The age range of 1.24-1.08 Ma has previously been suggested by Rafferty (1977) based on morphology and geographic location within the SAVF based on previously determined ages of other centres. There are three exposures at Pokeno West, two of which are ~10 m thick. All three can be roughly correlated based on accurate height measurements from GPS readings taken at the base of each column (Fig. 7.3). They indicate a complex eruptive history in which phreatomagmatic, and highly explosive volcanism dominated. Surtseyan style eruptions have likely also occurred, along with short phases of more magmatic, Strombolian style volcanism which has continuously alternated throughout the eruption history.

The localisation of the basaltic magma ascent is not clear. It is possible that magma ascended along the nearby Pukekawa or Waikato faults, and was then deflected by the weak overlying Miocene rocks as Cassidy and Locke (2011) hypothesise for the AVF. Magma could have also ascended through unknown faults in the highly block faulted basement (Schofield, 1958a; Rafferty, 1977), and then proceeded into the weak overlying rock units of the Waitemata Group. Magma would have then reacted violently when encountering high volumes of water within the Kaawa Formation and subsequently established a vent.

The earliest stages of the eruption near the vent are unknown because of lack of exposure. A distal outcrop of <4 m (location two) lies stratigraphically above the 1.0 Ma Kidnappers Ignimbrite. The tuff at this location has no indication of the early vent dynamics illustrated by Gibson (2011), Rout *et al.* (1993), Németh and White (1993), and Németh *et al.* (2008), who obtained evidence for early phases removing large accessory lithic fragments from the country rock walls. The section represents a finely fragmented fall and surge succession with beds dipping 19° inward of the tuff ring. While contacting the Kidnappers Ignimbrite, it is unlikely that this succession represents the very earliest stages in the tuff ring formation, rather is the result of phases proceeding early interactions, after the primary tuff ring forming stages have occurred due to its distal location.

There is a thin layer of silty clay that lies above the Kidnappers Ignimbrite only present in some locations. This might represent lake sediments in the area before the eruption. The time between deposition of the 1.0 Ma Kidnappers Ignimbrite and the eruption at Pokeno West might have only been several hundred years if sedimentation rates were sufficient for 30-40 cm of silt, mud, and tephras from the TVZ to accumulate. This stratigraphic data indicates the Rafferty (1977) age estimate of 1.24-1.08 Ma is incorrect, and the age is now known to be <1.0 Ma.

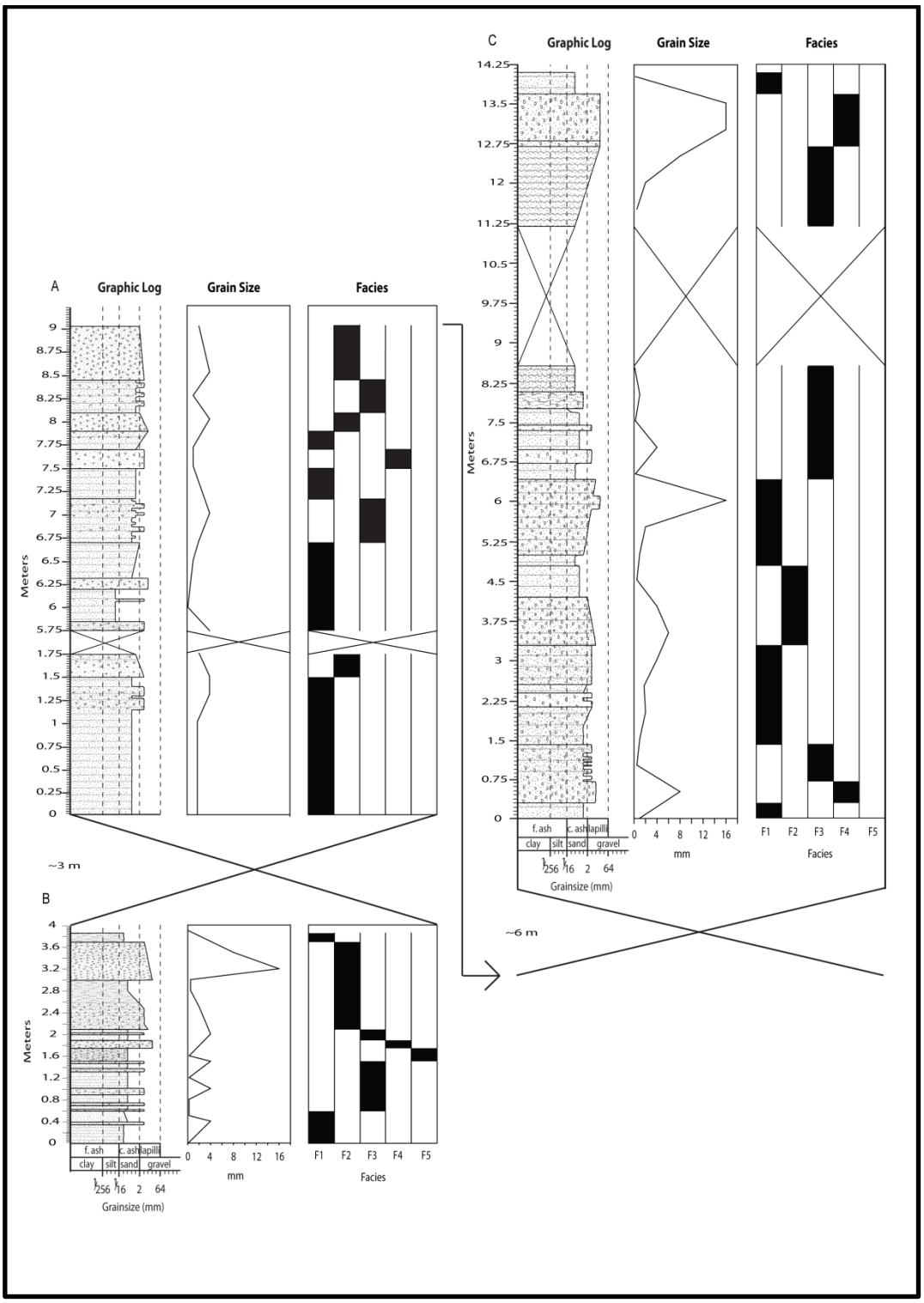


**Figure 7.3:** Compilation of stratigraphic columns of Pokeno West tuff ring III, indicating graphic log, grainsize, and facies. Location 1, 2, 3 labelled A, B, C respectfully.

The stratigraphically lowest exposed section at Pokeno West is an explosive phase dominated by fall with occasional surges (Fig. 7.4A). The phase represents varying explosive activity of highly fragmented material, suggesting a vent stabilising phase early in the eruption. Several pulses throughout this early stage

produced lapilli beds, and were likely the result of a weak Strombolian style eruption (cf. Allen *et al.*, 1996). Lithic abundance is moderate throughout the lower stratigraphic section (Fig. 7.3B), indicating high fragmentation energy levels (Németh *et al.*, 2001; Németh & White, 2003). Distal source areas likely received thin layers of highly fragmented ash. Surges in these areas deposited wavy or cross-bedded successions, and indicate unstable flow regimes from decreasing energy due to distance.

As the eruption progressed it entered a very complex eruptive phase. Explosive activity with occasional variable surges occurred (Fig. 7.4Bb), depositing planar bedded coarse ash and lapilli. The eruption at this time was phreatomagmatic. Magma ascent rates then increased substantially, depositing a massive lapilli fall unit from a Strombolian style eruption (Fig. 7.4C). The increased magma ascent rate likely dried out the eruption. With a reduction in magma ascent rate and an increase in the water to magma ratio, variable explosive and surge phases then proceeded. Fragmentation energy was high comparative to the strength of the country rock, removing and depositing large volumes of small lithics, suggesting unstable vent dynamics.

Several increases in magma ascent rate, and variable magma-water interaction, produced an almost identical phase. Variable explosive activity and surges deposited lithics, and fragmented material in planar beds due to fallout from a phreatomagmatic phase. The increased magma ascent rate produced a magmatic style eruption, depositing a thick lapilli layer with few accessory lithics. The range of vesicularities measured indicates that some stagnation and ponding of magma at the vent may have occurred, and allowed the degassing of magma while more, gas rich magma, exploded through the degassed crust (Allen *et al.*, 1996). Once the magma ascent rates declined, the explosive fall deposits returned, and the system reverted back into a phreatomagmatic phase.

The high lithic content throughout the final phases in the eruption suggest that water availability was abundant and continuous (Allen *et al.*, 1996; Németh & White, 2003; Houghton *et al.*, 2000). Many lithics were removed in violent explosive interactions, being deposited by falls and surges (Fig. 7.4D). Few

magmatic phases exist in the mid to upper section of the tuff ring indicating magma ascent rates waned and became more constant with time.

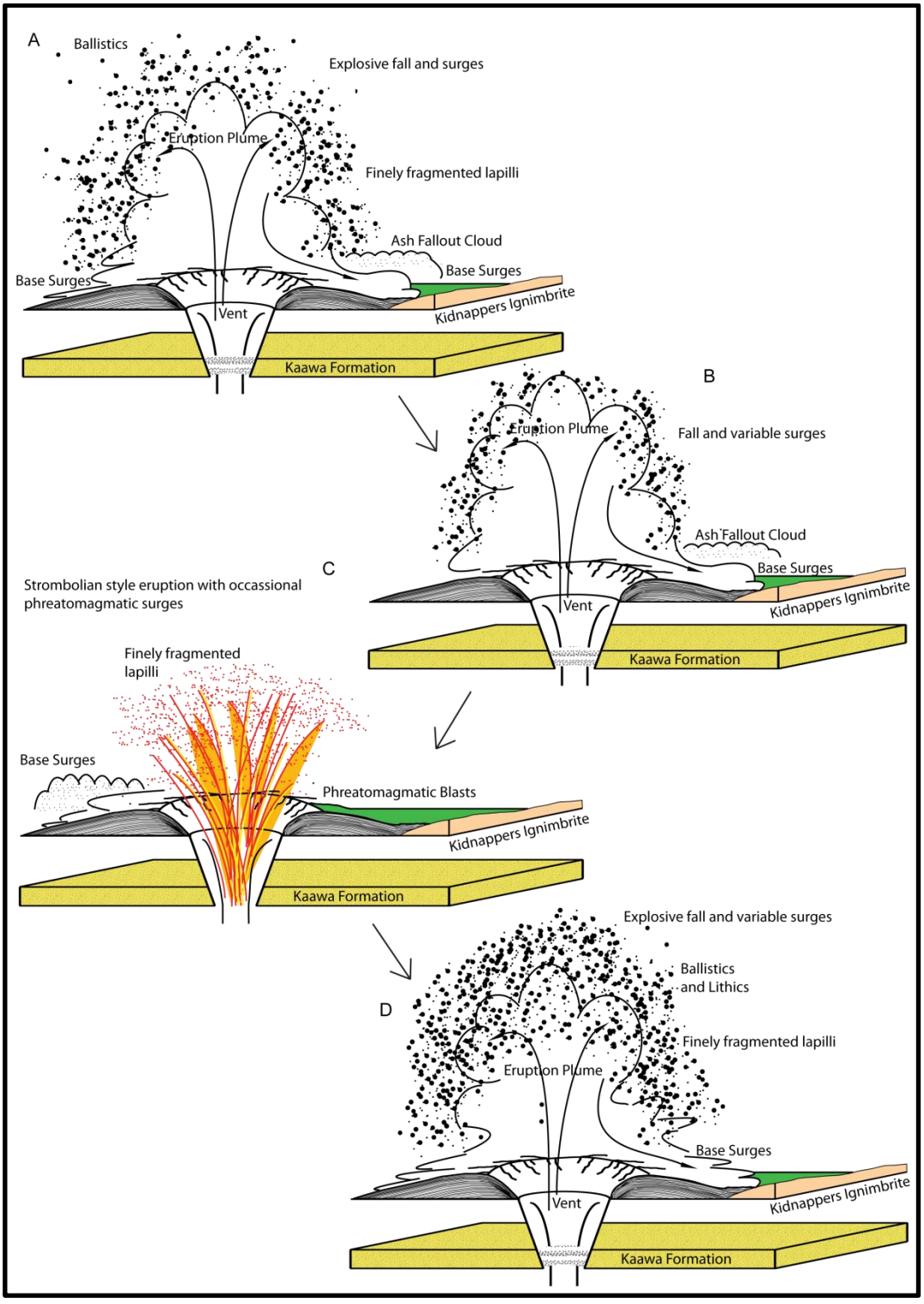


**Figure 7.4:** Swarm of bees eruption model for the Pokeno West tuff ring. (A) Explosive phase, fall and occasional surges. (B) Variable explosive fall and surges. (C) Strombolian style fall deposit. (D) Explosive falls and surge.

The sections at each location at Pokeno West are highly variable and alternate continuously. The variable range of vesicularities obtained indicates fragmentation of a non-homogenous magma occurred throughout the entire eruption (Németh *et al.*, 2001). To the southwest the Bluff Road cone erupted, with lavas flowing over the southern rim of the tuff ring without breaching it. Erosion since then has removed much of the entire tuff ring. Briggs *et al.* (1994) dated the lava of the Bluff Road cone to 0.64 Ma. During a later stage, lava breached the northern rim of the tuff ring, likely from magmatic centres occurring along the Drury Fault around Bombay. Rafferty (1977) suggested the northern lava originated from the Bombay cones based on petrographic evidence. The cones of Bombay have since been dated by Briggs *et al.* (1994) at 0.59 Ma, consistent with the timing of the Pokeno West tuff ring and observations of Rafferty (1977).

## 7.7 Comparisons to other centres

The centres of Raventhorpe, Ingram Road and Pokeno West can be compared. All three indicate sufficient evidence for their location based on proximity to faults. Rosenberg (1991) concluded there was strong structural control on the localisation of Barriball, Maketu, and Smeed Quarry tuff rings. The underlying geology of the three centres in this study is the same, with local variations in the thickness of the Kaawa Formation and overlying sediments and basalt eruptives. The deposits of the Raventhorpe tuff ring decrease in grainsize with increasing stratigraphic height, while the other two centres are monotonous in this regard. Rosenberg (1991) observed no grainsize trends occurring at the centres of Barriball and Aka Aka tuff rings contrasting to Gibson (2011) who observed grainsize fining at Kellyville. The deposits of Raventhorpe and Pokeno West indicate phases of changing eruption style, away from phreatomagmatic, towards a more Strombolian style, similar to that occurring in Maketu tuff ring (Rosenberg, 1991). Ingram Road tuff ring III does not indicate any change in style has occurred, comparable to Aka Aka tuff ring (Rosenberg, 1991).

Fragmentation energy at all locations was variable, and likely represents interactions between magma ascent rates and water availability (Houghton *et al.*,

2000). Fragmentation energy has been fairly high throughout the eruptions occurring at each centre. This contrasts to the findings of Rosenberg (1991), who observed very few lithics in the Aka Aka tuff ring. The lithic abundance throughout the centres of Raventhorpe and Ingram Road remained consistent, while the abundance at Pokeno West decreased with increasing stratigraphic height. At the centres of Onewhero and Kellyville, Gibson (2011) identified an increase in lithic content, contrasting to the observations made at Raventhorpe and Pokeno West volcanic complexes.

The juvenile abundance is consistent throughout each stratigraphic section and does not indicate any trend, except variable magma ascent rates and water availability. This is similar to the Onewhero tuff ring, but contrasts to that of Kellyville tuff ring, which showed a decrease with stratigraphic height (Gibson, 2011).

The dominant control on the style of volcanism occurring at Raventhorpe tuff ring is magma ascent rate, the variability of which produced a range of vesicular juvenile pyroclasts. The Kaawa Formation is also an important control, and had large implications providing water in the eruption. This is likely the dominant control on Ingram Road tuff ring III, and Barriball Road tuff ring (Rosenberg, 1991; Ilanko, 2010), however the short succession at Ingram Road allows little to be fully concluded. Pokeno West tuff ring was controlled by the highly variable magma ascent rate and the thick Kaawa Formation deposit in the area.

All centres indicate fall and surge processes have occurred and deposited similar amounts of material. Drying phases deposit ash and lapilli as more massive air fall units, while the more common wetter phreatomagmatic explosions deposit finely fragmented material as thin fallout and surges. Raventhorpe was the only centre which indicated a grainsize fining and predominant surge deposition towards the end of the eruption. Final stage surges before eruption termination were also described by Gibson (2011) at Onewhero tuff ring.

The main differences between the three centres studied, and others that occur in the SAVF are the hydrology, proximity to faults, and absence of any later, solely magmatic phase, as described by Rosenberg (1991) at Maketu, and Gibson (2011)

at Kellyville. The hydrology affecting the eruption style throughout the Manukau Lowlands is dominantly the Kaawa Formation aquifers, while to the south the Waikato River valley likely provided the water source such as at Kellyville tuff ring (Gibson, 2011). While many of the centres occur proximal to faults, some centres throughout the Manukau Lowlands occur with what appears to be an isolated distribution.

## 7.8 Conclusions

The focus of this thesis was to document the physical volcanology of several centres in the SAVF, and to study the field as a whole through spatial and temporal analysis. Two volcanic complexes were chosen: Raventhorpe, which included the Raventhorpe tuff ring, and the five Ingram Road tuff rings all interconnected, and the Pokeno West tuff ring with the nearby Bluff Road cone.

Field study was undertaken with the data presented using a facies concept. The petrography of the deposits were then described and analysed. Lava samples were studied using geochemistry, while individual crystals within the tuff were microprobed to determine their origin. These data were combined to give an account of the eruption mechanisms and evolutionary history occurring at each centre.

New information was discussed. This included: (1) the identification of Ingram Road tuff ring III as a type A magma based on petrographic analysis, (2) the use of slope analysis as a tool for tuff ring identification throughout the SAVF, and likely other monogenetic fields, (3) an eruption history for the Pokeno West tuff ring, (4) a newly constrained age range for the Pokeno West tuff ring, previously 1.24-1.08 Ma, now <1.0 Ma, and (5) statistical evidence for faulting and hydrology as the main controls on volcanism throughout the SAVF.

The second objective was to study the spatial and temporal relationships within the field. This returned results that were as predicted, and had been previously concluded by Rosenberg (1991) and Briggs *et al.* (1994). The data produced suggests: (1) the occurrence of centres is strongly fault controlled as previously

described (Rafferty, 1977; Rosenberg, 1991; Briggs *et al.*, 1994), (2) the underlying geology and hydrology influences the distribution of phreatomagmatic centres (Rosenberg, 1991), and is commonly the Kaawa Formation ranging in thickness over an irregular Waitemata Group surface, and (4) the distribution of volcanic centres and age correlation is random and proven statistically.

The SAVF can offer much in terms of studying ancient volcanic centres to better understand volcanic processes, mechanisms, and erosion rates of older fields in contrast to presently active fields. Modern spatial analysis tools can be used to produce statistics and outputs that can benefit our knowledge of the spatial and temporal relationships that are possibly occurring in monogenetic fields. The occurrence of volcanoes throughout the SAVF is strongly controlled by faulting and hydrology, and at a smaller scale, each centre is then controlled by localised factors including magma ascent rates and water availability. The evolution of the volcanic complexes in this thesis offer insights into the structure, and processes which have occurred throughout the SAVF, and can add to the understanding of presently or potentially, active volcanic fields such as the AVF.

# References


Allen, S. R., Bryner, V. F., Smith, I. E. M., Ballance, P. F. (1996). Facies analysis of pyroclastic deposits within basaltic tuff rings of the Auckland volcanic field, New Zealand. *New Zealand Journal of Geology and Geophysics*, 39 (2): 309-327.

ARC. (1996). *A model of recharge to Pukekohe volcanic aquifers, South Auckland: preliminary study*. Technical Publication no. 77, Auckland Regional Council, Auckland.

Barringer, J. R. F., Pairman, D., McNeill, S. J. (2002). *Development of a high resolution digital elevation model for New Zealand*. Landcare Research Contract Report, LC0102/170.

Bartrum, J. A., Branch, W. J. (1936). Geology of Bombay-Happy Valley Area, Franklin County, Auckland. *Transactions of the Royal Society of New Zealand*, 65: 386-404.

Battey, M. H. (1949). The Geology of the Tuakau-Mercer Area, Auckland. *Transactions of the Royal Society of New Zealand, 77*(3): 429-455.

Briggs, R. M., Okada, T., Itaya, T., Shibuya, H., Smith, I. E. M. (1994). K-Ar ages, paleomagnetism, and geochemistry of the South Auckland volcanic field, North Island, New Zealand. *New Zealand Journal of Geology and Geophysics*, 37: 143-153.

Briggs, R. M., Houghton, B. F., McWilliams, M., Wilson, C. J. N. (2005). $^{40}Ar/^{39}Ar$ ages of silicic volcanic rocks in the Tauranga-Kaimai area, NZ: dating the transition between volcanism in the Coromandel Arc and the Taupo Volcanic Zone. *New Zealand Journal of Geology and Geophysics*, 48: 459-469.

Briggs, R. M., Pittari, A., Rosenberg, M. D. (2010). *Controls on volcanism in the South Auckland volcanic field. GeoNZ 2010*: Joint Meeting of The Geoscience Society of New Zealand: The New Zealand Geothermal Works.

Carmona, J., Romero, C., Dóniz, J., García, A. (2011). Characterization and facies analysis of the hydrovolcanic deposits of Montaña Pelada tuff ring: Tenerife, Canary Islands. *Journal of African Earth Sciences*, 59: 41-50.

Cas, R. A. F., Wright, J. V. (1987). *Volcanic successions- Modern and ancient*. Allen and Unwin, London.

Cas, R. A. F. (1989). *Physical Volcanology*, in Johnson, R. W. (*ed*.), *Intraplate Volcanism*, Cambridge University Press, Cambridge, pp. 55-87.

Cas, R. A. F. (2006). Explosive mafic volcanism. *Journal of Volcanology and Geothermal Research*, 155, Preface: vi.

Cassidy, J. (2006). Geomagnetic excursion captured by multiple volcanoes in a monogenetic field. *Geophysical Research Letters*, 33: L21310, 5pp.

Cassidy, J., Locke, C. A. (2011). The Auckland volcanic field: Geophysical evidence for structural and spatio-temporal relationships. *Journal of Volcanology and Geothermal Research*, 195: 127-137.

Chough, S. K., Sohn, Y. K. (1990). Depositional mechanisms and sequences of base surges, Songakasan tuff ring, Cheju Island, Korea. *Sedimentology*, 37: 1115-1135.

Cole, J. W., (1986). Distribution and tectonic setting of late Cenozoic volcanism in New Zealand. *In*: Smith, I.E.M. (*ed*.), Late Cenozoic volcanism in New Zealand. *Royal Society of New Zealand Bulletin*, *23*:7-20.

Condit, C.D., Connor, C. B. (1996). Recurrence rates of volcanism in basaltic volcanic fields: An example from the Springerville volcanic field, Arizona. *Geological Society of America*, 108 (10): 1225-1241.

Cook, C. (2002). *Petrogenesis and evolution of alkalic basaltic magmas in a continental intraplate setting: the South Auckland volcanic field, New Zealand*. Thesis, University of Waikato.

Cook, C., Briggs, R. M., Smith, I. E. M., Maas, R. (2005). Petrology and geochemistry of intraplate basalts in the South Auckland volcanic field, New Zealand: Evidence for two coeval magma suites from distinct sources. *Journal of Petrology*, 46 (3): 473-503.

Cox, S. H. (1882). North Auckland District, Including Thames, Coromandel, Island of Kawau, and Drury Coal Field. *New Zealand Geological Survey Report for Geological Exploration 1881*, 14: 17-41.

Cox, S. H. (1877). Report on Waikato District. *New Zealand Geological Survey Report for Geological Exploration 1876-7*, 10: 11-26.

Edbrooke, S. W. (2001). *Geology of the Auckland Area*, Institute of Geological and Nuclear Sciences Limited, Lower Hutt, New Zealand.

ESRI. (2011). *ArcGIS Desktop: Release 10*. Environmental Systems Research Institute. Redlands, California.

Formenti, Y., Druitt, T. H. (2003). Vesicle connectivity in pyroclasts and implications for the fluidisation of fountain-collapse pyroclastic flows, Montserrat (West Indies). *Earth and Planetary Science Letters*, 214: 561-574.

Francis, P., Oppenheimer, C. (2004). *Volcanoes*, Oxford University Press, New York.

Furlong, K. P., Kamp, P. J. J. (2009). The lithospheric geodynamics of plate boundary transpression in New Zealand: Initiating and emplacing subduction along the Hikurangi margin, and the tectonic evolution of the Alpine Fault system. *Tectonophysics*, 474 (1-4): 449-462

Gibson, A. C. (2011). *Volcanology of tuff rings at Kellyville, Onewhero, and Bombay, South Auckland Volcanic Field*. Thesis, University of Waikato.

Greig, D. A. (1989). *A study of the Kaawa Formation aquifer system in the Manukau Lowlands*, Technical Publication No. 85, Auckland Regional Water Board, Auckland.

Hadfield, J. C. (1988). *Aspects of Kaawa Formation hydrogeology: A preliminary evaluation of a steady state finite element groundwater model*. Thesis, University of Waikato.

Hayward, B. W., Brook, F. J., (1984). Lithostratigraphy of the basal Waitemata Group, Kawau Subgroup (new), Auckland New Zealand. *New Zealand Journal of Geology and Geophysics*, 27: 101-123.

Hochstein, M. P., Nunns, A. G. (1976). Gravity measurements across the Waikato Fault, North Island, New Zealand. *New Zealand Journal of Geology and Geophysics*, 19: 347-358.

Hodder, A. P. W. (1984). Late Cenozoic rift development and intra-plate volcanism in northern New Zealand inferred from geochemical discrimination diagrams. *Tectonophysics*, 101: 293-318.

Hoernle, K., White, J. D. L., van den Bogaard, P., Hauff, F., Coombs, D. S., Werner, R., Timm, C., Garbe Schönberg, D., Rea, A., Cooper, A. F. (2006). Cenozoic intraplate volcanism on New Zealand: Upwelling induced by lithospheric removal. *Earth and Planetary Science Letters,* 248: 350-367.

Hollis, C. J., (1986). *The subsurface Kaawa Formation at Mauku, South Auckland*. Thesis, University of Auckland.

Houghton, B. F., Schminke, H-U. (1989). Rothenberg scoria cone, East Eifel: a complex Strombolian and phreatomagmatic volcano. *Bulletin of Volcanology,* 52: 28-48.

Houghton, B. F., Smith, R. T. (1993). Recycling of magmatic clasts during explosive eruptions: estimating the true juvenile content of phreatomagmatic deposits. *Bulletin of Volcanology,* 55: 414-420.

Houghton, B. F., Wilson, C. J. N. (1989). A vesicularity index for pyroclastic deposits. *Bulletin of Volcanology,* 51 (6): 451-462.

Houghton, B. F., Wilson, C. J. N., Pyle, D. M. (2000). *Pyroclastic fall deposits*, in Sigurdsson, H. (*ed*.), *Encyclopedia of Volcanoes,* Academic Press, California, pp. 555-570.

Huang, Y., Hawkesworth, C., Smith, I., van Calsteren, P., Smith, I., Black, P. (1997). Melt generation models for the Auckland volcanic field, New Zealand: constraints from U-Th isotopes. *Earth and Planetary Science Letters,* 149 (1-4): 67-84.

Ilanko, T. (2010). Eruption and Emplacement Processes of the Barriball Road Tuff Ring South Auckland. Thesis, University of Waikato.

Jukić, M. F., (1995). *A Geological and Geophysical Subsurface Investigation of the Auckland Volcanic Field*. Thesis, University of Auckland.

Kear, D. (1957). Stratigraphy of the Kaawa-Ohuka Coastal Area, West Auckland. *New Zealand Journal of Science and Technology Bulletin*, 38: 826-42.

Kear, D. (1960). Stratigraphy of Pokeno District, Auckland. *New Zealand Journal of Geology and Geophysics*, 4: 148-164.

Kereszturi, G., Dóniz-Páez, F. J., Guillen, C., Németh, K., Jordan, G. Cronin, S. J., Sohn, Y.K. (2010) *DEM-based methodology of scoria cone parameterization in the southern volcanic zone of Tenerife (Spain) and an implication to other monogenetic fields: Jeju Island (Korea) and Auckland (New Zealand).* GeoNZ 2010: Joint Meeting of The Geoscience Society of New Zealand: The New Zealand Geothermal Works.

King, P. R. (2000). Tectonic reconstructions of New Zealand: 40 Ma to Present. *New Zealand Journal of Geology and Geophysics*, 43: 611-638.

Klűgel, A. (1997). *Ascent rates of magmas and genesis, transport, and reactions of mantle and crustal xenoliths of the 1949 eruption on La Palma (Canary Islands)*. Thesis, Christian-Albrechts University, Kiel.

Le Maitre, R. W. (1989). *A classification of igneous rocks and glossary of terms: recommendations of the international Union of Geological Sciences Subcommission on the Systematics of Igneous Rocks.* Blackwell, London.

Lorenz, V. (2003). Maar-diatreme volcanoes, their formation, and their setting in hard-rock or soft-rock environments. *GeoLines*, 15: 72-83.

Michalski, J. R., Kraft, M. D., Sharp, T. G., Christensen, P. R. (2005). Palagonite-like alteration products on the earth and Mars I: spectroscopy (0.4-25 microns) of weathered basalts and silicate alteration products. *Lunar and Planetary Science*, XXXVI, Abstract: 1188.

Magill, C. R., McAneney, K. J., Smith, I. E. M. (2005). Probabilistic Assessment of Vent Locations for the Next Auckland Volcanic Field Event. *Mathematical Geology*, 37 (3): 227-242.

Needham, A. J., Lindsay, J. M., Smith, I. E. M., Augustinus, P., Shane, P. A. (2011). Sequential eruption of alkaline and sub-alkaline magmas from a small monogenetic volcano in the Auckland Volcanic Field, New Zealand. *Journal of Volcanology and Geothermal Research*, 201: 126-142.

Németh, K., Goth, K., Martin, U., Csillag, G., Suhr, P. (2008). Reconstructing paleoenvironment, eruption mechanism and paleomorphology of the Pliocene Pula Maar, (Hungary). *Journal of Volcanology and Geothermal Research*, 177: 441-456.

Németh, K., Martin, U., Harangi, Sz. (2001). Miocene phreatomagmatic volcanism at Tihany (Pannonian Basin, Hungary). *Journal of Volcanology and Geothermal Research*, 111: 111-135.

Németh, K., White, J. D. L. (2003). Reconstructing eruption processes of a Miocene monogenetic field from vent remnants: Waipiata Volcanic Field, South Island, *New Zealand. Journal of Volcanology and Geothermal Research*, 124: 1-21.

Nicholas, A. (1986). A melt extraction model based on structural studies in mantle peridotites. *Journal of Petrology*, 27: 999-1022.

Nixon, I. M. (1977). *A Geophysical Study of the Drury Fault, South Auckland*. Thesis, University of Auckland.

QMAP, GNS Science. (2009). *Digital QMAP Data.* Institute of Geological and Nuclear Sciences Limited, Lower Hutt, New Zealand.

Rafferty, W. J. (1977). *The volcanic geology and petrology of South Auckland*. Thesis, University of Auckland.

Rafferty, W. J., Heming, R. F. (1979). Quaternary alkalic and sub-alkalic volcanism in South Auckland, New Zealand. *Contributions to Mineralogy and Petrology*, 71: 139-150.

Rapela, C. W., Spalletti, L. A., Merodio, J. C., Aragón, E. (1988). Temporal evolution and spatial variation of early tertiary volcanism in the Patagonian Andes (40°S-42°30'S). *Journal of South American Earth Sciences*, 1 (1): 75-88.

Righter, K., Carmichael, I. S. E. (1993). Mega-xenocrysts in alkali olivine basalts: Fragments of disrupted mantle assemblages. *American Mineralogist*, 78: 1230-1245.

Rosenberg, M. D. (1991). *The nature and mechanisms of phreatomagmatic volcanism in the South Auckland volcanic field*. Thesis, University of Waikato.

Sanders, R. J. (1994). *Ultramafic and mafic xenoliths from the Okete, Ngatutura, and South Auckland volcanics.* Thesis, University of Waikato.

Schofield, J. C. (1958a). Notes on Volcanism and Structure in Franklin County. *New Zealand Journal of Geology and Geophysics*, 1 (3): 341-59.

Schofield, J. C. (1958b). Pliocene Shell Beds South of the Manukau Harbour. *New Zealand Journal of Geology and Geophysics*, 1 (2): 247-255.

Kear, D., Schofield, J. C. (1978). *Geology of the Ngaruawahia subdivision*, New Zealand, Department of Scientific and Industrial Research, Wellington.

Searle E. J. (1962a). Quartzose xenoliths and pyroxene aggregates in the Auckland Basalts. *New Zealand Journal of Geology and Geophysics*, 5 (1): 130-140.

Searle, E. J. (1962b). Xenoliths and metamorphosed rocks associated with the Auckland Basalts. *New Zealand Journal of Geology and Geophysics*, 5: 384-403.

Serpa, F. J. (1984). Carbon dioxide in petrogenesis. III. Role of volatiles in the ascent of alkaline magma with special reference to xenolith-bearing mafic lavas. *Contributions to Mineralogy and Petrology*, 88: 217-232.

Smith, I. E. M., Okada, T., Itaya, T. Black, P. M. (1993). Age relationships and tectonic implications of late Cenozoic basaltic volcanism in Northland, New Zealand. *New Zealand Journal of Geology and Geophysics*, 36, (3) 385-393.

Sohn, Y. K., Cough, S. K. (1989). Depositional processes of the Suwolbong tuff ring, Cheju Island (Korea). *Sedimentology*, 36: 837-855.

Spörli, K. B., Eastwood, V. R. (1997). Elliptical boundary of an intraplate volcanic field, Auckland, New Zealand. *Journal of Volcanology and Geothermal Research*, 79: 169-179.

Sprung, P., Schuth, S., Műnker, C., Hoke, L. (2007). Intraplate volcanism in New Zealand: the role of fossil plume material and variable lithospheric properties. *Contributions to Mineralogy and Petrology*, 153: 669-687.

Stroncik, N. A., Schminke, H. (2002). Palagonite- a review. *International Journal of Earth Science*, 91: 680-697.

Turcotte, D. L., Oxburgh, E. R. (1978). Intra-plate volcanism. *Philosophical Transaction of the Royal Society*, A288: 561-579.

Viljevac, Z. (1998). Western Springs Aquifer – Hydrogeological Characteristics and Computer Model. University of Auckland.

Viljevac, Z., Murphy, G., Smaill, A., Crowcroft, G., Bowden, D. (2002). *South Auckland Groundwater, Kaawa Aquifer Recharge Study and Management of the Volcanic and Kaawa Aquifers*. Technical Publication No. 133, Auckland Regional Council, Auckland.

Waterhouse, B. C. (1978). *Onewhero*, Department of Scientific and Industrial Research, Wellington.

Weaver, S. D., Smith, I. E. M. (1989). New Zealand Intraplate Volcanism, in Johnson, R. W. (*ed*.), *Intraplate Volcanism*, Cambridge University Press, Cambridge, pp. 157-187.

Weaver, S. D., Smith, I. E. M., Sewell, R. J., Gamble, J. A., Morris, P. A., Gibson, I. L. (1989). New Zealand Intraplate Volcanism: Trace element geochemistry. In Johnson, R. W., Knutson, J., Taylor, S. R. (*eds.*). *Intraplate Volcanism in Eastern Australia and New Zealand*. Cambridge University Press, Cambridge. pp. 180-183.

Weller, J. N., Martin, A. J., Connor, C. B., Connor, L. J., Karakhanian, A. (2006). *Modelling the Spatial Distribution of Volcanoes: An Example from Armenia*. In Mader, H. M., Coles, S. G., Connor, C. B., Connor, L. J. *(eds.), Statistics in Volcanology.* Special Publications of IAVCEI, 1. Geological Society of London, 77-87.

White, J. D. L. (1996) Impure coolants and interaction dynamics of phreatomagmatic eruptions. *Journal of Volcanology and Geothermal Research*, 74, 155-170.

White, J. D. L., Houghton, B. F. (2000). *Pyroclastic fall deposits*, in Sigurdsson, H. (*ed*.), *Encyclopedia of Volcanoes*, Academic Press, California, pp. 555-570.

White, P. J., Waterhouse, B. C. (1993). Lithostratigraphy of the Te Kuiti Group: a revision. *New Zealand Journal of Geology and Geophysics*, 36: 255-266.

Wilshire, H. G., Kirkby, S. H. (1989). Dykes, joints and faults in the upper mantle. *Tectonophysics*, 161: 23-31.

Wilson, C. J. N., Houghton, B. F., Kamp, P. J. J., McWilliams, M. O. (1995). An exceptionally widespread ignimbrite with implications for pyroclastic flow emplacement. *Nature*, 378: 605-607.

Wilson, L., Head III, J. W. 1981. Ascent and Eruption of Basaltic Magma on the Earth and Moon. *Journal of Geophysical Research*, 86 (B4): 2971-3001.

Wohletz, K. H. (1983). Mechanisms of hydrovolcanic pyroclast formation: grain-size-scanning electron microscopy, and experimental studies. *Journal of Volcanology and Geothermal Research*, 17: 31-63.

Wohletz, K., Krinsley, D. (1982). *Scanning Electron Microscopy of Basaltic Hydromagmatic Ash*. Los Alamos National Laboratory Report, LA-UR 82-1433. pp. 43.

Wohletz, K. H., McQueen, R. G. (1984). *Experimental studies of hydromagmatic volcanism*, In *Explosive Volcanism: Inception, Evolution, and Hazards*, Studies in Geophysics, National Academy Press, Washington, D.C., 158-169.

# *Appendices*

# *Appendix One*

## *General Reference Information*

| Sample Number | Collection Number | Location | Type | Height (m) | NZTM Easting | NZTM Northing | Facies | Thinsection | Modal Analysis | Vesicularity | XRF | SEM | EMP |
|---|---|---|---|---|---|---|---|---|---|---|---|---|---|
| R1 | 20110001 | Raventhorpe tuff ring | Bulk | 2.58-2.6 | 1774618.6 | 5884613.5 | 4 | X | X | | | | X |
| R2 | 20110002 | Raventhorpe tuff ring | Bulk | 0.1 | 1774618.6 | 5884613.5 | 1 | X | X | | | X | |
| R3 | 20110003 | Raventhorpe tuff ring | Bulk | 1 | 1774618.6 | 5884613.5 | 2 | X | X | | | | |
| R4 | 20110004 | Raventhorpe tuff ring | Juvenile | 1.35 | 1774618.6 | 5884613.5 | 3 | X | X | X | X | | |
| R4 | 20110005 | Raventhorpe tuff ring | Juvenile | 1.35 | 1774618.6 | 5884613.5 | 3 | X | X | X | X | | |
| R5 | 20110006 | Raventhorpe tuff ring | Bulk | 1.4-1.45 | 1774618.6 | 5884613.5 | 4 | X | X | | | | |
| R6 | 20110007 | Raventhorpe tuff ring | Bulk | 1.75-1.8 | 1774618.6 | 5884613.5 | 4 | X | X | X | | | |
| R7 | 20110008 | Raventhorpe tuff ring | Juvenile | 2.35-2.85 | 1774618.6 | 5884613.5 | 4 | X | X | X | | | |
| R8 | 20110009 | Raventhorpe tuff ring | Bulk | 2.6-2.7 | 1774618.6 | 5884613.5 | 5 | X | X | | | | |
| R9 | 20110010 | Raventhorpe tuff ring | Bulk | 2.9 | 1774618.6 | 5884613.5 | 5 | X | X | | | | |
| R10 | 20110011 | Raventhorpe tuff ring | Juvenile | 3.1-3.3 | 1774618.6 | 5884613.5 | 5 | X | X | X | | X | |
| R11 | 20110012 | Raventhorpe tuff ring | Bulk | 3.8 | 1774618.6 | 5884613.5 | 4 | X | X | | | | |
| R12 | 20110013 | Raventhorpe tuff ring | Lithic | 4.4 | 1774618.6 | 5884613.5 | 4 | X | X | | | | |
| R13 | 20110014 | Raventhorpe tuff ring | Juvenile | 4.45-4.5 | 1774618.6 | 5884613.5 | 4 | X | X | X | | | |
| R14 | 20110015 | Raventhorpe tuff ring | Bulk | 5.25 | 1774618.6 | 5884613.5 | 4 | X | X | | | | X |
| R15 | 20110016 | Raventhorpe tuff ring | Bulk | 4.4 | 1774618.6 | 5884613.5 | 4 | X | X | | | | |
| R16 | 20110017 | Raventhorpe tuff ring | Juvenile | 3.7 | 1774618.6 | 5884613.5 | 4 | | | X | | | |
| R17 | 20110018 | Raventhorpe tuff ring | Bulk | 3.7 | 1774618.6 | 5884613.5 | 4 | X | X | | | | |
| R18 | 20110019 | Raventhorpe tuff ring | Juvenile | 6.3-7 | 1774618.6 | 5884613.5 | 1 | X | X | X | | | |
| R19 | 20110020 | Raventhorpe tuff ring | Juvenile | 7.9-8.2 | 1774618.6 | 5884613.5 | 1 | X | X | X | X | | |
| R20 | 20110021 | Raventhorpe tuff ring | Bulk | 8 | 1774618.6 | 5884613.5 | 1 | X | X | | | | |
| I1 | 20110022 | Ingram Road tuff ring | Bulk | 2.05 | 1773922.9 | 5883556.5 | 2.1 | X | X | | | | |
| I2 | 20110023 | Ingram Road tuff ring | Bulk | 2.05-2.13 | 1773922.9 | 5883556.5 | 2.1 | X | X | | | | |
| I3 | 20110024 | Ingram Road tuff ring | Bulk | 2.48-2.6 | 1773922.9 | 5883556.5 | 2.2 | X | X | | | | |
| I4 | 20110025 | Ingram Road tuff ring | Bulk | 2.6-3.2 | 1773922.9 | 5883556.5 | 2.2 | X | X | | | | |
| I5 | 20110026 | Ingram Road tuff ring | Bulk | 3.2-3.5 | 1773922.9 | 5883556.5 | 2.2 | X | X | | | | |
| I6 | 20110027 | Ingram Road tuff ring | Bulk | 3.57-3.72 | 1773922.9 | 5883556.5 | 1 | X | X | | | | |
| I7 | 20110028 | Ingram Road tuff ring | Bulk | 3.8 | 1773922.9 | 5883556.5 | 1 | X | X | | | | |
| I8 | 20110029 | Ingram Road tuff ring | Bulk | 3.72-4.05 | 1773922.9 | 5883556.5 | 1 | X | X | | | | |
| I9 | 20110030 | Ingram Road tuff ring | Bulk | 4.5-4.7 | 1773922.9 | 5883556.5 | 1 | X | X | | | | |
| I10 | 20110031 | Ingram Road tuff ring | Bulk | 0.3-0.4 | 1773922.9 | 5883556.5 | 1 | X | X | | | | |
| I11 | 20110032 | Ingram Road tuff ring | Bulk | 0.8 | 1773922.9 | 5883556.5 | 1 | X | X | | | | |
| I12 | 20110033 | Ingram Road tuff ring | Bulk | 1.5 | 1773922.9 | 5883556.5 | 1 | X | X | | | | |
| I13 | 20110034 | Ingram Road tuff ring | Bulk | 1.5-1.7 | 1773922.9 | 5883556.5 | 2.1 | X | X | | | | |
| P1 | 20110035 | Pokeno Tuff ring ring | Bulk | 0.5 | 1780037.7 | 5875170.4 | 1 | X | X | | | | |

| Sample Number | Collection Number | Location | Type | Height (m) | NZTM Easting | NZTM Northing | Facies | Thinsection | Modal Analysis | Vesicularity | XRF | SEM | EMP |
|---|---|---|---|---|---|---|---|---|---|---|---|---|---|
| P2 | 20110036 | Pokeno Tuff Ring | Bulk | 1.5-1.75 | 1780037.7 | 5875170.4 | 2 | X | X | | | | |
| P3 | 20110037 | Pokeno Tuff Ring | Bulk | 5.75-5.9 | 1780037.7 | 5875170.4 | 1 | X | X | | | | |
| P4 | 20110038 | Pokeno Tuff Ring | Bulk | 6 | 1780037.7 | 5875170.4 | 1 | X | X | | | | |
| P5 | 20110039 | Pokeno Tuff Ring | Bulk | 6.2 | 1780037.7 | 5875170.4 | 1 | X | | | | | |
| P6 | 20110040 | Pokeno Tuff Ring | Juvenile | 6.2 | 1780037.7 | 5875170.4 | 1 | X | | X | | | |
| P7 | 20110041 | Pokeno Tuff Ring | Lithic | 6.2 | 1780037.7 | 5875170.4 | 1 | X | | | | | |
| P8 | 20110042 | Pokeno Tuff Ring | Bulk | 6.5 | 1780037.7 | 5875170.4 | 1 | | | | | | |
| P9 | 20110043 | Pokeno Tuff Ring | Bulk | 6.7-7.2 | 1780037.7 | 5875170.4 | 3 | X | X | | | | |
| P10 | 20110044 | Pokeno Tuff Ring | Bulk | 7.2-7.5 | 1780037.7 | 5875170.4 | 1 | X | X | | | | |
| P11 | 20110045 | Pokeno Tuff Ring | Bulk | 7.5-7.7 | 1780037.7 | 5875170.4 | 4 | X | X | | | | X |
| P12 | 20110046 | Pokeno Tuff Ring | Juvenile | 8.1-8.3 | 1780037.7 | 5875170.4 | 2 | X | X | X | | | |
| P13 | 20110047 | Pokeno Tuff Ring | Bulk | 7.7-7.9 | 1780037.7 | 5875170.4 | 1 | X | | | | | |
| P14 | 20110048 | Pokeno Tuff Ring | Bulk | 7.9-8.1 | 1780037.7 | 5875170.4 | 2 | X | X | | | | |
| P15 | 20110049 | Pokeno Tuff Ring | Bulk | 8.1-8.3 | 1780037.7 | 5875170.4 | 2 | X | X | | | | |
| P3 S1 | 20110050 | Pokeno Tuff Ring | Bulk | 0-0.3 | 1780072.8 | 5874980.1 | 1 | X | X | | | | |
| P3 S2 | 20110051 | Pokeno Tuff Ring | Juvenile | 0.3-0.7 | 1780072.8 | 5874980.1 | 4 | X | X | X | X | | |
| P3 S3 | 20110052 | Pokeno Tuff Ring | Bulk | 0.4 | 1780072.8 | 5874980.1 | 4 | X | X | | | X | |
| P3 S4 | 20110053 | Pokeno Tuff Ring | Bulk | 1.5-1.7 | 1780072.8 | 5874980.1 | 1 | X | X | | | | |
| P3 S5 | 20110054 | Pokeno Tuff Ring | Bulk | 2 | 1780072.8 | 5874980.1 | 1 | X | | | | | |
| P3 S6 | 20110055 | Pokeno Tuff Ring | Bulk | 2.15-2.4 | 1780072.8 | 5874980.1 | 1 | X | X | | | | |
| P3 S7 | 20110056 | Pokeno Tuff Ring | Bulk | 3 | 1780072.8 | 5874980.1 | 1 | X | X | | | | |
| P3 S8 | 20110057 | Pokeno Tuff Ring | Bulk | 3.6-4 | 1780072.8 | 5874980.1 | 2 | X | X | | | | |
| P3 S9 | 20110058 | Pokeno Tuff Ring | Bulk | 4.4-4.6 | 1780072.8 | 5874980.1 | 2 | X | X | | | | |
| P3 S10 | 20110059 | Pokeno Tuff Ring | Juvenile | 4-4.2 | 1780072.8 | 5874980.1 | 2 | X | | X | | | |
| P3 S11 | 20110060 | Pokeno Tuff Ring | Juvenile | 1.2-1.4 | 1780072.8 | 5874980.1 | 3 | X | | X | | | |
| P3 S12 | 20110061 | Pokeno Tuff Ring | Juvenile | 6.6 | 1780072.8 | 5874980.1 | 3 | | | X | | | |
| P3 S13 | 20110062 | Pokeno Tuff Ring | Bulk | 5.2-5.8 | 1780072.8 | 5874980.1 | 1 | X | X | | | | |
| P3 S14 | 20110063 | Pokeno Tuff Ring | Bulk | 6.42-6.72 | 1780072.8 | 5874980.1 | 3 | X | | | | | |
| P3 S15 | 20110064 | Pokeno Tuff Ring | Bulk | 6.72-6.98 | 1780072.8 | 5874980.1 | 3 | X | X | | | | |
| P3 S16 | 20110065 | Pokeno Tuff Ring | Juveniles | 6.72-6.98 | 1780072.8 | 5874980.1 | 3 | X | | X | | | |
| P3 S17 | 20110066 | Pokeno Tuff Ring | Bulk | 7-7.73 | 1780072.8 | 5874980.1 | 3 | X | X | | | | |
| P3 S18 | 20110067 | Pokeno Tuff Ring | Juvenile | 6.72-6.98 | 1780072.8 | 5874980.1 | 3 | X | | X | | | |
| P3 S19 | 20110068 | Pokeno Tuff Ring | Bulk | 7-7.73 | 1780072.8 | 5874980.1 | 3 | X | X | X | | | |
| P3 S20 | 20110069 | Pokeno Tuff Ring | Juvenile | 7.34-7.74 | 1780072.8 | 5874980.1 | 3 | X | | | | | |
| P3 S21 | 20110070 | Pokeno Tuff Ring | Juvenile | 7.5 | 1780072.8 | 5874980.1 | 3 | X | | | | | |
| P3 S22 | 20110071 | Pokeno Tuff Ring | Bulk | 7.76-8 | 1780072.8 | 5874980.1 | 3 | X | X | X | | | |

| Sample Number | Collection Number | Location | Type | Height (m) | NZTM Easting | NZTM Northing | Facies | Thinsection | Modal Analysis | Vesicularity | XRF | SEM | EMP |
|---|---|---|---|---|---|---|---|---|---|---|---|---|---|
| P3 S23 | 20110072 | Pokeno Tuff Ring | Bulk | 8.08-8.2 | 1780072.8 | 5874980.1 | 3 | X | X | X | | | |
| P3 S24 | 20110073 | Pokeno Tuff Ring | Juvenile | 12.7-12.8 | 1780072.8 | 5874980.1 | 3 | X | | | | | |
| P3 S25 | 20110074 | Pokeno Tuff Ring | Juvenile | 11.5-13.5 | 1780072.8 | 5874980.1 | 3 | X | | | | X | |
| P2 S1 | 20110075 | Pokeno Tuff Ring | Juvenile | 2.1 | 1779237.1 | 5874732.8 | 3 | | | | | | |
| P2 S2 | 20110076 | Pokeno Tuff Ring | Bulk | 0.3 | 1779237.1 | 5874732.8 | 1 | X | X | | | | |
| P2 S3 | 20110077 | Pokeno Tuff Ring | Bulk | 0.7 | 1779237.1 | 5874732.8 | 3 | X | X | | | | |
| P2 S4 | 20110078 | Pokeno Tuff Ring | Bulk | 1.1-1.4 | 1779237.1 | 5874732.8 | 3 | X | X | | | | |
| P2 S5 | 20110079 | Pokeno Tuff Ring | Bulk | 1.65 | 1779237.1 | 5874732.8 | 5 | X | X | | | | |
| P2 S6 | 20110080 | Pokeno Tuff Ring | Bulk | 2.2-2.6 | 1779237.1 | 5874732.8 | 2 | X | X | | | | |
| P2 S7 | 20110081 | Pokeno Tuff Ring | Bulk | 2.9-3.0 | 1779237.1 | 5874732.8 | 2 | X | X | | | | |
| P2 S8 | 20110082 | Pokeno Tuff Ring | Bulk | 3.1-3.2 | 1779237.1 | 5874732.8 | 2 | X | X | | | | |
| P2 S9 | 20110083 | Pokeno Tuff Ring | Bulk | 3.5-3.7 | 1779237.1 | 5874732.8 | 2 | X | X | | | | |
| P2 S10 | 20110084 | Pokeno Tuff Ring | Bulk | 3.7-3.8 | 1779237.1 | 5874732.8 | 1 | X | X | | | | |
| P2 S11 | 20110085 | Pokeno Tuff Ring | Juvenile | 3 | 1779237.1 | 5874732.8 | 2 | | | X | | | |
| BF2 S2 | 20110086 | Ingram Road | Boulder | - | 1773913.2 | 5883506.1 | | X | | | | | |
| H S1 | 20110087 | Great South Road | Lava | 0.5-1 | 1775953.3 | 5883573.7 | | X | x | | X | | |
| H S2 | 20110088 | Great South Road | Lava | 1-1.5 | 1775953.3 | 5883573.7 | | X | | | | | |
| H S3 | 20110089 | Great South Road | Lava | 2.85-3.2 | 1775953.3 | 5883573.7 | | X | X | | X | | |
| H S4 | 20110090 | Great South Road | Lava | 3.5 | 1775953.3 | 5883573.7 | | X | | | | | |
| H S5 | 20110091 | Great South Road | Lava | 3.8-4.2 | 1775953.3 | 5883573.7 | | X | | | | | |
| BF2 S1 | 20110092 | Ingram Road | Boulder | - | 1773913.2 | 5883506.1 | | X | X | | X | | |
| BF1 S1 | 20110093 | Flay Road | Boulder | - | 1775139.2 | 5885012.5 | | X | X | | | | |
| AL1 | 20110094 | Ambush Road | Lava | 1.5 | 1774556.2 | 5885351.1 | | X | X | | | | |
| AL2 | 20110095 | Ambush Road | Lava | 3.0-3.2 | 1774556.2 | 5885351.1 | | X | | | | | |
| AL3 | 20110096 | Ambush Road | Lava | 4.0-4.4 | 1774556.2 | 5885351.1 | | X | | | | | |
| BF3 S1 | 20110097 | Rutherford Road | Boulder | - | 1774404.9 | 5882814.8 | | X | | | | | |
| BF3 S2 | 20110098 | Rutherford Road | Boulder | - | 1774404.9 | 5882814.8 | | X | X | | X | | |
| BF4 S1 | 20110099 | Pukekohe East School | Boulder | - | 1772504.5 | 5883164.1 | | X | X | | X | | |
| BF4 S2 | 20110100 | Pukekohe East School | Boulder | - | 1772504.5 | 5883164.1 | | X | | | | | |
| BF5 S1 | 20110101 | Ambush Road | Boulder | - | 1774439.1 | 5885393.6 | | X | X | | X | | |
| BF5 S2 | 20110102 | Ambush Road | Boulder | - | 1774439.1 | 5885393.6 | | X | | | | | |
| BF5 S3 | 20110103 | Ambush Road | Boulder | - | 1774439.1 | 5885393.6 | | X | | | | | |
| BF6 S1 | 20110104 | Pokeno Tuff Ring | Boulder | - | 1779203.7 | 5874719.9 | | X | X | | X | | |
| BF7 S1 | 20110105 | Cole Road | Boulder | - | 1779305.2 | 5874264.1 | | X | X | | X | | |
| BF7 S2 | 20110106 | Cole Road | Boulder | - | 1779305.2 | 5874264.1 | | X | | | | | |
| BF3 S3 | 20110107 | Rutherford Road | Boulder | - | 1774404.9 | 5882814.8 | | X | | | X | | |

# *Appendix Two*

## *CIPW Normalised Oxide Values*

Norm Calculation Program  Program run: 15/01/2012  HELP

Sample Number: BF2S1

| | Rock Analysis | |
|---|---|---|
| SiO2 | 46.49 | % |
| TiO2 | 2.86 | % |
| Al2O3 | 14.29 | % |
| Fe2O3 | 14.07 | % |
| FeO | | % |
| MnO | 0.17 | % |
| MgO | 7.29 | % |
| CaO | 8.37 | % |
| Na2O | 3.25 | % |
| K2O | 1.07 | % |
| P2O5 | 0.46 | % |
| CO2 | | % |
| SO3 | | % |
| S | | % |
| F | | % |
| Cl | | % |
| Sr | | ppm |
| Ba | | ppm |
| Ni | | ppm |
| Cr | | ppm |
| Zr | | ppm |
| Total | 98.32 | |

| Normalization Factors | |
|---|---|
| Total=100%? Y/N | n |
| Fe3+/(Total Iron) | 0.1 |
| Total Fe as FeO | 12.66 |
| Desired Fe2O3 | 1.41 |
| Desired FeO | 11.39 |
| Weight corr. factor | 1.000 |

Zero values not shown

Norm calculation checks:

Norm seems OK

| Normalized Analysis |
|---|
| 46.49 |
| 2.86 |
| 14.29 |
| 1.41 |
| 11.39 |
| 0.17 |
| 7.29 |
| 8.37 |
| 3.25 |
| 1.07 |
| 0.46 |
| 97.05 |

| Normative Minerals | Weight % Norm | Volume % Norm |
|---|---|---|
| Quartz | | |
| Plagioclase | 48.29 | 56.35 |
| Orthoclase | 6.32 | 7.72 |
| Nepheline | 0.25 | 0.30 |
| Leucite | | |
| Kalsilite | | |
| Corundum | | |
| Diopside | 14.21 | 13.26 |
| Hypersthene | | |
| Wollastonite | | |
| Olivine | 19.44 | 16.53 |
| Larnite | | |
| Acmite | | |
| K2SiO3 | | |
| Na2SiO3 | | |
| Rutile | | |
| Ilmenite | 5.43 | 3.58 |
| Magnetite | 2.04 | 1.23 |
| Hematite | | |
| Apatite | 1.07 | 1.04 |
| Zircon | | |
| Perovskite | | |
| Chromite | | |
| Sphene | | |
| Pyrite | | |
| Halite | | |
| Fluorite | | |
| Anhydrite | | |
| Na2SO4 | | |
| Calcite | | |
| Na2CO3 | | |
| Total | 97.05 | 100.01 |

| | | |
|---|---|---|
| Fe3+/(Total Fe) in rock | 10.0 | 10.0 |
| Mg/(Mg+Total Fe) in rock | 50.7 | 50.7 |
| Mg/(Mg+Fe2+) in rock | 53.3 | 53.3 |
| Mg/(Mg+Fe2+) in silicates | 60.9 | 60.9 |
| Ca/(Ca+Na) in rock | 58.7 | 58.7 |
| Ca/(Ca+Na) in plagioclase | 42.5 | 42.5 |
| Differentiation Index | 54.9 | 64.4 |
| Calculated density, g/cc | 3.03 | 3.03 |
| Calculated liquid density, g/cc | 2.72 | 2.72 |
| Calculated viscosity, dry, Pas | 0.18 | 0.18 |
| Calculated viscosity, wet, Pas | 0.17 | 0.17 |
| Estimated liquidus temp., °C | 1252 | 1252 |
| Estimated H2O content, wt. % | 0.26 | 0.26 |

This program was written by Kurt Hollocher, Geology Department, Union College, Schenectady, NY, 12308, hollochk@union.edu

Norm Calculation Program  Program run: 15/01/2012  HELP

Sample Number: R19

| | Rock Analysis | |
|---|---|---|
| SiO2 | 48.69 | % |
| TiO2 | 2.11 | % |
| Al2O3 | 13.55 | % |
| Fe2O3 | 13.50 | % |
| FeO | | % |
| MnO | 0.16 | % |
| MgO | 7.77 | % |
| CaO | 8.80 | % |
| Na2O | 3.29 | % |
| K2O | 0.48 | % |
| P2O5 | 0.27 | % |
| CO2 | | % |
| SO3 | | % |
| S | | % |
| F | | % |
| Cl | | % |
| Sr | | ppm |
| Ba | | ppm |
| Ni | | ppm |
| Cr | | ppm |
| Zr | | ppm |
| Total | 98.62 | |

| Normalization Factors | |
|---|---|
| Total=100%? Y/N | n |
| Fe3+/(Total Iron) | 0.1 |
| Total Fe as FeO | 12.15 |
| Desired Fe2O3 | 1.35 |
| Desired FeO | 10.93 |
| Weight corr. factor | 1.000 |

Zero values not shown

Norm calculation checks:
Norm seems OK

| Normalized Analysis |
|---|
| 48.69 |
| 2.11 |
| 13.55 |
| 1.35 |
| 10.93 |
| 0.16 |
| 7.77 |
| 8.80 |
| 3.29 |
| 0.48 |
| 0.27 |
| 97.40 |

| Normative Minerals | Weight % Norm | Volume % Norm |
|---|---|---|
| Quartz | | |
| Plagioclase | 48.63 | 56.77 |
| Orthoclase | 2.84 | 3.46 |
| Nepheline | | |
| Leucite | | |
| Kalsilite | | |
| Corundum | | |
| Diopside | 17.34 | 16.19 |
| Hypersthene | 9.43 | 8.43 |
| Wollastonite | | |
| Olivine | 12.58 | 10.72 |
| Larnite | | |
| Acmite | | |
| K2SiO3 | | |
| Na2SiO3 | | |
| Rutile | | |
| Ilmenite | 4.01 | 2.64 |
| Magnetite | 1.96 | 1.18 |
| Hematite | | |
| Apatite | 0.63 | 0.61 |
| Zircon | | |
| Perovskite | | |
| Chromite | | |
| Sphene | | |
| Pyrite | | |
| Halite | | |
| Fluorite | | |
| Anhydrite | | |
| Na2SO4 | | |
| Calcite | | |
| Na2CO3 | | |
| Total | 97.42 | 100.00 |

| | | |
|---|---|---|
| Fe3+/(Total Fe) in rock | 10.0 | 10.0 |
| Mg/(Mg+Total Fe) in rock | 53.3 | 53.3 |
| Mg/(Mg+Fe2+) in rock | 55.9 | 55.9 |
| Mg/(Mg+Fe2+) in silicates | 61.7 | 61.7 |
| Ca/(Ca+Na) in rock | 59.6 | 59.6 |
| Ca/(Ca+Na) in plagioclase | 41.3 | 41.3 |
| Differentiation Index | 51.5 | 60.2 |
| Calculated density, g/cc | 3.05 | 3.05 |
| Calculated liquid density, g/cc | 2.71 | 2.71 |
| Calculated viscosity, dry, Pas | 0.21 | 0.21 |
| Calculated viscosity, wet, Pas | 0.20 | 0.20 |
| Estimated liquidus temp., °C | 1214 | 1214 |
| Estimated H2O content, wt. % | 0.38 | 0.38 |

This program was written by Kurt Hollocher, Geology Department, Union College, Schenectady, NY, 12308, hollochk@union.edu

Norm Calculation Program  Program run: 15/01/2012  HELP

Sample Number: R4

| | Rock Analysis | |
|---|---|---|
| SiO2 | 47.32 | % |
| TiO2 | 2.12 | % |
| Al2O3 | 14.14 | % |
| Fe2O3 | 14.00 | % |
| FeO | | % |
| MnO | 0.16 | % |
| MgO | 7.35 | % |
| CaO | 8.55 | % |
| Na2O | 3.20 | % |
| K2O | 0.30 | % |
| P2O5 | 0.44 | % |
| CO2 | | % |
| SO3 | | % |
| S | | % |
| F | | % |
| Cl | | % |
| Sr | | ppm |
| Ba | | ppm |
| Ni | | ppm |
| Cr | | ppm |
| Zr | | ppm |
| Total | 97.58 | |

| Normalization Factors | |
|---|---|
| Total=100%? Y/N | n |
| Fe3+/(Total Iron) | 0.1 |
| Total Fe as FeO | 12.60 |
| Desired Fe2O3 | 1.40 |
| Desired FeO | 11.34 |
| Weight corr. factor | 1.000 |

Zero values not shown

Norm calculation checks:

Norm seems OK

| Normalized Analysis |
|---|
| 47.32 |
| 2.12 |
| 14.14 |
| 1.40 |
| 11.34 |
| 0.16 |
| 7.35 |
| 8.55 |
| 3.20 |
| 0.30 |
| 0.44 |
| 96.32 |

| Normative Minerals | Weight % Norm | Volume % Norm |
|---|---|---|
| Quartz | | |
| Plagioclase | 50.41 | 59.48 |
| Orthoclase | 1.77 | 2.19 |
| Nepheline | | |
| Leucite | | |
| Kalsilite | | |
| Corundum | | |
| Diopside | 13.36 | 12.60 |
| Hypersthene | 11.31 | 10.19 |
| Wollastonite | | |
| Olivine | 12.39 | 10.61 |
| Larnite | | |
| Acmite | | |
| K2SiO3 | | |
| Na2SiO3 | | |
| Rutile | | |
| Ilmenite | 4.03 | 2.68 |
| Magnetite | 2.03 | 1.24 |
| Hematite | | |
| Apatite | 1.02 | 1.01 |
| Zircon | | |
| Perovskite | | |
| Chromite | | |
| Sphene | | |
| Pyrite | | |
| Halite | | |
| Fluorite | | |
| Anhydrite | | |
| Na2SO4 | | |
| Calcite | | |
| Na2CO3 | | |
| Total | 96.32 | 100.00 |

| | | |
|---|---|---|
| Fe3+/(Total Fe) in rock | 10.0 | 10.0 |
| Mg/(Mg+Total Fe) in rock | 51.0 | 51.0 |
| Mg/(Mg+Fe2+) in rock | 53.6 | 53.6 |
| Mg/(Mg+Fe2+) in silicates | 59.4 | 59.4 |
| Ca/(Ca+Na) in rock | 59.6 | 59.6 |
| Ca/(Ca+Na) in plagioclase | 44.8 | 44.8 |
| Differentiation Index | 52.2 | 61.7 |
| Calculated density, g/cc | 3.05 | 3.05 |
| Calculated liquid density, g/cc | 2.72 | 2.72 |
| Calculated viscosity, dry, Pas | 0.20 | 0.20 |
| Calculated viscosity, wet, Pas | 0.19 | 0.19 |
| Estimated liquidus temp., °C | 1229 | 1229 |
| Estimated H2O content, wt. % | 0.33 | 0.33 |

This program was written by Kurt Hollocher, Geology Department, Union College, Schenectady, NY, 12308, hollochk@union.edu

Norm Calculation Program  Program run: 15/01/2012  HELP

Sample Number: BF3S1

| | Rock Analysis | |
|---|---|---|
| SiO2 | 42.45 | % |
| TiO2 | 2.85 | % |
| Al2O3 | 12.35 | % |
| Fe2O3 | 14.38 | % |
| FeO | | % |
| MnO | 0.19 | % |
| MgO | 10.82 | % |
| CaO | 9.76 | % |
| Na2O | 2.68 | % |
| K2O | 1.18 | % |
| P2O5 | 0.60 | % |
| CO2 | | % |
| SO3 | | % |
| S | | % |
| F | | % |
| Cl | | % |
| Sr | | ppm |
| Ba | | ppm |
| Ni | | ppm |
| Cr | | ppm |
| Zr | | ppm |
| Total | 97.26 | |

| Normalization Factors | |
|---|---|
| Total=100%? Y/N | n |
| Fe3+/(Total Iron) | 0.1 |
| Total Fe as FeO | 12.94 |
| Desired Fe2O3 | 1.44 |
| Desired FeO | 11.65 |
| Weight corr. factor | 1.000 |

Zero values not shown

Norm calculation checks:

Norm seems OK

| Normalized Analysis |
|---|
| 42.45 |
| 2.85 |
| 12.35 |
| 1.44 |
| 11.65 |
| 0.19 |
| 10.82 |
| 9.76 |
| 2.68 |
| 1.18 |
| 0.60 |
| 95.97 |

| Normative Minerals | Weight % Norm | Volume % Norm |
|---|---|---|
| Quartz | | |
| Plagioclase | 28.40 | 34.01 |
| Orthoclase | 6.97 | 8.83 |
| Nepheline | 6.75 | 8.55 |
| Leucite | | |
| Kalsilite | | |
| Corundum | | |
| Diopside | 21.41 | 20.88 |
| Hypersthene | | |
| Wollastonite | | |
| Olivine | 23.55 | 21.32 |
| Larnite | | |
| Acmite | | |
| K2SiO3 | | |
| Na2SiO3 | | |
| Rutile | | |
| Ilmenite | 5.41 | 3.70 |
| Magnetite | 2.09 | 1.30 |
| Hematite | | |
| Apatite | 1.39 | 1.41 |
| Zircon | | |
| Perovskite | | |
| Chromite | | |
| Sphene | | |
| Pyrite | | |
| Halite | | |
| Fluorite | | |
| Anhydrite | | |
| Na2SO4 | | |
| Calcite | | |
| Na2CO3 | | |
| Total | 95.97 | 100.00 |

| | | |
|---|---|---|
| Fe3+/(Total Fe) in rock | 10.0 | 10.0 |
| Mg/(Mg+Total Fe) in rock | 59.8 | 59.8 |
| Mg/(Mg+Fe2+) in rock | 62.3 | 62.3 |
| Mg/(Mg+Fe2+) in silicates | 69.1 | 69.1 |
| Ca/(Ca+Na) in rock | 66.8 | 66.8 |
| Ca/(Ca+Na) in plagioclase | 62.6 | 62.6 |
| Differentiation Index | 42.1 | 51.4 |
| Calculated density, g/cc | 3.11 | 3.11 |
| Calculated liquid density, g/cc | 2.77 | 2.77 |
| Calculated viscosity, dry, Pas | 0.10 | 0.10 |
| Calculated viscosity, wet, Pas | 0.10 | 0.10 |
| Estimated liquidus temp., °C | 1319 | 1319 |
| Estimated H2O content, wt. % | 0.14 | 0.14 |

This program was written by Kurt Hollocher, Geology Department, Union College, Schenectady, NY, 12308, hollochk@union.edu

Norm Calculation Program  Program run: 15/01/2012  HELP

Sample Number: P3S2

| | Rock Analysis | |
|---|---|---|
| SiO2 | 66.30 | % |
| TiO2 | 0.65 | % |
| Al2O3 | 15.68 | % |
| Fe2O3 | 4.88 | % |
| FeO | | % |
| MnO | 0.06 | % |
| MgO | 1.40 | % |
| CaO | 1.94 | % |
| Na2O | 6.12 | % |
| K2O | 2.04 | % |
| P2O5 | 0.16 | % |
| CO2 | | % |
| SO3 | | % |
| S | | % |
| F | | % |
| Cl | | % |
| Sr | | ppm |
| Ba | | ppm |
| Ni | | ppm |
| Cr | | ppm |
| Zr | | ppm |
| Total | 99.23 | |

| Normalization Factors | |
|---|---|
| Total=100%? Y/N | n |
| Fe3+/(Total Iron) | 0.1 |
| Total Fe as FeO | 4.39 |
| Desired Fe2O3 | 0.49 |
| Desired FeO | 3.95 |
| Weight corr. factor | 1.000 |

Zero values not shown

Norm calculation checks:

Norm seems OK

| Normalized Analysis |
|---|
| 66.30 |
| 0.65 |
| 15.68 |
| 0.49 |
| 3.95 |
| 0.06 |
| 1.40 |
| 1.94 |
| 6.12 |
| 2.04 |
| 0.16 |
| 98.79 |

| Normative Minerals | Weight % Norm | Volume % Norm |
|---|---|---|
| Quartz | 14.42 | 15.04 |
| Plagioclase | 60.36 | 63.22 |
| Orthoclase | 12.06 | 13.01 |
| Nepheline | | |
| Leucite | | |
| Kalsilite | | |
| Corundum | 0.26 | 0.18 |
| Diopside | | |
| Hypersthene | 9.37 | 7.13 |
| Wollastonite | | |
| Olivine | | |
| Larnite | | |
| Acmite | | |
| K2SiO3 | | |
| Na2SiO3 | | |
| Rutile | | |
| Ilmenite | 1.23 | 0.72 |
| Magnetite | 0.71 | 0.38 |
| Hematite | | |
| Apatite | 0.37 | 0.32 |
| Zircon | | |
| Perovskite | | |
| Chromite | | |
| Sphene | | |
| Pyrite | | |
| Halite | | |
| Fluorite | | |
| Anhydrite | | |
| Na2SO4 | | |
| Calcite | | |
| Na2CO3 | | |
| Total | 98.78 | 100.00 |
| Fe3+/(Total Fe) in rock | 10.0 | 10.0 |
| Mg/(Mg+Total Fe) in rock | 36.2 | 36.2 |
| Mg/(Mg+Fe2+) in rock | 38.7 | 38.7 |
| Mg/(Mg+Fe2+) in silicates | 43.8 | 43.8 |
| Ca/(Ca+Na) in rock | 14.9 | 14.9 |
| Ca/(Ca+Na) in plagioclase | 13.5 | 13.5 |
| Differentiation Index | 86.8 | 91.3 |
| Calculated density, g/cc | 2.73 | 2.73 |
| Calculated liquid density, g/cc | 2.45 | 2.45 |
| Calculated viscosity, dry, Pas | 0.69 | 0.69 |
| Calculated viscosity, wet, Pas | 0.56 | 0.56 |
| Estimated liquidus temp., °C | 900 | 900 |
| Estimated H2O content, wt. % | 2.73 | 2.73 |

This program was written by Kurt Hollocher, Geology Department, Union College, Schenectady, NY, 12308, hollochk@union.edu

Norm Calculation Program  Program run: 15/01/2012  HELP

Sample Number: HS3

| | Rock Analysis | |
|---|---|---|
| SiO2 | 45.06 | % |
| TiO2 | 2.09 | % |
| Al2O3 | 16.10 | % |
| Fe2O3 | 14.26 | % |
| FeO | | % |
| MnO | 0.17 | % |
| MgO | 8.60 | % |
| CaO | 6.71 | % |
| Na2O | 2.50 | % |
| K2O | 0.30 | % |
| P2O5 | 0.29 | % |
| CO2 | | % |
| SO3 | | % |
| S | | % |
| F | | % |
| Cl | | % |
| Sr | | ppm |
| Ba | | ppm |
| Ni | | ppm |
| Cr | | ppm |
| Zr | | ppm |
| Total | 96.08 | |

| Normalization Factors | |
|---|---|
| Total=100%? Y/N | n |
| Fe3+/(Total Iron) | 0.1 |
| Total Fe as FeO | 12.83 |
| Desired Fe2O3 | 1.43 |
| Desired FeO | 11.55 |
| Weight corr. factor | 1.000 |

Zero values not shown

Norm calculation checks:

Norm seems OK

| Normalized Analysis |
|---|
| 45.06 |
| 2.09 |
| 16.10 |
| 1.43 |
| 11.55 |
| 0.17 |
| 8.60 |
| 6.71 |
| 2.50 |
| 0.30 |
| 0.29 |
| 94.80 |

| Normative Minerals | Weight % Norm | Volume % Norm |
|---|---|---|
| Quartz | | |
| Plagioclase | 52.55 | 62.57 |
| Orthoclase | 1.77 | 2.23 |
| Nepheline | | |
| Leucite | | |
| Kalsilite | | |
| Corundum | 0.16 | 0.13 |
| Diopside | | |
| Hypersthene | 20.74 | 19.12 |
| Wollastonite | | |
| Olivine | 12.87 | 11.31 |
| Larnite | | |
| Acmite | | |
| K2SiO3 | | |
| Na2SiO3 | | |
| Rutile | | |
| Ilmenite | 3.97 | 2.69 |
| Magnetite | 2.07 | 1.28 |
| Hematite | | |
| Apatite | 0.67 | 0.68 |
| Zircon | | |
| Perovskite | | |
| Chromite | | |
| Sphene | | |
| Pyrite | | |
| Halite | | |
| Fluorite | | |
| Anhydrite | | |
| Na2SO4 | | |
| Calcite | | |
| Na2CO3 | | |
| Total | 94.80 | 100.01 |

| | | |
|---|---|---|
| Fe3+/(Total Fe) in rock | 10.0 | 10.0 |
| Mg/(Mg+Total Fe) in rock | 54.4 | 54.4 |
| Mg/(Mg+Fe2+) in rock | 57.0 | 57.0 |
| Mg/(Mg+Fe2+) in silicates | 62.5 | 62.5 |
| Ca/(Ca+Na) in rock | 59.7 | 59.7 |
| Ca/(Ca+Na) in plagioclase | 58.3 | 58.3 |
| Differentiation Index | 54.3 | 64.8 |
| Calculated density, g/cc | 3.05 | 3.05 |
| Calculated liquid density, g/cc | 2.73 | 2.73 |
| Calculated viscosity, dry, Pas | 0.18 | 0.18 |
| Calculated viscosity, wet, Pas | 0.17 | 0.17 |
| Estimated liquidus temp., °C | 1259 | 1259 |
| Estimated H2O content, wt. % | 0.25 | 0.25 |

This program was written by Kurt Hollocher, Geology Department, Union College, Schenectady, NY, 12308, hollochk@union.edu

Norm Calculation Program  Program run: 15/01/2012  HELP

Sample Number: HS1

| | Rock Analysis | |
|---|---|---|
| SiO2 | 47.76 | % |
| TiO2 | 2.28 | % |
| Al2O3 | 14.28 | % |
| Fe2O3 | 13.24 | % |
| FeO | | % |
| MnO | 0.14 | % |
| MgO | 7.73 | % |
| CaO | 7.95 | % |
| Na2O | 3.73 | % |
| K2O | 0.97 | % |
| P2O5 | 0.40 | % |
| CO2 | | % |
| SO3 | | % |
| S | | % |
| F | | % |
| Cl | | % |
| Sr | | ppm |
| Ba | | ppm |
| Ni | | ppm |
| Cr | | ppm |
| Zr | | ppm |
| Total | 98.48 | |

| Normalization Factors | |
|---|---|
| Total=100%? Y/N | n |
| Fe3+/(Total Iron) | 0.1 |
| Total Fe as FeO | 11.91 |
| Desired Fe2O3 | 1.32 |
| Desired FeO | 10.72 |
| Weight corr. factor | 1.000 |

Zero values not shown

Norm calculation checks:
Norm seems OK

| Normalized Analysis |
|---|
| 47.76 |
| 2.28 |
| 14.28 |
| 1.32 |
| 10.72 |
| 0.14 |
| 7.73 |
| 7.95 |
| 3.73 |
| 0.97 |
| 0.40 |
| 97.28 |

| Normative Minerals | Weight % Norm | Volume % Norm |
|---|---|---|
| Quartz | | |
| Plagioclase | 49.03 | 56.78 |
| Orthoclase | 5.73 | 6.93 |
| Nepheline | 1.02 | 1.24 |
| Leucite | | |
| Kalsilite | | |
| Corundum | | |
| Diopside | 14.34 | 13.26 |
| Hypersthene | | |
| Wollastonite | | |
| Olivine | 19.99 | 16.92 |
| Larnite | | |
| Acmite | | |
| K2SiO3 | | |
| Na2SiO3 | | |
| Rutile | | |
| Ilmenite | 4.33 | 2.82 |
| Magnetite | 1.91 | 1.14 |
| Hematite | | |
| Apatite | 0.93 | 0.90 |
| Zircon | | |
| Perovskite | | |
| Chromite | | |
| Sphene | | |
| Pyrite | | |
| Halite | | |
| Fluorite | | |
| Anhydrite | | |
| Na2SO4 | | |
| Calcite | | |
| Na2CO3 | | |
| Total | 97.28 | 99.99 |

| | | |
|---|---|---|
| Fe3+/(Total Fe) in rock | 10.0 | 10.0 |
| Mg/(Mg+Total Fe) in rock | 53.6 | 53.6 |
| Mg/(Mg+Fe2+) in rock | 56.2 | 56.2 |
| Mg/(Mg+Fe2+) in silicates | 62.6 | 62.6 |
| Ca/(Ca+Na) in rock | 54.1 | 54.1 |
| Ca/(Ca+Na) in plagioclase | 38.1 | 38.1 |
| Differentiation Index | 55.8 | 65.0 |
| Calculated density, g/cc | 3.01 | 3.01 |
| Calculated liquid density, g/cc | 2.70 | 2.70 |
| Calculated viscosity, dry, Pas | 0.19 | 0.19 |
| Calculated viscosity, wet, Pas | 0.18 | 0.18 |
| Estimated liquidus temp., °C | 1230 | 1230 |
| Estimated H2O content, wt. % | 0.33 | 0.33 |

This program was written by Kurt Hollocher, Geology Department, Union College, Schenectady, NY, 12308, hollochk@union.edu

Norm Calculation Program  Program run: 15/01/2012  HELP

Sample Number: BF7S1

| | Rock Analysis | |
|---|---|---|
| SiO2 | 46.30 | % |
| TiO2 | 2.68 | % |
| Al2O3 | 14.28 | % |
| Fe2O3 | 13.90 | % |
| FeO | | % |
| MnO | 0.21 | % |
| MgO | 7.35 | % |
| CaO | 8.18 | % |
| Na2O | 4.08 | % |
| K2O | 1.55 | % |
| P2O5 | 0.61 | % |
| CO2 | | % |
| SO3 | | % |
| S | | % |
| F | | % |
| Cl | | % |
| Sr | | ppm |
| Ba | | ppm |
| Ni | | ppm |
| Cr | | ppm |
| Zr | | ppm |
| Total | 99.14 | |

| Normalization Factors | |
|---|---|
| Total=100%? Y/N | n |
| Fe3+/(Total Iron) | 0.1 |
| Total Fe as FeO | 12.51 |
| Desired Fe2O3 | 1.39 |
| Desired FeO | 11.26 |
| Weight corr. factor | 1.000 |

Zero values not shown

Norm calculation checks:
Norm seems OK

| Normalized Analysis |
|---|
| 46.30 |
| 2.68 |
| 14.28 |
| 1.39 |
| 11.26 |
| 0.21 |
| 7.35 |
| 8.18 |
| 4.08 |
| 1.55 |
| 0.61 |
| 97.89 |

| Normative Minerals | Weight % Norm | Volume % Norm |
|---|---|---|
| Quartz | | |
| Plagioclase | 37.59 | 43.34 |
| Orthoclase | 9.16 | 11.05 |
| Nepheline | 7.05 | 8.50 |
| Leucite | | |
| Kalsilite | | |
| Corundum | | |
| Diopside | 16.89 | 15.55 |
| Hypersthene | | |
| Wollastonite | | |
| Olivine | 18.69 | 15.69 |
| Larnite | | |
| Acmite | | |
| K2SiO3 | | |
| Na2SiO3 | | |
| Rutile | | |
| Ilmenite | 5.09 | 3.31 |
| Magnetite | 2.02 | 1.20 |
| Hematite | | |
| Apatite | 1.41 | 1.36 |
| Zircon | | |
| Perovskite | | |
| Chromite | | |
| Sphene | | |
| Pyrite | | |
| Halite | | |
| Fluorite | | |
| Anhydrite | | |
| Na2SO4 | | |
| Calcite | | |
| Na2CO3 | | |
| Total | 97.90 | 100.00 |

| | | |
|---|---|---|
| Fe3+/(Total Fe) in rock | 10.0 | 10.0 |
| Mg/(Mg+Total Fe) in rock | 51.2 | 51.2 |
| Mg/(Mg+Fe2+) in rock | 53.8 | 53.8 |
| Mg/(Mg+Fe2+) in silicates | 60.8 | 60.8 |
| Ca/(Ca+Na) in rock | 52.6 | 52.6 |
| Ca/(Ca+Na) in plagioclase | 41.3 | 41.3 |
| Differentiation Index | 53.8 | 62.9 |
| Calculated density, g/cc | 3.02 | 3.02 |
| Calculated liquid density, g/cc | 2.71 | 2.71 |
| Calculated viscosity, dry, Pas | 0.16 | 0.16 |
| Calculated viscosity, wet, Pas | 0.15 | 0.15 |
| Estimated liquidus temp., °C | 1263 | 1263 |
| Estimated H2O content, wt. % | 0.24 | 0.24 |

This program was written by Kurt Hollocher, Geology Department, Union College, Schenectady, NY, 12308, hollochk@union.edu

Norm Calculation Program  Program run: 15/01/2012  HELP

Sample Number: BF3S2

| | Rock Analysis | |
|---|---|---|
| $SiO_2$ | 61.69 | % |
| $TiO_2$ | 0.81 | % |
| $Al_2O_3$ | 16.25 | % |
| $Fe_2O_3$ | 6.41 | % |
| FeO | | % |
| MnO | 0.09 | % |
| MgO | 2.61 | % |
| CaO | 2.83 | % |
| $Na_2O$ | 3.70 | % |
| $K_2O$ | 2.69 | % |
| $P_2O_5$ | 0.19 | % |
| $CO_2$ | | % |
| $SO_3$ | | % |
| S | | % |
| F | | % |
| Cl | | % |
| Sr | | ppm |
| Ba | | ppm |
| Ni | | ppm |
| Cr | | ppm |
| Zr | | ppm |
| Total | 97.27 | |

| Normalization Factors | |
|---|---|
| Total=100%? Y/N | n |
| Fe3+/(Total Iron) | 0.1 |
| Total Fe as FeO | 5.77 |
| Desired $Fe_2O_3$ | 0.64 |
| Desired FeO | 5.19 |
| Weight corr. factor | 1.000 |

Zero values not shown

Norm calculation checks:

Norm seems OK

| Normalized Analysis |
|---|
| 61.69 |
| 0.81 |
| 16.25 |
| 0.64 |
| 5.19 |
| 0.09 |
| 2.61 |
| 2.83 |
| 3.70 |
| 2.69 |
| 0.19 |
| 96.69 |

| Normative Minerals | Weight % Norm | Volume % Norm |
|---|---|---|
| Quartz | 16.89 | 18.49 |
| Plagioclase | 44.11 | 48.12 |
| Orthoclase | 15.90 | 18.02 |
| Nepheline | | |
| Leucite | | |
| Kalsilite | | |
| Corundum | 2.56 | 1.87 |
| Diopside | | |
| Hypersthene | 14.33 | 11.65 |
| Wollastonite | | |
| Olivine | | |
| Larnite | | |
| Acmite | | |
| $K_2SiO_3$ | | |
| $Na_2SiO_3$ | | |
| Rutile | | |
| Ilmenite | 1.54 | 0.94 |
| Magnetite | 0.93 | 0.52 |
| Hematite | | |
| Apatite | 0.44 | 0.40 |
| Zircon | | |
| Perovskite | | |
| Chromite | | |
| Sphene | | |
| Pyrite | | |
| Halite | | |
| Fluorite | | |
| Anhydrite | | |
| $Na_2SO_4$ | | |
| Calcite | | |
| $Na_2CO_3$ | | |
| Total | 96.70 | 100.01 |

| | | |
|---|---|---|
| Fe3+/(Total Fe) in rock | 10.0 | 10.0 |
| Mg/(Mg+Total Fe) in rock | 44.7 | 44.7 |
| Mg/(Mg+Fe2+) in rock | 47.3 | 47.3 |
| Mg/(Mg+Fe2+) in silicates | 52.2 | 52.2 |
| Ca/(Ca+Na) in rock | 29.7 | 29.7 |
| Ca/(Ca+Na) in plagioclase | 27.8 | 27.8 |
| Differentiation Index | 76.9 | 84.6 |
| Calculated density, g/cc | 2.81 | 2.81 |
| Calculated liquid density, g/cc | 2.50 | 2.50 |
| Calculated viscosity, dry, Pas | 0.60 | 0.60 |
| Calculated viscosity, wet, Pas | 0.51 | 0.51 |
| Estimated liquidus temp., °C | 961 | 961 |
| Estimated $H_2O$ content, wt. % | 2.12 | 2.12 |

This program was written by Kurt Hollocher, Geology Department, Union College, Schenectady, NY, 12308, hollochk@union.edu

Norm Calculation Program  Program run: 15/01/2012  HELP

Sample Number: BF4S1

| Rock Analysis | | |
|---|---|---|
| $SiO_2$ | 47.77 | % |
| $TiO_2$ | 1.60 | % |
| $Al_2O_3$ | 13.30 | % |
| $Fe_2O_3$ | 13.46 | % |
| FeO | | % |
| MnO | 0.18 | % |
| MgO | 7.51 | % |
| CaO | 7.75 | % |
| $Na_2O$ | 3.03 | % |
| $K_2O$ | 0.38 | % |
| $P_2O_5$ | 0.14 | % |
| $CO_2$ | | % |
| $SO_3$ | | % |
| S | | % |
| F | | % |
| Cl | | % |
| Sr | | ppm |
| Ba | | ppm |
| Ni | | ppm |
| Cr | | ppm |
| Zr | | ppm |
| Total | 95.12 | |

| Normalization Factors | |
|---|---|
| Total=100%? Y/N | n |
| Fe3+/(Total Iron) | 0.1 |
| Total Fe as FeO | 12.11 |
| Desired $Fe_2O_3$ | 1.35 |
| Desired FeO | 10.90 |
| Weight corr. factor | 1.000 |

Zero values not shown

Norm calculation checks:
Norm seems OK

| Normalized Analysis |
|---|
| 47.77 |
| 1.60 |
| 13.30 |
| 1.35 |
| 10.90 |
| 0.18 |
| 7.51 |
| 7.75 |
| 3.03 |
| 0.38 |
| 0.14 |
| 93.91 |

| Normative Minerals | Weight % Norm | Volume % Norm |
|---|---|---|
| Quartz | | |
| Plagioclase | 47.21 | 57.14 |
| Orthoclase | 2.25 | 2.85 |
| Nepheline | | |
| Leucite | | |
| Kalsilite | | |
| Corundum | | |
| Diopside | 13.16 | 12.72 |
| Hypersthene | 18.17 | 16.80 |
| Wollastonite | | |
| Olivine | 7.81 | 6.87 |
| Larnite | | |
| Acmite | | |
| $K_2SiO_3$ | | |
| $Na_2SiO_3$ | | |
| Rutile | | |
| Ilmenite | 3.04 | 2.08 |
| Magnetite | 1.96 | 1.22 |
| Hematite | | |
| Apatite | 0.32 | 0.33 |
| Zircon | | |
| Perovskite | | |
| Chromite | | |
| Sphene | | |
| Pyrite | | |
| Halite | | |
| Fluorite | | |
| Anhydrite | | |
| $Na_2SO_4$ | | |
| Calcite | | |
| $Na_2CO_3$ | | |
| Total | 93.92 | 100.01 |

| | | |
|---|---|---|
| Fe3+/(Total Fe) in rock | 10.0 | 10.0 |
| Mg/(Mg+Total Fe) in rock | 52.5 | 52.5 |
| Mg/(Mg+Fe2+) in rock | 55.1 | 55.1 |
| Mg/(Mg+Fe2+) in silicates | 59.7 | 59.7 |
| Ca/(Ca+Na) in rock | 58.6 | 58.6 |
| Ca/(Ca+Na) in plagioclase | 44.2 | 44.2 |
| Differentiation Index | 49.5 | 60.0 |
| Calculated density, g/cc | 3.05 | 3.05 |
| Calculated liquid density, g/cc | 2.71 | 2.71 |
| Calculated viscosity, dry, Pas | 0.22 | 0.22 |
| Calculated viscosity, wet, Pas | 0.22 | 0.22 |
| Estimated liquidus temp., °C | 1198 | 1198 |
| Estimated $H_2O$ content, wt. % | 0.44 | 0.44 |

This program was written by Kurt Hollocher, Geology Department, Union College, Schenectady, NY, 12308, hollochk@union.edu

Norm Calculation Program  Program run: 15/01/2012  HELP

Sample Number: BF5S1

| | Rock Analysis | |
|---|---|---|
| SiO2 | 45.44 | % |
| TiO2 | 1.93 | % |
| Al2O3 | 14.76 | % |
| Fe2O3 | 13.61 | % |
| FeO | | % |
| MnO | 0.17 | % |
| MgO | 8.09 | % |
| CaO | 7.18 | % |
| Na2O | 3.69 | % |
| K2O | 0.40 | % |
| P2O5 | 0.26 | % |
| CO2 | | % |
| SO3 | | % |
| S | | % |
| F | | % |
| Cl | | % |
| Sr | | ppm |
| Ba | | ppm |
| Ni | | ppm |
| Cr | | ppm |
| Zr | | ppm |
| Total | 95.53 | |

| Normalization Factors | |
|---|---|
| Total=100%? Y/N | n |
| Fe3+/(Total Iron) | 0.1 |
| Total Fe as FeO | 12.25 |
| Desired Fe2O3 | 1.36 |
| Desired FeO | 11.02 |
| Weight corr. factor | 1.000 |

Zero values not shown

Norm calculation checks:
Norm seems OK

| Normalized Analysis |
|---|
| 45.44 |
| 1.93 |
| 14.76 |
| 1.36 |
| 11.02 |
| 0.17 |
| 8.09 |
| 7.18 |
| 3.69 |
| 0.40 |
| 0.26 |
| 94.30 |

| Normative Minerals | Weight % Norm | Volume % Norm |
|---|---|---|
| Quartz | | |
| Plagioclase | 52.22 | 62.42 |
| Orthoclase | 2.36 | 2.96 |
| Nepheline | 0.83 | 1.04 |
| Leucite | | |
| Kalsilite | | |
| Corundum | | |
| Diopside | 9.36 | 8.95 |
| Hypersthene | | |
| Wollastonite | | |
| Olivine | 23.29 | 20.35 |
| Larnite | | |
| Acmite | | |
| K2SiO3 | | |
| Na2SiO3 | | |
| Rutile | | |
| Ilmenite | 3.67 | 2.47 |
| Magnetite | 1.97 | 1.21 |
| Hematite | | |
| Apatite | 0.60 | 0.60 |
| Zircon | | |
| Perovskite | | |
| Chromite | | |
| Sphene | | |
| Pyrite | | |
| Halite | | |
| Fluorite | | |
| Anhydrite | | |
| Na2SO4 | | |
| Calcite | | |
| Na2CO3 | | |
| Total | 94.30 | 100.00 |

| | | |
|---|---|---|
| Fe3+/(Total Fe) in rock | 10.0 | 10.0 |
| Mg/(Mg+Total Fe) in rock | 54.1 | 54.1 |
| Mg/(Mg+Fe2+) in rock | 56.7 | 56.7 |
| Mg/(Mg+Fe2+) in silicates | 62.0 | 62.0 |
| Ca/(Ca+Na) in rock | 51.8 | 51.8 |
| Ca/(Ca+Na) in plagioclase | 41.7 | 41.7 |
| Differentiation Index | 55.4 | 66.4 |
| Calculated density, g/cc | 3.02 | 3.02 |
| Calculated liquid density, g/cc | 2.72 | 2.72 |
| Calculated viscosity, dry, Pas | 0.18 | 0.18 |
| Calculated viscosity, wet, Pas | 0.17 | 0.17 |
| Estimated liquidus temp., °C | 1247 | 1247 |
| Estimated H2O content, wt. % | 0.28 | 0.28 |

This program was written by Kurt Hollocher, Geology Department, Union College, Schenectady, NY, 12308, hollochk@union.edu

Norm Calculation Program  Program run: 15/01/2012  HELP

Sample Number: BF6S1

| | Rock Analysis | | Normalized Analysis |
|---|---|---|---|
| SiO2 | 45.26 | % | 45.26 |
| TiO2 | 2.82 | % | 2.82 |
| Al2O3 | 14.29 | % | 14.29 |
| Fe2O3 | 14.35 | % | 1.44 |
| FeO | | % | 11.62 |
| MnO | 0.20 | % | 0.20 |
| MgO | 6.56 | % | 6.56 |
| CaO | 8.14 | % | 8.14 |
| Na2O | 3.39 | % | 3.39 |
| K2O | 1.48 | % | 1.48 |
| P2O5 | 0.57 | % | 0.57 |
| CO2 | | % | |
| SO3 | | % | |
| S | | % | |
| F | | % | |
| Cl | | % | |
| Sr | | ppm | |
| Ba | | ppm | |
| Ni | | ppm | |
| Cr | | ppm | |
| Zr | | ppm | |
| Total | 97.06 | | 95.77 |

| Normalization Factors | |
|---|---|
| Total=100%? Y/N | n |
| Fe3+/(Total Iron) | 0.1 |
| Total Fe as FeO | 12.91 |
| Desired Fe2O3 | 1.44 |
| Desired FeO | 11.62 |
| Weight corr. factor | 1.000 |

Zero values not shown

Norm calculation checks:

Norm seems OK

| Normative Minerals | Weight % Norm | Volume % Norm |
|---|---|---|
| Quartz | | |
| Plagioclase | 42.42 | 50.07 |
| Orthoclase | 8.75 | 10.81 |
| Nepheline | 3.07 | 3.79 |
| Leucite | | |
| Kalsilite | | |
| Corundum | | |
| Diopside | 14.26 | 13.42 |
| Hypersthene | | |
| Wollastonite | | |
| Olivine | 18.51 | 15.76 |
| Larnite | | |
| Acmite | | |
| K2SiO3 | | |
| Na2SiO3 | | |
| Rutile | | |
| Ilmenite | 5.36 | 3.57 |
| Magnetite | 2.09 | 1.27 |
| Hematite | | |
| Apatite | 1.32 | 1.31 |
| Zircon | | |
| Perovskite | | |
| Chromite | | |
| Sphene | | |
| Pyrite | | |
| Halite | | |
| Fluorite | | |
| Anhydrite | | |
| Na2SO4 | | |
| Calcite | | |
| Na2CO3 | | |
| Total | 95.78 | 100.00 |

| | | |
|---|---|---|
| Fe3+/(Total Fe) in rock | 10.0 | 10.0 |
| Mg/(Mg+Total Fe) in rock | 47.5 | 47.5 |
| Mg/(Mg+Fe2+) in rock | 50.2 | 50.2 |
| Mg/(Mg+Fe2+) in silicates | 57.5 | 57.5 |
| Ca/(Ca+Na) in rock | 57.0 | 57.0 |
| Ca/(Ca+Na) in plagioclase | 44.3 | 44.3 |
| Differentiation Index | 54.2 | 64.7 |
| Calculated density, g/cc | 3.03 | 3.03 |
| Calculated liquid density, g/cc | 2.72 | 2.72 |
| Calculated viscosity, dry, Pas | 0.17 | 0.17 |
| Calculated viscosity, wet, Pas | 0.16 | 0.16 |
| Estimated liquidus temp., °C | 1264 | 1264 |
| Estimated H2O content, wt. % | 0.23 | 0.23 |

This program was written by Kurt Hollocher, Geology Department, Union College, Schenectady, NY, 12308, hollochk@union.edu

# *Appendix Three*

## *Modal Analysis*

Modal analysis for tuff samples

| Sample | Vesicles | Matrix | Juvenile Basalt | Olivine | Clinopyroxene | Plagioclase | Sed - Lithic | Ign - Lithic | Quartz Xenolith | Hornblende | Plagioclase | Hypersthene | Total |
|---|---|---|---|---|---|---|---|---|---|---|---|---|---|
| R1 | 12.67 | 32.67 | 30.67 | 8.67 | 4.33 | 0.67 | 1.67 | 2.00 | 5.67 | 0.33 | 0.67 | 0.00 | 100 |
| R2 | 6.33 | 52.00 | 15.33 | 10.00 | 6.00 | 1.00 | 3.67 | 1.67 | 2.00 | 1.00 | 0.00 | 1.00 | 100 |
| R2 | 12.67 | 41.67 | 23.67 | 6.33 | 5.33 | 0.67 | 3.00 | 1.67 | 4.33 | 0.67 | 0.00 | 0.00 | 100 |
| R3 | 7.00 | 38.00 | 34.67 | 5.33 | 1.33 | 0.33 | 3.67 | 4.00 | 5.33 | 0.00 | 0.00 | 0.33 | 100 |
| R5 | 13.00 | 29.33 | 51.33 | 3.00 | 0.67 | 0.00 | 2.33 | 0.33 | 0.00 | 0.00 | 0.00 | 0.00 | 100 |
| R6 | 10.00 | 30.00 | 38.33 | 2.67 | 1.00 | 0.00 | 12.67 | 3.00 | 2.33 | 0.00 | 0.00 | 0.00 | 100 |
| R6 | 11.67 | 36.67 | 37.00 | 4.00 | 0.33 | 0.33 | 7.00 | 0.33 | 2.67 | 0.00 | 0.00 | 0.00 | 100 |
| R6 | 17.00 | 21.33 | 53.33 | 2.67 | 1.00 | 0.00 | 0.33 | 1.33 | 3.00 | 0.00 | 0.00 | 0.00 | 100 |
| R8 | 21.67 | 32.00 | 32.00 | 4.67 | 2.67 | 0.33 | 1.67 | 0.33 | 4.67 | 0.00 | 0.00 | 0.00 | 100 |
| R8 | 26.67 | 19.33 | 46.33 | 3.67 | 0.67 | 0.00 | 0.33 | 0.67 | 2.33 | 0.00 | 0.00 | 0.33 | 100 |
| R9 | 3.33 | 70.00 | 11.00 | 3.33 | 4.00 | 0.00 | 1.00 | 1.67 | 2.67 | 1.67 | 1.00 | 0.00 | 100 |
| R9 | 10.67 | 48.00 | 29.33 | 3.33 | 1.67 | 0.00 | 0.00 | 1.33 | 4.33 | 0.00 | 0.67 | 0.67 | 100 |
| R11 | 9.00 | 50.33 | 28.33 | 1.00 | 3.00 | 0.00 | 2.33 | 2.33 | 2.67 | 0.00 | 0.67 | 0.33 | 100 |
| R11 | 6.67 | 69.33 | 11.33 | 3.33 | 3.33 | 0.00 | 1.00 | 1.33 | 2.00 | 0.67 | 1.00 | 0.00 | 100 |
| R14 | 10.00 | 65.67 | 7.67 | 5.00 | 4.33 | 0.00 | 1.00 | 2.33 | 3.67 | 0.00 | 0.33 | 0.00 | 100 |
| R14 | 8.67 | 72.00 | 11.33 | 2.00 | 1.33 | 0.00 | 1.67 | 0.00 | 1.33 | 0.67 | 0.67 | 0.33 | 100 |
| R15 | 11.67 | 21.67 | 54.67 | 1.00 | 1.33 | 0.00 | 2.33 | 6.67 | 0.67 | 0.00 | 0.00 | 0.00 | 100 |
| R15 | 12.00 | 29.00 | 50.33 | 2.00 | 0.33 | 0.00 | 1.67 | 2.67 | 2.00 | 0.00 | 0.00 | 0.00 | 100 |
| R12 | 17.00 | 64.00 | 12.33 | 4.00 | 0.33 | 0.00 | 0.00 | 2.00 | 0.33 | 0.00 | 0.00 | 0.00 | 100 |
| R17 | 3.67 | 58.33 | 26.33 | 1.00 | 4.67 | 0.00 | 0.00 | 2.00 | 4.00 | 0.00 | 0.00 | 0.00 | 100 |
| R20 | 5.00 | 31.67 | 36.33 | 2.33 | 0.00 | 0.00 | 17.00 | 5.33 | 2.00 | 0.33 | 0.00 | 0.00 | 100 |
| R20 | 11.33 | 32.33 | 42.67 | 0.67 | 1.00 | 0.00 | 9.67 | 1.33 | 1.00 | 0.00 | 0.00 | 0.00 | 100 |
| I1 | 24.67 | 65.67 | 5.00 | 1.33 | 0.00 | 0.00 | 0.00 | 1.67 | 1.67 | 0.00 | 0.00 | 0.00 | 100 |
| I1 | 23.00 | 68.00 | 3.33 | 3.33 | 0.33 | 0.00 | 0.33 | 0.33 | 1.33 | 0.00 | 0.00 | 0.00 | 100 |
| I2 | 16.00 | 74.67 | 3.00 | 2.00 | 0.33 | 0.00 | 0.00 | 0.00 | 3.00 | 0.67 | 0.33 | 0.00 | 100 |
| I2 | 12.67 | 80.00 | 3.00 | 1.00 | 1.33 | 0.00 | 0.00 | 0.33 | 1.33 | 0.00 | 0.33 | 0.00 | 100 |
| I3 | 16.67 | 57.67 | 18.33 | 2.33 | 0.00 | 0.00 | 2.67 | 1.00 | 0.33 | 0.00 | 0.33 | 0.67 | 100 |
| I4 | 12.67 | 27.67 | 48.33 | 2.67 | 0.00 | 0.00 | 5.33 | 3.33 | 0.00 | 0.00 | 0.00 | 0.00 | 100 |
| I4 | 14.67 | 36.33 | 41.67 | 3.67 | 0.00 | 0.00 | 0.67 | 2.67 | 0.33 | 0.00 | 0.00 | 0.00 | 100 |
| I4 | 13.67 | 35.33 | 39.33 | 1.00 | 0.00 | 0.00 | 1.00 | 9.33 | 0.00 | 0.00 | 0.00 | 0.33 | 100 |
| I4 | 18.33 | 22.33 | 45.33 | 0.00 | 0.00 | 0.00 | 0.67 | 13.33 | 0.00 | 0.00 | 0.00 | 0.00 | 100 |
| I5 | 28.67 | 57.00 | 8.33 | 1.33 | 1.00 | 0.00 | 0.00 | 1.00 | 2.00 | 0.00 | 0.67 | 0.00 | 100 |
| I6 | 11.33 | 40.67 | 30.67 | 3.00 | 1.00 | 0.00 | 6.00 | 6.00 | 1.33 | 0.00 | 0.00 | 0.00 | 100 |
| I6 | 12.33 | 49.33 | 28.33 | 3.67 | 1.33 | 0.00 | 3.33 | 1.33 | 0.33 | 0.00 | 0.00 | 0.00 | 100 |

| Sample | Vesicles | Matrix | Juvenile Basalt | Olivine | Clinopyroxene | Plagioclase | Sed - Lithic | Ign - Lithic | Quartz Xenolith | Hornblende | Plagioclase | Hypersthene | Total |
|---|---|---|---|---|---|---|---|---|---|---|---|---|---|
| I7 | 12.00 | 37.00 | 32.67 | 1.00 | 1.00 | 0.00 | 1.00 | 13.67 | 1.67 | 0.00 | 0.00 | 0.00 | 100 |
| I7 | 12.67 | 48.00 | 27.67 | 4.33 | 0.67 | 0.00 | 1.67 | 3.33 | 0.67 | 0.00 | 0.33 | 0.67 | 100 |
| I8 | 14.00 | 63.33 | 11.33 | 3.00 | 0.67 | 0.00 | 2.67 | 2.00 | 2.33 | 0.00 | 0.67 | 0.00 | 100 |
| I9 | 8.67 | 64.33 | 11.00 | 7.33 | 0.33 | 0.00 | 2.67 | 3.67 | 1.33 | 0.00 | 0.67 | 0.00 | 100 |
| I9 | 12.00 | 59.00 | 16.33 | 5.33 | 2.00 | 0.00 | 3.33 | 0.33 | 1.33 | 0.00 | 0.33 | 0.00 | 100 |
| I10 | 19.33 | 59.67 | 13.33 | 2.00 | 1.67 | 0.00 | 1.00 | 0.67 | 1.00 | 0.67 | 0.33 | 0.33 | 100 |
| I10 | 19.67 | 60.67 | 9.67 | 3.00 | 2.67 | 0.00 | 1.00 | 1.00 | 2.00 | 0.00 | 0.33 | 0.00 | 100 |
| I11 | 11.67 | 44.67 | 28.00 | 2.00 | 4.33 | 0.67 | 4.67 | 1.33 | 1.67 | 0.33 | 0.67 | 0.00 | 100 |
| I12 | 12.67 | 52.67 | 28.00 | 5.33 | 0.33 | 0.00 | 0.33 | 0.33 | 0.33 | 0.00 | 0.00 | 0.00 | 100 |
| I12 | 15.00 | 45.00 | 27.00 | 3.67 | 0.00 | 0.00 | 1.67 | 7.00 | 0.33 | 0.00 | 0.00 | 0.33 | 100 |
| I13 | 19.00 | 72.67 | 4.00 | 0.67 | 1.33 | 0.00 | 0.67 | 1.00 | 0.67 | 0.00 | 0.00 | 0.00 | 100 |
| I13 | 22.00 | 69.67 | 5.33 | 1.00 | 0.67 | 0.00 | 1.00 | 0.00 | 0.33 | 0.00 | 0.00 | 0.00 | 100 |
| P1 | 14.67 | 63.67 | 13.33 | 0.33 | 1.33 | 0.00 | 0.33 | 0.00 | 5.33 | 0.33 | 0.67 | 0.00 | 100 |
| P1 | 8.67 | 65.00 | 15.67 | 1.00 | 6.00 | 0.00 | 0.00 | 0.00 | 3.67 | 0.00 | 0.00 | 0.00 | 100 |
| P2 | 18.00 | 69.33 | 2.00 | 0.00 | 1.33 | 0.00 | 2.67 | 0.00 | 5.33 | 0.00 | 0.67 | 0.67 | 100 |
| P2 | 17.33 | 72.33 | 1.00 | 1.33 | 3.00 | 0.00 | 2.67 | 0.00 | 2.00 | 0.00 | 0.33 | 0.00 | 100 |
| P3 | 10.67 | 63.00 | 13.33 | 1.00 | 2.00 | 0.00 | 4.33 | 0.00 | 4.67 | 0.00 | 0.67 | 0.33 | 100 |
| P3 | 8.00 | 64.67 | 15.33 | 0.00 | 0.33 | 0.00 | 5.33 | 0.00 | 5.33 | 0.33 | 0.67 | 0.00 | 100 |
| P4 | 9.33 | 73.00 | 6.33 | 1.00 | 2.67 | 0.00 | 3.67 | 0.00 | 3.67 | 0.33 | 0.00 | 0.00 | 100 |
| P4 | 11.00 | 77.33 | 3.33 | 0.67 | 0.67 | 0.00 | 3.00 | 0.00 | 3.67 | 0.00 | 0.00 | 0.33 | 100 |
| P8 | 6.67 | 37.67 | 43.67 | 1.33 | 0.33 | 0.00 | 8.00 | 0.00 | 2.33 | 0.00 | 0.00 | 0.00 | 100 |
| P8 | 6.67 | 42.00 | 43.00 | 0.33 | 2.00 | 0.00 | 3.67 | 0.00 | 1.67 | 0.33 | 0.33 | 0.00 | 100 |
| P9 | 12.00 | 42.00 | 37.00 | 1.00 | 1.00 | 0.00 | 3.00 | 0.00 | 3.00 | 0.00 | 1.00 | 0.00 | 100 |
| P11 | 8.33 | 30.67 | 39.00 | 0.33 | 1.67 | 0.00 | 19.00 | 0.00 | 0.67 | 0.33 | 0.00 | 0.00 | 100 |
| P11 | 5.00 | 38.00 | 40.33 | 1.00 | 0.67 | 0.00 | 8.33 | 4.00 | 2.33 | 0.00 | 0.00 | 0.33 | 100 |
| P14 | 5.67 | 34.33 | 44.00 | 2.67 | 1.00 | 0.00 | 11.00 | 0.00 | 1.00 | 0.00 | 0.33 | 0.00 | 100 |
| P14 | 4.33 | 44.33 | 37.33 | 0.33 | 2.67 | 0.00 | 9.33 | 0.00 | 1.00 | 0.00 | 0.67 | 0.00 | 100 |
| P15 | 5.67 | 39.33 | 27.67 | 2.67 | 1.67 | 0.00 | 22.00 | 0.00 | 1.00 | 0.00 | 0.00 | 0.00 | 100 |
| P15 | 10.67 | 48.67 | 25.00 | 1.33 | 2.33 | 0.00 | 10.33 | 0.33 | 1.00 | 0.33 | 0.00 | 0.00 | 100 |
| P3S1 | 10.67 | 40.67 | 38.00 | 0.00 | 3.33 | 0.67 | 2.33 | 0.00 | 3.33 | 0.33 | 0.33 | 0.33 | 100 |
| P3S1 | 18.00 | 38.00 | 36.33 | 0.00 | 2.67 | 1.00 | 1.67 | 0.00 | 1.67 | 0.00 | 0.67 | 0.00 | 100 |
| P3S3 | 13.33 | 27.67 | 51.00 | 1.00 | 2.00 | 0.00 | 2.00 | 0.67 | 2.00 | 0.00 | 0.33 | 0.00 | 100 |
| P3S3 | 9.67 | 29.33 | 50.33 | 0.33 | 1.00 | 0.00 | 7.00 | 0.00 | 1.67 | 0.33 | 0.33 | 0.00 | 100 |
| P3S4 | 9.67 | 53.67 | 22.33 | 0.67 | 5.33 | 0.00 | 3.33 | 1.00 | 3.00 | 0.33 | 0.33 | 0.33 | 100 |
| P3S4 | 6.33 | 56.00 | 27.00 | 1.33 | 4.00 | 0.00 | 3.33 | 0.00 | 1.33 | 0.33 | 0.33 | 0.00 | 100 |
| P3S6 | 9.67 | 44.00 | 34.67 | 2.67 | 2.67 | 0.33 | 5.33 | 0.00 | 0.33 | 0.00 | 0.33 | 0.00 | 100 |
| P3S6 | 5.00 | 37.67 | 48.00 | 2.00 | 3.67 | 0.00 | 2.33 | 0.00 | 1.33 | 0.00 | 0.00 | 0.00 | 100 |

| Sample | Vesicles | Matrix | Juvenile Basalt | Olivine | Clinopyroxene | Plagioclase | Sed - Lithic | Ign - Lithic | Quartz Xenolith | Hornblende | Plagioclase | Hypersthene | Total |
|---|---|---|---|---|---|---|---|---|---|---|---|---|---|
| P3S7 | 10.00 | 44.33 | 30.67 | 2.00 | 1.67 | 0.67 | 9.33 | 0.33 | 1.00 | 0.00 | 0.00 | 0.00 | 100 |
| P3S7 | 5.33 | 51.67 | 24.33 | 0.33 | 4.33 | 0.33 | 7.33 | 1.67 | 3.33 | 0.00 | 1.33 | 0.00 | 100 |
| P3S8 | 8.33 | 36.00 | 40.33 | 0.00 | 3.00 | 0.00 | 8.67 | 0.00 | 3.00 | 0.00 | 0.67 | 0.00 | 100 |
| P3S8 | 15.33 | 28.67 | 45.00 | 0.33 | 1.00 | 0.00 | 3.67 | 1.00 | 4.00 | 0.00 | 0.67 | 0.33 | 100 |
| P3S9 | 5.00 | 58.33 | 24.00 | 3.00 | 2.00 | 0.00 | 4.00 | 0.33 | 3.33 | 0.00 | 0.00 | 0.00 | 100 |
| P3S9 | 3.00 | 46.67 | 36.33 | 1.33 | 0.00 | 0.33 | 6.00 | 0.00 | 5.67 | 0.00 | 0.67 | 0.00 | 100 |
| P3S13 | 7.33 | 28.33 | 48.33 | 0.67 | 2.00 | 0.00 | 4.33 | 8.00 | 0.67 | 0.00 | 0.33 | 0.00 | 100 |
| P3S13 | 9.67 | 27.33 | 52.00 | 0.33 | 2.00 | 0.00 | 6.33 | 0.00 | 1.67 | 0.00 | 0.67 | 0.00 | 100 |
| P3S15 | 9.00 | 47.00 | 35.00 | 1.00 | 0.67 | 0.33 | 6.00 | 0.00 | 0.00 | 0.67 | 0.33 | 0.00 | 100 |
| P3S15 | 8.67 | 45.67 | 34.00 | 0.00 | 3.67 | 0.00 | 5.33 | 0.00 | 1.67 | 0.00 | 1.00 | 0.00 | 100 |
| P3S17 | 5.67 | 74.33 | 9.67 | 0.33 | 2.67 | 0.00 | 2.33 | 0.67 | 3.33 | 0.00 | 1.00 | 0.00 | 100 |
| P3S17 | 9.33 | 68.67 | 13.33 | 0.67 | 2.67 | 0.00 | 2.00 | 0.00 | 2.67 | 0.33 | 0.00 | 0.33 | 100 |
| P3S20 | 4.33 | 34.00 | 49.00 | 0.67 | 1.33 | 0.67 | 3.33 | 0.33 | 5.67 | 0.33 | 0.33 | 0.00 | 100 |
| P3S20 | 2.00 | 46.67 | 35.00 | 0.33 | 4.67 | 0.00 | 8.00 | 0.00 | 3.00 | 0.00 | 0.33 | 0.00 | 100 |
| P3S24 | 8.67 | 26.00 | 61.00 | 0.00 | 0.33 | 0.00 | 2.00 | 0.00 | 2.00 | 0.00 | 0.00 | 0.00 | 100 |
| P3S24 | 8.67 | 27.67 | 53.00 | 0.00 | 3.67 | 0.00 | 2.67 | 0.00 | 3.67 | 0.00 | 0.33 | 0.33 | 100 |
| P3S25 | 6.33 | 21.33 | 58.33 | 0.00 | 1.33 | 0.00 | 9.00 | 0.00 | 3.33 | 0.00 | 0.33 | 0.00 | 100 |
| P3S25 | 3.33 | 32.00 | 57.00 | 0.33 | 1.67 | 0.00 | 4.33 | 0.00 | 1.33 | 0.00 | 0.00 | 0.00 | 100 |
| P2S2 | 8.00 | 80.67 | 1.00 | 0.67 | 4.67 | 0.00 | 3.33 | 0.00 | 1.67 | 0.00 | 0.00 | 0.00 | 100 |
| P2S2 | 6.33 | 77.33 | 5.00 | 0.00 | 3.67 | 0.00 | 4.00 | 0.33 | 3.33 | 0.00 | 0.00 | 0.00 | 100 |
| P2S3 | 13.33 | 48.67 | 33.67 | 0.00 | 1.00 | 0.00 | 2.67 | 0.00 | 0.67 | 0.00 | 0.00 | 0.00 | 100 |
| P2S3 | 10.33 | 47.00 | 32.00 | 2.33 | 0.67 | 0.00 | 6.33 | 0.00 | 1.33 | 0.00 | 0.00 | 0.00 | 100 |
| P2S4 | 3.33 | 76.00 | 4.33 | 0.00 | 2.33 | 0.00 | 8.33 | 0.00 | 4.33 | 0.67 | 0.67 | 0.00 | 100 |
| P2S4 | 9.00 | 61.33 | 18.67 | 1.00 | 2.33 | 0.00 | 6.00 | 0.00 | 1.67 | 0.00 | 0.00 | 0.00 | 100 |
| P2S5 | 8.33 | 68.67 | 7.33 | 1.67 | 2.00 | 0.00 | 7.67 | 0.00 | 4.33 | 0.00 | 0.00 | 0.00 | 100 |
| P2S6 | 6.33 | 47.33 | 34.33 | 0.33 | 2.00 | 0.00 | 8.33 | 0.00 | 1.33 | 0.00 | 0.00 | 0.00 | 100 |
| P2S6 | 6.67 | 49.33 | 32.33 | 0.33 | 0.00 | 0.00 | 7.33 | 0.00 | 4.00 | 0.00 | 0.00 | 0.00 | 100 |
| P2S8 | 6.33 | 47.67 | 36.33 | 0.33 | 1.33 | 0.00 | 7.00 | 0.00 | 1.00 | 0.00 | 0.00 | 0.00 | 100 |
| P2S9 | 12.33 | 51.67 | 23.33 | 1.67 | 6.00 | 0.00 | 3.33 | 0.67 | 1.00 | 0.00 | 0.00 | 0.00 | 100 |
| P2S9 | 9.00 | 56.00 | 27.33 | 1.33 | 1.00 | 0.00 | 4.00 | 0.00 | 1.00 | 0.00 | 0.33 | 0.00 | 100 |
| P2S10 | 6.67 | 74.67 | 6.00 | 1.33 | 2.67 | 0.00 | 3.67 | 0.00 | 4.33 | 0.67 | 0.00 | 0.00 | 100 |
| P2S10 | 6.33 | 74.00 | 9.00 | 0.67 | 2.33 | 0.00 | 3.33 | 0.00 | 4.00 | 0.00 | 0.33 | 0.00 | 100 |

Modal analysis for Juvenile Basalt

| Sample | Vesicles | Plagioclase | Glass | Plagioclase | Olivine | Clinopyroxene | Tuff Xenolith | Sed Xenolith | Ig Xenolith | Xenocryst | Total |
|---|---|---|---|---|---|---|---|---|---|---|---|
| R4 | 12.67 | 56.33 | 6.33 | 2.00 | 22.67 | 0.00 | 0.00 | 0.00 | 0.00 | 0.00 | 100.00 |
| R7 | 21.33 | 46.67 | 17.33 | 1.67 | 7.33 | 1.00 | 4.67 | 0.00 | 0.00 | 0.00 | 100.00 |
| R10 | 14.67 | 69.00 | 3.33 | 0.00 | 5.33 | 6.00 | 1.67 | 0.00 | 0.00 | 0.00 | 100.00 |
| R10 | 15.67 | 66.67 | 3.00 | 0.00 | 7.00 | 6.67 | 1.00 | 0.00 | 0.00 | 0.00 | 100.00 |
| R13 | 23.00 | 55.67 | 0.00 | 1.33 | 10.67 | 6.67 | 2.67 | 0.00 | 0.00 | 0.00 | 100.00 |
| R13 | 20.33 | 57.67 | 0.33 | 0.67 | 12.33 | 8.67 | 0.00 | 0.00 | 0.00 | 0.00 | 100.00 |
| R18 | 1.33 | 83.33 | 3.33 | 0.33 | 7.33 | 4.33 | 0.00 | 0.00 | 0.00 | 0.00 | 100.00 |
| R19 | 1.00 | 77.67 | 3.00 | 0.00 | 15.33 | 3.00 | 0.00 | 0.00 | 0.00 | 0.00 | 100.00 |
| P12 | 0.00 | 77.00 | 0.33 | 9.67 | 5.00 | 2.00 | 0.33 | 0.00 | 2.67 | 0.00 | 100.00 |
| P3S2 | 27.70 | 0.00 | 60.00 | 0.70 | 5.30 | 4.30 | 1.30 | 0.70 | 0.00 | 0.00 | 100.00 |
| P3S2 | 30.30 | 0.00 | 58.33 | 0.30 | 6.00 | 2.77 | 1.00 | 1.33 | 0.00 | 0.00 | 100.00 |
| P3S18 | 20.67 | 59.67 | 7.33 | 1.33 | 8.00 | 3.00 | 0.00 | 0.00 | 0.00 | 0.00 | 100.00 |
| P3S18 | 14.67 | 61.00 | 14.00 | 0.00 | 7.00 | 3.33 | 0.00 | 0.00 | 0.00 | 0.00 | 100.00 |
| P3S22 | 19.33 | 67.33 | 0.67 | 0.00 | 7.67 | 4.00 | 1.00 | 0.00 | 0.00 | 0.00 | 100.00 |
| P3S22 | 28.33 | 57.67 | 0.67 | 0.00 | 8.00 | 5.33 | 0.00 | 0.00 | 0.00 | 0.00 | 100.00 |
| P3S23 | 1.67 | 65.67 | 0.00 | 8.67 | 12.00 | 10.00 | 0.00 | 0.00 | 0.00 | 2.00 | 100.00 |
| P3S23 | 20.67 | 66.33 | 0.00 | 0.00 | 8.00 | 5.00 | 0.00 | 0.00 | 0.00 | 0.00 | 100.00 |

# *Appendix Four*

## *Vesicularity*

Vesicularity results from the method of Houghton and Wilson (1989).

| Sample | Stratigraphic Height | Size Range | Clast Number | Dry Weight | Wet Weight | Number of Wax Sheets | Weight Difference | DRE ($g/cm^3$) | Specific Gravity | Vesicularity |
|---|---|---|---|---|---|---|---|---|---|---|
| P3 S16 | 6.72-6.98 | 13-45 | 1 | 202.79 | 126.65 | 6 | -0.18 | 3 | 2.66 | 11.22 |
| P3 S16 | 6.72-6.98 | 13-45 | 2 | 57.43 | 35.36 | 4 | -0.12 | 3 | 2.60 | 13.26 |
| P3 S16 | 6.72-6.98 | 13-45 | 3 | 56.07 | 34.54 | 3 | -0.09 | 3 | 2.60 | 13.19 |
| P3 S16 | 6.72-6.98 | 13-45 | 4 | 22.27 | 13.71 | 2 | -0.06 | 3 | 2.60 | 13.28 |
| P3 S16 | 6.72-6.98 | 13-45 | 5 | 18.48 | 9.21 | 2 | -0.06 | 3 | 1.99 | 33.55 |
| P3 S16 | 6.72-6.98 | 13-45 | 6 | 15.31 | 7.49 | 2 | -0.06 | 3 | 1.96 | 34.74 |
| P3 S16 | 6.72-6.98 | 13-45 | 7 | 19.14 | 9.34 | 2 | -0.06 | 3 | 1.95 | 34.90 |
| P3 S16 | 6.72-6.98 | 13-45 | 8 | 14.79 | 9.05 | 2 | -0.06 | 3 | 2.58 | 14.11 |
| P3 S16 | 6.72-6.98 | 13-45 | 9 | 11.74 | 7.29 | 2 | -0.06 | 3 | 2.64 | 12.06 |
| P3 S16 | 6.72-6.98 | 13-45 | 10 | 4.74 | 1.57 | 1 | -0.03 | 3 | 1.50 | 50.16 |
| P3 S16 | 6.72-6.98 | 13-45 | 11 | 9.31 | 5.54 | 1 | -0.03 | 3 | 2.47 | 17.68 |
| P3 S16 | 6.72-6.98 | 13-45 | 12 | 10.36 | 6.32 | 1 | -0.03 | 3 | 2.56 | 14.52 |
| P3 S16 | 6.72-6.98 | 13-45 | 13 | 5.96 | 3.64 | 1 | -0.03 | 3 | 2.57 | 14.37 |
| P3 S16 | 6.72-6.98 | 13-45 | 14 | 4.61 | 2.37 | 1 | -0.03 | 3 | 2.06 | 31.40 |
| P3 S16 | 6.72-6.98 | 13-45 | 15 | 2.77 | 1.1 | 1 | -0.03 | 3 | 1.66 | 44.71 |
| P3 S16 | 6.72-6.98 | 13-45 | 16 | 4.09 | 2.47 | 1 | -0.03 | 3 | 2.52 | 15.84 |
| P3 S16 | 6.72-6.98 | 13-45 | 17 | 4.35 | 2.61 | 1 | -0.03 | 3 | 2.50 | 16.67 |

| Sample | Stratigraphic Height | Size Range | Clast Number | Dry Weight | Wet Weight | Number of Wax Sheets | Weight Difference | DRE ($g/cm^3$) | Specific Gravity | Vesicularity |
|---|---|---|---|---|---|---|---|---|---|---|
| R7 | 6.2 | 16-120 | 1 | 27.08 | 16.09 | 2 | -0.06 | 3 | 2.46 | 17.86 |
| R7 | 6.2 | 16-120 | 2 | 26.8 | 16.69 | 2 | -0.06 | 3 | 2.65 | 11.64 |
| R7 | 6.2 | 16-120 | 3 | 27.8 | 16.7 | 2 | -0.06 | 3 | 2.50 | 16.52 |
| R7 | 6.2 | 16-120 | 4 | 20.76 | 12.43 | 2 | -0.06 | 3 | 2.49 | 16.93 |
| R7 | 6.2 | 16-120 | 5 | 16.33 | 9.71 | 2 | -0.06 | 3 | 2.47 | 17.77 |
| R7 | 6.2 | 16-120 | 6 | 12.83 | 8.19 | 1 | -0.03 | 3 | 2.77 | 7.83 |
| R7 | 6.2 | 16-120 | 7 | 5.91 | 3.69 | 1 | -0.03 | 3 | 2.66 | 11.26 |
| R7 | 6.2 | 16-120 | 8 | 5.91 | 3.38 | 1 | -0.03 | 3 | 2.34 | 22.13 |
| R7 | 6.2 | 16-120 | 9 | 11.13 | 6.33 | 2 | -0.06 | 3 | 2.32 | 22.71 |
| R7 | 6.2 | 16-120 | 10 | 7.1 | 4.02 | 1 | -0.03 | 3 | 2.31 | 23.16 |
| R7 | 6.2 | 16-120 | 11 | 664.01 | 404.89 | 15 | -0.45 | 3 | 2.56 | 14.58 |

| Sample | Stratigraphic Height | Size Range | Clast Number | Dry Weight | Wet Weight | Number of Wax Sheets | Weight Difference | DRE ($g/cm^3$) | Specific Gravity | Vesicularity |
|---|---|---|---|---|---|---|---|---|---|---|
| R4 | 6 | 24-67 | 1 | 145.16 | 89.74 | 5 | -0.15 | 3 | 2.62 | 12.69 |
| R4 | 6 | 24-67 | 2 | 128.77 | 81.46 | 5 | -0.15 | 3 | 2.72 | 9.27 |
| R4 | 6 | 24-67 | 3 | 222.39 | 135.67 | 6 | -0.18 | 3 | 2.56 | 14.52 |
| R4 | 6 | 24-67 | 4 | 142.97 | 86.33 | 5 | -0.15 | 3 | 2.52 | 15.86 |
| R4 | 6 | 24-67 | 5 | 80.33 | 47.17 | 4 | -0.12 | 3 | 2.42 | 19.25 |
| R4 | 6 | 24-67 | 6 | 114.67 | 60.07 | 5 | -0.15 | 3 | 2.10 | 29.99 |
| R4 | 6 | 24-67 | 7 | 104.77 | 63.93 | 4 | -0.12 | 3 | 2.57 | 14.49 |
| R4 | 6 | 24-67 | 8 | 70.7 | 39.98 | 3 | -0.09 | 3 | 2.30 | 23.29 |
| R4 | 6 | 24-67 | 9 | 80.66 | 48.55 | 3 | -0.09 | 3 | 2.51 | 16.27 |
| R4 | 6 | 24-67 | 10 | 57.09 | 31.67 | 4 | -0.12 | 3 | 2.25 | 25.14 |
| R4 | 6 | 24-67 | 11 | 62.41 | 36.86 | 3 | -0.09 | 3 | 2.44 | 18.58 |
| R4 | 6 | 24-67 | 12 | 55.07 | 30.85 | 3 | -0.09 | 3 | 2.27 | 24.21 |
| R4 | 6 | 24-67 | 13 | 52.07 | 28.77 | 3 | -0.09 | 3 | 2.23 | 25.51 |
| R4 | 6 | 24-67 | 14 | 45.33 | 27.38 | 3 | -0.09 | 3 | 2.53 | 15.82 |
| R4 | 6 | 24-67 | 15 | 36.8 | 22.53 | 2 | -0.06 | 3 | 2.58 | 14.04 |
| R4 | 6 | 24-67 | 16 | 39.27 | 25.2 | 2 | -0.06 | 3 | 2.79 | 6.97 |
| R4 | 6 | 24-67 | 17 | 31.46 | 18.51 | 2 | -0.06 | 3 | 2.43 | 19.02 |
| R4 | 6 | 24-67 | 18 | 21.42 | 12.94 | 2 | -0.06 | 3 | 2.53 | 15.80 |
| R4 | 6 | 24-67 | 19 | 23.88 | 14.12 | 2 | -0.06 | 3 | 2.45 | 18.44 |

| Sample | Stratigraphic Height | Size Range | Clast Number | Dry Weight | Wet Weight | Number of Wax Sheets | Weight Difference | DRE (g/cm$^3$) | Specific Gravity | Vesicularity |
|---|---|---|---|---|---|---|---|---|---|---|
| P3 S11 | 1.2-1.4 | 15-49 | 1 | 118.04 | 72.07 | 5 | -0.15 | 3 | 2.57 | 14.41 |
| P3 S11 | 1.2-1.4 | 15-49 | 2 | 65.58 | 39.82 | 4 | -0.12 | 3 | 2.55 | 15.14 |
| P3 S11 | 1.2-1.4 | 15-49 | 3 | 112.24 | 69.11 | 5 | -0.15 | 3 | 2.60 | 13.25 |
| P3 S11 | 1.2-1.4 | 15-49 | 4 | 45.22 | 19.03 | 4 | -0.12 | 3 | 1.73 | 42.45 |
| P3 S11 | 1.2-1.4 | 15-49 | 5 | 37.37 | 18.39 | 3 | -0.09 | 3 | 1.97 | 34.37 |
| P3 S11 | 1.2-1.4 | 15-49 | 6 | 33.3 | 16.38 | 3 | -0.09 | 3 | 1.97 | 34.40 |
| P3 S11 | 1.2-1.4 | 15-49 | 7 | 22.64 | 9.47 | 3 | -0.09 | 3 | 1.72 | 42.70 |
| P3 S11 | 1.2-1.4 | 15-49 | 8 | 18.25 | 11.17 | 2 | -0.06 | 3 | 2.58 | 14.08 |
| P3 S11 | 1.2-1.4 | 15-49 | 9 | 23.59 | 14.38 | 2 | -0.06 | 3 | 2.56 | 14.62 |
| P3 S11 | 1.2-1.4 | 15-49 | 10 | 14.04 | 5.33 | 2 | -0.06 | 3 | 1.61 | 46.27 |
| P3 S11 | 1.2-1.4 | 15-49 | 11 | 10.38 | 4.17 | 2 | -0.06 | 3 | 1.67 | 44.28 |
| P3 S11 | 1.2-1.4 | 15-49 | 12 | 11.47 | 4.2 | 2 | -0.06 | 3 | 1.58 | 47.41 |
| P3 S11 | 1.2-1.4 | 15-49 | 13 | 12.84 | 7.76 | 1 | -0.03 | 3 | 2.53 | 15.75 |
| P3 S11 | 1.2-1.4 | 15-49 | 14 | 14.86 | 9.07 | 1 | -0.03 | 3 | 2.57 | 14.45 |
| P3 S11 | 1.2-1.4 | 15-49 | 15 | 10.89 | 6.73 | 1 | -0.03 | 3 | 2.62 | 12.74 |
| P3 S11 | 1.2-1.4 | 15-49 | 16 | 11.42 | 4.61 | 2 | -0.06 | 3 | 1.68 | 44.10 |
| P3 S11 | 1.2-1.4 | 15-49 | 17 | 13.57 | 8.35 | 1 | -0.03 | 3 | 2.60 | 13.35 |
| P3 S11 | 1.2-1.4 | 15-49 | 18 | 10.97 | 5.61 | 2 | -0.06 | 3 | 2.05 | 31.78 |
| P3 S11 | 1.2-1.4 | 15-49 | 19 | 8.6 | 4.52 | 1 | -0.03 | 3 | 2.11 | 29.74 |
| P3 S11 | 1.2-1.4 | 15-49 | 20 | 5.76 | 2.41 | 1 | -0.03 | 3 | 1.72 | 42.69 |
| P3 S11 | 1.2-1.4 | 15-49 | 21 | 7.77 | 3.21 | 1 | -0.03 | 3 | 1.70 | 43.20 |
| P3 S11 | 1.2-1.4 | 15-49 | 22 | 7.6 | 3.27 | 1 | -0.03 | 3 | 1.76 | 41.49 |
| P3 S11 | 1.2-1.4 | 15-49 | 23 | 5.74 | 2.12 | 1 | -0.03 | 3 | 1.59 | 47.15 |
| P3 S11 | 1.2-1.4 | 15-49 | 24 | 3.95 | 1.55 | 1 | -0.03 | 3 | 1.65 | 45.14 |
| P3 S11 | 1.2-1.4 | 15-49 | 25 | 5.3 | 1.94 | 1 | -0.03 | 3 | 1.58 | 47.42 |
| P3 S11 | 1.2-1.4 | 15-49 | 26 | 4.47 | 2.25 | 1 | -0.03 | 3 | 2.01 | 32.88 |
| P3 S11 | 1.2-1.4 | 15-49 | 27 | 2.95 | 1.33 | 1 | -0.03 | 3 | 1.82 | 39.30 |
| P3 S11 | 1.2-1.4 | 15-49 | 28 | 4.35 | 2.63 | 1 | -0.03 | 3 | 2.53 | 15.70 |

| Sample | Stratigraphic Height | Size Range | Clast Number | Dry Weight | Wet Weight | Number of Wax Sheets | Weight Difference | DRE (g/cm$^3$) | Specific Gravity | Vesicularity |
|---|---|---|---|---|---|---|---|---|---|---|
| P3 S2 | 0.3-0.7 | 11-58 | 1 | 297 | 182.63 | 8 | -0.24 | 3 | 2.60 | 13.44 |
| P3 S2 | 0.3-0.7 | 11-58 | 2 | 89.22 | 68.08 | 5 | -0.15 | 3 | 4.22 | -40.68 |
| P3 S2 | 0.3-0.7 | 11-58 | 3 | 111.5 | 54.97 | 4 | -0.12 | 3 | 1.97 | 34.25 |
| P3 S2 | 0.3-0.7 | 11-58 | 4 | 78.76 | 37.31 | 4 | -0.12 | 3 | 1.90 | 36.66 |
| P3 S2 | 0.3-0.7 | 11-58 | 5 | 36.95 | 13.76 | 3 | -0.09 | 3 | 1.59 | 46.89 |
| P3 S2 | 0.3-0.7 | 11-58 | 6 | 30.71 | 9.89 | 3 | -0.09 | 3 | 1.48 | 50.83 |
| P3 S2 | 0.3-0.7 | 11-58 | 7 | 64.6 | 39.68 | 3 | -0.09 | 3 | 2.59 | 13.59 |
| P3 S2 | 0.3-0.7 | 11-58 | 8 | 23.91 | 8.5 | 3 | -0.09 | 3 | 1.55 | 48.28 |
| P3 S2 | 0.3-0.7 | 11-58 | 9 | 23.18 | 8.23 | 2 | -0.06 | 3 | 1.55 | 48.32 |
| P3 S2 | 0.3-0.7 | 11-58 | 10 | 22.2 | 8.1 | 2 | -0.06 | 3 | 1.57 | 47.52 |
| P3 S2 | 0.3-0.7 | 11-58 | 11 | 20.7 | 8.69 | 2 | -0.06 | 3 | 1.72 | 42.55 |
| P3 S2 | 0.3-0.7 | 11-58 | 12 | 44 | 27.23 | 2 | -0.06 | 3 | 2.62 | 12.54 |
| P3 S2 | 0.3-0.7 | 11-58 | 13 | 42.17 | 25.93 | 3 | -0.09 | 3 | 2.60 | 13.44 |
| P3 S2 | 0.3-0.7 | 11-58 | 14 | 25.45 | 15.6 | 2 | -0.06 | 3 | 2.58 | 13.87 |
| P3 S2 | 0.3-0.7 | 11-58 | 15 | 42.96 | 25.81 | 2 | -0.06 | 3 | 2.50 | 16.50 |
| P3 S2 | 0.3-0.7 | 11-58 | 16 | 20.84 | 9.83 | 2 | -0.06 | 3 | 1.89 | 36.91 |
| P3 S2 | 0.3-0.7 | 11-58 | 17 | 20.14 | 10.68 | 2 | -0.06 | 3 | 2.13 | 29.03 |
| P3 S2 | 0.3-0.7 | 11-58 | 18 | 17.36 | 10.38 | 2 | -0.06 | 3 | 2.49 | 17.10 |
| P3 S2 | 0.3-0.7 | 11-58 | 19 | 16.6 | 10.03 | 2 | -0.06 | 3 | 2.53 | 15.78 |
| P3 S2 | 0.3-0.7 | 11-58 | 20 | 8.98 | 3.57 | 2 | -0.06 | 3 | 1.66 | 44.67 |
| P3 S2 | 0.3-0.7 | 11-58 | 21 | 9.9 | 4.25 | 2 | -0.06 | 3 | 1.75 | 41.59 |
| P3 S2 | 0.3-0.7 | 11-58 | 22 | 8.98 | 2.77 | 2 | -0.06 | 3 | 1.45 | 51.80 |
| P3 S2 | 0.3-0.7 | 11-58 | 23 | 6.67 | 2.54 | 1 | -0.03 | 3 | 1.62 | 46.17 |
| P3 S2 | 0.3-0.7 | 11-58 | 24 | 9.22 | 5.7 | 1 | -0.03 | 3 | 2.62 | 12.69 |
| P3 S2 | 0.3-0.7 | 11-58 | 25 | 7.49 | 2.85 | 1 | -0.03 | 3 | 1.61 | 46.19 |
| P3 S2 | 0.3-0.7 | 11-58 | 26 | 8.14 | 3.2 | 1 | -0.03 | 3 | 1.65 | 45.07 |
| P3 S2 | 0.3-0.7 | 11-58 | 27 | 8.45 | 5.15 | 1 | -0.03 | 3 | 2.56 | 14.65 |
| P3 S2 | 0.3-0.7 | 11-58 | 28 | 6.08 | 2.6 | 1 | -0.03 | 3 | 1.75 | 41.76 |
| P3 S2 | 0.3-0.7 | 11-58 | 29 | 3.48 | 1.09 | 1 | -0.03 | 3 | 1.46 | 51.46 |
| P3 S2 | 0.3-0.7 | 11-58 | 30 | 4.07 | 1.71 | 1 | -0.03 | 3 | 1.72 | 42.51 |
| P3 S2 | 0.3-0.7 | 11-58 | 31 | 3.61 | 1.66 | 1 | -0.03 | 3 | 1.85 | 38.29 |
| P3 S2 | 0.3-0.7 | 11-58 | 32 | 2.74 | 1.01 | 1 | -0.03 | 3 | 1.58 | 47.21 |

| Sample | Stratigraphic Height | Size Range | Clast Number | Dry Weight | Wet Weight | Number of Wax Sheets | Weight Difference | DRE (g/cm$^3$) | Specific Gravity | Vesicularity |
|---|---|---|---|---|---|---|---|---|---|---|
| P3 S10 | 4-4.2 | 13-64 | 1 | 268.13 | 147.82 | 9 | -0.27 | 3 | 2.23 | 25.71 |
| P3 S10 | 4-4.2 | 13-64 | 2 | 164.58 | 87.41 | 7 | -0.21 | 3 | 2.13 | 28.91 |
| P3 S10 | 4-4.2 | 13-64 | 3 | 78.58 | 44.6 | 4 | -0.12 | 3 | 2.31 | 22.92 |
| P3 S10 | 4-4.2 | 13-64 | 4 | 28.81 | 17.53 | 2 | -0.06 | 3 | 2.55 | 14.86 |
| P3 S10 | 4-4.2 | 13-64 | 5 | 50.2 | 27.71 | 3 | -0.09 | 3 | 2.23 | 25.60 |
| P3 S10 | 4-4.2 | 13-64 | 6 | 25.26 | 13.01 | 2 | -0.06 | 3 | 2.06 | 31.27 |
| P3 S10 | 4-4.2 | 13-64 | 7 | 26.43 | 16.18 | 2 | -0.06 | 3 | 2.58 | 14.05 |
| P3 S10 | 4-4.2 | 13-64 | 8 | 41.8 | 25.88 | 2 | -0.06 | 3 | 2.63 | 12.48 |
| P3 S10 | 4-4.2 | 13-64 | 9 | 11.06 | 4.64 | 2 | -0.06 | 3 | 1.72 | 42.58 |
| P3 S10 | 4-4.2 | 13-64 | 10 | 17.49 | 10.51 | 2 | -0.06 | 3 | 2.51 | 16.48 |
| P3 S10 | 4-4.2 | 13-64 | 11 | 12.45 | 7.57 | 1 | -0.03 | 3 | 2.55 | 14.96 |
| P3 S10 | 4-4.2 | 13-64 | 12 | 14.87 | 8.98 | 2 | -0.06 | 3 | 2.52 | 15.85 |
| P3 S10 | 4-4.2 | 13-64 | 13 | 11.32 | 5.79 | 1 | -0.03 | 3 | 2.05 | 31.77 |
| P3 S10 | 4-4.2 | 13-64 | 14 | 4.39 | 2.31 | 1 | -0.03 | 3 | 2.11 | 29.65 |
| P3 S10 | 4-4.2 | 13-64 | 15 | 3.31 | 1.51 | 1 | -0.03 | 3 | 1.84 | 38.70 |



| Sample | Stratigraphic Height | Size Range | Clast Number | Dry Weight | Wet Weight | Number of Wax Sheets | Weight Difference | DRE (g/cm$^3$) | Specific Gravity | Vesicularity |
|---|---|---|---|---|---|---|---|---|---|---|
| P3 S18 | 6.72-6.98 | 16-48 | 1 | 44.33 | 20.09 | 3 | -0.09 | 3 | 1.83 | 39.04 |
| P3 S18 | 6.72-6.98 | 16-48 | 2 | 43.1 | 26.19 | 3 | -0.09 | 3 | 2.55 | 15.04 |
| P3 S18 | 6.72-6.98 | 16-48 | 3 | 32.32 | 19.78 | 2 | -0.06 | 3 | 2.58 | 14.09 |
| P3 S18 | 6.72-6.98 | 16-48 | 4 | 26.21 | 12.67 | 2 | -0.06 | 3 | 1.94 | 35.48 |
| P3 S18 | 6.72-6.98 | 16-48 | 5 | 21.27 | 10.52 | 2 | -0.06 | 3 | 1.98 | 34.05 |
| P3 S18 | 6.72-6.98 | 16-48 | 6 | 13.36 | 6.76 | 2 | -0.06 | 3 | 2.02 | 32.53 |
| P3 S18 | 6.72-6.98 | 16-48 | 7 | 15.34 | 8.45 | 2 | -0.06 | 3 | 2.23 | 25.79 |
| P3 S18 | 6.72-6.98 | 16-48 | 8 | 9.45 | 4.59 | 1 | -0.03 | 3 | 1.94 | 35.19 |
| P3 S18 | 6.72-6.98 | 16-48 | 9 | 9.16 | 4.22 | 1 | -0.03 | 3 | 1.85 | 38.19 |
| P3 S18 | 6.72-6.98 | 16-48 | 10 | 5.42 | 2.55 | 1 | -0.03 | 3 | 1.89 | 37.05 |
| P3 S18 | 6.72-6.98 | 16-48 | 11 | 4.55 | 2.29 | 1 | -0.03 | 3 | 2.01 | 32.89 |
| P3 S18 | 6.72-6.98 | 16-48 | 12 | 2.63 | 1.12 | 1 | -0.03 | 3 | 1.74 | 41.94 |
| P3 S18 | 6.72-6.98 | 16-48 | 13 | 3.5 | 2.1 | 1 | -0.03 | 3 | 2.50 | 16.67 |

| Sample | Stratigraphic Height | Size Range | Clast Number | Dry Weight | Wet Weight | Number of Wax Sheets | Weight Difference | DRE (g/cm$^3$) | Specific Gravity | Vesicularity |
|---|---|---|---|---|---|---|---|---|---|---|
| P3 S23 | 8.08-8.2 | 10-44 | 1 | 45.62 | 21.28 | 3 | -0.09 | 3 | 1.87 | 37.52 |
| P3 S23 | 8.08-8.2 | 10-44 | 2 | 38.75 | 21.33 | 3 | -0.09 | 3 | 2.22 | 25.85 |
| P3 S23 | 8.08-8.2 | 10-44 | 3 | 24.98 | 14.82 | 2 | -0.06 | 3 | 2.46 | 18.04 |
| P3 S23 | 8.08-8.2 | 10-44 | 4 | 19.36 | 8.8 | 2 | -0.06 | 3 | 1.83 | 38.89 |
| P3 S23 | 8.08-8.2 | 10-44 | 5 | 14.55 | 6.87 | 2 | -0.06 | 3 | 1.89 | 36.85 |
| P3 S23 | 8.08-8.2 | 10-44 | 6 | 17.98 | 8.4 | 2 | -0.06 | 3 | 1.88 | 37.44 |
| P3 S23 | 8.08-8.2 | 10-44 | 7 | 18.36 | 11.05 | 2 | -0.06 | 3 | 2.51 | 16.28 |
| P3 S23 | 8.08-8.2 | 10-44 | 8 | 19.27 | 11.66 | 2 | -0.06 | 3 | 2.53 | 15.59 |
| P3 S23 | 8.08-8.2 | 10-44 | 9 | 17.38 | 10.54 | 2 | -0.06 | 3 | 2.54 | 15.30 |
| P3 S23 | 8.08-8.2 | 10-44 | 10 | 16.13 | 8.31 | 2 | -0.06 | 3 | 2.06 | 31.24 |
| P3 S23 | 8.08-8.2 | 10-44 | 11 | 14.69 | 8.98 | 2 | -0.06 | 3 | 2.57 | 14.24 |
| P3 S23 | 8.08-8.2 | 10-44 | 12 | 17.07 | 10.4 | 2 | -0.06 | 3 | 2.56 | 14.69 |
| P3 S23 | 8.08-8.2 | 10-44 | 13 | 10.98 | 6.69 | 1 | -0.03 | 3 | 2.56 | 14.69 |
| P3 S23 | 8.08-8.2 | 10-44 | 14 | 9.71 | 4.36 | 2 | -0.06 | 3 | 1.81 | 39.50 |
| P3 S23 | 8.08-8.2 | 10-44 | 15 | 11.65 | 7.15 | 1 | -0.03 | 3 | 2.59 | 13.70 |
| P3 S23 | 8.08-8.2 | 10-44 | 16 | 9.41 | 4.94 | 2 | -0.06 | 3 | 2.11 | 29.83 |
| P3 S23 | 8.08-8.2 | 10-44 | 17 | 12.94 | 7.81 | 2 | -0.06 | 3 | 2.52 | 15.92 |
| P3 S23 | 8.08-8.2 | 10-44 | 18 | 7.2 | 3.05 | 1 | -0.03 | 3 | 1.73 | 42.17 |
| P3 S23 | 8.08-8.2 | 10-44 | 19 | 6.82 | 3.52 | 1 | -0.03 | 3 | 2.07 | 31.11 |
| P3 S23 | 8.08-8.2 | 10-44 | 20 | 12.3 | 7.54 | 1 | -0.03 | 3 | 2.58 | 13.87 |
| P3 S23 | 8.08-8.2 | 10-44 | 21 | 5.12 | 2.64 | 1 | -0.03 | 3 | 2.06 | 31.18 |
| P3 S23 | 8.08-8.2 | 10-44 | 22 | 4.55 | 2.25 | 1 | -0.03 | 3 | 1.98 | 34.06 |
| P3 S23 | 8.08-8.2 | 10-44 | 23 | 3.11 | 0.55 | 1 | -0.03 | 3 | 1.21 | 59.51 |
| P3 S23 | 8.08-8.2 | 10-44 | 24 | 4.93 | 2.49 | 1 | -0.03 | 3 | 2.02 | 32.65 |
| P3 S23 | 8.08-8.2 | 10-44 | 25 | 4.53 | 2.29 | 1 | -0.03 | 3 | 2.02 | 32.59 |
| P3 S23 | 8.08-8.2 | 10-44 | 26 | 2.78 | 1.17 | 1 | -0.03 | 3 | 1.73 | 42.44 |
| P3 S23 | 8.08-8.2 | 10-44 | 27 | 6.06 | 3.38 | 1 | -0.03 | 3 | 2.26 | 24.63 |
| P3 S23 | 8.08-8.2 | 10-44 | 28 | 2.91 | 1.29 | 1 | -0.03 | 3 | 1.80 | 40.12 |
| P3 S23 | 8.08-8.2 | 10-44 | 29 | 2.71 | 1.25 | 1 | -0.03 | 3 | 1.86 | 38.13 |
| P3 S23 | 8.08-8.2 | 10-44 | 30 | 2.93 | 1.32 | 1 | -0.03 | 3 | 1.82 | 39.34 |

| Sample | Stratigraphic Height | Size Range | Clast Number | Dry Weight | Wet Weight | Number of Wax Sheets | Weight Difference | DRE ($g/cm^3$) | Specific Gravity | Vesicularity |
|---|---|---|---|---|---|---|---|---|---|---|
| P3 S22 | 7.76-8 | 12-34 | 1 | 16.84 | 6.66 | 2 | -0.06 | 3 | 1.65 | 44.86 |
| P3 S22 | 7.76-8 | 12-34 | 2 | 61.78 | 24.28 | 5 | -0.15 | 3 | 1.65 | 45.08 |
| P3 S22 | 7.76-8 | 12-34 | 3 | 61.06 | 36.91 | 3 | -0.09 | 3 | 2.53 | 15.72 |
| P3 S22 | 7.76-8 | 12-34 | 4 | 31.14 | 13.64 | 3 | -0.09 | 3 | 1.78 | 40.69 |
| P3 S22 | 7.76-8 | 12-34 | 5 | 34.47 | 18.55 | 3 | -0.09 | 3 | 2.17 | 27.83 |
| P3 S22 | 7.76-8 | 12-34 | 6 | 17.89 | 8.23 | 2 | -0.06 | 3 | 1.85 | 38.27 |
| P3 S22 | 7.76-8 | 12-34 | 7 | 13.17 | 5.09 | 2 | -0.06 | 3 | 1.63 | 45.67 |
| P3 S22 | 7.76-8 | 12-34 | 8 | 14.81 | 8.08 | 2 | -0.06 | 3 | 2.20 | 26.65 |
| P3 S22 | 7.76-8 | 12-34 | 9 | 5.88 | 1.8 | 1 | -0.03 | 3 | 1.44 | 51.96 |
| P3 S22 | 7.76-8 | 12-34 | 10 | 10.91 | 5.12 | 2 | -0.06 | 3 | 1.88 | 37.19 |
| P3 S22 | 7.76-8 | 12-34 | 11 | 8.91 | 2.96 | 2 | -0.06 | 3 | 1.50 | 50.08 |
| P3 S22 | 7.76-8 | 12-34 | 12 | 8.59 | 4.38 | 1 | -0.03 | 3 | 2.04 | 31.99 |
| P3 S22 | 7.76-8 | 12-34 | 13 | 6.22 | 3.07 | 1 | -0.03 | 3 | 1.97 | 34.18 |
| P3 S22 | 7.76-8 | 12-34 | 14 | 5.89 | 3.49 | 1 | -0.03 | 3 | 2.45 | 18.19 |
| P3 S22 | 7.76-8 | 12-34 | 15 | 5.48 | 3.08 | 1 | -0.03 | 3 | 2.28 | 23.89 |
| P3 S22 | 7.76-8 | 12-34 | 16 | 6.3 | 3.02 | 1 | -0.03 | 3 | 1.92 | 35.98 |
| P3 S22 | 7.76-8 | 12-34 | 17 | 4.31 | 1.51 | 1 | -0.03 | 3 | 1.54 | 48.69 |
| P3 S22 | 7.76-8 | 12-34 | 18 | 6.42 | 3.87 | 1 | -0.03 | 3 | 2.52 | 16.08 |
| P3 S22 | 7.76-8 | 12-34 | 19 | 4.54 | 2.39 | 1 | -0.03 | 3 | 2.11 | 29.61 |
| P3 S22 | 7.76-8 | 12-34 | 20 | 3.49 | 1.63 | 1 | -0.03 | 3 | 1.88 | 37.46 |
| P3 S22 | 7.76-8 | 12-34 | 21 | 4.79 | 2.8 | 1 | -0.03 | 3 | 2.41 | 19.77 |
| P3 S22 | 7.76-8 | 12-34 | 22 | 3.93 | 2.18 | 1 | -0.03 | 3 | 2.25 | 25.14 |
| P3 S22 | 7.76-8 | 12-34 | 23 | 2.65 | 0.71 | 1 | -0.03 | 3 | 1.37 | 54.47 |

| Sample | Stratigraphic Height | Size Range | Clast Number | Dry Weight | Wet Weight | Number of Wax Sheets | Weight Difference | DRE ($g/cm^3$) | Specific Gravity | Vesicularity |
|---|---|---|---|---|---|---|---|---|---|---|
| P6 | 6.2 | 14-43 | 1 | 83.13 | 51.54 | 4 | -0.12 | 3 | 2.63 | 12.28 |
| P6 | 6.2 | 14-43 | 2 | 37.42 | 23.03 | 3 | -0.09 | 3 | 2.60 | 13.32 |
| P6 | 6.2 | 14-43 | 3 | 45.49 | 24.3 | 3 | -0.09 | 3 | 2.15 | 28.44 |
| P6 | 6.2 | 14-43 | 4 | 29.11 | 17.83 | 2 | -0.06 | 3 | 2.58 | 13.98 |
| P6 | 6.2 | 14-43 | 5 | 21.86 | 13.23 | 2 | -0.06 | 3 | 2.53 | 15.57 |
| P6 | 6.2 | 14-43 | 6 | 30.59 | 18.63 | 2 | -0.06 | 3 | 2.56 | 14.74 |
| P6 | 6.2 | 14-43 | 7 | 14.87 | 9.08 | 2 | -0.06 | 3 | 2.57 | 14.39 |
| P6 | 6.2 | 14-43 | 8 | 12.5 | 7.49 | 2 | -0.06 | 3 | 2.50 | 16.83 |
| P6 | 6.2 | 14-43 | 9 | 8.34 | 5.03 | 1 | -0.03 | 3 | 2.52 | 16.01 |
| P6 | 6.2 | 14-43 | 10 | 7.53 | 4.6 | 1 | -0.03 | 3 | 2.57 | 14.33 |
| P6 | 6.2 | 14-43 | 11 | 5.65 | 3.39 | 1 | -0.03 | 3 | 2.50 | 16.67 |
| P6 | 6.2 | 14-43 | 12 | 8.45 | 5.15 | 1 | -0.03 | 3 | 2.56 | 14.65 |
| P6 | 6.2 | 14-43 | 13 | 5.61 | 3.27 | 1 | -0.03 | 3 | 2.40 | 20.09 |

| Sample | Stratigraphic Height | Size Range | Clast Number | Dry Weight | Wet Weight | Number of Wax Sheets | Weight Difference | DRE (g/cm$^3$) | Specific Gravity | Vesicularity |
|---|---|---|---|---|---|---|---|---|---|---|
| P12 | 8.1-8.3 | 14-51 | 1 | 267.93 | 163.94 | 7 | -0.21 | 3 | 2.58 | 14.12 |
| P12 | 8.1-8.3 | 14-51 | 2 | 123.09 | 75.82 | 5 | -0.15 | 3 | 2.60 | 13.20 |
| P12 | 8.1-8.3 | 14-51 | 3 | 39.95 | 24.55 | 3 | -0.09 | 3 | 2.59 | 13.53 |
| P12 | 8.1-8.3 | 14-51 | 4 | 27 | 11.43 | 3 | -0.09 | 3 | 1.73 | 42.20 |
| P12 | 8.1-8.3 | 14-51 | 5 | 41.84 | 26.1 | 2 | -0.06 | 3 | 2.66 | 11.39 |
| P12 | 8.1-8.3 | 14-51 | 6 | 36.85 | 22.65 | 3 | -0.09 | 3 | 2.60 | 13.50 |
| P12 | 8.1-8.3 | 14-51 | 7 | 46 | 28.01 | 3 | -0.09 | 3 | 2.56 | 14.77 |
| P12 | 8.1-8.3 | 14-51 | 8 | 20.74 | 12.97 | 2 | -0.06 | 3 | 2.67 | 11.03 |
| P12 | 8.1-8.3 | 14-51 | 9 | 27.6 | 13.87 | 3 | -0.09 | 3 | 2.01 | 32.99 |
| P12 | 8.1-8.3 | 14-51 | 10 | 17.18 | 10.12 | 1 | -0.03 | 3 | 2.43 | 18.89 |
| P12 | 8.1-8.3 | 14-51 | 11 | 16.49 | 9.98 | 2 | -0.06 | 3 | 2.53 | 15.57 |
| P12 | 8.1-8.3 | 14-51 | 12 | 15.15 | 9.24 | 2 | -0.06 | 3 | 2.56 | 14.55 |
| P12 | 8.1-8.3 | 14-51 | 13 | 8.85 | 5.29 | 1 | -0.03 | 3 | 2.49 | 17.13 |
| P12 | 8.1-8.3 | 14-51 | 14 | 14.32 | 8.39 | 2 | -0.06 | 3 | 2.41 | 19.51 |
| P12 | 8.1-8.3 | 14-51 | 15 | 6.32 | 2.98 | 1 | -0.03 | 3 | 1.89 | 36.93 |
| P12 | 8.1-8.3 | 14-51 | 16 | 5.34 | 2.3 | 1 | -0.03 | 3 | 1.76 | 41.45 |
| P12 | 8.1-8.3 | 14-51 | 17 | 4.7 | 1.81 | 1 | -0.03 | 3 | 1.63 | 45.79 |
| P12 | 8.1-8.3 | 14-51 | 18 | 4.3 | 1.85 | 1 | -0.03 | 3 | 1.76 | 41.50 |
| P12 | 8.1-8.3 | 14-51 | 19 | 9.93 | 6.07 | 1 | -0.03 | 3 | 2.57 | 14.25 |
| P12 | 8.1-8.3 | 14-51 | 20 | 5.26 | 2.13 | 1 | -0.03 | 3 | 1.68 | 43.98 |
| P12 | 8.1-8.3 | 14-51 | 21 | 5.08 | 2.01 | 1 | -0.03 | 3 | 1.65 | 44.84 |
| P12 | 8.1-8.3 | 14-51 | 22 | 7.62 | 4.57 | 1 | -0.03 | 3 | 2.50 | 16.72 |

Analysis for 1” pycnometer cores

| Sample | Weight | Volume (cc) | Density (g/cc) | Radius (mm) | Core Height (mm) | Volume ($cm^3$) | Connected Vesicularity | Total Vesicularity |
|---|---|---|---|---|---|---|---|---|
| P12(1) | 14.19 | 5.31 | 2.67 | 11.86 | 12.49 | 5.51 | 0.04 | 0.14 |
| P12(2) | 13.47 | 4.96 | 2.72 | 11.82 | 11.68 | 5.12 | 0.03 | 0.12 |
| P12(3) | 13.92 | 5.22 | 2.67 | 11.86 | 12.26 | 5.42 | 0.04 | 0.14 |
| P12(4) | 12.09 | 4.51 | 2.68 | 11.87 | 10.8 | 4.78 | 0.06 | 0.16 |
| P2S11(1) | 10.57 | 3.91 | 2.70 | 11.89 | 9.83 | 4.36 | 0.10 | 0.19 |
| P2S11(2) | 5.68 | 2.09 | 2.72 | 11.88 | 5.42 | 2.40 | 0.13 | 0.21 |
| P3S10(1) | 17.61 | 5.03 | 3.32 | 11.92 | 16.98 | 7.58 | 0.34 | 0.23 |
| P3S10(2) | 12.36 | 5.31 | 2.33 | 11.90 | 12.48 | 5.55 | 0.04 | 0.26 |
| P3S10(3) | 10.61 | 5.04 | 2.00 | 11.98 | 10.97 | 4.94 | -0.02 | 0.28 |
| P3S10(4) | 7.9 | 2.32 | 3.41 | 11.89 | 8.27 | 3.67 | 0.37 | 0.28 |
| P3S11 | 16.09 | 6.06 | 2.65 | 11.86 | 14.18 | 6.27 | 0.03 | 0.14 |
| P3S16(1) | 12.42 | 4.55 | 2.73 | 11.95 | 10.52 | 4.72 | 0.04 | 0.12 |
| P3S16(2) | 11.96 | 4.34 | 2.75 | 11.90 | 10.1 | 4.49 | 0.03 | 0.11 |
| P3S19(1) | 16.35 | 6.08 | 2.69 | 11.88 | 14.26 | 6.32 | 0.04 | 0.14 |
| P3S19(2) | 14.52 | 5.39 | 2.69 | 11.89 | 12.79 | 5.68 | 0.05 | 0.15 |
| P3S19(3) | 19.17 | 7.10 | 2.70 | 11.90 | 16.38 | 7.29 | 0.03 | 0.12 |
| P3S19(4) | 16.93 | 6.29 | 2.69 | 11.92 | 14.38 | 6.41 | 0.02 | 0.12 |
| P3S19(5) | 13.22 | 4.91 | 2.69 | 11.89 | 11.3 | 5.02 | 0.02 | 0.12 |
| P3S2(1) | 18.3 | 6.85 | 2.67 | 11.89 | 15.42 | 6.84 | 0.00 | 0.11 |
| P3S2(2) | 17.64 | 6.59 | 2.68 | 11.85 | 15.22 | 6.71 | 0.02 | 0.12 |
| P3S2(3) | 14.82 | 5.54 | 2.68 | 11.86 | 12.93 | 5.71 | 0.03 | 0.13 |
| P3S2(4) | 13.58 | 5.06 | 2.68 | 11.89 | 11.78 | 5.23 | 0.03 | 0.13 |
| P3S2(5) | 11.46 | 4.26 | 2.68 | 11.93 | 9.94 | 4.44 | 0.04 | 0.14 |
| P3S2(6) | 17.78 | 6.60 | 2.69 | 11.90 | 14.99 | 6.67 | 0.01 | 0.11 |
| P6 | 13.78 | 5.08 | 2.71 | 11.90 | 11.98 | 5.33 | 0.05 | 0.14 |
| R10(1) | 9.93 | 3.31 | 3.00 | 11.84 | 7.8 | 3.44 | 0.04 | 0.04 |
| R10(1.1) | 20.74 | 6.78 | 3.06 | 11.89 | 17.82 | 7.91 | 0.14 | 0.13 |
| R10(2) | 11.9 | 3.98 | 2.99 | 11.89 | 9.24 | 4.10 | 0.03 | 0.03 |
| R10(2.1) | 12.83 | 4.20 | 3.06 | 11.85 | 11.06 | 4.88 | 0.14 | 0.12 |
| R10(3) | 11.63 | 3.90 | 2.99 | 11.91 | 9.06 | 4.03 | 0.03 | 0.04 |
| R10(3.1) | 9.89 | 3.24 | 3.06 | 11.94 | 8.82 | 3.95 | 0.18 | 0.16 |
| R10(4) | 10.51 | 3.46 | 3.04 | 11.90 | 10.94 | 4.87 | 0.29 | 0.28 |

| Sample | Weight | Volume (cc) | Density (g/cc) | Radius (mm) | Core Height (mm) | Volume ($cm^3$) | Connected Vesicularity | Total Vesicularity |
|---|---|---|---|---|---|---|---|---|
| R10(4.1) | 10.11 | 3.39 | 2.99 | 11.88 | 8.05 | 3.57 | 0.05 | 0.06 |
| R10(5) | 7.8 | 2.56 | 3.05 | 11.90 | 7.64 | 3.40 | 0.25 | 0.23 |
| R13(1) | 20.44 | 6.71 | 3.05 | 11.84 | 17.08 | 7.52 | 0.11 | 0.09 |
| R13(2) | 19.11 | 6.26 | 3.05 | 11.91 | 15.91 | 7.08 | 0.12 | 0.10 |
| R13(3) | 13.45 | 4.51 | 2.98 | 11.84 | 16.79 | 7.39 | 0.39 | 0.39 |
| R13(4) | 14.32 | 4.48 | 3.20 | 11.94 | 17.08 | 7.64 | 0.41 | 0.38 |
| R13(5) | 15.61 | 5.12 | 3.05 | 11.90 | 13.08 | 5.82 | 0.12 | 0.11 |
| R13(6) | 11.88 | 4.03 | 2.95 | 11.97 | 9.91 | 4.46 | 0.10 | 0.11 |
| R13(7) | 11.57 | 3.88 | 2.98 | 11.97 | 9.36 | 4.21 | 0.08 | 0.08 |
| R13(8) | 6.52 | 2.09 | 3.12 | 11.89 | 5.45 | 2.42 | 0.14 | 0.10 |
| R16(1) | 19.99 | 6.85 | 2.92 | 11.89 | 15.6 | 6.93 | 0.01 | 0.04 |
| R16(2) | 13.86 | 4.58 | 3.02 | 11.87 | 12.14 | 5.37 | 0.15 | 0.14 |
| R16(3) | 11.77 | 4.01 | 2.93 | 11.92 | 9.52 | 4.25 | 0.06 | 0.08 |
| R16(4) | 7.59 | 2.59 | 2.93 | 11.93 | 6.31 | 2.82 | 0.08 | 0.10 |
| R16(5) | 4.52 | 1.55 | 2.91 | 11.91 | 3.53 | 1.57 | 0.01 | 0.04 |
| R16(6) | 5.87 | 2.00 | 2.94 | 11.96 | 4.7 | 2.11 | 0.05 | 0.07 |
| R18(1) | 13.39 | 4.44 | 3.02 | 11.90 | 14.35 | 6.38 | 0.31 | 0.30 |
| R18(1.1) | 24.33 | 8.36 | 2.91 | 11.89 | 19.43 | 8.62 | 0.03 | 0.06 |
| R18(2) | 8.28 | 2.73 | 3.03 | 11.94 | 7.44 | 3.33 | 0.18 | 0.17 |
| R18(2.1) | 23.42 | 8.03 | 2.92 | 11.86 | 18.43 | 8.14 | 0.01 | 0.04 |
| R18(3) | 3.92 | 1.25 | 3.14 | 11.89 | 4.22 | 1.87 | 0.33 | 0.30 |
| R18(3.1) | 15.78 | 5.25 | 3.01 | 11.89 | 16.14 | 7.16 | 0.27 | 0.27 |
| R18(4) | 3.98 | 1.27 | 3.13 | 11.84 | 4.43 | 1.95 | 0.35 | 0.32 |
| R18(4.1) | 17.21 | 5.86 | 2.94 | 11.93 | 13.47 | 6.02 | 0.03 | 0.05 |
| R18(5.1) | 18.55 | 6.36 | 2.92 | 11.89 | 15.15 | 6.73 | 0.05 | 0.08 |
| R18(6.1) | 15.98 | 5.47 | 2.92 | 11.89 | 12.56 | 5.58 | 0.02 | 0.05 |
| R19(1) | 11.82 | 4.04 | 2.93 | 11.89 | 9.26 | 4.11 | 0.02 | 0.04 |
| R19(1.1) | 17.04 | 5.77 | 2.95 | 11.90 | 13.92 | 6.19 | 0.07 | 0.08 |
| R19(2) | 10.77 | 3.63 | 2.97 | 11.94 | 8.89 | 3.98 | 0.09 | 0.10 |
| R19(2.1) | 17.33 | 5.90 | 2.94 | 11.91 | 13.68 | 6.09 | 0.03 | 0.05 |
| R19(3) | 15.91 | 5.25 | 3.03 | 11.97 | 14.42 | 6.49 | 0.19 | 0.18 |
| R19(3.1) | 16.33 | 5.09 | 2.77 | 11.89 | 13.62 | 6.05 | 0.16 | 0.10 |
| R19(4) | 17.94 | 5.86 | 3.06 | 11.92 | 16.09 | 7.18 | 0.18 | 0.11 |
| R19(4.1) | 15.58 | 5.90 | 2.64 | 11.95 | 13.28 | 5.96 | 0.01 | 0.17 |
| R19(5) | 16.15 | 5.86 | 2.75 | 11.85 | 16.44 | 7.25 | 0.19 | 0.13 |
| R19(5.1) | 12.81 | 4.30 | 2.98 | 11.83 | 10.77 | 4.73 | 0.09 | 0.26 |
| R19(6.1) | 9.79 | 3.27 | 2.99 | 11.88 | 8.59 | 3.81 | 0.14 | 0.10 |

| Sample | Weight | Volume (cc) | Density (g/cc) | Radius (mm) | Core Height (mm) | Volume ($cm^3$) | Connected Vesicularity | Total Vesicularity |
|---|---|---|---|---|---|---|---|---|
| R19(7.1) | 10.44 | 3.55 | 2.94 | 11.95 | 8.67 | 3.89 | 0.09 | 0.14 |
| R4(1) | 17.12 | 6.75 | 2.54 | 11.88 | 18.95 | 8.40 | 0.20 | 0.10 |
| R4(2) | 21.78 | 7.25 | 3.01 | 11.92 | 18.57 | 8.28 | 0.13 | 0.32 |
| R4(3) | 14.36 | 4.69 | 3.06 | 11.89 | 12.45 | 5.53 | 0.15 | 0.12 |
| R4(4) | 9.38 | 3.08 | 3.04 | 11.91 | 8.96 | 3.99 | 0.23 | 0.13 |
| R4(5) | 18.86 | 6.48 | 2.91 | 11.94 | 15.36 | 6.87 | 0.06 | 0.22 |
| R4(6) | 11.72 | 3.84 | 3.05 | 11.89 | 10.52 | 4.67 | 0.18 | 0.09 |
| R4.1(1) | 12.33 | 4.12 | 2.99 | 11.85 | 14.47 | 6.38 | 0.35 | 0.16 |
| R4.1(1.1) | 15.58 | 5.22 | 2.98 | 11.83 | 18.66 | 8.20 | 0.36 | 0.36 |
| R4.1(10.1) | 10.19 | 3.38 | 3.01 | 11.76 | 12.65 | 5.50 | 0.38 | 0.37 |
| R4.1(11.1) | 9.43 | 3.12 | 3.02 | 11.85 | 11.84 | 5.22 | 0.40 | 0.38 |
| R4.1(12.1) | 9.58 | 3.16 | 3.03 | 11.71 | 12.02 | 5.18 | 0.39 | 0.40 |
| R4.1(2) | 12.16 | 4.02 | 3.02 | 11.80 | 13.13 | 5.74 | 0.30 | 0.38 |
| R4.1(2.1) | 15.39 | 5.23 | 2.94 | 11.84 | 16.84 | 7.42 | 0.30 | 0.29 |
| R4.1(3) | 11.01 | 3.64 | 3.03 | 11.78 | 12.23 | 5.33 | 0.32 | 0.31 |
| R4.1(3.1) | 15.32 | 5.16 | 2.97 | 11.74 | 17.89 | 7.74 | 0.33 | 0.31 |
| R4.1(4) | 14.12 | 4.73 | 2.99 | 11.84 | 16.13 | 7.10 | 0.33 | 0.34 |
| R4.1(4.1) | 12.02 | 4.32 | 3.01 | 11.82 | 14.37 | 6.31 | 0.31 | 0.34 |
| R4.1(5) | 11.05 | 3.72 | 2.97 | 11.84 | 12.61 | 5.55 | 0.33 | 0.36 |
| R4.1(5.1) | 12.51 | 4.24 | 2.95 | 11.81 | 14.01 | 6.13 | 0.31 | 0.34 |
| R4.1(6) | 9.81 | 3.28 | 2.99 | 11.96 | 11.22 | 5.04 | 0.35 | 0.32 |
| R4.1(6.1) | 13.09 | 4.36 | 3.00 | 11.83 | 13.76 | 6.05 | 0.28 | 0.35 |
| R4.1(7.1) | 11.31 | 4.37 | 2.59 | 11.85 | 14.13 | 6.23 | 0.30 | 0.28 |
| R4.1(8.1) | 13.37 | 4.37 | 3.06 | 11.83 | 15.21 | 6.68 | 0.35 | 0.39 |
| R4.1(9.1) | 9.96 | 3.34 | 2.98 | 11.82 | 12.24 | 5.37 | 0.38 | 0.33 |
| R7(1) | 17.95 | 5.86 | 3.06 | 11.89 | 16.16 | 7.18 | 0.18 | 0.38 |
| R7(2) | 19.94 | 6.54 | 3.05 | 11.90 | 17.68 | 7.87 | 0.17 | 0.17 |
| R7(3) | 15.71 | 5.15 | 3.05 | 11.84 | 14.68 | 6.46 | 0.20 | 0.15 |
| R7(4) | 8.06 | 2.62 | 3.08 | 11.88 | 7.42 | 3.29 | 0.20 | 0.19 |

Analysis for 1.5” pycnometer cores

| Sample | Weight | Volume (cc) | Density (g/cc) | Radius (mm) | Core Height (mm) | Volume ($cm^3$) | Connected Vesicularity | Total Vesicularity |
|---|---|---|---|---|---|---|---|---|
| P3S12 | 123.12 | 44.90 | 3.00 | 19.26 | 39.5 | 46.03 | 0.02 | 0.11 |
| P3S19(1) | 121.51 | 45.56 | 3.00 | 19.24 | 39.8 | 46.29 | 0.02 | 0.12 |
| R16(1) | 132.28 | 45.10 | 3.00 | 19.24 | 39.04 | 45.38 | 0.01 | 0.03 |
| R16(3) | 133.62 | 45.31 | 3.00 | 19.21 | 39.9 | 46.23 | 0.02 | 0.04 |
| R16(4) | 132.32 | 44.99 | 3.00 | 19.23 | 39.21 | 45.53 | 0.01 | 0.03 |
| R16(5) | 131.41 | 44.74 | 3.00 | 19.23 | 39.15 | 45.46 | 0.02 | 0.04 |
| R18(1) | 117.21 | 38.78 | 3.00 | 19.24 | 38.84 | 45.15 | 0.14 | 0.13 |
| R18(2) | 100.64 | 28.96 | 3.00 | 19.26 | 39.86 | 46.45 | 0.38 | 0.28 |
| R19 | 118.18 | 39.41 | 3.00 | 19.21 | 40.75 | 47.24 | 0.17 | 0.17 |
| R10 | 119.79 | 39.62 | 3.00 | 19.08 | 39.99 | 45.71 | 0.13 | 0.13 |
| R4(1) | 87.37 | 29.99 | 3.00 | 19.19 | 39.1 | 45.24 | 0.34 | 0.36 |
| R4(2) | 88.76 | 28.96 | 3.00 | 19.22 | 38.49 | 44.67 | 0.35 | 0.34 |
| R4(3) | 87.44 | 30.09 | 3.00 | 19.21 | 39.28 | 45.54 | 0.34 | 0.36 |
| R4(4) | 94.15 | 32.23 | 3.00 | 19.20 | 39.87 | 46.17 | 0.30 | 0.32 |
| R4(5) | 88.86 | 30.12 | 3.00 | 19.22 | 38.55 | 44.74 | 0.33 | 0.34 |
| R6(1) | 91.15 | 28.96 | 3.00 | 19.23 | 38.99 | 45.27 | 0.36 | 0.33 |
| R16(2) | 106.62 | 36.59 | 3.00 | 19.23 | 31.89 | 37.03 | 0.01 | 0.04 |
| P3S19(2) | 39.58 | 14.65 | 3.00 | 19.22 | 13.49 | 15.66 | 0.06 | 0.16 |

# *Appendix Five*

## *Electron Microprobe Analysis*

| Analysis | Sample | $SiO_2$ | $TiO_2$ | $Al_2O_3$ | FeO | MnO | MgO | CaO | $Na_2O$ | $K_2O$ | $P_2O_5$ | $SO_3$ | Cl | $Cr_2O_3$ | NiO | TOTAL |
|---|---|---|---|---|---|---|---|---|---|---|---|---|---|---|---|---|
| ID = 3652 | P11 | 41.73 | 0.01 | 0 | 7.03 | 0.09 | 50.35 | 0 | 0 | 0.06 | -0.04 | 0 | 0.02 | 0.02 | 0.4 | 99.67 |
| ID = 3653 | P11 | 67.73 | 0.04 | 19.59 | 0.14 | 0.04 | 0 | 0.39 | 11.33 | 0.24 | 0.1 | 0.01 | 0 | 0.01 | 0.04 | 99.65 |
| ID = 3654 | P11 | 68.34 | -0.02 | 19.47 | 0.01 | 0.05 | -0.03 | 0.15 | 11.55 | 0.21 | 0.07 | 0.02 | 0.03 | -0.03 | -0.04 | 99.78 |
| ID = 3655 | P11 | 40.86 | 5.09 | 13.66 | 10.07 | 0.14 | 13.37 | 10.41 | 2.81 | 1.84 | -0.09 | 0.08 | 0 | -0.03 | 0.02 | 98.24 |
| ID = 3656 | P11 | 41.34 | 5.12 | 13.71 | 9.93 | 0.02 | 13.49 | 10.23 | 2.8 | 1.91 | 0.01 | -0.05 | 0 | -0.05 | -0.07 | 98.39 |
| ID = 3657 | P11 | 69.6 | 0.26 | 12.55 | 2.15 | 0.14 | 0.09 | 1.41 | 2.46 | 2.73 | 0.01 | -0.08 | 0.14 | 0.06 | 0.06 | 91.59 |
| ID = 3658 | P11 | 68.97 | 0.13 | 12.36 | 2.06 | -0.05 | 0.21 | 1.47 | 1.98 | 3.69 | 0 | -0.08 | 0.21 | 0.07 | -0.08 | 90.94 |
| ID = 3659 | P11 | 98.14 | -0.08 | -0.17 | 0.01 | 0 | 0.01 | 0.09 | -0.04 | 0.03 | 0.05 | -0.13 | 0.04 | -0.04 | 0.04 | 97.95 |
| ID = 3661 | P11 | 56.92 | 0.04 | 26.23 | 0.48 | 0.1 | -0.03 | 9.63 | 5.07 | 0.68 | 0.02 | 0.09 | 0.08 | 0.04 | -0.12 | 99.23 |
| ID = 3662 | P11 | 55.59 | 0.17 | 27.63 | 0.47 | -0.05 | 0.04 | 10.17 | 5.39 | 0.35 | 0.05 | -0.06 | 0.06 | 0.15 | -0.12 | 99.84 |
| ID = 3663 | P11 | 49.33 | 0.07 | 6.82 | 22.45 | 0.03 | 3.31 | 0.12 | 0 | 8.04 | 0.19 | -0.04 | 0 | 0.1 | -0.07 | 90.34 |
| ID = 3664 | P11 | 50.7 | 0.07 | 7.35 | 22.17 | -0.05 | 3.69 | 0.15 | -0.02 | 8.25 | 0.28 | 0 | 0 | -0.03 | 0.09 | 92.65 |
| ID = 3665 | P11 | 41.15 | 0.02 | -0.02 | 9.67 | 0.13 | 48.49 | 0.09 | -0.01 | 0.08 | -0.06 | -0.13 | -0.02 | 0.15 | 0.46 | 99.99 |
| ID = 3666 | P11 | 41.45 | 0 | -0.02 | 10.61 | 0.12 | 48.88 | 0.08 | 0.13 | 0.08 | -0.11 | -0.1 | -0.01 | -0.09 | 0.21 | 101.23 |
| ID = 3667 | P11 | 50.27 | 0.23 | 10.48 | 18.34 | -0.02 | 3.72 | 0.28 | -0.03 | 7.34 | -0.15 | -0.15 | 0.01 | -0.02 | 0.16 | 90.47 |
| ID = 3669 | P11 | 41.3 | -0.01 | -0.03 | 12.18 | 0.22 | 47.05 | 0.08 | -0.06 | 0.07 | -0.03 | -0.25 | -0.04 | -0.04 | 0.44 | 100.88 |
| ID = 3670 | P11 | 40.69 | 0.03 | 0.01 | 12.13 | 0.06 | 46.5 | 0.12 | -0.02 | 0.13 | -0.15 | -0.03 | -0.01 | 0.07 | 0.25 | 99.77 |
| ID = 3671 | P11 | 53.61 | 0.42 | 4.12 | 12.93 | 0.24 | 27.62 | 0.9 | -0.07 | 0.07 | -0.13 | 0.07 | 0.02 | 0.48 | 0.04 | 100.31 |
| ID = 3673 | P11 | 40.86 | 4.98 | 13.99 | 9.22 | -0.02 | 13.74 | 10.64 | 2.41 | 1.9 | -0.1 | 0.05 | 0.06 | 0.19 | 0.17 | 98.1 |
| ID = 3674 | P11 | 41.33 | 4.95 | 14.26 | 8.69 | 0.08 | 13.67 | 10.45 | 2.92 | 1.75 | 0.05 | 0.05 | 0.05 | 0.14 | 0.09 | 98.47 |
| ID = 3675 | R14 | 45.62 | 2.2 | 8.64 | 14.02 | 0.19 | 13.74 | 10.7 | 1.8 | 0.49 | 0.06 | 0.07 | 0.02 | 0.04 | 0 | 97.6 |
| ID = 3676 | R14 | 46.03 | 2.38 | 8.4 | 13.83 | 0.15 | 13.96 | 10.95 | 1.69 | 0.5 | -0.11 | 0.02 | 0.15 | -0.03 | -0.05 | 97.87 |
| ID = 3677 | R14 | 38.53 | 0 | -0.11 | 22.07 | 0.16 | 38.15 | 0.18 | 0.17 | 0.09 | -0.08 | -0.05 | -0.01 | 0.06 | 0.15 | 99.3 |
| ID = 3678 | R14 | 39.12 | 0.14 | 0.09 | 22.09 | 0.35 | 38.6 | 0.19 | 0.06 | -0.02 | -0.03 | -0.07 | 0.01 | 0.02 | 0.04 | 100.6 |
| ID = 3679 | R14 | 45.42 | 1.93 | 8.29 | 14.7 | 0.15 | 13.08 | 10.77 | 1.79 | 0.48 | 0 | 0.02 | 0.09 | 0.01 | -0.07 | 96.66 |
| ID = 3680 | R14 | 46.26 | 1.87 | 8.16 | 15.49 | 0.42 | 12.97 | 10.49 | 1.74 | 0.51 | -0.05 | -0.08 | 0.12 | -0.07 | 0.18 | 98.01 |
| ID = 3681 | R14 | 51.18 | 1.2 | 1.91 | 9.51 | 0.18 | 14.38 | 20.18 | 0.28 | 0.13 | 0.23 | -0.12 | 0 | 0.11 | 0.07 | 99.25 |
| ID = 3682 | R14 | 50.99 | 1.42 | 2.66 | 7.8 | 0.01 | 14.92 | 20.55 | 0.2 | 0.08 | 0.16 | -0.09 | -0.01 | 0.32 | -0.12 | 98.9 |
| ID = 3683 | R14 | 46.49 | 1.96 | 7.69 | 14.34 | 0.18 | 13.76 | 10.49 | 1.52 | 0.41 | -0.04 | -0.01 | 0.16 | 0.08 | -0.1 | 96.92 |
| ID = 3684 | R14 | 46.97 | 1.75 | 7.83 | 14.24 | 0.25 | 13.89 | 10.95 | 1.81 | 0.47 | 0 | -0.04 | 0.09 | 0 | -0.08 | 98.13 |
| ID = 3685 | R14 | 41.85 | 0.03 | -0.02 | 8.08 | 0.09 | 50.68 | 0.13 | 0.38 | 0.02 | -0.11 | 0.1 | 0.1 | -0.03 | 0.21 | 101.51 |
| ID = 3686 | R14 | 41.76 | -0.02 | -0.03 | 9.09 | 0.04 | 49.58 | 0.07 | 0.08 | 0.11 | -0.1 | -0.07 | 0.01 | -0.01 | 0.37 | 100.88 |
| ID = 3687 | R14 | 54.02 | 0.39 | 0.98 | 16.69 | 0.36 | 25.41 | 1.32 | 0.11 | 0.06 | -0.09 | -0.01 | -0.04 | 0.04 | -0.07 | 99.17 |
| ID = 3688 | R14 | 53.87 | 0.32 | 1.08 | 17.03 | 0.29 | 25.86 | 1.4 | 0.28 | 0.08 | 0.13 | 0.01 | 0.04 | 0.05 | 0.19 | 100.63 |
| ID = 3689 | R14 | 40.85 | 0.06 | -0.04 | 13.38 | 0.26 | 45.72 | 0.24 | 0.15 | 0.01 | -0.07 | 0.1 | -0.02 | 0.03 | 0.53 | 101.2 |
| ID = 3690 | R14 | 40.81 | 0.07 | -0.04 | 14.25 | 0.27 | 44.92 | 0.34 | 0.11 | 0.06 | 0.06 | 0.1 | 0.03 | 0.1 | 0.38 | 101.46 |

| Analysis | Sample | $SiO_2$ | $TiO_2$ | $Al_2O_3$ | FeO | MnO | MgO | CaO | $Na_2O$ | $K_2O$ | $P_2O_5$ | $SO_3$ | Cl | $Cr_2O_3$ | NiO | TOTAL |
|---|---|---|---|---|---|---|---|---|---|---|---|---|---|---|---|---|
| ID = 3691 | R1 | 58.55 | 0.07 | 25.26 | 0.29 | -0.09 | 0 | 7.43 | 6.98 | 0.45 | -0.06 | -0.12 | -0.01 | 0.15 | 0.22 | 99.1 |
| ID = 3692 | R1 | 56.75 | 0.07 | 27.06 | 0.26 | -0.07 | 0.05 | 9.26 | 6.02 | 0.4 | -0.07 | -0.03 | 0.01 | -0.03 | 0.13 | 99.81 |
| ID = 3693 | R1 | 61.34 | 0.19 | 23.63 | 0.21 | 0.13 | -0.05 | 5.71 | 7.6 | 0.67 | -0.06 | -0.04 | -0.01 | 0.04 | -0.11 | 99.25 |
| ID = 3694 | R1 | 60.92 | -0.05 | 23.65 | 0.23 | 0.08 | 0 | 5.51 | 8 | 0.7 | -0.13 | -0.01 | 0.01 | -0.08 | -0.14 | 98.7 |
| ID = 3695 | R1 | 45.13 | 1.02 | 10.51 | 17.12 | 0.45 | 11.77 | 9.7 | 1.28 | 0.48 | -0.05 | 0.04 | 0.09 | 0.07 | 0.06 | 97.65 |
| ID = 3696 | R1 | 44.51 | 1.17 | 10.39 | 16.51 | 0.32 | 11.64 | 9.72 | 1.1 | 0.49 | -0.01 | -0.02 | 0.09 | 0.02 | 0.08 | 96.02 |
| ID = 3697 | R1 | 54.57 | 0.11 | 28.74 | 0.2 | -0.09 | 0.03 | 11.13 | 5.02 | 0.31 | -0.04 | 0.06 | 0 | -0.06 | -0.09 | 99.88 |
| ID = 3698 | R1 | 53.98 | 0 | 28.74 | 0.38 | 0.12 | -0.07 | 11.08 | 4.86 | 0.25 | -0.06 | -0.02 | 0 | 0.04 | 0.09 | 99.39 |
| ID = 3699 | R1 | 46.11 | 2.42 | 8.57 | 13.89 | 0.34 | 13.93 | 11.01 | 1.79 | 0.58 | -0.08 | 0.03 | 0.12 | -0.08 | 0.07 | 98.71 |
| ID = 3700 | R1 | 45.95 | 2.26 | 8.43 | 13.23 | 0.22 | 14.13 | 10.8 | 1.85 | 0.52 | 0.01 | 0.01 | 0.07 | 0.01 | 0.16 | 97.64 |
| ID = 3701 | R1 | 41.52 | 0.04 | -0.02 | 9.28 | 0.21 | 49.47 | 0.04 | 0.13 | 0.06 | -0.13 | -0.07 | 0.04 | -0.04 | 0.3 | 100.83 |
| ID = 3702 | R1 | 42.04 | -0.03 | -0.03 | 8.88 | 0.19 | 49.33 | 0.1 | -0.07 | 0.02 | -0.09 | -0.05 | 0.05 | 0.12 | 0.45 | 100.89 |
| ID = 3703 | R1 | 39.4 | -0.03 | 0 | 20.32 | 0.29 | 40.67 | 0.15 | 0.13 | 0.04 | -0.07 | -0.02 | -0.01 | -0.03 | 0.03 | 100.88 |
| ID = 3704 | R1 | 39.62 | -0.04 | -0.11 | 20.26 | 0.22 | 40.81 | 0.05 | 0.22 | 0.01 | 0 | 0.12 | 0 | 0 | 0.16 | 101.32 |
| ID = 3705 | R1 | 60.26 | 0.19 | 23.84 | 0.27 | 0.05 | -0.03 | 5.96 | 7.77 | 0.6 | -0.01 | -0.01 | 0.03 | 0.13 | -0.14 | 98.9 |
| ID = 3706 | R1 | 58.32 | 0.05 | 25.37 | 0.27 | -0.09 | -0.06 | 7.5 | 6.8 | 0.47 | -0.07 | -0.06 | 0.02 | 0.19 | -0.07 | 98.65 |
| ID = 3707 | R1 | 48.45 | 1.63 | 7.79 | 7.27 | 0.1 | 14.44 | 17.91 | 0.84 | 0.03 | -0.06 | -0.05 | -0.02 | 0.63 | 0.02 | 98.98 |
| ID = 3708 | R1 | 49.34 | 1.37 | 6.37 | 7.08 | 0.11 | 14.6 | 18.63 | 0.9 | 0.09 | 0.21 | 0.06 | 0.05 | 0.19 | -0.13 | 98.88 |
| ID = 3709 | R1 | 49.42 | -0.01 | 7.58 | 22.39 | 0.03 | 3.34 | 0.23 | 0.17 | 8 | -0.05 | 0 | 0.03 | -0.06 | 0.01 | 91.09 |
| ID = 3710 | R1 | 49.86 | 0.07 | 6.76 | 22.18 | 0.02 | 3.25 | 0.26 | -0.1 | 8.11 | 0 | -0.13 | -0.02 | 0.05 | -0.06 | 90.24 |
| ID = 3711 | R1 | 97.06 | 0.03 | -0.1 | 0.04 | 0.11 | -0.08 | 0.01 | -0.02 | 0.11 | 0.24 | 0.13 | 0 | -0.06 | -0.01 | 97.47 |